Centre Eau Terre Environnement

EXPLOITATION DE LA TOMOGRAPHIE HYDRAULIQUE OSCILLATOIRE POUR LA REPRÉSENTATION DE L'HÉTÉROGÉNÉITÉ ET DE L'ANISOTROPIE D'UN AQUIFÈRE GRANULAIRE

Par

Aymen Nefzi

Thèse présentée pour l'obtention du grade
de Philosophiae Doctor, Ph.D.
en sciences de la terre

Jury d'évaluation

Président du jury et	Richard Martel
Examinateur interne	INRS, Centre Eau Terre Environnement
Examinateur externe	Denis Millette
	Département des Génies civil, Géologique et des Mines
	École Polytechnique de Montréal
Examinateur externe	Pierre Fischer
	Département Géosciences
	Université de Poitiers, France
Directeur de recherche	Daniel Paradis
	INRS, Centre Eau Terre Environnement
Codirecteur de recherche	René Lefebvre
	INRS, Centre Eau Terre Environnement
Codirecteur de recherche	Olivier Bour
	Géosciences Rennes
	Université de Rennes

REMERCIEMENTS

Je souhaite exprimer ma gratitude envers mon directeur de thèse, René Lefebvre, pour avoir initié ce sujet de recherche et pour m'avoir accordé sa confiance pour mener à bien ce projet. Je te remercie particulièrement pour ta grande disponibilité tout le long de ce parcours. Tes exigences élevées et ta rigueur m'ont souvent poussé à repousser mes limites pour atteindre l'excellence dans ce projet. Je te remercie également pour ton humanité, ton écoute attentive et ta compréhension lors des moments difficiles. Ton soutien indéfectible m'a souvent encouragé à persévérer jusqu'au terme de ce travail. Merci de m'avoir accompagné et conseillé jusqu'à la soutenance.

J'adresse de chaleureux remerciements à mon co-directeur de thèse, Daniel Paradis, pour son attention de tout instant sur mes travaux, pour ses conseils avisés et son écoute qui ont été prépondérants pour la bonne réussite de cette thèse. Son énergie et sa confiance ont été des éléments moteurs pour moi. J'ai pris un grand plaisir à travailler avec lui. Un grand merci à mon co-directeur, Olivier Bour, pour son engagement dans le projet et sa disponibilité, malgré la distance qui nous sépare.

J'ai une grosse pensée pour tous mes amis qui ont partagé une petite ou grande partie de ces années de thèse : Zakher, Lap, Khalil, Mourad, Omar, Lazar, Manel, Ahmed, Albotros, Kenza, Chahine, Lyticia, Mahdieh, Saif, Boubaker, Mejdi, et Eya. Grâce à eux, j'ai pu me détendre après de longues journées intellectuellement éprouvantes. Malgré les fréquentes périodes de doute et d'angoisse, leur soutien m'a permis de ne jamais perdre de vue mon objectif final. Ces moments passés ensemble ont indéniablement été essentiels pour me permettre de tenir le coup et de mener à bien ce projet de recherche unique.

Je remercie ma famille en particulier ma petite fille Sophia, qui illumine mes journées, ainsi que mon épouse Maha, qui a été présente à mes côtés, et à mon écoute, tout au long de ce parcours si enrichissant mais si prenant. Ton incroyable patience et compréhension face à mes moments de doutes, de colère et de tristesse ont été plus que précieux. Je souhaite également exprimer ma reconnaissance envers ma belle-mère, Raoudha, pour son soutien et sa présence tout au long de cette période.

Un immense merci à mon frère Louay et ma sœur Oumaima pour leur soutien indéfectible, même à distance, et pour leur présence constante à mes côtés tout au long de ce parcours. Leur soutien inestimable m'a été d'un grand réconfort et m'a donné la force nécessaire pour poursuivre mes efforts.

Je réserve la fin de ces remerciements à mes parents. Merci à mon père sans qui je n’aurai même pas commencé cette thèse. Je te suis reconnaissant pour tes sacrifices, papa. Tu m'as toujours rendu fier en sacrifiant tant de choses pour moi. J'espère sincèrement que tu es fier de moi, car maintenant, ton fils est Docteur. Merci à ma mère Atika pour son écoute attentive et sa compréhension, qui m'ont souvent permis de rebondir dans les moments difficiles. Maman, tu sais à quel point je t'aime plus que tout, car tu as toujours été à mes côtés et tu m'as encouragé pour mon bien-être. Tu mérites bien plus qu'un simple merci !

RÉSUMÉ

L'hétérogénéité et l'anisotropie des aquifères contrôlent l'écoulement de l'eau souterraine et la migration des contaminants, mais la caractérisation de la distribution spatiale hétérogène des propriétés hydrauliques représente un défi majeur. La tomographie hydraulique permet la caractérisation des propriétés hydrauliques entre les puits d'observation, sur des coupes 2D ou sur des volumes 3D, permettant ainsi de caractériser à la fois les propriétés et leur continuité dans l'espace. La tomographie est une méthode de caractérisation qui implique la génération d'un signal hydraulique à partir d'un puits source, puis la mesure de la déformation de ce signal à travers l'aquifère, à différents niveaux dans un ou plusieurs puits d'observation. Dans la littérature, la tomographie hydraulique a principalement été réalisée à l'aide d'essais de pompage à débit constant ou d'essais à choc hydraulique. Pour cette thèse, une approche récemment développée a été explorée : la tomographie hydraulique utilisant des variations sinusoïdales du niveau d'eau avec différentes périodes, dans le puits source.

Le but fondamental de cette thèse est d'offrir un exemple exhaustif de l'application concrète de la tomographie hydraulique oscillatoire (THO) à un aquifère granulaire. Cet objectif englobe l'ensemble des étapes essentielles, depuis les procédures de terrain jusqu'au traitement des données et à l'inversion des résultats obtenus. Dans cette démarche, il s'agit également d'explorer le contenu informationnel de la tomographie hydraulique oscillatoire, avec pour ambition d'améliorer notre compréhension de cette technique dans des conditions de terrain authentiques et de mettre en évidence sa faisabilité pour caractériser l'hétérogénéité des aquifères.

Tout d'abord, les procédures de terrain et le traitement des données sont présentés, en mettant particulièrement l'accent sur l'inversion des résultats. Pour ce faire, les signaux périodiques des tests tomographiques ont été obtenus mécaniquement avec une tige reliée à un treuil contrôlé par ordinateur. Malgré les défis liés à la caractérisation de l'hétérogénéité des aquifères non consolidés anisotropes, des mesures de charge robustes dépassant les niveaux de bruit estimés ont été obtenues au site expérimental de Saint-Lambert-de-Lauzon près de Québec. Dans cette thèse, des techniques d'inversion utilisant l'algorithme de Levenberg-Marquardt ont été appliquées pour estimer l'hétérogénéité des propriétés hydrauliques (conductivité hydraulique horizontale K_h, anisotropie de K à partir du rapport de K verticale et horizontale K_v/K_h, et emmagasinement spécifique S_s) en simulant les effets de l'écoulement radial des eaux souterraines et du stockage dans les puits.

Dans la thèse, nous avons exploré les avancées et les applications de la THO à travers trois études complémentaires. La première démontre la faisabilité de la THO sur le site de St-Lambert, mettant en évidence sa capacité à caractériser l'hétérogénéité et l'anisotropie des propriétés hydrauliques (K_h, K_v/K_h et S_s), en mettant l'accent sur l'utilisation de multiples périodes et leur combinaison. La deuxième analyse compare les réponses de modèles homogènes et hétérogènes pour diverses périodes de signal oscillatoire, proposant des recommandations pour améliorer la résolution des paramètres des aquifères. Enfin, la troisième évalue le contenu informationnel de la THO par rapport à la TH avec essais de perméabilité par choc hydraulique, soulignant ses avantages dans le traitement des données malgré des exigences techniques plus complexes. Cette thèse montre que la combinaison de plusieurs périodes améliore légèrement la résolution de la caractérisation de l'aquifère.

Mots-clés: Hydrogéologie, Caractérisation des aquifères, Tomographie hydraulique oscillatoire, Anisotropie de la conductivité hydraulique, Hétérogénéité, Analyse de résolution, Inversion numérique.

ABSTRACT

Heterogeneity and anisotropy of aquifers control groundwater flow and contaminant migration but characterizing the heterogeneous spatial distribution of hydraulic properties poses a major challenge. Hydraulic tomography (HT) enables the characterization of hydraulic properties between observation wells, in 2D cross-sections or 3D volumes, thus allowing characterization of both properties and their spatial continuity. Hydraulic tomography is a characterization method involving the emission of a hydraulic signal from a source well and the capture of this signal at multiple levels in one or more observation wells. In the literature, hydraulic tomography has primarily been conducted using pumping tests or slug tests. For this thesis, a novel approach was explored: hydraulic tomography using sinusoidal water level variations with different periods in the source well.

The fundamental aim of this thesis is to provide a comprehensive example of the practical application of oscillatory hydraulic tomography (OHT) to a granular aquifer. This objective encompasses all essential steps, from field procedures to data processing and inversion of obtained results. In this endeavor, there is also an exploration of the information content of oscillatory hydraulic tomography, with the ambition of enhancing our understanding of this technique under real field conditions and highlighting its feasibility in characterizing aquifer heterogeneity.

Firstly, the field procedures and data processing are presented, with a particular emphasis on data inversion. For this purpose, the periodic signals from tomographic tests were mechanically obtained using a rod connected to a computer-controlled winch. In this thesis, inversion techniques employing the Levenberg-Marquardt algorithm were applied to estimate the heterogeneity of hydraulic properties (horizontal hydraulic conductivity K_h, K anisotropy through the ratio of vertical to horizontal hydraulic conductivity K_v/K_h, and specific storage S_s) by simulating the effects of radial groundwater flow and wellbore storage effects. Despite the challenges of characterizing the heterogeneity of anisotropic unconsolidated aquifers, robust head measurements exceeding estimated noise levels were obtained at the experimental site of Saint-Lambert-de-Lauzon near Quebec City.

In the thesis, we explore the advancements and applications of OHT through three complementary studies. The first study demonstrates the feasibility of OHT at the St-Lambert site, highlighting its ability to characterize the heterogeneity and anisotropy of hydraulic properties (K_h, K_v/K_h, and S_s), with a focus on the use of multiple periods and their combination. The second

study compares the responses of homogeneous and heterogeneous models across various signal periods, offering recommendations to improve aquifer parameter resolution. Finally, the third study evaluates the information content of OHT compared to HT using slug tests, emphasizing its advantages in data processing despite more complex technical requirements. This thesis shows that combining multiple periods slightly enhances aquifer resolution.

Keywords : Hydrogeology, Aquifer Characterization, Oscillatory Hydraulic Tomography, Hydraulic Conductivity Anisotropy, Heterogeneity, Resolution Analysis, Numerical Inversion.

TABLE DES MATIÈRES

LISTE DES FIGURES

LISTE DES TABLEAUX

LISTE DES ABRÉVIATIONS

THO	Tomographie hydraulique oscillatoire
TH	Tomographie hydraulique
K	Conductivité hydraulique (m/s)
K_h	Conductivité hydraulique horizontale (m/s)
K_v/K_h	Anisotropie de K (rapport K verticale sur K horizontale) (-)
S_s	Coefficient d'emmagasinement spécifique (m^{-1})
r_o	Rayon de la tige (m)
r_{eq}	Rayon équivalent (m)
r_i	Rayon du tubage (m)
r_w	Rayon du puits (m)
A_0	Amplitude maximale du déplacement de la tige (m)
A_{eq}	Variation équivalente de charge hydraulique induite par la tige (m)
T_0	Période du signal (s)
Q_i	Variation périodique du volume d'eau (m^3/s)
L	Longueur de l'intervalle source (m)
S18	Puits source
O21	Puits d'observation
H_o	Variation de charge hydraulique mesurée dans l'intervalle source (m)
h_0 max	Charge hydraulique maximale mesurée dans les intervalles d'observation (m)
h_0 min	Charge hydraulique minimale mesurée dans les intervalles d'observation (m)
Obs	Observation
s	Seconde
SD	Écart type (standard deviation)
Q_a	Débit échangé entre le puits et l'aquifère (m^3/s)
Q_w	Changement d'emmagasinement relié d'eau dans le puits (m^3/s)
J	Matrice de sensibilité
R^2	Coefficient de détermination
m	Pente de régression linéaire
h	Charge hydraulique (m)
F^{-1}	Processus inverse
J†	Inverse généralisée
SVD	Décomposition en valeurs singulières (single value decomposition)
RD	Degré de résolution
tx	Source ou transmetteur
rx	Observateur ou receveur
min	Minute
$m_\dagger$	Solution généralisée du vecteur des paramètres

1 INTRODUCTION

1.1 Méthodes de caractérisation in situ des propriétés hydrauliques

En hydrogéologie, l'étude du fonctionnement hydrodynamique d'un aquifère est basée sur la caractérisation des propriétés hydrauliques qui contrôlent l'écoulement de l'eau et le transport des contaminants. L'hétérogénéité de la distribution spatiale de ces propriétés représente un défi pour la caractérisation hydrogéologique (de Marsily et al., 2005). Généralement, les problèmes de transport de contaminants à partir de sources ponctuelles nécessitent une caractérisation fine de l'hétérogénéité des aquifères. En revanche, les problèmes d'écoulement à l'échelle régionale en hydrogéologie exigent plutôt une évaluation à grande échelle des propriétés hydrauliques. Diverses approches permettent d'obtenir des informations sur la distribution spatiale des propriétés hydrauliques, en fonction du type de caractérisation requise.

Plusieurs méthodes in situ d'estimation des propriétés hydrauliques ont été développées. Les essais de pompages et les essais à choc hydraulique sont les techniques de terrain les plus couramment utilisées pour caractériser les propriétés hydrauliques d'un aquifère (Kruseman et Ridder, 1994; Butler, 2005). Les essais de pompages peuvent fournir des informations précieuses, nous aider à comprendre l'hydraulique des puits, définir les limites d'un aquifère et fournir ses propriétés hydrauliques globales. Les essais à choc hydraulique sont aussi utiles pour fournir les propriétés hydrauliques. Toutefois, les volumes d'eau impliqués sont généralement beaucoup plus faibles qu'avec les essais de pompage, ce qui limite le rayon d'investigation. Ces essais, généralement réalisés sur des crépines pleine longueur, permettent d'estimer la conductivité hydraulique horizontale (K_h) globale des aquifères. Afin d'obtenir plus de détails sur la distribution verticale des propriétés hydrauliques, des essais de pompage ou à choc hydraulique entre obturateurs peuvent être réalisés (Rehfeldt et al., 1992; Ross et McElwee, 2007; Lancaster-Jones, 1975; Quinn et al., 2011).

Cependant, les essais hydrauliques conventionnels, qui induisent principalement des écoulements horizontaux, ne permettent pas d'estimer la composante verticale de la conductivité hydraulique (K_v). Pour y remédier, plusieurs auteurs ont proposé diverses méthodes d'essais hydrauliques en forage pour estimer K_v, telles que les essais en dipôle avec un seul puits (Kabala, 1993; Xiang et Kabala, 1997; Zlotnik et Ledder, 1996; Zlotnik et Zurbuchen, 1998; Hvilshøj et al., 2000; Zlotnik et al., 2001) ou deux puits (Goltz et al., 2008), ainsi que les essais d'interférence

verticale sur un seul puits (Paradis et Lefebvre, 2013). L'ajout des estimations de K_v à celles de K_h permet d'obtenir une meilleure représentation de l'hydraulique des aquifères.

Dans l'ensemble, les essais hydrauliques réalisés sur un seul puits ou sur de grands intervalles crépinés renseignent difficilement sur la distribution spatiale des hétérogénéités à distance des puits. La précision dans l'imagerie spatiale des caractéristiques hydrauliques est soulignée par Illman et al. (2010) comme étant essentielle pour affiner les prévisions concernant la migration des contaminants dans des aquifères hétérogènes affectés par des polluants. Ces prédictions jouent un rôle clé dans l'élaboration de méthodes de réhabilitation adaptées aux environnements contaminés. De ce fait, la détermination précise des propriétés hydrauliques dans les zones polluées constitue un domaine de recherche très actif. Pour pallier les limitations des méthodes conventionnelles, plusieurs travaux ont été réalisés au cours de la dernière décennie sur la tomographie hydraulique (TH), qui a le potentiel de fournir une description détaillée de la distribution spatiale des propriétés hydrauliques des aquifères (Carrera et Neuman, 1986; Bohling, 1993; Tosaka et al., 1993; Yeh et Liu, 2000; Lavenue et al., 1995). La TH implique la production d'un signal hydraulique à un puits source et la mesure de son effet dans plusieurs intervalles d'un ou plusieurs puits d'observation. La TH est une technique émergente pour l'imagerie de l'hétérogénéité détaillée des aquifères qui peut intégrer les réponses des aquifères à partir de nombreux tests de pompage (Hochstetler et al., 2016; Yeh et al., 2008; Zha et al., 2019; Zhao et Illman, 2018; Zhu et Yeh, 2005).

Afin de caractériser les distributions 2D ou 3D (tomogrammes) des propriétés hydrauliques, la TH repose sur l'inversion des mesures effectuées entre les puits, à partir de variations de charge hydraulique mesurées à différents intervalles d'observation (Bohling, 1993; Tosaka et al., 1993; Gottlieb et Dietrich, 1995). La TH a été suggérée pour la première fois par Neuman (1987) comme analogue à la tomographie géophysique. Plusieurs types de sollicitation hydraulique peuvent être utilisés, notamment le pompage et les chocs hydrauliques. Dans la plupart des études de terrain utilisant la tomographie hydraulique, des essais de pompage ont été effectués à un débit constant pour générer une sollicitation. Lors de l'analyse de la tomographie des essais de pompage, différentes approches ont été utilisées. Certaines études se sont appuyées sur l'analyse de la forme quasi-stationnaire ou sur la charge hydraulique en régime permanent(Li et al., 2008; Cardiff et al., 2009). D'autres ont exploité les réponses transitoires complètes (Illman et al., 2009; Berg et Illman, 2011; Cardiff et al., 2012, 2013a; Tiedeman et Barrash, 2020) ont été utilisées. La robustesse de la TH a été confirmée dans des aquifères synthétiques à petite échelle (Illman et al., 2008, 2010), des bacs à sable de laboratoire (Illman et al., 2007; Liu et al., 2007; Zhao et al.,

2016), ainsi que dans des applications de terrain (Berg et Illman, 2011; Cardiff et al., 2012; Fischer et al., 2017; Kuhlman et al., 2008; Zha et al., 2016). D'autres applications de terrain de la tomographie hydraulique ont reposé sur des essais à choc hydraulique (Brauchler et al., 2011, 2013; Lochbühler et al., 2013; Paradis et al., 2016; Liu et al., 2023). Ces expériences de terrain et des essais en laboratoire ont généralement bien démontré la capacité de la TH à définir l'hétérogénéité des aquifères entre les puits, à des échelles plus larges que celles obtenues avec des essais sur des puits individuels.

Outre les méthodes de la TH classiques en régime permanent (Yeh et Liu, 2000) et transitoire (Zhu et Yeh, 2005), il a été proposé d'utiliser les informations sur les variations du niveau d'eau dérivées des courbes de rabattement pour l'analyse TH. Par exemple, afin de surmonter l'impact des conditions limites incertaines dans la modélisation inverse, Bohling et al. (2002) ont proposé une analyse de forme stationnaire des données TH transitoires pour la caractérisation de l'hétérogénéité de *K*. Plus tard, Bohling et al. (2007) ont validé l'approche de forme stationnaire TH par une étude de terrain menée dans un aquifère alluvial situé au Kansas, aux États-Unis, et ils ont conclu que l'analyse de forme stationnaire des données TH transitoires offrait une performance comparable à celle de la TH transitoire pour estimer les profils de *K*. Par ailleurs, Brauchler et al. (2003) ont proposé une approche TH basée sur le temps de parcours afin d'obtenir la distribution de la diffusivité (D=K/Ss) entre les puits testés. Hu et al. (2011) ont ensuite combiné les analyses TH par temps de parcours et forme stationnaire pour estimer les variations spatiales de *K* et S_s. En outre, Zhu et Yeh (2006) ont proposé l'analyse TH des moments temporels des données de récupération de rabattement pour cartographier l'hétérogénéité de *K* et S_s, ce qui a ensuite été validé par une étude en laboratoire dans un bac à sable par Yin et Illman (2009).

Cependant, la sollicitation de l'ensemble d'un aquifère à grande échelle présente des défis. En effet, pomper un puits pour générer des réponses détectables dans tout l'aquifère est difficilement réalisable. Yeh et al. (2008) ont suggéré l'utilisation de sollicitations naturelles (tels que les variations de pression atmosphérique, les éclairs, les marées terrestres ou les fluctuations de niveau des rivières) comme sources d'énergie pour des études tomographiques à l'échelle du bassin. Ils ont conclu aussi que les données recueillies lors de telles études tomographiques offrent de nombreuses contraintes pour la calibration des modèles numériques d'écoulement, permettant d'obtenir des estimations plus précises des champs de *K* et S_s avec moins d'incertitude par rapport aux méthodes de caractérisation traditionnelles.

Yeh et al. (2009) ont ensuite démontré la faisabilité d'utiliser les variations de niveau des rivières pour la caractérisation d'aquifères à grande échelle dans un contexte synthétique, tandis que Wang et al. (2017) ont appliqué ce concept pour caractériser l'aquifère dans l'éventail de la rivière Zhuoshui, à Taïwan. Ces avancées montrent un potentiel important pour l'imagerie de l'hétérogénéité des aquifères à grande échelle, surtout lorsque la rentabilité est accrue par la collecte d'informations non redondantes à partir d'un nombre limité de puits (Sun et al., 2013; Yeh et al., 2014). De nouvelles approches exploitant ces sollicitations pour recueillir davantage d'informations non redondantes dans des puits d'observation existants s'avèrent prometteuses (Cardiff et al., 2013a, 2013b; Tso et al., 2016). Par exemple, Zha et al. (2019) ont tiré parti des modifications des champs d'écoulement causées par les variations de pompage et de traitement pour une étude de TH à grande échelle, permettant de localiser des zones à faible perméabilité en vue d'améliorer l'efficacité de l'assainissement à l'usine 44 de l'US Air Force à Tucson, en Arizona, aux États-Unis.

Bien que la TH ait démontré une performance robuste dans la caractérisation de l'hétérogénéité des propriétés hydrauliques du sous-sol, l'estimation de la distribution spatiale des paramètres hydrauliques par inversion géostatistique des données TH reste sujette à un effet de lissage, particulièrement dans les zones dépourvues de données d'observation utilisées pour la modélisation inverse (Cardiff et al., 2013b; Illman et al., 2015). Cet effet de lissage dépend essentiellement de la contrainte imposée par le variogramme utilisé et du poids qui lui est attribué dans la fonction objectif. Un variogramme fortement contraignant ou fortement pondéré favorise des modèles plus lisses, en limitant les variations spatiales abruptes. Soueid et al. (2015) expliquent cet effet de lissage par l'estimation des moyennes conditionnelles, un élément central de la plupart des approches d'inversion géostatistique (Kitanidis, 1995; Yeh et al., 1996). Bien que ces tomogrammes lissés de K et S_s soient souvent suffisants pour prévoir les distributions de rabattement lors de tests de pompage indépendants non impliqués dans l'étalonnage, une résolution plus fine, incluant les limites des couches, est probablement nécessaire pour des représentations plus précises des processus de transport de solutés et de contaminants.

Pour atténuer l'effet de lissage, plusieurs études recommandent l'incorporation d'informations structurelles dans la modélisation inverse. Par exemple, Jiménez et al. (2013) ont utilisé une inversion basée sur le temps de parcours des réponses de charge hydraulique pour identifier les caractéristiques structurelles du domaine, ensuite employées pour guider une inversion TH basée sur des points pilotes et ainsi cartographier la distribution spatiale de K. De plus, Zhao et al. (2016) ont étudié l'ajout d'informations géologiques dans une étude TH en créant un champ initial de K

fondé sur des données géologiques pour des analyses spécifiques de TH, démontrant qu'un modèle géologique précis pouvait améliorer la qualité du tomogramme de *K*. Zhao et Illman (2017) ont appliqué cette approche pour caractériser la distribution de *K* sur un site de recherche à l'Université de Waterloo. Enfin, Zha et al. (2017) ont intégré des informations structurelles préalables en utilisant les moyennes et covariances des paramètres hydrauliques conditionnées par les caractéristiques géologiques spécifiques du site.

Une difficulté liée aux essais de pompage traditionnels, aux essais à choc hydraulique ainsi qu'à la tomographie hydraulique basée sur ces méthodes réside dans l'atténuation du signal avec la distance, jusqu'à ce qu'il devienne indiscernable du bruit ambiant au-delà d'un certain point. La charge hydraulique est particulièrement sensible aux perturbations externes, telles que les variations du niveau des rivières adjacentes, les activités de pompage ou d'irrigation à proximité des puits d'observation, les effets de marée, les variations de pression barométrique, les changements de charge lithostatique, entre autres. Ces sources de bruit peuvent altérer les résultats de diverses manières (Spane et Mackley, 2011). Par ailleurs, un inconvénient de la tomographie hydraulique utilisant des essais de pompage à débit constant est que le signal généré par la tomographie hydraulique peut être difficile à distinguer de ces bruits et tendances parasites.

Les difficultés rencontrées par la TH ont mené au développement de la tomographie hydraulique oscillatoire (THO), qui est une méthode d'imagerie souterraine basée sur l'analyse tomographique de signaux oscillatoires. Dans les essais utilisant des signaux oscillatoires, une variation de pression périodique est imposée à un point de stimulation (ou à plusieurs de manière séquentielle), tandis que les effets transmis de ce signal sont enregistrés dans un ou plusieurs puits d'observation. Le concept des tests harmoniques a été initialement proposé dans la littérature pétrolière par Kuo (1972) comme une extension des tests impulsionnels (Johnson et al., 1966; McKinley et al., 1968). Rosa et Horne (1997) ont démontré qu'un signal périodique en forme d'onde carrée, alternant des périodes de débit constant et nul, peut fournir davantage d'informations qu'un signal généré par un essai de pompage conventionnel à débit constant, pour une même configuration expérimentale. Cette meilleure performance s'explique par le fait que le signal périodique contient plusieurs composantes sinusoïdales, chacune explorant une région différente de l'aquifère. En modifiant la période d'un signal sinusoïdal pur, il est également possible d'examiner différentes zones de l'aquifère. Plus récemment, des études portant sur la caractérisation des réservoirs à l'aide de tests harmoniques incluent plusieurs travaux (Fokker et al., 2012; Fokker et Verga, 2011; Ahn et Horne, 2011). De manière similaire, les essais

oscillatoires sur les aquifères ont été utilisés pour estimer les paramètres hydrauliques des aquifères (Lavenue et de Marsily, 2001; Engard et al., 2005; Wachter et al., 2008; Becker et Guiltinan, 2010). Ainsi, l'analyse combinée de ces signaux peut potentiellement améliorer la caractérisation de l'hétérogénéité (Black et Kipp, 1981; Hollaender et al., 2002; Ahn et Horne, 2010; Cardiff et al., 2013b; Paradis et al., 2024).

L'utilisation de signaux oscillatoires présente plusieurs avantages par rapport aux essais de pompage traditionnels, notamment (1) une réduction des coûts associés à l'évacuation des eaux contaminées, notamment lorsque l'oscillation est générée sans extraction d'eau significative (par exemple via un slug test ou une pression pneumatique), contrairement aux essais de pompage, ce qui constitue un avantage pour la caractérisation des sites contaminés (Bakhos et al., 2014 ; Cardiff et Sayler, 2016), (2) une diminution des coûts de calcul grâce à l'utilisation d'un modèle périodique stationnaire et (3) les réponses oscillatoires se distinguent plus facilement du bruit ambiant (ex. interférence due à un pompage à proximité). Cependant, ces tests présentent également certains inconvénients, dont (1) la nécessité d'utiliser un équipement spécifique pour générer une stimulation périodique et (2) l'amplitude des signaux observés qui peut être nettement inférieure à celle des signaux générés par un pompage à débit constant.

Pour la THO, différents dispositifs de sollicitations oscillatoires ont été proposés. Premièrement, mécaniquement, cela peut être réalisé à l'aide d'une tige mobile contrôlée par un treuil (Guiltinan et Becker, 2015; Nefzi et al., 2025) ou un piston motorisé (Cardiff et al., 2020). Deuxièmement, un débit périodique peut être généré pneumatiquement en contrôlant la pression de l'air au-dessus du niveau de l'eau dans un puits pressurisé (Sayler et al., 2018). Troisièmement, un dispositif de pompage-injection stocke temporairement l'eau extraite dans un réservoir avant de la réinjecter dans l'aquifère et génère un signal oscillatoire. Ce signal se caractérise par des taux de pompage variant entre des extrêmes positifs (injection) et négatifs (pompage) (Rasmussen et al., 2003; Renner et Messar, 2006). Finalement, une sollicitation oscillatoire peut également être obtenue en utilisant uniquement le pompage. Dans ce cas, le niveau d'eau dans le puits source est d'abord abaissé par un pompage à débit constant, puis la sollicitation périodique est générée en faisant varier le débit de pompage autour du débit initial (Lavenue et de Marsily, 2001; Fischer et al., 2018, 2020).

1.2 Besoins de démonstration du potentiel de la THO

Bien que la THO semble présenter certains avantages par rapport aux méthodes hydrauliques conventionnelles, il existe peu d'exemples de terrain illustrant son application dans des cas réels,

et l'information contenue dans les signaux oscillatoires n'est pas encore pleinement démontrée. Cela limite évidemment la compréhension de son potentiel et a un impact sur son adoption dans la pratique.

1.2.1 Application de la THO sur le terrain

Une des premières applications de la THO en hydrogéologie provient de Lavenue et de Marsily (2001). Ces auteurs ont réalisé trois essais de pompage sinusoïdal dans un aquifère dolomitique. Ces essais ont débuté avec un débit constant pour établir un régime d'écoulement stationnaire avant de passer à un débit sinusoïdal avec une période unique de 72 min. Les variations de charge hydraulique ont été mesurées à 14 intervalles répartis dans 7 puits. L'inversion des données de charge a suivi une approche en deux étapes : une simulation catégorielle de la lithologie (roche fracturée ou non fracturée), suivie d'une méthode par points pilotes pour estimer K au sein de chaque catégorie lithologique. Le coefficient d'emmagasinement spécifique (S_s) et la conductivité hydraulique (K) de l'aquifère ont été ajustés par essais successifs. La moyenne d'ensemble de 100 modèles 3D calibrés a permis de localiser avec précision la frontière entre les zones fracturées et non fracturées et de reproduire fidèlement un test périodique indépendant utilisé pour validation.

Fischer et al. (2018) ont mené des essais de pompage harmonique dans 4 puits avec deux périodes distinctes (2 et 5 min) dans un réseau karstique, en enregistrant les réponses de charge hydraulique dans 13 puits d'observation. La méthode de stimulation suivait celle de Lavenue et de Marsily (2001), mais sans phase de stabilisation. À la place, les réponses de charge ont été traitées pour éliminer la composante transitoire. L'algorithme d'inversion impliquait deux étapes : une simulation de la structure du réseau karstique par automates cellulaires et un algorithme d'optimisation non linéaire déterministe combiné à un modèle d'écoulement souterrain dans le domaine fréquentiel. L'atténuation des amplitudes et les déphasages des réponses de charge ont été inversés pour estimer la transmissivité (T) et le coefficient d'emmagasinement (S) des matrices et des canaux dans un plan horizontal en 2D. Les résultats ont montré des structures distinctes du réseau karstique pour chaque période.

Fischer et al. (2020) ont cartographié l'hétérogénéité d'un aquifère alluvial à l'aide d'essais de pompage dans 2 puits avec deux périodes différentes (5 et 10 min), en enregistrant les charges hydrauliques dans 13 puits d'observation. La méthode de stimulation et le traitement des données de charge étaient similaires à ceux de Fischer et al. (2018). Les amplitudes et les phases ont été inversées en utilisant un algorithme d'optimisation non linéaire déterministe couplé à un modèle

d'écoulement souterrain formulé dans le domaine fréquentiel. Les cartes de transmissivité (*T*) et de coefficient d'emmagasinement (*S*) issues des inversions séparées et conjointes des deux périodes étaient légèrement différentes, mais cohérentes avec la géologie et l'historique de contamination du site.

Récemment, Cardiff et al. (2020) ont présenté une application sur le terrain de la tomographie hydraulique oscillatoire dans un aquifère fluviatile, avec une série de périodes comprises entre 5 et 70 sec. Ils ont réalisé 6 essais à des intervalles verticaux d'un mètre dans 2 puits et ont enregistré les charges hydrauliques dans 25 intervalles d'observation répartis dans trois puits voisins. Le signal oscillatoire a été généré à l'aide d'un système motorisé à double piston permettant de modifier le volume total d'eau échangé et la période du cycle. Une approche d'inversion géostatistique combinée à un modèle d'écoulement dans le domaine fréquentiel a été utilisée pour inverser le champ 3D de *K*, en supposant S_s constant. Les amplitudes et phases ont été inversées simultanément pour toutes les périodes. Cardiff et al. (2020) ont observé des corrélations positives modérées à fortes entre les profils de conductivité hydraulique (K) estimés par différentes méthodes à plusieurs puits, ainsi qu'une corrélation modérée entre les volumes tridimensionnels (3D) de K estimés, en comparant leurs résultats aux caractérisations antérieures réalisées sur le site du BHRS (Boise Hydrogeophysical Research Site).

La description de ces études met en évidence le peu d'applications pratiques de la THO, couvrant l'ensemble du processus, depuis les méthodes de terrain jusqu'aux techniques de traitement des données et les procédures d'inversion. Une comparaison de cette technique avec les méthodes plus courantes, ou d'autres types de sollicitations utilisées pour la TH, serait également nécessaire. Il est crucial de combler cette lacune afin de tirer pleinement parti des avantages potentiels de la THO et d'identifier des opportunités d'amélioration.

1.2.2 Contenu en information de la THO

Même si les études de terrain décrites précédemment fournissent des résultats intéressants, l'absence de connaissance des champs véritables des propriétés hydrauliques rend difficile l'établissement de règles pour maximiser les bénéfices des essais périodiques.

Par exemple, Ahn et Horne (2010) ont développé des solutions analytiques pour l'atténuation et le déphasage lors de tests de pulsation de pression dans un écoulement radial 1-D à travers trois couches concentriques de perméabilités différentes (comportant 10 blocs de perméabilité inconnues) entourant le puits d'essai. Ils ont montré que (1) l'atténuation et le déphasage

fournissaient une « caractéristique indicatrice » permettant de révéler l'hétérogénéité du réservoir et (2) les signaux de différentes fréquences peuvent révéler les perméabilités en reflétant divers rayons d'influence, augmentant ainsi la résolution des hétérogénéités avec l'utilisation de multiples périodes.

De la même manière, Cardiff et al. (2013b) ont confirmé ces analyses dans une étude sur un aquifère synthétique de type canal, en montrant que l'inclusion de données de charge hydraulique provenant de pompages à différentes fréquences peut améliorer les estimations des paramètres hydrauliques de l'aquifère, même si le pompage est réalisé dans un seul puits. En utilisant des expériences numériques, Cardiff et al. (2013b) ont mis en évidence des avantages supplémentaires offerts par les stimulations multi-fréquences, notamment une réduction significative du coût de calcul grâce à l'utilisation d'un modèle numérique périodique stationnaire, ainsi qu'une meilleure exploitation des informations sur l'hétérogénéité de l'aquifère fournies par les réponses à différentes fréquences. En réalisant d'abord une modélisation numérique transitoire complète pour des aquifères hétérogènes, ils ont pu démontrer que des résultats équivalents peuvent être obtenus en utilisant un modèle numérique périodique stationnaire plus rapide basé sur les oscillations périodiques. La sensibilité de la réponse du signal observé aux hétérogénéités de l'aquifère a été déterminée à l'aide d'une approche basée sur l'état adjoint, montrant que les stimulations à différentes fréquences fournissent des informations complémentaires. Enfin, Cardiff et al. (2013b) ont présenté une application en 2D dans laquelle des signaux sinusoïdaux de différentes fréquences sont utilisés comme source de données et inversés pour obtenir des estimations de l'hétérogénéité de l'aquifère. Ces analyses révèlent les différentes informations sur l'hétérogénéité que l'on peut obtenir en utilisant diverses fréquences de stimulation, et montrent que les données de plusieurs tests de pompage sinusoïdal peuvent être inversées rapidement grâce à ce cadre périodique stationnaire.

D'autres auteurs, tels que Wang et al. (2021), ont utilisé la THO couplée à des expériences de Monte Carlo pour estimer les champs de transmissivité (T) et de coefficient d'emmagasinement spécifique (S). Leur étude a mis en évidence que l'exploitation des réponses de charge hydraulique obtenues lors d'un pompage périodique, qu'il soit à fréquence unique ou multiple, produit des métriques de performance des estimations qui varient d'une réalisation à une autre. Cependant, les résultats de leurs simulations Monte Carlo ont confirmé que l'utilisation de multi-fréquences n'améliore pas nécessairement la résolution de la caractérisation de l'aquifère. Wang et al. (2021) ont également clarifié certaines idées préconçues sur les tests multi-fréquences, avancées dans des études précédentes, en soulignant deux points cruciaux. (1) La variation des

valeurs de sensibilité ne garantit pas automatiquement une amélioration des estimations. Bien que les excitations multi-fréquences puissent sembler apporter des informations supplémentaires sur l'aquifère, la localisation des hétérogénéités reste incertaine en l'absence de puits d'observation supplémentaires. (2) L'hypothèse d'ergodicité, sous-jacente aux problèmes inverses mal posés, est souvent ignorée. En d'autres termes, les résultats provenant d'une seule réalisation ou d'un seul test THO peuvent s'avérer trompeurs. Ces conclusions soulignent l'importance de recourir aux simulations de Monte Carlo pour évaluer la robustesse des résultats de telles modélisations inverses. De plus, ils ont noté que les signaux oscillants permettent de discriminer plus facilement les signaux de fond, tels que le bruit ou la dérive des capteurs, ainsi que d'autres influences hydrauliques, comme le pompage à proximité ou les variations du niveau des rivières. Cependant, ils reconnaissent également que des tests de pompage à débit constant peuvent pallier ces problèmes si l'échantillonnage temporel est suffisamment dense et le rapport signal/bruit assez élevé.

Récemment, Paradis et al. (2024) nuancent les travaux antérieurs en démontrant que le choix de la période et l'analyse du signal transitoire exercent une influence déterminante sur le pouvoir de résolution de la THO. Ils mettent en évidence que la capacité de résoudre des champs de propriétés hétérogènes dépend également des caractéristiques du milieu à caractériser. Ainsi, pour maximiser le potentiel de la THO, les essais doivent être optimisés en fonction des propriétés spécifiques de l'aquifère étudié. Leur étude révèle qu'une meilleure résolution est obtenue en intégrant la phase transitoire, où les premiers cycles du signal périodique contiennent la majorité des informations sur les propriétés hydrauliques grâce à l'intensité des effets transitoires.

En revanche, Paradis et al. (2024) soulignent que les cycles ultérieurs n'apportent pas d'informations supplémentaires significatives et sont même moins informatifs. De plus, ils soulignent que les périodes courtes offrent une résolution supérieure car elles comportent une composante transitoire plus importante. La combinaison de plusieurs périodes peut également améliorer la résolution spatiale, mais cette amélioration reste marginale. Paradis et al. (2024) expliquent également les limites observées dans certaines études, comme celle de Wang et al. (2021) qui ont utilisé des périodes excessivement longues (400 à 10 800 min) par rapport à la transmissivité simulée de l'aquifère. Ils montrent que ces longues périodes transmettent peu d'informations et n'améliorent pas notablement la résolution des champs d'hétérogénéité. Cette analyse souligne l'importance de concevoir des essais THO adaptés aux propriétés du milieu étudié, en sélectionnant des périodes optimales et en intégrant pleinement les phases transitoires pour maximiser la précision et la robustesse des résultats.

La revue de ces études illustre la complexité et l'ambiguïté actuelles concernant le potentiel informatif de la THO, soulignant la nécessité de recherches supplémentaires pour optimiser son utilisation.

1.3 Objectifs de la thèse

L'objectif général de cette thèse est d'évaluer comment la THO peut contribuer à définir l'hétérogénéité et l'anisotropie d'un aquifère granulaire. Plus spécifiquement, elle vise à déterminer si des sollicitations hydrauliques de différentes périodes permettent une résolution distincte de l'hétérogénéité des propriétés hydrauliques. Les résultats obtenus avec la THO seront également comparés à ceux issus des sollicitations conventionnelles (choc hydraulique), tant du point de vue de la définition de l'hétérogénéité que de l'efficacité de mise-en-œuvre (gain en information par rapport au temps investi pour réaliser les essais).

Pour répondre à cet objectif général, trois objectifs spécifiques sont visés:

1) **Faire l'application de la THO**. Faire l'acquisition et l'interprétation des mesures de THO au site expérimental de Saint-Lambert afin de démontrer la possibilité de réaliser les mesures dans un contexte hydrogéologique difficile (grande anisotropie et K limitée) et pour illustrer une démarche rigoureuse d'analyse;
2) **Mieux comprendre l'hydraulique de la THO**. À cette fin, une analyse de résolution sera réalisée de façon similaire à Paradis et al. (2015b, 2016, 2024) pour évaluer le contenu en information des mesures tomographiques réalisées sur le terrain avec différentes périodes de sollicitations ainsi que leur analyse combinée. Cette analyse permettra également d'évaluer les possibilités d'amélioration des procédures expérimentales sur le terrain;
3) **Comparer la THO à d'autres méthodes hydrauliques**. La THO sera comparée à d'autres méthodes tomographiques réalisées au site de Saint-Lambert, soit la TH par choc hydraulique. Cette comparaison sera faite à plusieurs niveaux : contenu en information (analyse de résolution spatiale et des paramètres) et logistique de réalisation des essais sur le terrain. Les résultats obtenus au site de Saint-Lambert avec ces différentes méthodes permettront aussi d'illustrer ce qui peut être tiré de ces méthodes et leurs avantages relatifs.

Ce projet est mené dans le cadre du Laboratoire International Associé (LIA) France-Québec RESO (« REsources-SOciété » : Exploitation des ressources profondes et protection des ressources de surface : rapports entre sciences et décisions).

1.4 Méthodologie générale

Cette section présente de manière générale la région d'étude dans laquelle la THO a été appliquée, ainsi que la procédure adoptée pour la réalisation de l'essai de terrain et les méthodes utilisées pour le traitement et l'analyse des données.

1.4.1 Zone d'étude

L'application de la THO dans cette thèse a été réalisée sur le site expérimental de St-Lambert-de-Lauzon, situé à environ 35 km au sud-ouest de la ville de Québec (Figure 1-1A). L'accès principal du site se trouve au 517, rue St-Aimé à Saint-Lambert-de-Lauzon. Le site d'étude est situé dans une région de 12 km^2 d'un sous-bassin versant qui englobe un ancien site d'enfouissement sanitaire où la migration et l'atténuation d'un panache de lixiviation ont fait l'objet d'études. La topographie de la zone est relativement plane entre 109 et 124 m au-dessus du niveau de la mer, et des petits ruisseaux constituent des exutoires pour les eaux souterraines.

La zone d'étude est limitée à l'est par une ligne de partage des eaux souterraines entre le sous-bassin versant de la rivière Beaurivage et le bassin versant de la rivière Chaudière déterminée à l'aide de la carte piézométrique de la région d'étude (Figure 1-1B). Au sud et au nord, le site d'étude est bordé par des petits ruisseaux et la frontière ouest est délimitée par la rivière Cugnet qui reçoit de l'eau de tous les ruisseaux de la zone étudiée.

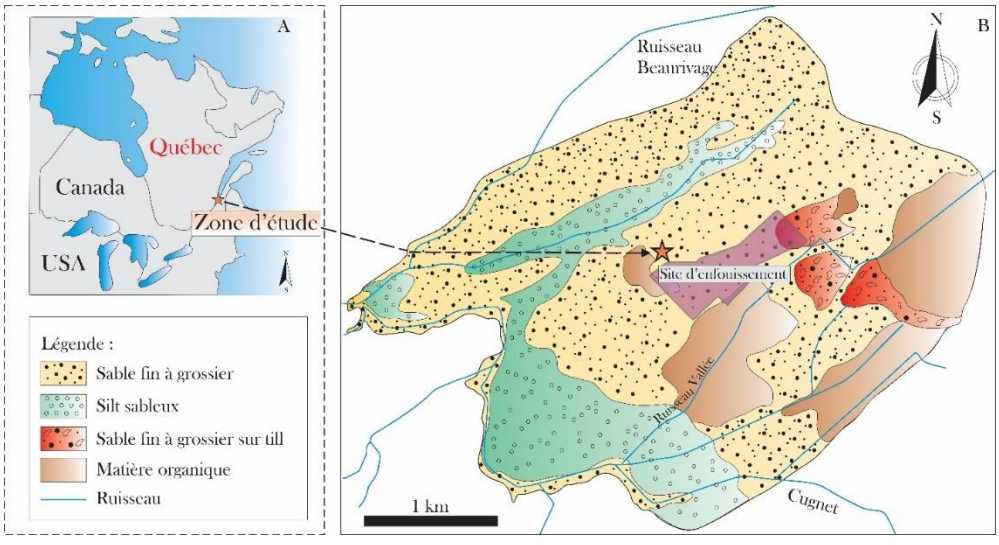

Figure 1-1 : (A) Localisation générale du site expérimental de St-Lambert près de Québec (Canada). (B) Délimitation du sous-bassin versant de la rivière Cugnet entourant le site d'enfouissement avec la carte des dépôts superficielles (l'étoile localise le site des essais tomographiques).

La zone d'étude comprend deux types d'aquifères : un aquifère régional dans les roches fracturées à une profondeur d'environ 20 m et un aquifère dans des dépôts granulaires à la surface. Ces deux aquifères sont séparés par des dépôts glaciaires peu perméables (aquitard) (Tremblay et al., 2014). L'étude présentée dans cette thèse se concentre spécifiquement sur l'aquifère dans les dépôts granulaires. Les sédiments liés à la dernière glaciation dominent dans la région de Saint-Lambert. L'aquifère granulaire est à nappe semi-captive en raison de la présence de sédiments moins perméables à la surface, et la surface de la nappe est très proche de la surface du sol, généralement d'une profondeur inférieure à 1 m au site d'enfouissement. Cette interprétation est appuyée par les réponses observées lors des essais de pompage, qui indiquent un comportement typique d'un aquifère semi-confiné (Gauthier et Guillemette Consultants Inc., 1993).

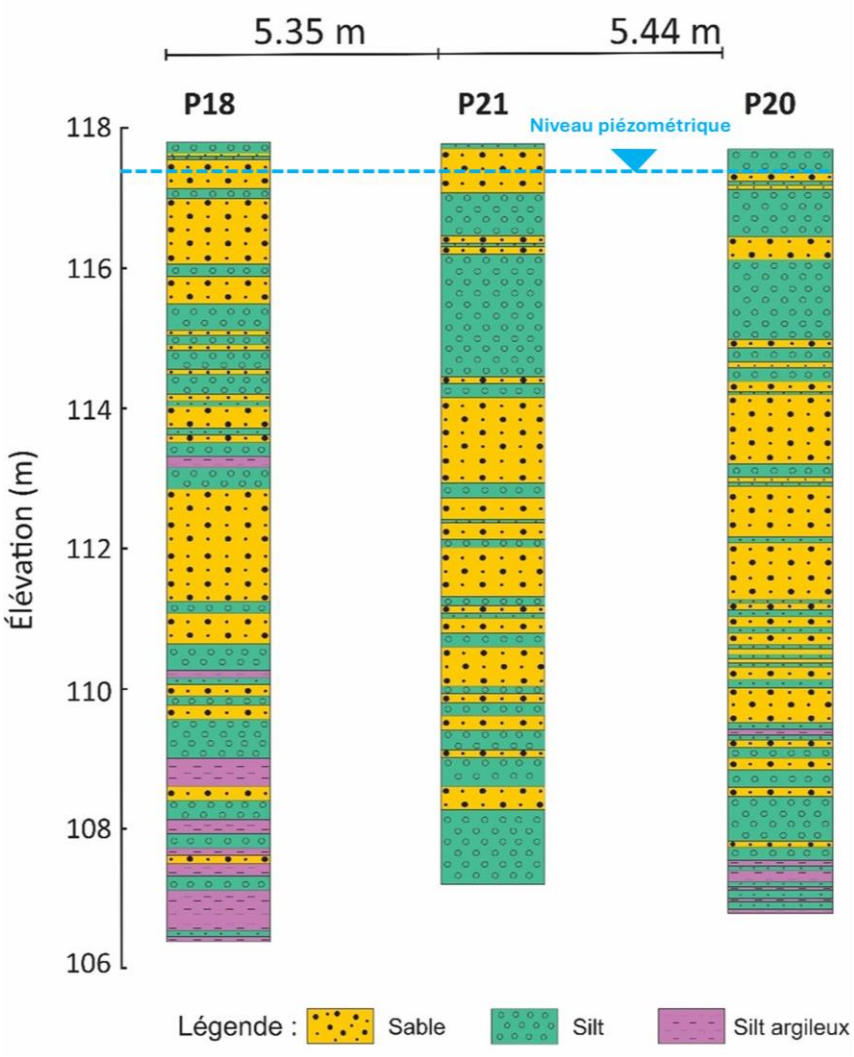

Figure 1-2 : Profils lithologiques pour illustrer la nature hétérogène du site expérimental de St-Lambert.

La géologie de surface est composée de sables et de silts d'âge Quaternaire récent qui ont été déposés durant le retrait de la mer de Champlain (Bolduc, 2003). La granulométrie des sédiments de l'aquifère varie du sable fin jusqu'au silt très fin (silt argileux), la répartition granulométrique allant de mal à très mal trié (Figure 1-2). La classification des sables et des silts sur le site de St-Lambert conduit à des valeurs de conductivité hydraulique relativement inférieures à celles de sédiments bien mieux classés, par exemple, comme dans les environnements deltaïques (Paradis et al., 2014). Ces dépôts reposent sur un socle rocheux particulièrement accidenté, composé essentiellement de roches de l'Ordovicien inférieur et moyen (schistes à blocs, grès, calcaires et conglomérats) (Hocq et Dubé, 1994; Landry et Mercier, 1983).

1.4.2 Site expérimental pour la tomographie

Le site expérimental pour la tomographie a une superficie d'environ 400 m^2 et est localisé à l'intérieur de la propriété du site d'enfouissement (Figure 1-3). Ce site est utilisé pour le développement d'approches de caractérisation hydrogéologique et la recherche sur le transport des contaminants. Ce site a fait l'objet d'une caractérisation de l'hétérogénéité et de l'anisotropie des aquifères granulaires par essais hydrauliques et géophysique (Paradis et al., 2011; Paradis et Lefebvre, 2013; Paradis et al., 2015a; Paradis et al., 2016; Gernez et al., 2019).

Un total de 5 puits disposés en forme de losange (un dans chaque coin et un au centre) avec un grand axe de 15,92 m et un petit axe de 10,79 m sont installés sur le site d'essai (Figure 1-3) (Paradis et al., 2016). Les puits crépinés sur toute l'épaisseur saturée de l'aquifère ont été installés à l'aide d'une foreuse géotechnique (Geotech 605D) selon la méthode dite de « crépine protégée » (ASTM 2004; Paradis et al., 2016). Ces puits ont été installés en contact direct avec les sédiments naturels (sans sable filtrant) pour minimiser les effets des courts-circuits hydrauliques lors des essais haute-résolution (Paradis et Lefebvre, 2013).

Les puits ont un diamètre de 5,1 cm avec une longueur de crépine allant de 7,62 à 9,24 m. Avant les essais, les puits ont été développés pour assurer un bon contact hydraulique entre les crépines et les sédiments (Paradis et al., 2011). Ces puits crépinés sur la totalité de l'aquifère permettent une grande flexibilité dans la configuration des intervalles pour la tomographie avec des obturateurs.

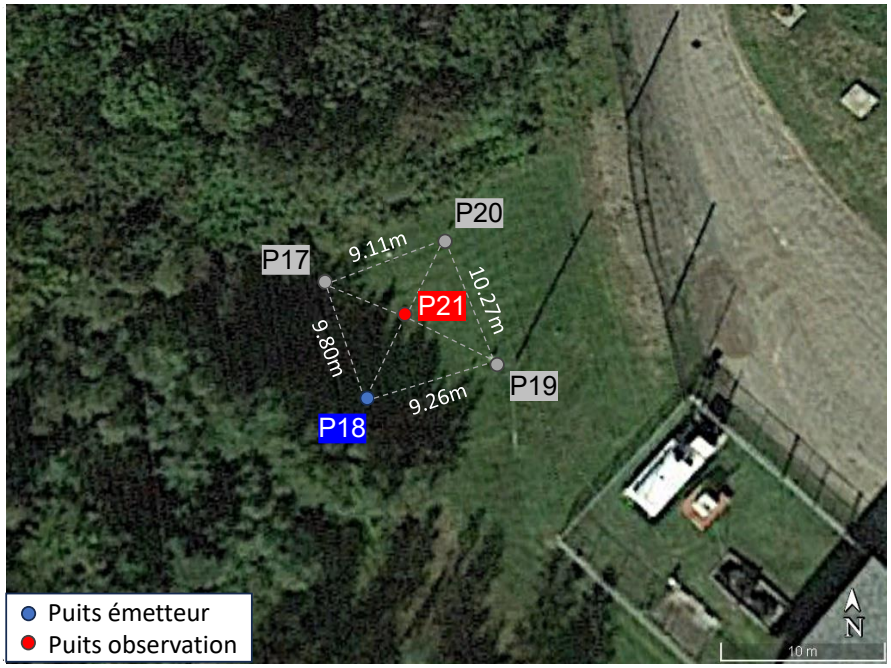

Figure 1-3 : Localisation des puits sur le site expérimental de St-Lambert.

1.4.3 Système de perturbation oscillatoire et acquisition des mesures

L'instrumentation utilisée pour effectuer les sollicitations périodiques provient de l'Université de Rennes. Il s'agit d'un treuil mécanique à commande numérique actionnant une tige en aluminium de 2,81 m de longueur et de 1,07 cm de rayon pour faire varier le niveau d'eau dans le puits (Figure 1-4). Le diamètre de la tige a été sélectionné pour optimiser le volume d'eau déplacé lors des essais, tout en permettant à l'eau de circuler librement entre la tige et l'intérieur du tubage retenant les obturateurs (Figure 1-5B) (Nefzi et al., 2025). Avant le début d'un essai, la tige était partiellement immergée et un programme informatique était utilisé pour contrôler précisément l'amplitude et la période de son mouvement vertical dans le puits (Figure 1-4). Il s'agit du même type de dispositif expérimental utilisé par Guiltinan et Becker (2015).

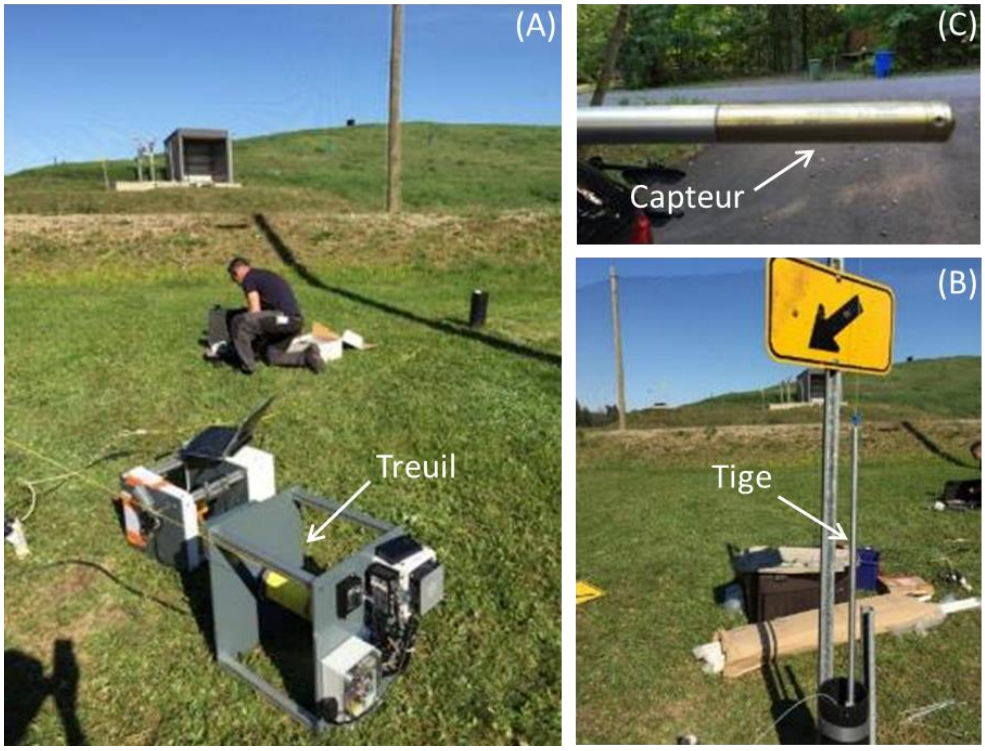

Figure 1-4 : Photographies des composantes du système de perturbation oscillatoire utilisé pour les essais de tomographie hydraulique. (A) Treuil mécanique utilisé pour contrôler l'amplitude et la période de la (B) tige d'aluminium servant à induire les sollicitations périodiques. (C) Capteur de pression installé à l'extrémité de la tige pour enregistrer les variations de niveaux d'eau dans le puits source.

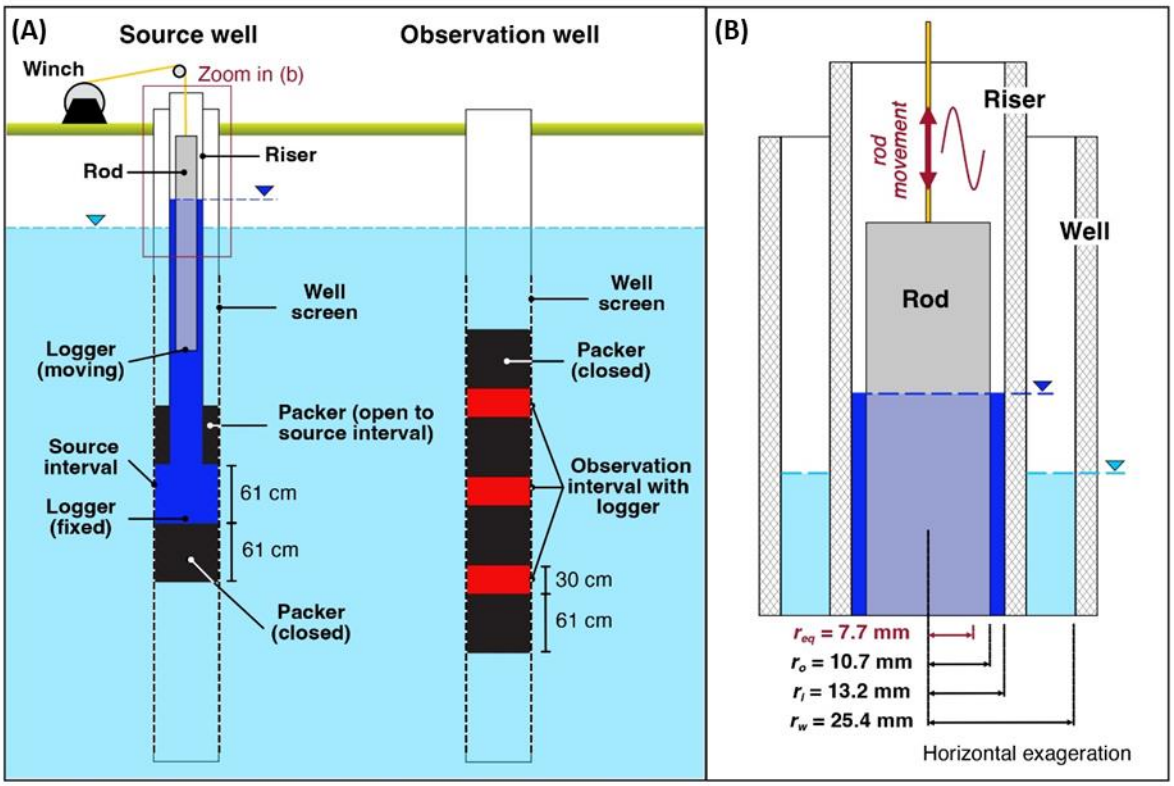

Figure 1-5 : (A) Vue schématique du système de test dans les puits source et d'observation utilisés pour l'expérience tomographique. (B) Coupe transversale détaillée montrant les dimensions radiales des matériaux dans le puits source.

Dans le cadre de cette thèse, l'expérience de tomographie a été réalisée entre les puits O21 et S18 (Figure 1-6). Le puits S18 a été utilisé comme puits source alors que O21 comme puits d'observation. L'expérimentation sur le terrain a donc inclus une série d'essais utilisant trois périodes différentes (150, 300 et 600 secondes) utilisées dans 8 intervalles dans le puits source avec la mesure des charges induites dans le puits source et à trois intervalles dans le puits d'observation. Afin d'optimiser la durée de collecte des données, le système d'obturateur n'a été repositionné dans le puits source qu'avant chaque test, tandis que celui dans le puits d'observation était ajusté après tous les trois tests.

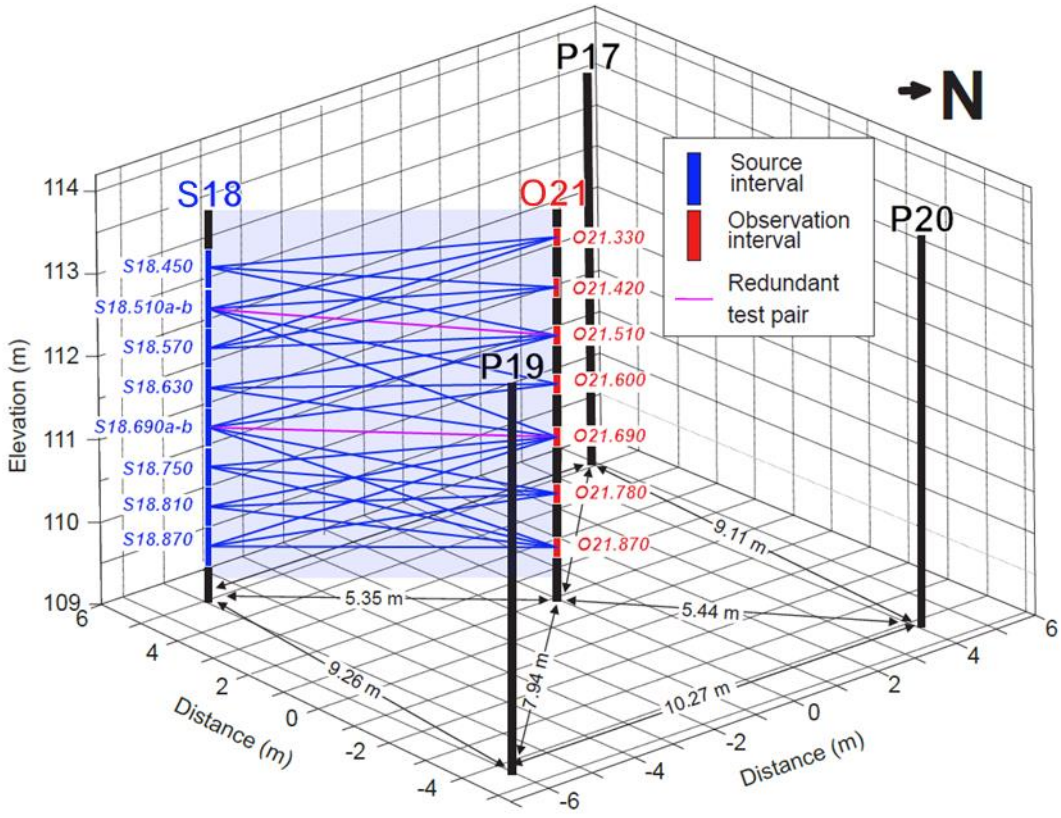

Figure 1-6 : Configuration des intervalles de source et d'observation (lignes bleues) utilisés pour les expériences de tomographie entre le puits source S18 et le puits d'observation O21. Les suffixes après les noms des puits indiquent la profondeur du sommet des crépines en millimètres par rapport à la tête de puits. Les désignations S18.510a-b et S18.690a-b indiquent que ces intervalles ont été testés deux fois avec des configurations différentes des intervalles d'observation dans O21.

1.4.4 Traitement des charges hydrauliques

Un processus de traitement des données a été fait pour rectifier les valeurs de charge qui ont subi certaines déviations au cours de l'expérimentation. Ces tendances sont attribuées à une stabilisation incomplète de certains intervalles par rapport à la charge ambiante après le gonflement des obturateurs dans les matériaux moins perméables. Une correction linéaire a généralement éliminé toutes les déviations des données originales (Figure 1-7). Ces déviations ont été observées dans la plupart des essais dont les variations de charges étaient très faibles (74 intervalles corrigés sur un total de 75). Aucune déviation significative n'a été observée pour les intervalles source.

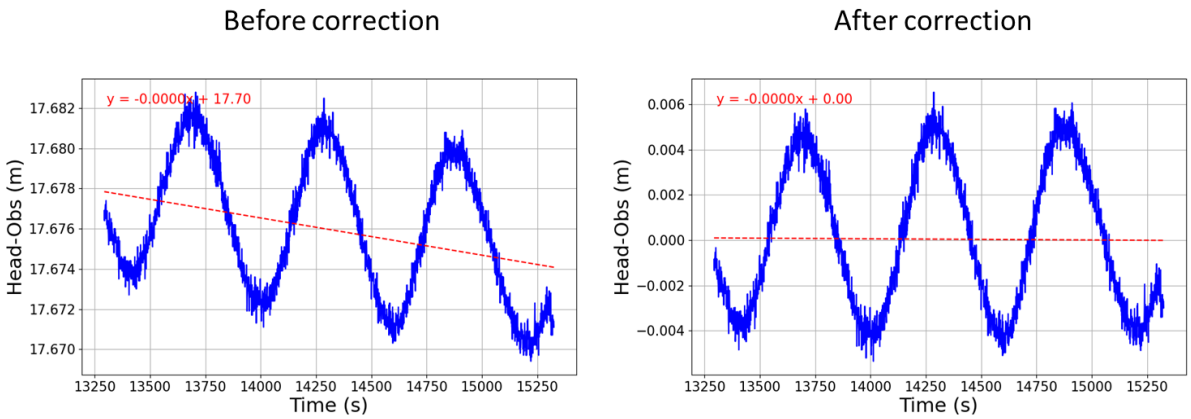

Figure 1-7 : Graphiques des réponses mesurées dans le puits observation (Test rx.870) pour la période 600 secondes montrant le traitement du signal réalisé sur toutes les mesures effectuées.

Une évaluation du niveau de bruit induit par le dispositif expérimental a également été réalisée. Ce niveau de bruit est pris en compte lors de l'analyse de la résolution des essais de tomographie, afin d'obtenir une évaluation réaliste des résolutions, cohérente avec les mesures de terrain. Cette évaluation du bruit a été réalisée en ajustant une fonction sinusoïdale aux charges mesurées (Figure 1-8), et en calculant la résiduelle entre la courbe sinusoïdale et les mesures. L'ajustement a été appliqué à un cycle complet durant la phase où le régime permanent périodique est atteint, après la disparition de la phase transitoire.

La Figure 1-9 montre que le niveau de bruit est plus prononcé dans les intervalles source que dans les intervalles d'observation. De plus, le niveau de bruit dans les intervalles sources est plus élevé pour les périodes courtes. Ceci est attribuable à la plus grande turbulence induite par le mouvement rapide de la tige pour les courtes périodes. Le bruit généré est fonction de l'amplitude du signal, ce qui influence directement le niveau de bruit observé. L'amplitude des signaux sources (la tige) est généralement fixée à 1,25 m pour toutes les périodes, sauf dans certains essais. Concernant les intervalles d'observation, le niveau de bruit reste constant pour toutes les périodes, ce qui suggère que ce dernier est principalement déterminé par la précision des instruments de mesure de la charge hydraulique. Le niveau de bruit pour les intervalles sources varie de $1{,}4 \times 10^{-2}$ à $8{,}6 \times 10^{-3}$ m. Pour les intervalles d'observation, le niveau de bruit varie de $4{,}9 \times 10^{-4}$ à $5{,}3 \times 10^{-4}$ m.

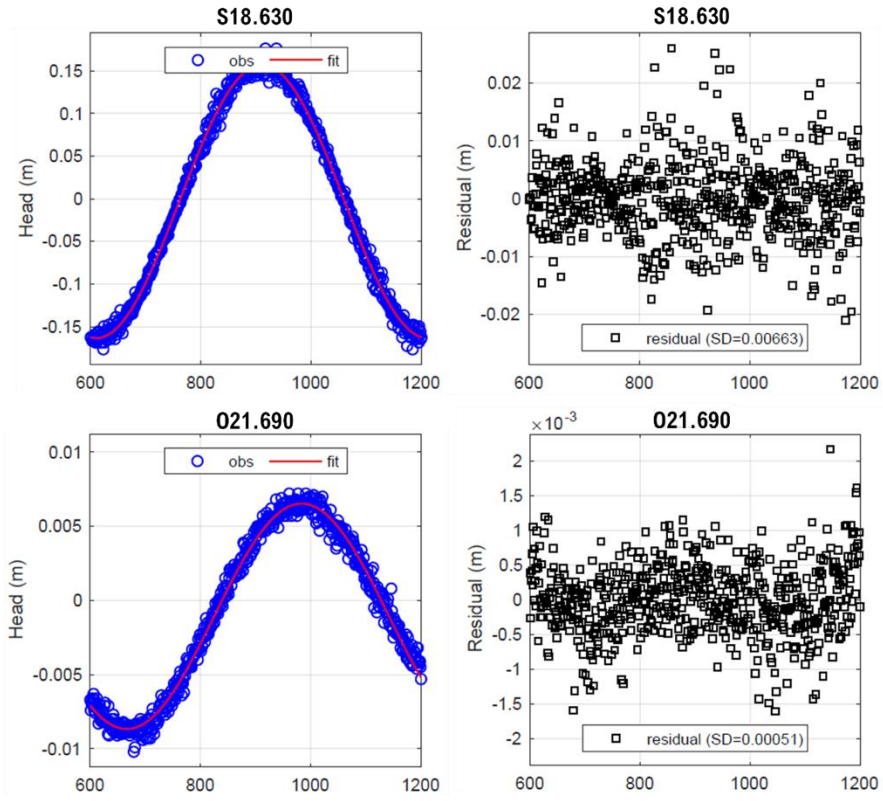

Figure 1-8 : Exemple d'estimation du niveau de bruit à l'aide de données de terrain pour le test S18-630 avec une période de 600 secondes à l'intervalle source (S18.630) et un des intervalles d'observation (O21.690).

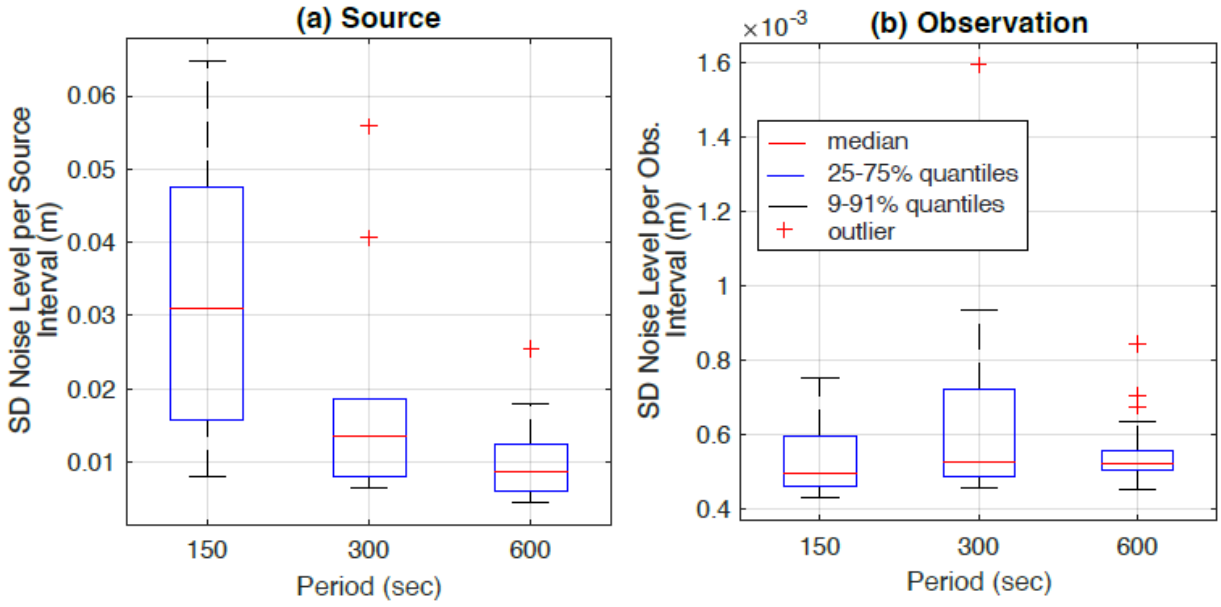

Figure 1-9 : Distribution du niveau de bruit standard (écart-type) par intervalle source et d'observation pour différentes périodes (150, 300, 600 sec).

1.4.5 Inversion des données de terrain de THO

Dans le cadre de nos travaux, l'inversion des données de THO de terrain a été réalisée à l'aide du simulateur numérique Ir2dinv, un programme conçu pour l'analyse inverse d'essais hydrauliques (Bohling et Butler, 2001). Ce simulateur est un modèle en différences finies axisymétrique bidimensionnel (2D) avec un maillage à croissance exponentielle qui permet de représenter les plus forts gradients hydrauliques à proximité du puits source. Le simulateur permet également la simulation explicite de l'emmagasinement de puits et l'utilisation d'obturateurs dans le puits source. Ce programme permet à l'utilisateur de spécifier des zones arbitraires et indépendantes pour les trois propriétés hydrauliques simulées, soit K_h, K_v/K_h et S_s.

La charge hydraulique h (m), générée dans un aquifère lors d'un essai hydraulique dans un puits, est décrite par l'équation suivante :

$$\frac{1}{r}\frac{\partial}{\partial r}\left(rK_r\frac{\partial h}{\partial r}\right)+\frac{\partial}{\partial z}\left(K_z\frac{\partial h}{\partial z}\right)=S_s\frac{\partial h}{\partial t} \tag{1.1}$$

Où r (m) est la coordonnée radiale à partir du centre du puits, z (m) est la coordonnée verticale, t (s) est le temps, S_s (m^{-1}) est le coefficient d'emmagasinement spécifique, et K_r (ou K_h) et K_z (m/s) sont les conductivités hydrauliques dans les directions radiale (ou horizontale) et verticale. L'équation (1.1) est résolue à l'aide d'une formulation en différences finies centrées sur des blocs, après avoir appliqué une transformation logarithmique de l'équation d'écoulement radial pour l'exprimer sous une forme équivalente en coordonnées cartésiennes (Butler et McElwee, 1990; Bohling et Butler, 2001).

Le flux périodique Q (m^3s^{-1}) est imposé dans l'intervalle crépiné pour induire un échange d'eau avec l'aquifère au niveau de la crépine du puits, qui possède un rayon r_w (m) :

$$Q=\pi r_c^2\frac{\partial(A_0\sin(2\pi/T_0t))}{\partial t}\ =2\pi r_wLK_h\frac{\partial h}{\partial r} \tag{1.2}$$

Où r_c (m) représente le rayon de tubage, L (m) la longueur de l'intervalle source, et $A_0 sin(2\pi/T_0\ t)$ (m) est le signal hydraulique sinusoïdal, avec A_0 (m) et T_0 (s) correspondant respectivement à l'amplitude maximale et à la période du signal périodique. Sur le terrain, un flux périodique peut être généré de plusieurs façons : (1) mécaniquement, à l'aide d'une tige mobile contrôlée par un treuil (Becker et Guiltinan, 2010; Guiltinan et Becker, 2015; Nefzi et al., 2025) ou d'un piston motorisé (Cardiff et al., 2020); (2) pneumatiquement, en contrôlant la pression d'air au-dessus du niveau d'eau dans un puits pressurisé (Sayler et al., 2018); et (3) hydrauliquement, en utilisant un système à double pompe permettant de contrôler les débits d'injection et de

pompage (Rasmussen et al., 2003; Renner et Messar, 2006). Pour les simulations, le flux périodique est approximé par une série de paliers, chaque palier étant modélisé comme une condition limite de débit constant avec un temps de début et de fin spécifiques. La durée des paliers est choisie de manière arbitraire, en fonction d'un compromis entre la meilleure représentation possible du signal sinusoïdal et les contraintes liées aux données et au temps de simulation. La simulation en régime fréquentiel n'a pas été retenue car notre intérêt porte principalement sur la phase transitoire, là où se trouve le maximum d'information pour la résolution spatiale des propriétés hydrauliques (Paradis et al., 2024).

Les modèles hétérogènes des propriétés hydrauliques dans le domaine simulé ont été estimés par inversion à l'aide de l'algorithme de Levenberg-Marquardt (Marquardt, 1963; Press et al., 1992) en considérant K_h, K_v/K_h, et S_s comme variables. L'inversion numérique des expériences de tomographie a été réalisée en minimisant la différence entre les charges mesurées h_i et les charges prédites par le modèle $f_i(\boldsymbol{p})$ basé sur le vecteur estimé des propriétés hydrauliques $\boldsymbol{p}$. Cette fonction objective quadratique pondérée est formalisée comme suit :

$$\chi^2 = \sum_{i=1}^{n} \left(\frac{h_i - f_i(\mathrm{p})}{\sigma_i} \right)^2 \tag{1.3}$$

Où σ_i est un facteur d'échelle associé à chaque mesure. Ces facteurs d'échelle ont été utilisés pour pondérer la fonction objective en fonction de l'amplitude relative des charges dans les intervalles source et d'observation. La pondération des données selon leur amplitude relative est nécessaire pour équilibrer leur influence dans la fonction objective. En effet, les charges mesurées dans les intervalles sources sont généralement très élevées, tandis que celles dans les intervalles d'observation sont beaucoup plus faibles. Si l'on utilise les valeurs originales sans pondération, l'inversion privilégiera les données de forte amplitude, c'est-à-dire celles des sources. Pour éviter ce biais, les charges des intervalles d'observation sont pondérées afin qu'elles aient un poids équivalent dans le processus d'inversion. La minimisation de la fonction objective a été réalisée à l'aide d'une méthode implicite itérative par lignes directionnelles orientées par rangées. Les lignes directionnelles orientées par rangées font référence à une méthode de résolution numérique, souvent utilisée dans les algorithmes d'inversion ou d'optimisation, où les mises à jour des paramètres sont effectuées rangée par rangée. Le simulateur *lr2dinv* a permis une analyse simultanée des données issues de plusieurs essais.

1.4.6 Analyse de résolution

À la suite d'un essai hydraulique induisant des variations de charge hydraulique dans un aquifère, la capacité à résoudre les différents paramètres hydrauliques de l'aquifère dépend de l'amplitude relative et de la corrélation entre les sensibilités des charges par rapport à ces paramètres hydrauliques (Bohling, 2009; Paradis et al., 2015b; Vasco et al., 1997). La sensibilité exprime la réponse de la charge hydraulique à une variation de la valeur d'un paramètre hydraulique. Pour qu'un paramètre soit résolu, sa sensibilité doit avoir une valeur non négligeable. Plus la différence entre l'amplitude de la sensibilité d'un paramètre et celle des paramètres voisins est grande, meilleure sera sa résolution. De plus, un paramètre est mieux résolu si son motif de sensibilité diffère de celui des autres paramètres au fil du temps, à mesure que les charges varient en réponse à une sollicitation hydraulique imposée.

Bien que le problème inverse de l'écoulement souterrain soit non linéaire, l'analyse de résolution présentée dans cette thèse repose sur une approximation linéaire du comportement du modèle dans le voisinage des paramètres hydrauliques supposés. Ainsi, la matrice de sensibilité est utilisée comme une représentation linéaire approximative de l'écoulement non linéaire. On considère également qu'une analyse de résolution basée sur un modèle radial 2D constitue une approximation valide qui peut être généralisée à des modèles 2D planaires ou 3D. Paradis et al. (2024) ont démontré que la résolution pour des puits dans un aquifère confiné 2D planaire est principalement centrée dans le plan contenant les puits, avec des motifs similaires à ceux obtenus avec un modèle radial. Dans le cas d'un milieu homogène isotrope, le modèle radial peut fournir une représentation adéquate des écoulements. Cependant, l'utilisation de ce modèle radial doit être soigneusement évaluée lorsqu'il s'agit d'un aquifère présentant des hétérogénéités significatives susceptibles de provoquer des écoulements latéraux importants en dehors du plan des puits. L'analyse de résolution présentée dans cette thèse a été réalisée à l'aide de la Regularization Toolbox de MATLAB (MathWorks, 2023) développée par Hansen (2023).

1.4.6.1 Problème inverse

L'analyse de résolution repose sur l'étude du problème inverse associé à une expérience tomographique spécifique. Un problème inverse hydraulique consiste à déterminer un modèle décrivant la distribution spatiale des paramètres hydrauliques d'un aquifère, pour lequel des données de charge hydraulique ont été mesurées dans des puits à différents moments et emplacements après une sollicitation hydraulique imposée (Aster et al., 2005):

$$\mathrm{m} = F^{-1}\mathrm{d} \tag{1.4}$$

Où *m* est un vecteur contenant *n* paramètres hydrauliques à estimer à partir du vecteur de données de charge *d* comprenant *m* observations. F^{-1} représente le processus inverse de l'opérateur direct *F*, qui décrit le comportement non linéaire de l'écoulement souterrain

Cependant, la résolution d'un problème inverse est complexe et soulève plusieurs enjeux majeurs : (1) l'existence de la solution: il peut arriver qu'aucun modèle ne corresponde aux observations; (2) l'unicité de la solution: en cas de déficience de rang, plusieurs modèles peuvent s'ajuster également bien aux observations; et (3) l'instabilité du processus de résolution : en cas de mauvais conditionnement, de petites variations dans les observations peuvent entraîner des différences significatives dans les modèles obtenus. Ces problématiques sont caractéristiques des problèmes inverses hydrauliques (Aster et al., 2005) et nécessitent des approches spécifiques pour garantir des solutions stables et fiables.

1.4.6.2 L'inverse généralisée

Pour faciliter la recherche d'une solution inverse *m*, l'inverse généralisé $J^{\dagger}$ de la matrice de sensibilité *J* est utilisé en tant qu'opérateur inverse F^{-1} (Moore, 1920; Penrose, 1955):

$$\mathrm{m}_{\dagger} = \mathrm{J}^{\dagger}\mathrm{d} \tag{1.5}$$

La matrice de sensibilité J est définie comme une matrice $m \times n$, où m représente le nombre d'observations (par exemple, les niveaux d'eau mesurés aux différents points d'observation) et n le nombre de paramètres hydrauliques, tels que la conductivité hydraulique. Chaque élément $J_{m,n}$ de la matrice exprime la sensibilité de l'observation d_m par rapport au paramètre m_n. Mathématiquement, cela s'exprime par :

$$J_{m,n} = \frac{\partial d_m}{\partial m_n / m_n} \tag{1.6}$$

Cette formulation normalisée permet de comparer l'influence relative de différents paramètres, indépendamment de leurs échelles respectives (Bohling et Butler, 2001).

Pour évaluer les éléments de la matrice de sensibilité, l'approche de perturbation séquentielle est utilisée. Cette méthode consiste à perturber légèrement (1%) un paramètre du modèle m_n tout en gardant les autres constants, et à observer les variations induites dans les résultats du modèle. La sensibilité est fonction des variations induites à la suite des perturbations. Plus les variations de charges sont grandes pour un paramètre donné, plus le modèle est sensible à ce paramètre.

Une fois la matrice de sensibilité établie, la décomposition en valeurs singulières (SVD) est utilisée pour calculer l'inverse généralisée de la matrice J. Cette technique est particulièrement utile dans les cas où le problème inverse est mal conditionné ou lorsque la matrice de sensibilité est de rang déficient.

$$\mathrm{J}^{\dagger} = \mathrm{VS}^{-1}\mathrm{U}^{T}\mathrm{d} \tag{1.7}$$

La SVD décompose J en trois matrices : U, S, et V, où U et V sont des matrices orthogonales, et S est une matrice diagonale contenant les valeurs singulières $\mathrm{s_i}$ de J. L'inverse généralisée $J^{\dagger}$ est ensuite obtenue et utilisée pour résoudre le problème inverse, permettant d'estimer les paramètres du modèle à partir des données d'observation avec une précision accrue.

1.4.6.3 Régularisation de Tikhonov

La présence de très petites valeurs singulières dans *S* de l'équation (1.7) peut rendre la solution de l'inverse généralisé extrêmement instable (Aster et al., 2005). Par conséquent, une régularisation de la solution est nécessaire. L'une des méthodes de régularisation les plus couramment utilisées est la technique de Tikhonov (Tikhonov et Goncharsky, 1987):

$$\mathrm{m}_{\lambda} = \mathrm{VFS}^{\dagger}\mathrm{U}^{T}\mathrm{d} \tag{1.8}$$

Où **F** est une matrice diagonale de taille *n*-by-*n*, dont les éléments diagonaux sont déterminés par les facteurs de filtrage :

$$f_i = \frac{s_i^2}{s_i^2 + \lambda^2} \tag{1.9}$$

Cette matrice est introduite pour réduire l'influence des petites valeurs singulières s_i. La pondération des valeurs singulières est contrôlée par le paramètre λ. Si λ est beaucoup plus grand que s_i, f_i tend vers zéro, ce qui entraîne une pondération plus faible. À l'inverse, si λ est beaucoup plus petit, f_i augmente, entraînant une pondération plus forte. La matrice $S^{\dagger}$ représente l'inverse généralisé de *S*, soit $S^{\dagger} = \mathrm{V}\Sigma^{\dagger}\mathrm{U}^{T}$, où $\Sigma^{\dagger}$ est une matrice diagonale dont chaque élément diagonal non nul est l'inverse de la valeur singulière correspondante non nulle de la matrice *S*. Les zéros sur la diagonale de $S^{\dagger}$ correspondent aux valeurs singulières nulles de *S*.

1.4.6.4 Évaluation de la matrice de résolution

Le concept de résolution permet d'évaluer les propriétés de la solution d'inverse généralisée pour une expérience hydraulique spécifique. Une matrice de résolution reflète la physique et la géométrie de l'expérience. Dans le cadre de la méthode de régularisation de Tikhonov, la matrice de résolution des paramètres hydrauliques est définie par :

$$\mathrm{R_{m,\lambda}} = \mathrm{VFV^T} \tag{1.10}$$

Où les éléments de $R_{m,\lambda}$ indiquent l'amplitude relative et la corrélation entre les sensibilités des charges hydrauliques vis-à-vis des paramètres hydrauliques. Ainsi, si $\mathrm{R}_{m,\lambda} = I$, ou I est la matrice identité, la résolution est parfaite et les véritables paramètres hydrauliques sont déterminés avec exactitude. À l'inverse, une valeur de résolution tendant vers zéro signifie qu'un paramètre ne peut pas être résolu sur la base des charges hydrauliques mesurées.

1.4.6.5 Sélection d'une solution optimale

Il convient de noter que la matrice de résolution du modèle dépend de la valeur de λ. Pour assurer la cohérence lors de la comparaison des différentes simulations, nous sélectionnons la valeur de λ en suivant le critère de la courbe en L (Hansen, 1992). Une courbe en L est construite à partir de la minimisation de l'équation des moindres carrés régularisés pour une plage de valeurs de λ. Ce processus est réalisé pour un ensemble de paramètres (m) définis selon un choix empirique, basé sur l'expérience du modélisateur et des essais-erreurs.:

$$min\ \|\mathrm{Jm_\lambda} - \mathrm{d}\|_2^2 + \lambda^2 \|\mathrm{m_\lambda}\|_2^2 \tag{1.11}$$

où le terme de gauche représente la norme au carré du résidu des données de charge hydraulique, tandis que le terme de droite correspond à la norme au carré du vecteur des paramètres du modèle. Représentée sur une échelle logarithmique, la courbe des valeurs optimales des normes du résidu et des paramètres du modèle prend souvent la forme d'un « L » (Figure 1-10). Le segment horizontal de la courbe est dominé par l'erreur de régularisation, où des valeurs très élevées de λ entraînent un lissage excessif des solutions avec une norme de résidu importante. À l'inverse, le segment vertical est caractérisé par des valeurs très faibles de λ, ce qui conduit à un surajustement des données de charge hydraulique. Ainsi, la solution optimale, équilibrant la sensibilité au bruit et la résolution des paramètres, correspond à la valeur de λ située au point d'inflexion de la courbe en L. L'algorithme de sélection adaptative proposé

par Hansen et al. (2007) a été utilisé pour localiser le point d'inflexion de la courbe en L pour chaque ensemble de simulations.

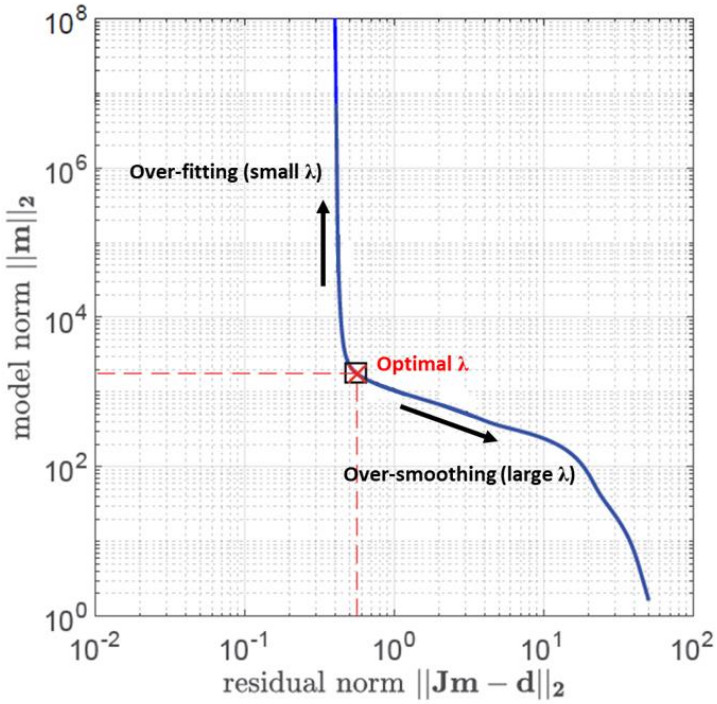

Figure 1-10 : Un exemple de courbe en L pour l'expérience tomographique (période 1,25 min). La valeur optimale de λ située au point d'inflexion de la courbe en L, représente un compromis entre le surajustement des données de charge hydraulique et le lissage excessif des paramètres hydrauliques estimés.

1.4.6.6 Niveau de bruit

Pour obtenir une évaluation réaliste des résolutions, les charges générées par le modèle d'écoulement souterrain doivent être perturbées par un niveau de bruit cohérent avec les mesures de terrain. Le niveau de bruit est basé sur une application pratique des tests périodiques à choc hydraulique réalisés par les auteurs. Ce bruit est supposé suivre une distribution normale avec une moyenne nulle attendue et un écart type de $8{,}5\times10^{-3}$ m pour les intervalles sources et $1{,}8\times10^{-4}$ m pour les intervalles d'observation. Un bruit plus élevé est appliqué aux charges des intervalles sources pour tenir compte de l'écoulement turbulent généré par le mouvement de la tige utilisée pour produire le signal périodique.

1.4.6.7 Métriques

Pour évaluer la qualité de la résolution dans les modèles hydrauliques, deux métriques sont utilisées (Günther, 2004): le contenu informationnel total (IC) et le degré de résolution (RD).

Le contenu informationnel total (IC) est une mesure quantitative qui indique l'efficacité globale de la résolution des paramètres au sein d'une zone d'intérêt spécifique pour une expérimentation donnée. IC est calculé en sommant tous les éléments diagonaux de la matrice de résolution $R_{m,\lambda}$ tel qu'exprimé par l'équation suivante :

$$IC = \sum_i^N R_{m,\lambda,ii}^N \tag{1.12}$$

Où N représente le nombre total de paramètres au sein de la zone d'étude. Un IC élevé signifie que la plupart des paramètres sont bien résolus, indiquant une forte capacité du modèle à distinguer les différents paramètres à partir des observations disponibles.

Le degré de résolution (RD) est pour sa part utilisé pour évaluer la résolution spécifique de chaque propriété hydraulique. Le RD est obtenu en divisant l'IC associé à chaque propriété hydraulique par le nombre de paramètres associés à cette propriété, tel que donnée par l'équation suivante :

$$RD_j = \frac{IC_j}{N_j} \tag{1.13}$$

Où j=1 à 3 correspond respectivement à K_h, K_v/K_h et S_s. Le RD fournit une mesure de la résolution moyenne obtenue pour chaque propriété, avec des valeurs allant de 0 (indiquant que la propriété n'est pas résolue) à 1 (indiquant une résolution parfaite).

1.5 Contributions originales de la thèse

1.5.1 Liste des publications originales

Mon parcours de recherche doctorale a été marqué par des contributions significatives à l'avancement de la tomographie hydraulique oscillatoire (THO) pour la caractérisation des aquifères granulaires hétérogènes et anisotropes. En combinant des approches expérimentales et des analyses théoriques, j'ai approfondi la compréhension de la mesure par THO de la distribution spatiale des propriétés hydrauliques, telles que la conductivité horizontale (K_h), l'anisotropie hydraulique (K_v/K_h) et l'emmagasinement spécifique (S_s), avec un accent particulier sur l'optimisation des pratiques de terrain et la résolution des hétérogénéités.

Cette thèse comprend trois articles scientifiques rédigés en vue de publication, et qui explorent chacun des aspects clés de la THO, de sa faisabilité sur le terrain à son évaluation comparative avec des techniques conventionnelles.

Article I: Nefzi, A., D. Paradis, R. Lefebvre, O. Bour, N. Lavenant (2025) Field deployment and analysis of hydraulic tomography experiments with periodic slug tests in an anisotropic littoral aquifer. Online 26 January 2-25, Journal of Hydrology, 653, June 2025, 132747, doi: 10.1016/j.jhydrol.2025.132747

- Cet article présente l'application innovante de la THO sur le site expérimental de St-Lambert (Québec), démontrant la faisabilité de cette technique dans des aquifères granulaires fortement hétérogènes et anisotropes. Il s'agit de la première étude à évaluer la capacité de la THO à imager non seulement l'hétérogénéité de la conductivité hydraulique horizontale (K_h), mais aussi l'anisotropie de la conductivité hydraulique (K_v/K_h) et l'emmagasinement spécifique (S_s) sur le terrain. En produisant des signaux oscillatoires de qualité et en comparant les résultats avec des simulations numériques, l'article valide la méthodologie employée. L'étude révèle également la distribution spatiale des propriétés hydrauliques à différentes échelles, offrant ainsi une nouvelle perspective pour la caractérisation des aquifères hétérogènes.

Article II: Nefzi, A., D. Paradis, R. Lefebvre (En préparation "a") Responses and resolution of oscillatory hydraulic tomography under a wide range of single and combined signal periods. (En préparation pour soumission à Water Resources Research)

- Cet article apporte une contribution significative en analysant et comparant les réponses théoriques de modèles homogènes et hétérogènes pour une large gamme de signaux périodiques. Bien que basée sur les résultats de l'essai de l'article I, cette étude étend l'analyse au-delà des essais de terrain en explorant des signaux plus variés aux niveaux des périodes et de la génération du signal au puits source. Les travaux permettent d'abord une meilleure compréhension de la propagation des signaux oscillatoires dans les aquifères en fonction de leurs propriétés et de la période des signaux. Ces travaux permettent aussi une évaluation critique des conditions d'essai utilisées et supportent la proposition d'améliorations aux méthodologies des test de THO, notamment pour ajuster la plage des périodes de sollicitation hydraulique pour une meilleure résolution de l'hétérogénéité des aquifères. Les recommandations fournies dans ce travail visent à optimiser les futurs essais THO, rendant l'étude précieuse pour perfectionner les pratiques de terrain et maximiser l'efficacité des résultats obtenus.

Article III: Nefzi, A., D. Paradis, R. Lefebvre, O. Bour (En préparation "b") Evaluation of the informational content and practical effectiveness of periodic and conventional slug test hydraulic tomography. (En préparation pour soumission à Hydrogeology Journal)

- Cette étude offre une évaluation comparative originale du contenu informationnel entre la THO et la tomographie hydraulique basée sur des essais à choc hydraulique conventionnels (*slug tests*), tous deux réalisés sur le terrain au site expérimental de St-Lambert. Les résultats montrent que les deux méthodes capturent de manière similaire la distribution de K_h, K_v/K_h et S_s dans l'aquifère. Toutefois, la THO présente un léger avantage dans le traitement des données de charge hydraulique grâce à la périodicité du signal, qui est plus facile à isoler du bruit ambiant. Cependant, la THO nécessite un équipement plus sophistiqué pour générer et contrôler les signaux oscillatoires, et les essais sont généralement plus longs en raison de la nécessité de produire plusieurs signaux sur différents cycles avec des périodes différentes.

1.5.2 Contributions des auteurs

Dans le cadre de ces publications, les contributions des auteurs se répartissent comme suit :

Aymen Nefzi : Responsable du traitement et de l'interprétation des données, il a pris en charge l'écriture des versions initiales des articles ainsi que la réalisation des figures et des tableaux. Il a également effectué la modélisation numérique, contribué aux orientations générales du projet et assuré la numérisation et la recherche de documents pertinents. Aymen a validé les données, calculé les flux nécessaires à leur intégration dans le modèle, et préparé les structures des premières versions des manuscrits.

Daniel Paradis : Il a planifié et coordonné l'acquisition des données de terrain, en plus de contribuer directement à cette acquisition. Daniel a joué un rôle central dans les orientations stratégiques du projet et a supervisé la modélisation numérique. Il a révisé toutes les versions des articles, modifié et créé des figures pour l'article 1, et contribué aux calculs de flux ainsi qu'à la modification des équations et des structures des manuscrits.

René Lefebvre : En tant que coordinateur du projet, René a encadré l'étudiant impliqué et révisé toutes les versions des articles. Il a également participé aux orientations stratégiques, aux calculs de flux, à la modification des équations, ainsi qu'à l'ajustement des structures des manuscrits.

Olivier Bour : Pendant sa présence au Québec, Olivier a participé à des rencontres pour discuter de l'avancement du projet et du travail réalisé. Il a contribué aux orientations stratégiques du projet et a également révisé l'article 1.

Nicolas Lavenant : Il a développé le système d'essais hydraulique oscillatoire et il a supervisé l'acquisition des données de terrain avec son système au cours des campagnes de terrain de 2017 et 2018.

Chaque auteur a joué un rôle clé dans la conception, la réalisation, et la finalisation des articles, permettant de garantir la qualité scientifique et la pertinence des travaux publiés.

1.5.3 Contributions originales de la thèse

Cette thèse aborde à la fois les aspects pratiques et fondamentaux de la caractérisation des propriétés hydrauliques des aquifères, en apportant des contributions significatives à l'avancement des connaissances. Ces contributions se situent à deux niveaux principaux :

1. Amélioration des pratiques pour la caractérisation de l'hétérogénéité des propriétés hydrauliques

La thèse propose des avancées méthodologiques et expérimentales pour l'application de la tomographie hydraulique oscillatoire (THO), notamment en :

- Proposant et appliquant une approche expérimentale innovante pour l'acquisition et l'analyse des données basée sur la THO, démontrant sa faisabilité dans des aquifères granulaires hétérogènes et anisotropes (Nefzi et al., 2025);
- Validant et comparant les résultats des analyses issues des essais de THO avec ceux obtenus par des essais hydrauliques conventionnels, mettant en évidence les avantages et les limites de chaque méthode (Nefzi et al., 2025; Nefzi et al., En préparation "b")

2. Compréhension approfondie des fondements physiques des écoulements hydrauliques

La thèse enrichit également les connaissances fondamentales sur les mécanismes qui régissent l'écoulement lors des essais hydrauliques, en :

- Expliquant beaucoup mieux comment se fait la transmission des signaux périodiques dans les aquifères granulaires en fonction de leurs propriétés hydrauliques et aussi de la période des signaux.
- Explorant les possibilités et les limites de la THO à travers l'analyse du contenu informationnel des essais de terrain, en particulier pour la résolution des hétérogénéités

des propriétés hydrauliques, telles que la conductivité horizontale (K_h), l'anisotropie (K_v/K_h) et l'emmagasinement spécifique (S_s) (Nefzi et al., En préparation "a").

- Les travaux montrent que les périodes optimales des signaux sources dépendent des propriétés de l'aquifère et que la combinaison de mesures prises avec des signaux de différentes périodes améliore la résolution des paramètres (Nefzi et al., En préparation "a").
- Soulignant que la résolution des propriétés hydrauliques ne dépend pas que de la amplitude du signal induit au puits source, mais aussi du volume d'eau échangé entre le puits source et l'aquifère (Nefzi et al., En préparation "a"). La période du signal au puits source va contrôler à la fois la magnitude et le volume d'eau, en fonction des propriétés de l'aquifère.

Ces contributions, à la fois théoriques et pratiques, permettent de mieux comprendre les potentialités de la THO pour caractériser les propriétés hydrauliques des aquifères et de fournir des recommandations précieuses pour optimiser les essais sur le terrain et améliorer leur interprétation.

1.5.4 Communications scientifiques supplémentaires

En plus des articles scientifiques publiés et en préparation, plusieurs communications scientifiques ont été réalisées au cours de cette thèse :

- Présentation d'une affiche au *Venice International University Graduate Seminar*. Le thème du séminaire portait sur l'inversion hydrogéophysique et l'assimilation des données pour la caractérisation et le suivi des aquifères côtiers;
- Passation de l'examen pré-doctoral comprenant la présentation d'un premier exemple des essais préliminaires sur le site de Saint-Lambert ;
- Participation à un cours de terrain intensif en hydrogéologie en collaboration avec l'Université de Rennes 1 ;
- Présentation orale lors de la Journée des Sciences de la Terre et de l'Environnement au Canada 2020;
- Présentation orale des premiers résultats de nos travaux de recherche au GeoNiagara 2021 (conférence de l'AIH canadien) ;
- Participation à l'Assemblée Générale de l'EGU à Vienne avec une présentation orale. Le thème de la session était l'hydrologie générale (Aymen Nefzi, Daniel Paradis, René

Lefebvre, Olivier Bour. Data acquisition and processing of multi-frequency oscillatory hydraulic tomography in a granular aquifer. EGU General Assembly 2023, Apr 2023, Vienna, Austria. pp. EGU23-10693, 2023, ⟨10.5194/egusphere-egu23-10693⟩. ⟨insu-04080669⟩).

1.6 Bibliographie

Ahn, S.,, Horne, R.N., 2011. The use of attenuation and phase shift to estimate permeability distributions from pulse tests. In Proceedings - SPE Annual Technical Conference and Exhibition, 3:2092–2106. Denver, CO. https://doi.org/10.2118/146636-MS.

Ahn, S., Horne, R.N., 2010. Estimating permeability distributions from pressure pulse testing. In: Proceedings of the SPE Annual Technical Conference and Exhibition, 3, pp. 2388–2403. https://doi.org/10.2118/134391-MS.

American Society for Testing and Materials-ASTM., 2004. D6724: standard guide for installation of direct push ground water monitoring wells. ASTM International, p 9

Aster, R.C., Borchers, B., Thurber, C., 2005. Parameter Estimation and Inverse Problems Elsevier, Amsterdam, p. 301.

Bakhos, T., Cardiff, M., Barrash, W., Kitanidis, P.K., 2014. Data processing for oscillatory pumping tests. Journal of Hydrology 511, 310–319. https://doi.org/10.1016/j.jhydrol.2014.01.007.

Becker, M., Guiltinan, E., 2010. Cross-Hole Periodic Hydraulic Testing of Inter-Well Connectivity. Stanford Geothermal Workshop SGP-TR-188.

Berg, S.J., Illman, W.A., 2011. Three-dimensional transient hydraulic tomography in a highly heterogeneous glaciofluvial aquifer-aquitard system. Water Resour. Res. 47. https://doi.org/10.1029/2011WR010616.

Bianchi, M., Zheng, C., Wilson, C., Tick, G.R., Liu, G., Gorelick, S.M., 2011. Spatial connectivity in a highly heterogeneous aquifer: From cores to preferential flow paths. Water Resources Research 47. https://doi.org/10.1029/2009WR008966.

Black, J.H., Kipp, K.L., 1981. Determination of hydrogeological parameters using sinusoidal pressure tests: A theoretical appraisal. Water Resour. Res. 17, 686–692. https://doi.org/10.1029/WR017i003p00686.

Bohling, G.C., 2009. Sensitivity and resolution of tomographic pumping tests in an alluvial aquifer. Water Resour. Res. 45. https://doi.org/10.1029/2008WR007249.

Bohling, G.C., 1993. Hydraulic tomography in two-dimensional, steady-state groundwater flow. Eos Trans. AGU 74, 141.

Bohling, G.C., Butler, J.J., 2001. lr2dinv: A finite-difference model for inverse analysis of two-dimensional linear or radial groundwater flow. Computers & Geosciences 27, 1147–1156. https://doi.org/10.1016/S0098-3004(01)00036-X.

Bohling, G.C., Butler, J.J., Zhan, X., Knoll, M.D., 2007. A field assessment of the value of steady shape hydraulic tomography for characterization of aquifer heterogeneities. Water Resour. Res. 43. https://doi.org/10.1029/2006WR004932.

Bohling, G.C., Zhan, X., Butler, J.J., Zheng, L., 2002. Steady shape analysis of tomographic pumping tests for characterization of aquifer heterogeneities. Water Resour. Res. 38, 60-1-60–15. https://doi.org/10.1029/2001WR001176.

Bolduc, A., 2003. Géologie des formations superficielles, Charny, Québec. Commission Géologique du Canada.

Brauchler, R., Hu, R., Dietrich, P., Sauter, M., 2011. A field assessment of high-resolution aquifer characterization based on hydraulic travel time and hydraulic attenuation tomography. Water Resour. Res. 47. https://doi.org/10.1029/2010WR009635.

Brauchler, R., Hu, R., Hu, L., Jiménez, S., Bayer, P., Dietrich, P., Ptak, T., 2013. Rapid field application of hydraulic tomography for resolving aquifer heterogeneity in unconsolidated sediments. Water Resour. Res. 49, 2013–2024. https://doi.org/10.1002/wrcr.20181.

Brauchler, R., Liedl, R., Dietrich, P., 2003. A travel time based hydraulic tomographic approach. Water Resour. Res. 39. https://doi.org/10.1029/2003WR002262.

Butler, J.J., 2005. Hydrogeological Methods for Estimation of Spatial Variations in Hydraulic Conductivity, in: Rubin, Y., Hubbard, S.S. (Eds.), Hydrogeophysics, Water Science and Technology Library. Springer Netherlands, Dordrecht, pp. 23–58. https://doi.org/10.1007/1-4020-3102-5_2.

Butler, J.J., McElwee, C.D., 1990. Variable-rate pumping tests for radially symmetric nonuniform aquifers. Water Resour. Res. 26, 291–306. https://doi.org/10.1029/WR026i002p00291.

Cardiff, M., Bakhos, T., Kitanidis, P.K., Barrash, W., 2013b. Aquifer heterogeneity characterization with oscillatory pumping: Sensitivity analysis and imaging potential. Water Resour. Res. 49, 5395–5410. https://doi.org/10.1002/wrcr.20356.

Cardiff, M., Barrash, W., Kitanidis, P. k., Malama, B., Revil, A., Straface, S., Rizzo, E., 2009. A Potential-Based Inversion of Unconfined Steady-State Hydraulic Tomography. Groundwater 47, 259–270. https://doi.org/10.1111/j.1745-6584.2008.00541.x.

Cardiff, M., Barrash, W., Kitanidis, P.K., 2012. A field proof-of-concept of aquifer imaging using 3-D transient hydraulic tomography with modular, temporarily-emplaced equipment. Water Resour. Res. 48. https://doi.org/10.1029/2011WR011704.

Cardiff, M., Barrash, W., Kitanidis, P.K., 2013a. Hydraulic conductivity imaging from 3-D transient hydraulic tomography at several pumping/observation densities. Water Resour. Res. 49, 7311–7326. https://doi.org/10.1002/wrcr.20519.

Cardiff, M., Sayler, C., 2016. Strategies for avoiding errors and ambiguities in the analysis of oscillatory pumping tests. Journal of Hydrology 540, 1016–1021. https://doi.org/10.1016/j.jhydrol.2016.06.045.

Cardiff, M., Zhou, Y., Barrash, W., Kitanidis, P.K., 2020. Aquifer imaging with oscillatory hydraulic tomography: application at the field scale. Groundwater 58, 710–722. https://doi.org/10.1111/gwat.12960.

Carrera, J., Neuman, S.P., 1986. Estimation of Aquifer Parameters Under Transient and Steady State Conditions: 1. Maximum Likelihood Method Incorporating Prior Information. Water Resources Research 22, 199–210. https://doi.org/10.1029/WR022i002p00199.

de Marsily, Gh., Delay, F., Gonçalvès, J., Renard, Ph., Teles, V., Violette, S., 2005. Dealing with spatial heterogeneity. Hydrogeol J 13, 161–183. https://doi.org/10.1007/s10040-004-0432-3.

Engard, B., McElwee, C., Healey, J.,, Devlin, J., 2005. Hydraulic tomography and high-resolution slug testing to determine hydraulic conductivity distributions – year 1. Project Report to the Strategic Environmental Research and Development Program, U.S. DoD, EPA, and DOE, KGS Open-File Report no. 2005-36, 81 pp.

Fischer, P., De Clercq, T., Jardani, A., Thannberger, L., Massei, N., Abbas, M., 2020. Imaging the hydraulic properties of a contaminated alluvial aquifer perturbed with periodic signals. Hydrogeol J 28, 2713–2726. https://doi.org/10.1007/s10040-020-02233-8.

Fischer, P., Jardani, A., Jourde, H., Cardiff, M., Wang, X., Chedeville, S., Lecoq, N., 2018. Harmonic pumping tomography applied to image the hydraulic properties and interpret the connectivity

of a karstic and fractured aquifer (Lez aquifer, France). Advances in Water Resources 119, 227–244. https://doi.org/10.1016/j.advwatres.2018.07.002.

Fischer, P., Jardani, A., Soueid Ahmed, A., Abbas, M., Wang, X., Jourde, H., Lecoq, N., 2017. Application of Large-Scale Inversion Algorithms to Hydraulic Tomography in an Alluvial Aquifer. Groundwater 55, 208–218. https://doi.org/10.1111/gwat.12457.

Fokker, P.A., Salina Borello, E., Serazio, C., Verga, F., 2012. Estimating reservoir heterogeneities from pulse testing. Journal of Petroleum Science and Engineering 86–87, 15–26. https://doi.org/10.1016/j.petrol.2012.03.017.

Fokker, P.A., Verga, F., 2011. Application of harmonic pulse testing to water–oil displacement. Journal of Petroleum Science and Engineering 79, 125–134. https://doi.org/10.1016/j.petrol.2011.09.004.

Gauthier et Guillemette Consultants Inc., Dessau Environnement ltée, and Serrener Consultation Inc ., 1993. Étude hydrogéologique complémentaire du lieu d'enfouissement sanitaire de saint-lambert-de-lauzon. Technical report, Comité intermunicipal d'enfouissement sanitaire des Chutes-de-la-Chaudière.

Gernez, S., Bouchedda, A., Gloaguen, E., Paradis, D., 2019. Comparison Between Hydraulic Conductivity Anisotropy and Electrical Resistivity Anisotropy From Tomography Inverse Modeling. Front. Environ. Sci. 7, 67. https://doi.org/10.3389/fenvs.2019.00067.

Goltz, M.N., Huang, J., Close, M.E., Flintoft, M.J., Pang, L., 2008. Use of tandem circulation wells to measure hydraulic conductivity without groundwater extraction. Journal of Contaminant Hydrology 100, 127–136. https://doi.org/10.1016/j.jconhyd.2008.06.003.

Gottlieb, J., Dietrich, P., 1995. Identification of the permeability distribution in soil by hydraulic tomography. Inverse Problems 11, 353–360. https://doi.org/10.1088/0266-5611/11/2/005.

Guiltinan, E., Becker, M.W., 2015. Measuring well hydraulic connectivity in fractured bedrock using periodic slug tests. Journal of Hydrology 521, 100–107. https://doi.org/10.1016/j.jhydrol.2014.11.066.

Günther, T., 2004. Inversion Methods and Resolution Analysis For the 2D/3D Reconstruction of Resistivity Structures from DC Measurements. Technische Universit¨at Bergakademie Freiberg, p. 160. Ph.D. Thesis.

Hansen, P.C., 2023. Regularization tools: A MATLAB Package For Analysis and Solution of Discrete Ill-Posed Problems. Version 4.1. regtools (https://www.mathworks.com /matlabcentral/fileexchange/52-regtools), MATLAB Central File Exchange. Retrieved February 6, 2023.

Hansen, P.C., 1992. Analysis of discrete Ill-posed problems by means of the L-curve. SIAM Rev. 34, 561–580. https://doi.org/10.1137/1034115.

Hansen, P.C., Jensen, T.K., Rodriguez, G., 2007. An adaptive pruning algorithm for the discrete L-curve criterion. Journal of Computational and Applied Mathematics, Special Issue: Applied Computational Inverse Problems 198, 483–492. https://doi.org/10.1016/j.cam.2005.09.026.

Hochstetler, D.L., Barrash, W., Leven, C., Cardiff, M., Chidichimo, F., Kitanidis, P.K., 2016. Hydraulic tomography: continuity and discontinuity of high-K and low-K zones. Groundwater 54, 171–185. https://doi.org/10.1111/gwat.12344.

Hocq M,, Dubé C, 1994. Géologie du Québec: Hocq M, Dubé C Ed., Ministère des Ressources Naturelles du Québec, Les Publications du Québec, 154 p.

Hollaender, F., Hammond, P.S., Gringarten, A.C., 2002. Harmonic Testing for Continuous Well and Reservoir Monitoring, in: All Days. Presented at the SPE Annual Technical Conference and Exhibition, SPE, San Antonio, Texas, p. SPE-77692-MS. https://doi.org/10.2118/77692-MS.

Hu, R., Brauchler, R., Herold, M., Bayer, P., 2011. Hydraulic tomography analog outcrop study: Combining travel time and steady shape inversion. Journal of Hydrology 409, 350–362. https://doi.org/10.1016/j.jhydrol.2011.08.031.

Hvilshøj, S., Jensen, K. h., Madsen, B., 2000. Single-Well Dipole Flow Tests: Parameter Estimation and Field Testing. Groundwater 38, 53–62. https://doi.org/10.1111/j.1745-6584.2000.tb00202.x.

Illman, W.A., Berg, S.J., Zhao, Z., 2015. Should hydraulic tomography data be interpreted using geostatistical inverse modeling? A laboratory sandbox investigation. Water Resources Research 51, 3219–3237. https://doi.org/10.1002/2014WR016552.

Illman, W.A., Craig, A.J., Liu, X., 2008. Practical Issues in Imaging Hydraulic Conductivity through Hydraulic Tomography. Groundwater 46, 120–132. https://doi.org/10.1111/j.1745-6584.2007.00374.x.

Illman, W.A., Liu, X., Craig, A., 2007. Steady-state hydraulic tomography in a laboratory aquifer with deterministic heterogeneity: Multi-method and multiscale validation of hydraulic conductivity tomograms. Journal of Hydrology 341, 222–234. https://doi.org/10.1016/j.jhydrol.2007.05.011.

Illman, W.A., Liu, X., Takeuchi, S., Yeh, T.-C.J., Ando, K., Saegusa, H., 2009. Hydraulic tomography in fractured granite: Mizunami Underground Research site, Japan. Water Resour. Res. 45. https://doi.org/10.1029/2007WR006715.

Illman, W.A., Zhu, J., Craig, A.J., Yin, D., 2010. Comparison of aquifer characterization approaches through steady state groundwater model validation: A controlled laboratory sandbox study. Water Resources Research 46. https://doi.org/10.1029/2009WR007745.

Jiménez, S., Brauchler, R., Bayer, P., 2013. A new sequential procedure for hydraulic tomographic inversion. Advances in Water Resources 62, 59–70. https://doi.org/10.1016/j.advwatres.2013.10.002.

Johnson, C.R., Greenkorn, R.A., Woods, E.G., 1966. Pulse-Testing: A New Method for Describing Reservoir Flow Properties Between Wells. Journal of Petroleum Technology 18, 1599–1604. https://doi.org/10.2118/1517-PA.

Kabala, Z.J., 1993. The dipole flow test: A new single-borehole test for aquifer characterization. Water Resources Research 29, 99–107. https://doi.org/10.1029/92WR01820.

Kitanidis, P.K., 1995. Quasi-Linear Geostatistical Theory for Inversing. Water Resources Research 31, 2411–2419. https://doi.org/10.1029/95WR01945.

Kruseman, G.P., Ridder, N.A. de, 1994. Analysis and evaluation of pumping test data, 2. ed. (completely rev.), reprint. ed, ILRI publication. Internat. Inst. for Land Reclamation and Improvement, Wageningen.

Kuhlman, K.L., Hinnell, A.C., Mishra, P.K., Yeh, T.-C.J., 2008. Basin-Scale Transmissivity and Storativity Estimation Using Hydraulic Tomography. Groundwater 46, 706–715. https://doi.org/10.1111/j.1745-6584.2008.00455.x.

Kuo, C.H., 1972. Determination of Reservoir Properties from Sinusoidal and Multirate Flow Tests in One or More Wells. Society of Petroleum Engineers Journal 12, 499–507. https://doi.org/10.2118/3632-PA.

Lancaster-Jones, P.F.F., 1975. The interpretation of the Lugeon water-test. Quarterly Journal of Engineering Geology 8, 151–154. https://doi.org/10.1144/GSL.QJEG.1975.008.02.05.

Landry B,, Mercier M, 1983. Notion de géologie : avec exemple du Québec, Modulo, Outremont.

Lavenue, A.M., RamaRao, B.S., De Marsily, G., Marietta, M.G., 1995. Pilot Point Methodology for Automated Calibration of an Ensemble of Conditionally Simulated Transmissivity Fields: 2. Application. Water Resources Research 31, 495–516. https://doi.org/10.1029/94WR02259.

Lavenue, M., de Marsily, G., 2001. Three-dimensional interference test interpretation in a fractured aquifer using the Pilot Point Inverse Method. Water Resour. Res. 37, 2659–2675. https://doi.org/10.1029/2000WR000289.

Li, W., Englert, A., Cirpka, O.A., Vereecken, H., 2008. Three-Dimensional Geostatistical Inversion of Flowmeter and Pumping Test Data. Groundwater 46, 193–201. https://doi.org/10.1111/j.1745-6584.2007.00419.x.

Liu, Q., Hu, L., Hu, R., Brauchler, R., Xing, Y., Qi, J., Ptak, T., 2023. Characterization of aquifer heterogeneity by tomographic slug test responses considering wellbore effects. Journal of Hydrology 627, 130472. https://doi.org/10.1016/j.jhydrol.2023.130472.

Liu, X., Illman, W.A., Craig, A.J., Zhu, J., Yeh, T.-C.J., 2007. Laboratory sandbox validation of transient hydraulic tomography. Water Resources Research 43. https://doi.org/10.1029/2006WR005144.

Lochbühler, T., Doetsch, J., Brauchler, R., Linde, N., 2013. Structure-coupled joint inversion of geophysical and hydrological data. GEOPHYSICS 78, ID1–ID14. https://doi.org/10.1190/geo2012-0460.1.

Marquardt, D. W, 1963. An algorithm for the least-squares estimation of nonlinear parameters, SIAM, J. Appl. Math., 11, 431–441.

McKinley, R.M., Vela, S., Carlton, L.A., 1968. A Field Application of Pulse-Testing for Detailed Reservoir Description. Journal of Petroleum Technology 20, 313–321. https://doi.org/10.2118/1822-PA.

Michael Tso, C.-H., Zha, Y., Jim Yeh, T.-C., Wen, J.-C., 2016. The relative importance of head, flux, and prior information in hydraulic tomography analysis. Water Resources Research 52, 3–20. https://doi.org/10.1002/2015WR017191.

Moore, E.H, 1920. On the reciprocal of the general algebraic matrix. Bull. Am. Math. Soc. 26, 394–395.

Nefzi, A., Paradis, D., Lefebvre, R., En préparation “b.” Evaluation of the informational content and practical effectiveness of periodic and conventional slug test hydraulic tomography. Article en préparation.

Nefzi, A., Paradis, D., Lefebvre, R., En préparation “a.” Responses and resolution of oscillatory hydraulic tomography under a wide range of single and combined signal periods. Article en préparation.

Nefzi, A., Paradis, D., Lefebvre, R., Bour, O., Lavenant, N., 2025. Field deployment and analysis of hydraulic tomography experiments with periodic slug tests in an anisotropic littoral aquifer. Journal of Hydrology 653, 132747. https://doi.org/10.1016/j.jhydrol.2025.132747.

Neuman, S.P., 1987. On Methods of Determining Specific Yield. Groundwater 25, 679–684. https://doi.org/10.1111/j.1745-6584.1987.tb02208.x.

Paradis, D., Gloaguen, E., Lefebvre, R., Giroux, B., 2016. A field proof-of-concept of tomographic slug tests in an anisotropic littoral aquifer. Journal of Hydrology 536, 61–73. https://doi.org/10.1016/j.jhydrol.2016.02.041.

Paradis, D., Gloaguen, E., Lefebvre, R., Giroux, B., 2015b. Resolution analysis of tomographic slug test head data: Two-dimensional radial case. Water Resour. Res. 51, 2356–2376. https://doi.org/10.1002/2013WR014785.

Paradis, D., Lefebvre, R., 2013. Single-well interference slug tests to assess the vertical hydraulic conductivity of unconsolidated aquifers. Journal of Hydrology 478, 102–118. https://doi.org/10.1016/j.jhydrol.2012.11.047.

Paradis, D., Lefebvre, R., Gloaguen, E., Rivera, A., 2015a. Predicting hydrofacies and hydraulic conductivity from direct-push data using a data-driven relevance vector machine approach: Motivations, algorithms, and application. Water Resour. Res. 51, 481–505. https://doi.org/10.1002/2014WR015452.

Paradis, D., Lefebvre, R., Morin, R.H., Gloaguen, E., 2011. Permeability Profiles in Granular Aquifers Using Flowmeters in Direct-Push Wells. Ground Water 49, 534–547. https://doi.org/10.1111/j.1745-6584.2010.00761.x.

Paradis, D., Lefebvre, R., Nefzi, A., 2024. Parameter resolution of simulated responses to periodic hydraulic tomography signals in aquifers. Advances in Water Resources 190, 104734. https://doi.org/10.1016/j.advwatres.2024.104734.

Paradis, D., Tremblay, L., Lefebvre, R., Gloaguen, E., Rivera, A., Parent, M., Ballard, J.-M., Michaud, Y., Brunet, P., 2014. Field characterization and data integration to define the hydraulic heterogeneity of a shallow granular aquifer at a sub-watershed scale. Environ Earth Sci 72, 1325–1348. https://doi.org/10.1007/s12665-014-3318-2.

Penrose, R., 1955. A generalized inverse for matrices. Proc. Camb. Philos. Soc. 51, 406–413.

Press, W. H., Teukolsky, S. A., Vetterling, W. T, Flannery, B. P., 1992. Numerical Recipes in C: The Art of Scientific Computing, 2nd edition, Cambridge Univ. Press, Cambridge.

Quinn, P.M., Cherry, J.A., Parker, B.L., 2011. Quantification of non-Darcian flow observed during packer testing in fractured sedimentary rock. Water Resources Research 47. https://doi.org/10.1029/2010WR009681.

Rasmussen, T.C., Haborak, K.G., Young, M.H., 2003. Estimating aquifer hydraulic properties using sinusoidal pumping at the Savannah River site, South Carolina, USA. Hydrogeology Journal 11, 466–482. https://doi.org/10.1007/s10040-003-0255-7.

Rehfeldt, K.R., Boggs, J.M., Gelhar, L.W., 1992. Field study of dispersion in a heterogeneous aquifer: 3. Geostatistical analysis of hydraulic conductivity. Water Resources Research 28, 3309–3324. https://doi.org/10.1029/92WR01758.

Renner, J., Messar, M., 2006. Periodic pumping tests. Geophysical Journal International 167, 479–493. https://doi.org/10.1111/j.1365-246X.2006.02984.x.

Rosa, A.J., Horne, R.N., 1997. Reservoir Description by Well-Test Analysis by Use of Cyclic Flow-Rate Variation. SPE Formation Evaluation 12, 247–254. https://doi.org/10.2118/22698-PA.

Ross, H.C., McElwee, C.D., 2007. Multi-Level Slug Tests to Measure 3-D Hydraulic Conductivity Distributions. Natural Resources Research 16, 67–79. https://doi.org/10.1007/s11053-007-9034-9.

Sayler, C., Cardiff, M., Fort, M.D., 2018. Understanding the Geometry of Connected Fracture Flow with Multiperiod Oscillatory Hydraulic Tests. Groundwater 56, 276–287. https://doi.org/10.1111/gwat.12580.

Soueid Ahmed, A., Zhou, J., Jardani, A., Revil, A., Dupont, J.P., 2015. Image-guided inversion in steady-state hydraulic tomography. Advances in Water Resources 82, 83–97. https://doi.org/10.1016/j.advwatres.2015.04.001.

Spane, F.A., Mackley, R.D., 2011. Removal of River-Stage Fluctuations from Well Response Using Multiple Regression. Groundwater 49, 794–807. https://doi.org/10.1111/j.1745-6584.2010.00780.x.

Sun, R., Yeh, T.-C.J., Mao, D., Jin, M., Lu, W., Hao, Y., 2013. A temporal sampling strategy for hydraulic tomography analysis. Water Resources Research 49, 3881–3896. https://doi.org/10.1002/wrcr.20337.

Tiedeman, C.R., Barrash, W., 2020. Hydraulic Tomography: 3D Hydraulic Conductivity, Fracture Network, and Connectivity in Mudstone. Groundwater 58, 238–257. https://doi.org/10.1111/gwat.12915.

Tikhonov, A.N.,, Goncharsky, A.V., 1987. Ill-posed problems in the natural sciences.

Tosaka, H., Masumoto, K., Kojima, K.., 1993. Hydropulse tomography for identifying 3-D permeability distribution. American Nuclear Society, Inc, United States.

Tremblay, L., Lefebvre, R., Paradis, D., Gloaguen, E., 2014. Conceptual model of leachate migration in a granular aquifer derived from the integration of multi-source characterization data (St-Lambert, Canada). Hydrogeol J 22, 587–608. https://doi.org/10.1007/s10040-013-1065-1.

Vasco, D.W., Datta-Gupta, A., Long, J.C.S., 1997. Resolution and uncertainty in hydrologic characterization. Water Resources Research 33, 379–397. https://doi.org/10.1029/96WR03301.

Wachter, B., McElwee, C., Devlin, J., 2008. Hydraulic tomography and highresolution slug testing to determine hydraulic conductivity distributions year 4. Project Report to the Strategic Environmental Research and Development Program, U.S. DoD, EPA, and DOE, KGS Open-File Report no. 2008-23, 74 pp.

Wang, Y.-L., Yeh, T.-C.J., Wen, J.-C., Huang, S.-Y., Zha, Y., Tsai, J.-P., Hao, Y., Liang, Y., 2017. Characterizing subsurface hydraulic heterogeneity of alluvial fan using riverstage fluctuations. Journal of Hydrology 547, 650–663. https://doi.org/10.1016/j.jhydrol.2017.02.032.

Wang, Y.-L., Yeh, T.-C.J., Xu, D., Li, K., Wen, J.-C., Huang, S.-Y., Wang, W., Hao, Y., 2021. Stochastic analysis of oscillatory hydraulic tomography. Journal of Hydrology 596, 126105. https://doi.org/10.1016/j.jhydrol.2021.126105.

Xiang, J., Kabala, Z.J., 1997. Performance of the steady-state dipole flow test in layered aquifers. Hydrological Processes 11, 1595–1605. https://doi.org/10.1002/(SICI)1099-1085(19971015)11:12<1595::AID-HYP489>3.0.CO;2-0.

Yeh, T.-C.J., Jin, M., Hanna, S., 1996. An Iterative Stochastic Inverse Method: Conditional Effective Transmissivity and Hydraulic Head Fields. Water Resources Research 32, 85–92. https://doi.org/10.1029/95WR02869.

Yeh, T.-C.J., Lee, C.-H., Hsu, K.-C., Illman, W.A., Barrash, W., Cai, X., Daniels, J., Sudicky, E., Wan, L., Li, G., Winter, C.L., 2008. A view toward the future of subsurface characterization: CAT scanning groundwater basins. Water Resources Research 44. https://doi.org/10.1029/2007WR006375.

Yeh, T.-C.J., Liu, S., 2000. Hydraulic tomography: Development of a new aquifer test method. Water Resour. Res. 36, 2095–2105. https://doi.org/10.1029/2000WR900114.

Yeh, T.-C.J., Mao, D., Zha, Y., Hsu, K.-C., Lee, C.-H., Wen, J.-C., Lu, W., Yang, J., 2014. Why Hydraulic Tomography Works? Groundwater 52, 168–172. https://doi.org/10.1111/gwat.12129.

Yeh, T.-C.J., Xiang, J., Suribhatla, R.M., Hsu, K.-C., Lee, C.-H., Wen, J.-C., 2009. River stage tomography: A new approach for characterizing groundwater basins. Water Resources Research 45. https://doi.org/10.1029/2008WR007233.

Yin, D., Illman, W.A., 2009. Hydraulic tomography using temporal moments of drawdown recovery data: A laboratory sandbox study. Water Resources Research 45. https://doi.org/10.1029/2007WR006623.

Zha, Y., Yeh, T.-C.J., Illman, W.A., Mok, C.M.W., Tso, C.-H.M., Carrera, B.A., Wang, Y.-L., 2019. Exploitation of pump-and-treat remediation systems for characterization of hydraulic heterogeneity. Journal of Hydrology 573, 324–340. https://doi.org/10.1016/j.jhydrol.2019.03.089.

Zha, Y., Yeh, T.-C.J., Illman, W.A., Onoe, H., Mok, C.M.W., Wen, J.-C., Huang, S.-Y., Wang, W., 2017. Incorporating geologic information into hydraulic tomography: A general framework based on geostatistical approach. Water Resources Research 53, 2850–2876. https://doi.org/10.1002/2016WR019185.

Zha, Y., Yeh, T.-C.J., Illman, W.A., Tanaka, T., Bruines, P., Onoe, H., Saegusa, H., Mao, D., Takeuchi, S., Wen, J.-C., 2016. An Application of Hydraulic Tomography to a Large-Scale Fractured Granite Site, Mizunami, Japan. Groundwater 54, 793–804. https://doi.org/10.1111/gwat.12421.

Zhao, Z., Illman, W.A., 2018. Three-dimensional imaging of aquifer and aquitard heterogeneity via transient hydraulic tomography at a highly heterogeneous field site. Journal of Hydrology 559, 392–410. https://doi.org/10.1016/j.jhydrol.2018.02.024.

Zhao, Z., Illman, W.A., 2017. On the importance of geological data for three-dimensional steady-state hydraulic tomography analysis at a highly heterogeneous aquifer-aquitard system. Journal of Hydrology 544, 640–657. https://doi.org/10.1016/j.jhydrol.2016.12.004.

Zhao, Z., Illman, W.A., Berg, S.J., 2016. On the importance of geological data for hydraulic tomography analysis: Laboratory sandbox study. Journal of Hydrology 542, 156–171. https://doi.org/10.1016/j.jhydrol.2016.08.061.

Zhu, J., Yeh, T.-C.J., 2006. Analysis of hydraulic tomography using temporal moments of drawdown recovery data. Water Resources Research 42. https://doi.org/10.1029/2005WR004309.

Zhu, J., Yeh, T.-C.J., 2005. Characterization of aquifer heterogeneity using transient hydraulic tomography. Water Resour. Res. 41. https://doi.org/10.1029/2004WR003790.

Zlotnik, V., Ledder, G., 1996. Theory of Dipole Flow in Uniform Anisotropic Aquifers. Water Resources Research 32, 1119–1128. https://doi.org/10.1029/95WR03813.

Zlotnik, V.A., Zurbuchen, B.R., 1998. Dipole Probe: Design and Field Applications of a Single-Borehole Device for Measurements of Vertical Variations of Hydraulic Conductivity. Groundwater 36, 884–893. https://doi.org/10.1111/j.1745-6584.1998.tb02095.x.

Zlotnik, V.A., Zurbuchen, B.R., Ptak, T., 2001. The Steady-State Dipole-Flow Test for Characterization of Hydraulic Conductivity Statistics in a Highly Permeable Aquifer: Horkheimer Insel Site, Germany. Groundwater 39, 504–516. https://doi.org/10.1111/j.1745-6584.2001.tb02339.x.

2 FIELD DEPLOYMENT AND ANALYSIS OF HYDRAULIC TOMOGRAPHY EXPERIMENTS WITH PERIODIC SLUG TESTS IN AN ANISOTROPIC LITTORAL AQUIFER

Titre de l'article : Déploiement et analyse des expérimentations de tomographie hydraulique par essais périodiques dans un aquifère littoral anisotrope

Auteurs :

Aymen Nefzi[1], Daniel Paradis[1,2], René Lefebvre[1], Olivier Bour[3] & Nicolas Lavenant[3]

[1] Centre Eau Terre Environnement (INRS-ETE) - Institut national de la recherche scientifique, Québec, Canada

[2] Ressources Naturelles Canada - Commission géologique du Canada, Québec, Canada

[3] Université Rennes, CNRS, Géosciences Rennes, UMR 6118, 35000 Rennes, France

Titre de la revue ou de l'ouvrage :

Article accepté le 12 janvier 2025, dans la revue Journal of Hydrology.

Abstract

Accurate mapping of the heterogeneity of hydraulic properties, including hydraulic conductivity (K_h) and its anisotropy (K_v/K_h), is crucial for predicting groundwater flow and solute transport in aquifers. This study investigates the use of hydraulic tomography with periodic signals to map K_h, K_v/K_h and specific storage (S_s) in an unconsolidated littoral aquifer. The periodic signals were generated by the movement of a rod numerically controlled by a winch, which allowed the signal

amplitude and period to be imposed. Thirty periodic slug tests with periods of 150, 300 and 600 s were conducted between isolated intervals in a source well and an observation well, generating 120 head responses (3 periods x 10 tests x 4 intervals). Numerical inversion in the time domain used the rod-induced flow rates and associated heads to estimate the heterogeneous fields. Significant differences in head amplitude and phase shift between test intervals at different locations highlighted the heterogeneity of the aquifer. The inversion results for single and combined periods are consistent with the values of previous studies and the heterogeneous nature of the littoral aquifer. Comparison of models from different periods revealed slight spatial and statistical variations in hydraulic properties and different hydraulic behavior when tested with independent hydraulic tests. While the fundamentals of understanding the information in the different periodic signals need to be further clarified, this study advances the application of hydraulic tomography under real field conditions and highlights its effectiveness in characterizing aquifer heterogeneity and anisotropy.

Keywords: Unconsolidated aquifers, aquifer characterization, field tests, hydraulic tomography, periodic testing, anisotropy, heterogeneity

2.1 Introduction

The heterogeneity of hydraulic properties in aquifers plays a crucial role in controlling groundwater flow (e.g. Frei et al., 2009; Yetbarek et al., 2020; Zeyrek et al., 2023; Chen et al., 2023) and influences processes such as solute transport and dispersivity (e.g. Leblanc et al., 1991; Boggs et al., 1992; Sudicky and Illman, 2011; Hoque and Burgess, 2020; Yin et al., 2023). Accurately mapping this heterogeneity remains an ongoing challenge that requires continuous development of field methods (de Marsily et al., 2005).

Several field methods have been developed to estimate hydraulic properties along wells, especially hydraulic conductivity (*K*). These methods usually require tests at small intervals to capture vertical variations of *K*. The most common method is to use inflatable packers to isolate discrete intervals (deca-metric to sub-metric) along open holes or screened wells and perform slug tests or pumping tests. In a slug test, a known volume of water is instantaneously withdrawn or injected into the well (e.g., Rehfeldt et al., 1992; Ross and McElwee, 2007), whereas in pumping tests, water is withdrawn or injected at a constant rate (e.g., Lancaster-Jones, 1975; Price et al., 1982; Quinn et al., 2011). In these tests, the changes in head over time in response to the hydraulic stimulation are measured and evaluated using analytical or numerical methods (e.g., Kruseman and de Ridder, 2000). Flowmeter tests are another technique that has been used

to obtain vertical profiles of transmissivity (*T*) (e.g., Morin et al., 1988; Molz et al., 1989; Hanson and Nishikawa, 1996; Paillet, 1998; Crisman et al., 2001; Paradis et al., 2011). Flowmeters use impellers, heat pulses, or electromagnetic devices to measure flow rates at discrete intervals along a well during pumping. Recent advances include FLUTe tests, which involve deploying a flexible liner into an open well under a controlled driving head. By measuring the rate of descent of the liner, the test can profile the transmissivity (T) of the well (e.g., Keller et al., 2014; Quinn et al., 2015). Slug tests and permeameter tests have been adapted for use with direct-push equipment (e.g., Butler et al., 2007; Dietrich et al., 2008; Liu et al., 2009). In these methods, a system of casing and screen is driven into unconsolidated sediments to the desired depths to perform tests. This approach allows for very fine vertical resolution of K, often in the centimeter range.

While 1D profiles are invaluable in identifying vertical variations in hydraulic properties at individual wells, mapping heterogeneity between these wells is better assessed by inter-well interference tests, such as hydraulic tomography (Berg and Illman, 2015). Hydraulic tomography is based on inverse modeling of multiple hydraulic tests with head measurements at multiple observation intervals to map 2D or 3D distributions (tomograms) of hydraulic properties (e.g. Bohling, 1993; Tosaka et al., 1993; Gottlieb and Dietrich, 1995). In most field studies using hydraulic tomography, pumping tests were performed at a constant rate to generate a stimulation. When analyzing pumping test tomography, either steady-state shape (e.g., Bohling et al., 2007) or steady-state head (e.g., Li et al., 2008; Cardiff et al., 2009) or full transient responses (e.g., Illman et al., 2009; Berg and Illman, 2011; Cardiff et al., 2012; 2013; Hochstetler et al., 2015; Tiedeman and Barrash, 2020) were used. Few other field applications of hydraulic tomography have relied on slug tests (e.g. Brauchler et al, 2011; 2013; Lochbühler et al, 2013; Paradis et al, 2016; Liu et al, 2023). All these previous studies have shown that the obtained tomograms of hydraulic properties are generally consistent with the geology of the sites or independent profiles of hydraulic conductivity obtained with other techniques along the wells. Some of them also successfully reproduce independent hydraulic tests, suggesting that the spatial structure of the heterogeneity is well reproduced.

The use of hydraulic tomography with periodic signals has also been proposed for the characterization of aquifer heterogeneity. Rosa and Horne (1997) have shown that a periodic square-wave signal, with alternating periods of constant and zero flow rates, can provide more information than a signal generated by a conventional constant-rate pumping test for the same test configuration. The reason for the better performance is that the periodic signal contains

multiple sinusoidal components, each of which investigates a different region of the aquifer. Varying the period of a pure sinusoidal signal also allows the investigation of different aquifer regions. Therefore, their combined analysis can possibly improve heterogeneity characterization (Black and Kipp, 1981; Hollaender et al., 2002; Ahn and Horne, 2010; Cardiff et al., 2013; Paradis et al. 2024).

However, only a few published field applications of periodic hydraulic tomography have revealed its potential for mapping aquifer heterogeneity. Lavenue and Marsilly (2001) performed sinusoidal pumping tests with a single period (72 min) to estimate K of an unconfined dolomite aquifer. Although the recovered model accurately reproduced an independent periodic test used for validation, the information content of the single period was not assessed. Fischer et al. (2018) conducted harmonic pumping tests with two different periods (2 and 5 min) to estimate the transmissivity (T) and the storativity (S) of the conduits and the matrix of a karst network in the horizontal 2D plane. Their results show very different structures of the karst network for each period, which was attributed to the relative change in the induced flow field for each period. Fischer et al. (2020) also mapped the heterogeneity of an alluvial aquifer using oscillatory pumping tests with two different periods (5 and 10 min). The resulting maps of T and S values, averaged over 2D depth, for the separate and joint inversions of the two periods differed only slightly and were all consistent with the geology and contamination history of the site (Fischer et al., 2020). However, they concluded that a joint inversion with the two periods “provided more information on the heterogeneous distribution of the field properties” based on the analysis of the uncertainty maps of the separate and joint inversions. Finally, Cardiff et al. (2020) reported on a field application of oscillatory hydraulic tomography with a series of periods ranging between 5 and 70 seconds in a fluvial aquifer. Data from all periods were inverted together to reconstruct the 3D K-field (S_s was fixed). This joint inversion reveals a strong positive correlation with K profiles obtained by slug tests. However, a rather moderate correlation with tomograms obtained by constant pumping rate tomography from a previous study was found.

While this review highlights successful applications of hydraulic tomography with periodic signals, none of them considered the anisotropy in K (or the ratio of vertical (K_v) to horizontal (K_h) hydraulic conductivity, K_v/K_h). K_v/K_h expresses the effects of small-scale heterogeneity in K at a larger scale and controls groundwater flow and solute transport at different scales (e.g. Hart et al. 2006; Barry et al. 2009; Falta et al. 2005). According to Shepley (2024), K_v tend to be overestimated in groundwater models due to a general lack of knowledge about this hydraulic parameter. The aim of this paper is to provide a practical example of hydraulic tomography with periodic tests

considering K_v/K_h. The examination of new applications is crucial to understand the benefits of this method and to identify opportunities for improvement. This includes the entire process, from field methods to data processing techniques and data inversion procedures. This study therefore presents the field experimentation and analysis of such an experiment conducted in a littoral aquifer at the St-Lambert Test Site in Canada. This site is known for its strong contrasts between K_v and K_h, reaching up to two orders of magnitude on a decimetric scale (Paradis and Lefebvre, 2013; Paradis et al., 2014). This highlights the interest in exploring the effectiveness of hydraulic tomography with periodic signals in highly heterogeneous (or anisotropic) aquifers.

In this proof-of-concept experiment on periodic tomography in an anisotropic aquifer, the head responses of a series of 10 periodic slug tests at 0.61-m intervals in a source well are described and analyzed. The head was recorded in the source interval itself and in 3 observation intervals in a nearby well. The periodic signal was generated by the movement of a rod in the source interval, with the amplitude and period numerically controlled by a winch. Three different periods were applied (150, 300 and 600 s). This resulted in 120 (3 periods x 10 tests x 4 intervals) recordings of head responses that could be analyzed. The heterogeneous fields of K_h, K_v/K_h and S_s were estimated by inversion using the Levenberg-Marquardt algorithm in combination with a groundwater flow model accounting for wellbore storage. The tomography experiments with different period were analyzed individually and together. Inverted tomograms were also verified by a cross-verification procedure and the simulation of conventional slug tests carried out in a tomographic arrangement to assess the information content of the different periods. The estimation of K_v/K_h from hydraulic tomography experiment with periodic tests was also explored.

2.2 Test site

The test site is located at Saint-Lambert-de-Lauzon, 40 km south of Quebec City (Canada). This site has been extensively studied to support the development of varied aquifer characterization techniques (Dubreuil-Boisclair et al., 2011; Gloaguen et al., 2012; Gernez et al., 2019; Paradis and Lefebvre, 2013; Paradis et al., 2011; Paradis et al., 2014; Paradis et al., 2015; Paradis et al., 2016; Ruggeri et al., 2014; Tremblay et al., 2014). The aquifer is made up of unconsolidated Late Quaternary sediments deposited in the Champlain Sea, an arm of the Atlantic Ocean that invaded the St. Lawrence Valley at the end of the last glaciation. Due to the changing energy levels along the shores of the Champlain Sea, this littoral and sublittoral sedimentary environment is characterized by overlapping thin layers of sand and silt (Bolduc, 2003; Parent and Occhietti, 1988) (Figure 2-1). These sediments typically exhibit poor to very poor grain size sorting and

frequent transitions in sediment composition. Figure 2-2 compares the vertical hydraulic conductivity K_v measured in the lab on 0.15 m long sediment samples to the horizontal hydraulic conductivity K_h obtained from slug tests between packers covering the same intervals. The figure shows that these rapid vertical variations in sediment grain size have led to heterogeneous and severely anisotropic conditions. The values of K_v/K_h for small 0.15 m intervals vary from 1 (isotropic condition) to very anisotropic conditions with values as low as 0.01 (two orders of magnitude difference between K_v and K_h).

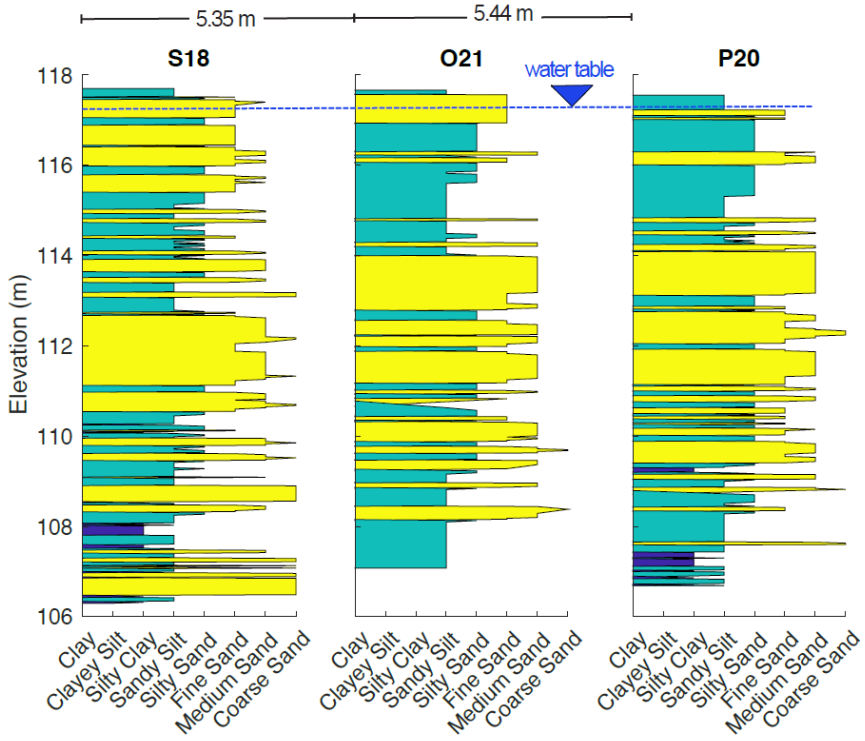

Figure 2-1 : Synthetic lithologic profiles derived from the mechanical properties of cone penetrometer soundings illustrating the heterogeneity of the test site (Paradis et al. 2014). Soundings were taken at the exact same locations where the wells were installed.

Previous field tests by Paradis and Lefebvre (2013) and Paradis et al. (2016) have shown that this anisotropy can be estimated using vertical interference tests obtained from slug tests between packers in a single well or between wells in a tomographic configuration. The granular, semi-confined aquifer is up to 20 m thick (12 m at the test site) and has an impermeable base made up of a glaciomarine diamicton. The shallow water table is less than 1 m below the land surface.

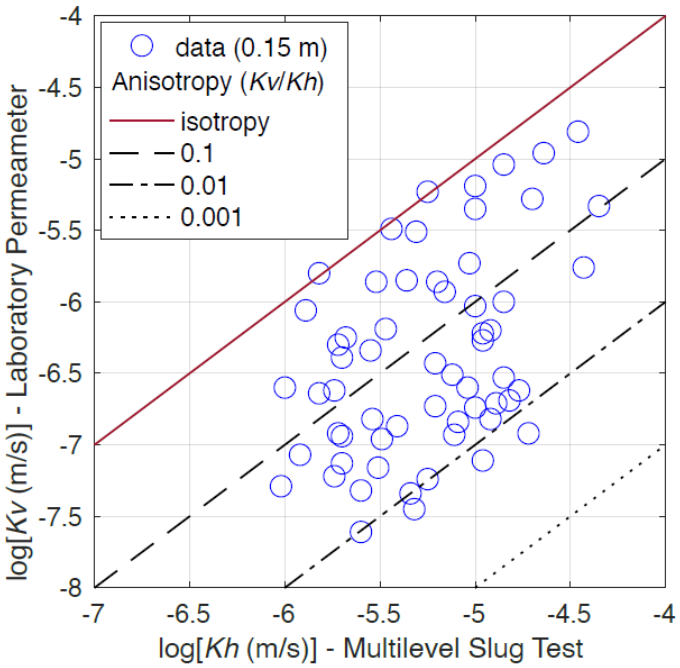

Figure 2-2 : Comparison of horizontal hydraulic conductivity (Kh) estimated using multilevel slug tests with vertical hydraulic conductivity (Kv) estimated on sediment samples using lab permeameter tests as described by Paradis et al. (2014). The length of the test intervals for slug tests and soil samples was 0.15 m. The intervals and samples were at the same depth, with well and sediment sample locations within 1 m of each other. Data was collected at various locations in the study area, including the tomography test site.

2.3 Test equipment and procedures

2.3.1 Direct-push wells

Figure 2-3 shows the spatial arrangement of wells S18 and O21 used for the field experiment. The wells are screened over the entire saturated thickness of the aquifer. They were installed without sand packs (screens in direct contact with the natural sediments) using direct-push equipment according to the protected screen method (Paradis et al., 2011). The diameter of each well is 0.051 m with a screen length of 7.6 m. Before the experiment, the wells were developed with an inertial pump and a surge block to ensure that the screens were free of sediment deposits.

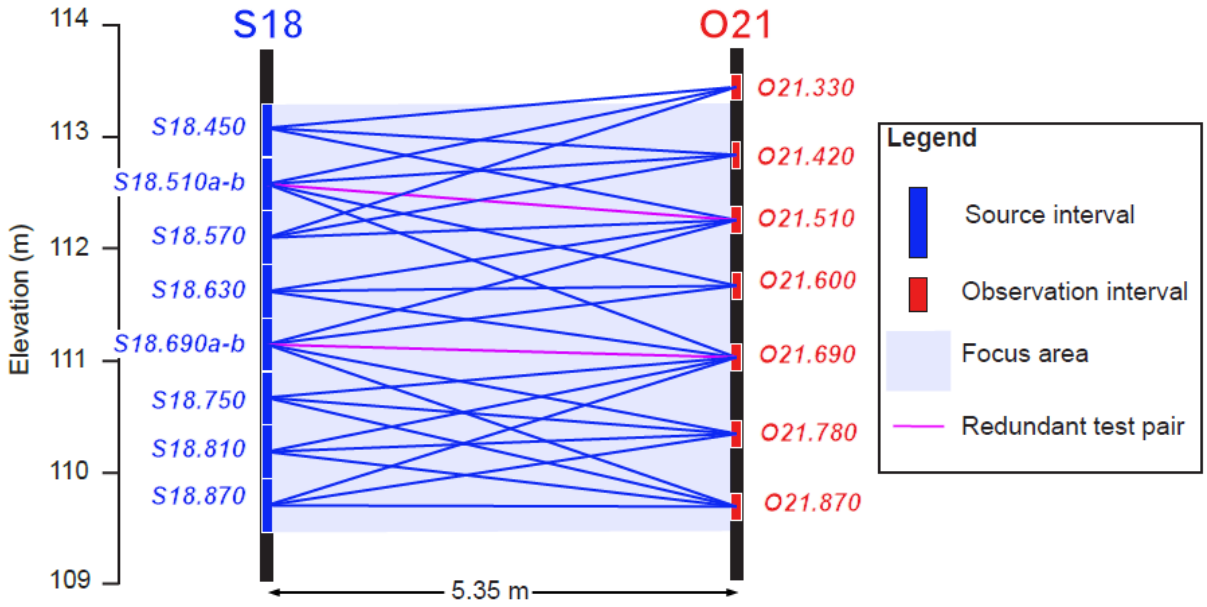

Figure 2-3 : Spatial arrangement of wells at the test site. Configuration of the source and observation intervals (blue lines) used for the tomography experiments between the source well S18 and the observation well O21. The suffixes after the well names indicate the depth of the top of the screens in centimeter with respect to the well collar. The designations S18.510a-b and S18.690a-b indicate that these intervals were tested twice with different configurations of the observation intervals in O21.

2.3.2 Packer system and pressure loggers

To increase flexibility in the design of the experiment, inflatable low-pressure packers and screens with threaded tubes were made. This design allows the length of the screens between the packers to be adjusted to accommodate different experimental setups. A double packer arrangement with 0.61 m long packers was used to isolate 0.61 m long source intervals along S18 (Figure 2-4a). This assembly was connected to the surface via a riser tube into which the periodic source was immersed (see Section 2.3.3). In O21, an arrangement of four packers was set up to isolate three observation intervals, each 0.30 m long and 0.91 m apart (center to center) (Figure 2-4a). To reduce data collection time, the packer arrangement in O21 was moved every three tests in S18. After each packer arrangement movement in the source or observation wells, there was a rest period until the head had stabilized.

A network of pressure loggers (Solinst Levelogger 3001 with a scale of 10 m and a resolution of 0.006 m) was installed in the source interval and in the three observation intervals. The logger in the source interval was placed inside the screen (“fixed logger” in Figure 2-4a) to ensure that the

head loss due to turbulence or friction along the riser tube did not affect the measurements (e.g., Hommersen et al., 2021). However, analysis of the heads measured in the source screen together with those measured by another logger at the lower end of the rod ("moving logger" in Figure 2-4a) revealed no significant head loss. The clocks of the pressure loggers were synchronized at the beginning of each day and a sampling rate of 1 Hz was used to record head data.

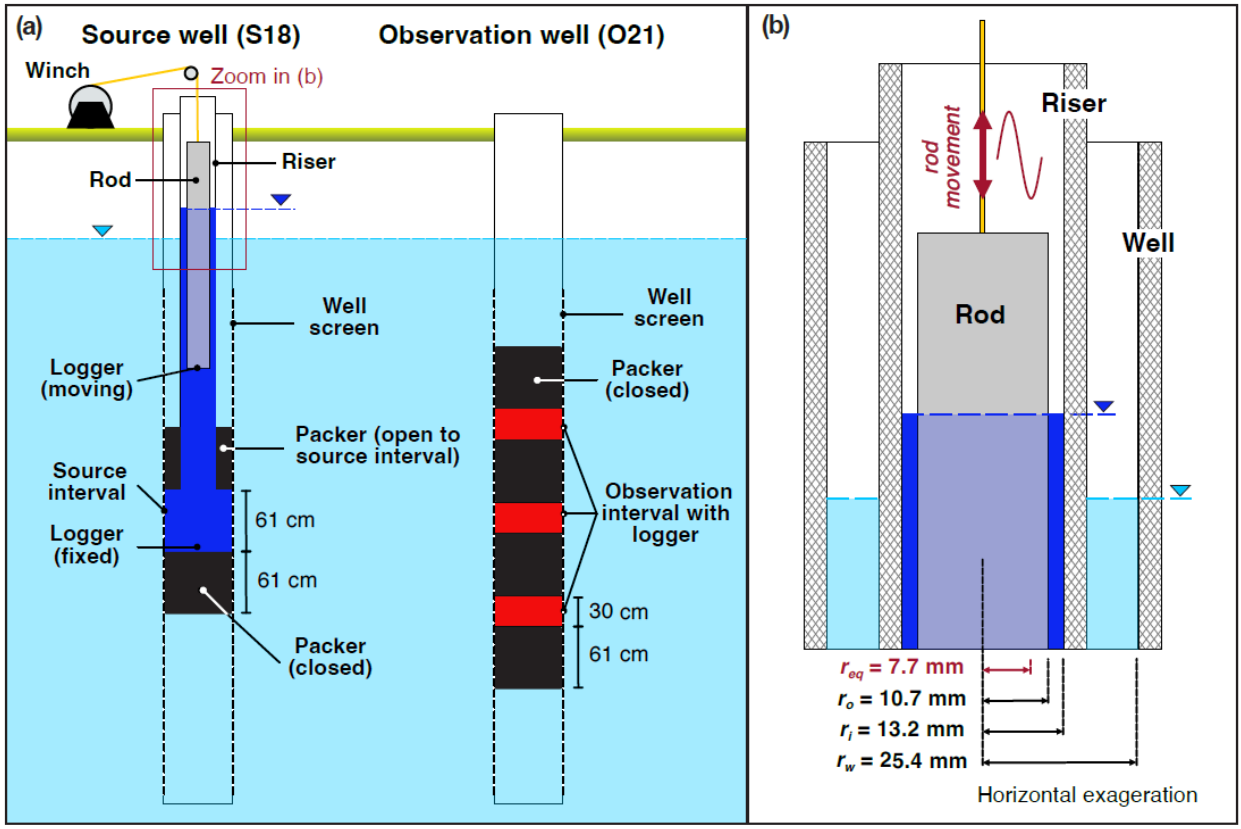

Figure 2-4 : (a) Schematic representation of the packer configurations used for the tomography experiments. (b) Cross-section of the source well, riser tube and rod arrangement with their corresponding radius.

2.3.3 Periodic source

The periodic stimulation was performed with a 2.8 m long aluminum rod immersed in the riser tube. The rod was attached to a winch that was numerically controlled (Figure 2-4a). Moving the rod upwards is like pumping water out of the riser, whereas lowering the rod is like injecting water. A similar setup was used by Becker and Guiltinan (2010) and Guiltinan and Becker (2015). The diameter of the rod was chosen to maximize the volume of water displaced for the tests while ensuring that the water could move freely between the rod and the inside of the riser tube (Figure 2-4b). Before starting a test, the rod was semi-submerged, and a computer program was used to

control the amplitude and period of the vertical movement. The amplitude of the rod displacement was adjusted for each test (Table 2-1) to ensure that the water level fluctuations always occurred within the annular space between the rod and the riser tube (i.e., no dewatering or flooding of the rod). Three different periods were used for the source signal: 150, 300 and 600 s. These periods were chosen to obtain maximum head variations in the observation intervals. The tests were performed by running the three periods in each source interval sequentially, with a rest period between each period. At least three cycles were performed for each period. The displacement of the rod was monitored and used to calculate the flow induced in the well for each test (see Section 2.4.4).

2.3.4 Field experiment description

The entire field experiment consisted of a series of three tomography experiments between S18 and O21 with the three different periods (Figure 2-3). The distance between the wells is 5.35 m. Each tomography experiment comprised 10 periodic slug tests performed in 8 source intervals in S18, with the head recorded in the source interval itself and in three observation intervals in O21 (Table 2-1). Source intervals S18.510 and S18.690 in S18 were tested twice with a different configuration of observation intervals in O21. Tests were conducted along S18 at successive intervals of 0.61 m with three observation intervals in O21 every 0.91 m (center to center). A total of 120 head responses (3 periods x 10 tests x 4 intervals) were available for analysis.

Table 2-1 : Description of periodic tests with corresponding sources and observation intervals, test periods, and peak amplitudes corresponding to the displacement of the rod (A0). Positions of tested intervals is shown in Figure 2-3. The bold observation intervals indicate redundant tests.

Interval				Period (s)		
				150	300	600
Source	Observation			A_0 (m)		
S18.450	O21.330	O21.420	O21.510	0.85	1.10	1.10
S18.510b	O21.330	O21.420	O21.510	1.00	1.25	1.25
S18.510a	O21.510	O21.600	O21.690	1.00	1.25	1.25
S18.570	O21.510	O21.600	O21.690	1.00	1.25	1.25
S18.630	O21.510	O21.600	O21.690	1.25	1.25	1.25
S18.690b	O21.510	O21.600	O21.690	1.25	1.25	1.25
S18.690a	O21.690	O21.780	O21.870	1.25	1.25	1.25
S18.750	O21.700	O21.790	O21.880	1.25	1.25	1.25
S18.810	O21.700	O21.790	O21.880	1.25	1.25	1.25
S18.870	O21.690	O21.780	O21.870	0.75	0.75	0.75

2.4 Description and processing of the data set

2.4.1 Head data

The time and head for each of the 120 head responses was extracted from the raw logger data. Each head recording was referenced to the start time of the corresponding test and normalized relative to the static head prior to the start of the test (e.g.,Figure 2-5). The periodic signal was then corrected to eliminate the influence of incomplete stabilization with the ambient head. This was only observed for a few observation intervals after the packers had been inflated in less permeable material. For these intervals, a linear equation representing the global deviation was fitted to the measurements and then subtracted from them to obtain only the periodic component of the signal (e.g. Fischer et al., 2020). No correction was required for the source intervals. Table 2-2 summarizes the head recordings extracted for the field experiment. It can be observed that the variation of the head for the source intervals is between 0.126 and 1.386 m (H0 in Table 2-2), while the variations for the observation intervals are between 0.001 and 0.0189 m (h0 min and h0

max in Table 2-2). The comparison of the head between the source and the observation intervals indicates a strong attenuation of the head in the aquifer.

Table 2-2 : Signals and responses of the periodic tests with the peak amplitude corresponding to the displacement of the rod (A0), the equivalent variation of the head induced by the rod in the source interval (Aeq), the variation of the head measured in the source interval (H_0), and the maximum (h_0 max) and minimum (h_0 min) heads measured in the observation intervals. A_{eq} is defined by Equation (2.7).

Test	Period (sec)	Peak amplitude (m)					H_0/A_{eq}
		Rod		Interval			
				Source	Observation		
		A_0	A_{eq}	H_0	h_0 max	h_0 min	
S18.450	150	0.85	1.63	1.3855	0.0060	0.0010	0.85
	300	1.10	2.11	1.3379	0.0091	0.0028	0.63
	600	1.10	2.11	0.8262	0.0084	0.0015	0.39
S18.510b	150	1.00	1.92	1.3402	0.0087	0.0017	0.70
	300	1.25	2.40	1.0850	0.0130	0.0017	0.45
	600	1.25	2.40	0.5924	0.0116	0.0014	0.25
S18.510a	150	1.00	1.92	1.3238	0.0089	0.0014	0.69
	300	1.25	2.40	1.0874	0.0131	0.0017	0.45
	600	1.25	2.40	0.5956	0.0102	0.0012	0.25
S18.570	150	1.00	1.92	1.1600	0.0095	0.0019	0.60
	300	1.25	2.40	0.8716	0.0114	0.0026	0.36
	600	1.25	2.40	0.4495	0.0089	0.0021	0.19
S18.630	150	1.25	2.40	0.6820	0.0155	0.0023	0.28
	300	1.25	2.40	0.3261	0.0112	0.0020	0.14
	600	1.25	2.40	0.1631	0.0088	0.0022	0.07
S18.690b	150	1.25	2.40	0.4498	0.0189	0.0017	0.19
	300	1.25	2.40	0.2411	0.0136	0.0014	0.10

	600	1.25	2.40	0.1260	0.0086	0.0017	0.05
S18.690a	150	1.25	2.40	0.4606	0.0171	0.0057	0.19
	300	1.25	2.40	0.2336	0.0131	0.0060	0.10
	600	1.25	2.40	0.1274	0.0096	0.0074	0.05
S18.750	150	1.25	2.40	0.6995	0.0063	0.0061	0.29
	300	1.25	2.40	0.3687	0.0060	0.0058	0.15
	600	1.25	2.40	0.1925	0.0042	0.0042	0.08
S18.810	150	1.25	2.40	1.2747	0.0054	0.0052	0.53
	300	1.25	2.40	0.7584	0.0057	0.0057	0.32
	600	1.25	2.40	0.4065	0.0047	0.0047	0.17
S18.870	150	0.75	1.44	1.2199	0.0036	0.0016	0.85
	300	0.75	1.44	1.1597	0.0064	0.0024	0.80
	600	0.75	1.44	0.6864	0.0069	0.0056	0.48

Figure 2-5 shows examples of head recordings in the source interval and the three observation intervals for test S18.630 for the three periods. Several observations can be derived from the data. First, while the variation of the displacement of the rod is the same for all periods (A_0=1.25 m in Table 2.1), the variation of the head in the source interval decreases with the length of the period. The variation for the period of 600 s is less than a quarter of the variation for the period of 150 s. This is explained by the fact that the slower the displacement of the water column in the riser (e.g., period of 600 s), the more water is exchanged with the aquifer and the less is stored in the borehole (Paradis et al. 2024). Second, the variation of the head for the observation intervals is similar for all periods, although the head in the source interval is much larger for the shortest period. This illustrates the concept of attenuation of head in aquifers, which is more significant for shorter periods (e.g., Ferris, 1952). When planning periodic slug tests, wellbore storage and aquifer attenuation must therefore be considered. Finally, it is noted that the head for the intervals O21.690 and O21.600, which are 0.91 m apart as shown in Figure 2-3, show similarities. However, a comparison of the amplitudes and phase shifts between O21.600 and O21.510, which are also 0.91 m apart, shows clear differences. This indicates strong contrasts in the hydraulic properties between the two pairs of intervals.

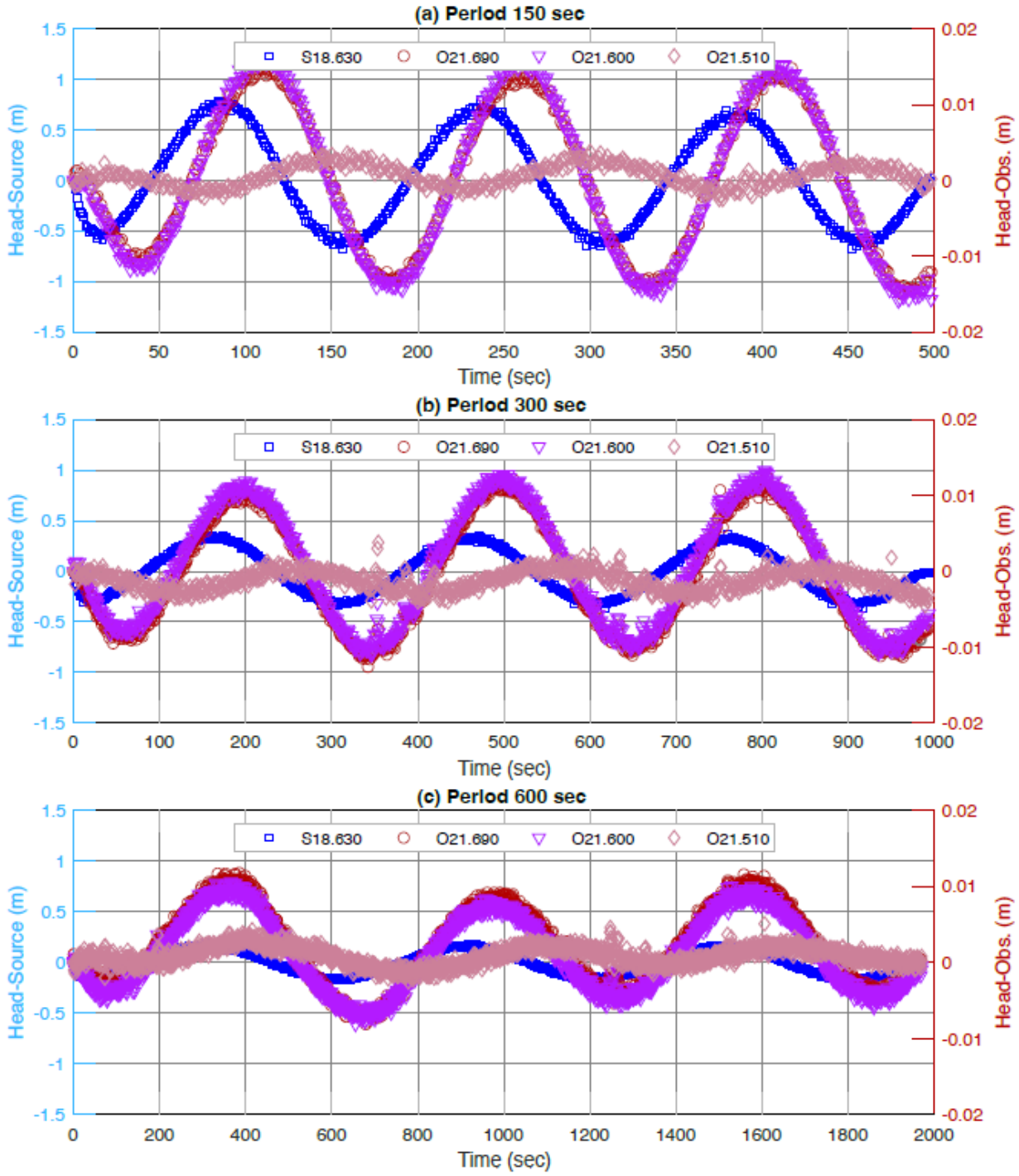

Figure 2-5 : Example of head recordings in the source interval and the three observation intervals for test S18.630 for periods of: (a) 150 s; (b) 300 s; and (c) 600 s. The head represents the variation of the head with respect to the static head measured before each test.

To reduce the computation time of the numerical inversions, the original 1 Hz head measurements were subsampled to 15 points per cycle (Figure 2-6). First, a moving average with window sizes

of 10, 20 and 40 s were applied to tests with periods of 150, 300 and 600 s, respectively. The head values in the middle of these time windows were then selected to represent the average head at intervals of 10, 20 or 40 s.

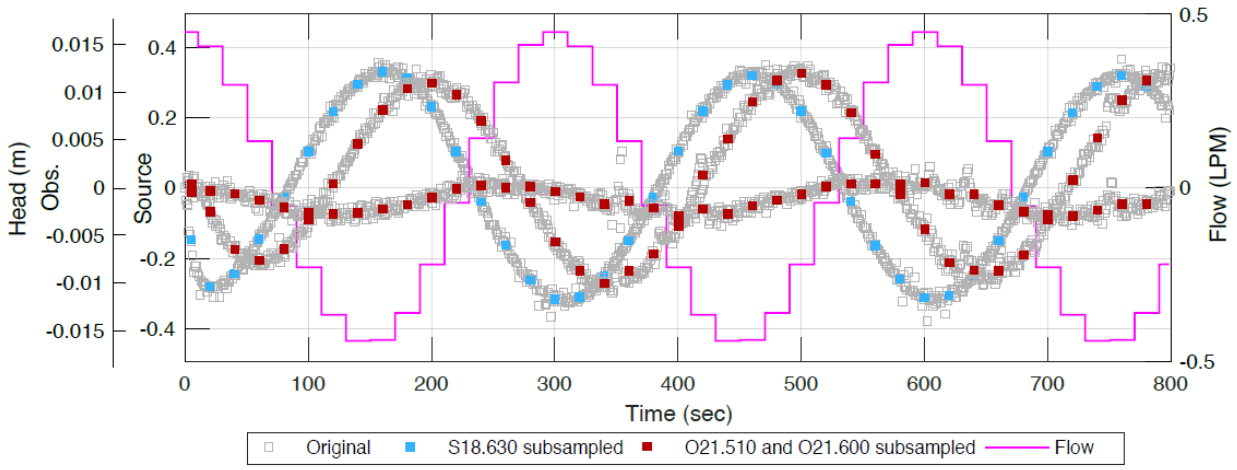

Figure 2-6 : Examples of subsampled head recordings for the source interval S18.630 and two observation intervals (O21.510 and O21.600) for the period of 300 s in relation to the original measurements. An example of a step function representing the modeled flow induced by the rod (Q in liters/minute-LPM) for the numerical simulation is also shown. A positive flow indicates that pumping is taking place (or that the rod is moving upwards).

2.4.2 Noise level

The noise level of the head data was assessed by fitting a sinusoidal curve to the original head measurements (Figure 2-7). The fit was applied to a complete cycle after the early transient effect had disappeared. The noise level is expressed as the standard deviation of the residual between the sinusoid and the measurements. Figure 2-7 shows that the noise level in the source interval is higher than in the observation intervals. The noise level also remains constant across the observation intervals, regardless of the variation of the head. For example, the intervals O21.690 and O21.600, which have four times the amplitude of O21.510, have similar standard deviations.

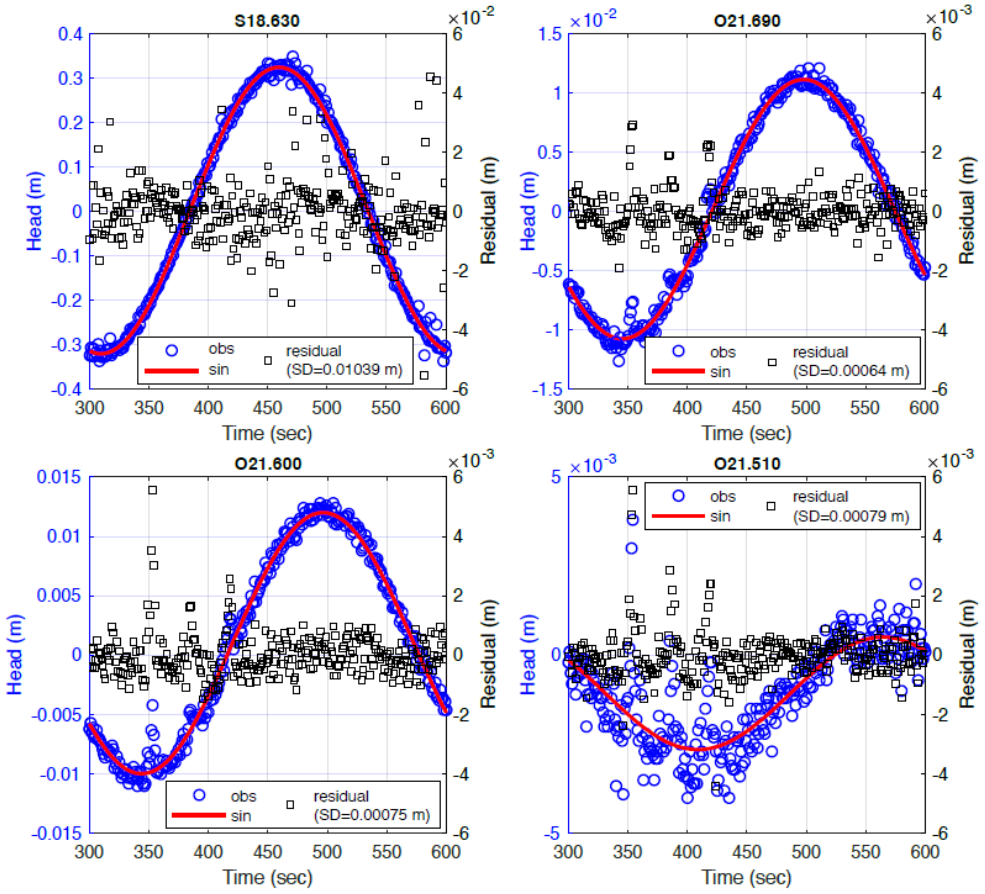

Figure 2-7 : Example of noise level estimation using field data for test S18-630 with a period of 300 s at the source interval (S18.630) and three observation intervals (O21.690, O21.600, and O21.510). The standard deviation (SD) of the residuals is given in the legend.

Figure 2-8 and Table 2-3 also show that the noise level in the source intervals is larger for the shortest period. This is due to the faster movement of the rod at shorter periods, which causes more turbulent flow in the annular space between the rod and the riser tube (Figure 2-4b). For the observation intervals, the noise level is similar for all periods and depends only on the precision of the pressure loggers used for the experiment. It is unlikely that the noise generated in the source intervals will be transferred to the observation intervals, as the head in the aquifer is strongly attenuated. The median standard deviation of the noise level for the source intervals is 3.1×10^{-2}, 1.4×10^{-2}, and 8.6×10^{-3} m for the periods of 150, 300, and 600 sec, respectively. For the observation intervals, the noise level ranges from 4.9×10^{-4} to 5.3×10^{-4} m. Although the variation of the head in the observation intervals is small (Table 2-2), the experiment provided head data with a high signal-to-noise ratio, indicating excellent data quality.

Table 2-3 : Median standard deviation (SD) of the residual between a sinusoid and the original head measurements recorded at 1 sample per second. The SD of the subsampled head used for the inversion is also provided. The amount of data for the subsampled data set is the same for all periods and corresponds to 15 measurements per cycle. The median is obtained from the SD of the residuals for all individually evaluated source and observation intervals.

Period (s)	Median SD of the residual (m)			
	Original (1/s)		Subsampled (15/cycle)	
	Source	Obs.	Source	Obs.
150	3.1×10^{-2}	4.9×10^{-4}	2.6×10^{-2}	1.8×10^{-4}
300	1.4×10^{-2}	5.3×10^{-4}	5.9×10^{-3}	1.8×10^{-4}
600	8.6×10^{-3}	5.2×10^{-4}	1.9×10^{-3}	1.4×10^{-4}

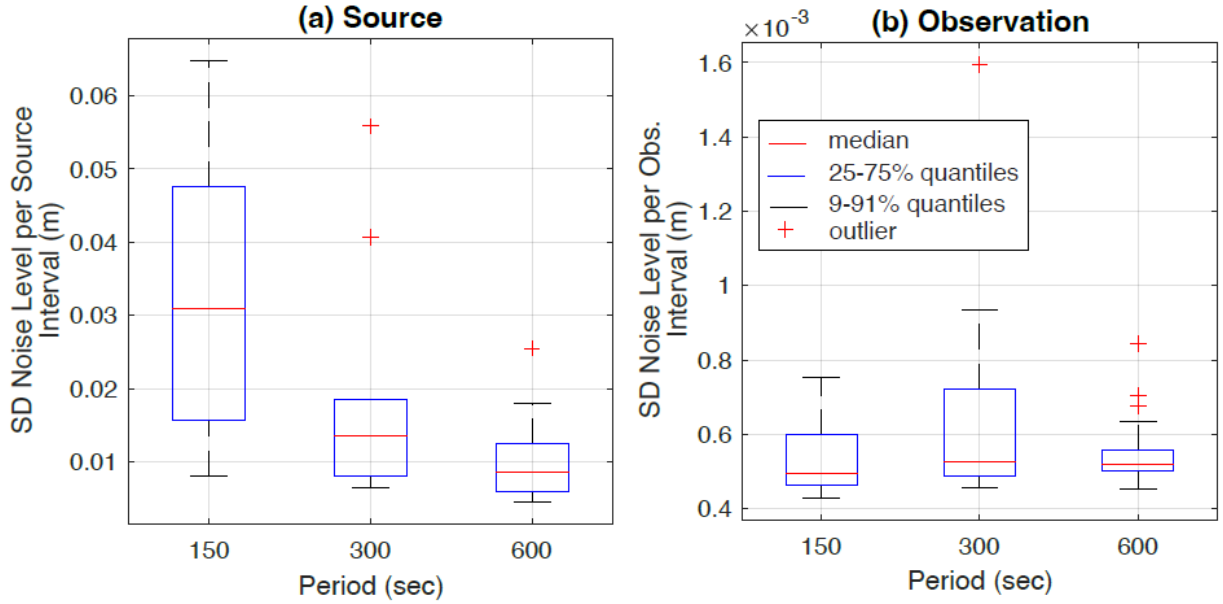

Figure 2-8 : Statistical distribution of the standard deviation of the noise level (residual between the sinusoid and the measurements) per period for the (a) source and the (b) observation intervals. The statistical distributions are determined from the residuals for all individually evaluated source and observation intervals.

2.4.3 Test redundancy

To validate the reproducibility of the head recordings, redundant tests were incorporated into the experiment (Figure 2-2 and Table 2-1). For example, the test S18.510a was performed with O21.510 as the lower observation interval of the packer arrangement in O21. After the packer arrangement in O21 was moved down, test S18.510b was performed with O21.510 as the upper intervals of the arrangement. The same was done for S18.690a-b and O21.690. Figure 2-9 shows the redundant head recordings, which demonstrate the excellent reproducibility of the tests.

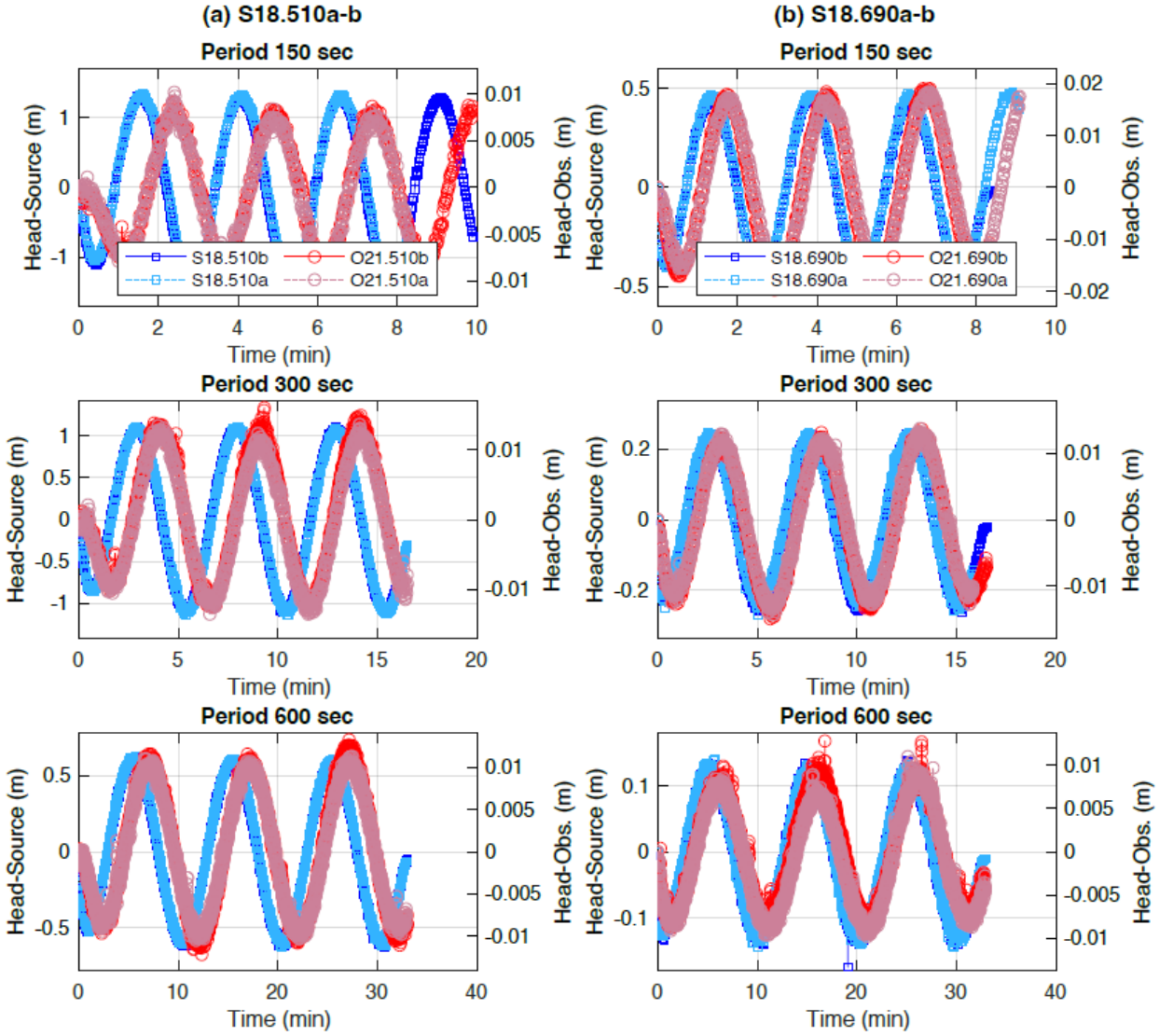

Figure 2-9 : Comparison of the head records for redundant observation intervals (a) O21.510 and (b) O21.690 for tests S18.510a-b and S18.690a-b, respectively.

2.4.4 Calculation of the periodic flow rate

To simulate the periodic tests, the volume of water displaced into the riser tube by the movement of the rod is calculated (Figure 2-4). The periodic change in the volume of water Q at each time t is calculated using the following formula:

$$Q = \frac{2A_0 r_o^2 \pi^2}{T_0} \cos\left(\frac{2\pi}{T_0} t\right) \tag{2.1}$$

where r_o is the radius of the rod, A_0 the peak amplitude of the displacement of the rod and T_0 the period of the signal. A sinusoidal displacement of the rod is assumed here; therefore Equation (2.1) is the derivative of the sinusoidal displacement ($A_0 \sin\left(\frac{2\pi}{T_0} t\right)$) multiplied by the cross-section of the rod (πr_o^2).

For the simulations, Q is approximated as a series of steps, where each step is modeled as a constant flow boundary condition with a start and end time (Figure 2-6). The number of steps corresponds to the number of measurements of the subsampled head recordings with a measurement in the middle of each flow rate step.

2.5 Simulation of the tomography experiments

The numerical inversion of each tomography experiment was performed using a parallelized version of the lr2dinv simulator (Bohling and Butler, 2001) modified by the authors. In the lr2dinv simulator, a forward radial groundwater flow model is coupled with the Levenberg–Marquardt algorithm to simultaneously estimate the spatial distribution of K_h, K_v/K_h, and S_s. The radial groundwater flow equation is solved using a block-centered finite-difference formulation after a logarithmic transformation of the radial flow equation to an equivalent equation in Cartesian coordinates (Butler and McElwee, 1995; Bohling and Butler, 2001). The Levenberg-Marquardt algorithm is a hybrid approach that combines the gradient descent and the Gauss-Newton methods to iteratively solve nonlinear least squares parameter estimation problems (Marquardt, 1963; Press et al., 1992). A series of four simulations were run, with three independent inversions for each of the periods and a fourth combining data from the three periods (Table 2-4). The same model structure was used for all simulations. The next sections describe the development of the numerical model applied to the inversion of the experiment data.

Table 2-4 : Simulation program for the inversion of the tomography experiments with different periods. Note that the final hydraulic parameters obtained from the inversion of the homogeneous model (a) are used as initial parameters for the heterogeneous model (b).

Inversion	Period (sec)	Number of test (interval)	a-Homogeneous model for all tests (1 zone)		b-Heterogeneous model for all tests (104 zones)	
			Hydraulic parameters			
			Initial	Final	Initial	Final
1a-b	150	10 (40)	K_h 1×10^{-5} ms^{-1} K_v/K_h 1×10^{-1} S_s 1×10^{-5} m^{-1}	K_h 1.10×10^{-5} ms^{-1} K_v/K_h 1.23×10^{-1} S_s 4.74×10^{-5} m^{-1}		Fig. 2-15a
2a-b	300	10 (40)		K_h 1.19×10^{-5} ms^{-1} K_v/K_h 8.15×10^{-2} S_s 6.88×10^{-5} m^{-1}		Fig. 2-15b
3a-b	600	10 (39)		K_h 1.18×10^{-5} ms^{-1} K_v/K_h 6.09×10^{-2} S_s 8.00×10^{-5} m^{-1}		Fig. 2-15c
4a-b	combi: 150, 300 and 600	30 (119)		K_h 1.18×10^{-5} ms^{-1} K_v/K_h 8.80×10^{-2} S_s 6.12×10^{-5} m^{-1}		Fig. 2-15d

2.5.1 Simulation and parameter grids

All inversions used a simulation grid consisting of 43 cells with an exponentially increasing width along the radial axis and 34 cells with a constant height of 0.30 m along the vertical axis (Figure 2-10a). The width of radial cells is smaller near the source well to better simulate the higher hydraulic gradients in this zone. The simulation grid was designed to match the locations of the packers and screens used for the field experiment. Thus, the packers and source intervals vertically comprise two simulation cells, while the observation intervals are represented by a single cell. The observation well, 5.35 m from the source well, is also placed directly on the nodes of the simulation grid.

The choice of parameter grid cell size was made iteratively by testing several configurations (14, 32, 52, 56, 104, 156, and 187 zones) to find a balance between resolution and computational time.

The simulation grid is overlaid with a parameter grid including 13 layers (numbered L1 to L13 in Figure 2-10a) and 8 columns (C1 to C8). Layers L2 to L12 have a thickness of 0.61 m to correspond to the length of the source intervals, while the layers above and below the tested zone were made thicker. Along the horizontal, the parameter grid consists of seven columns between the source and observation wells (C1 to C7), with an average width of 1.0 m. The width of columns is variable to adapt them to the simulation grid, which has an exponentially increasing size. A larger column of 54.85 m width is used beyond the observation well to average the influence of the hydraulic properties outside the tested zone. The same discretization of the parameter grid is used for K_h, $K_v/K_{h,}$ and S_s.

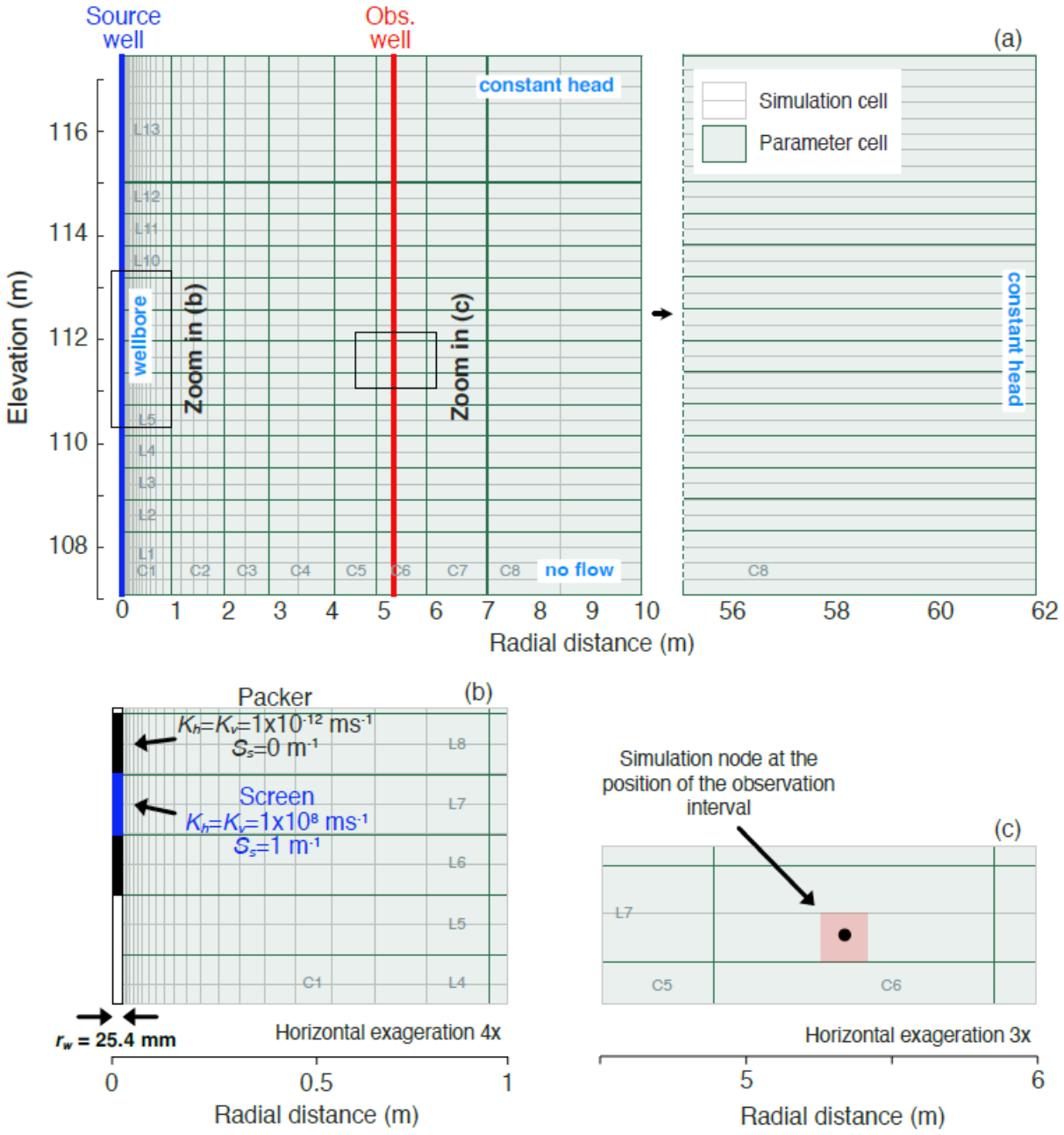

Figure 2-10 : (a) Simulation and parameter grids used for the inversion of the tomography experiments with the relative locations of the wells and boundary conditions. (b) Close-up at the source well showing the position and hydraulic properties of the packers and the screen (packers and screens are integrated in the model). (c) Close-up around the observation well at the position of an observation interval (packers and screens are not explicitly integrated in the model).

2.5.2 Boundary and wellbore conditions

To accurately simulate the variation of the head measured by the logger located in the screen of the source intervals ("fixed logger" in Figure 2-4a), the annular space between the rod and the riser tube is converted to a corresponding radius. The equivalent radius r_{eq} is obtained using the following formula:

$$r_{eq} = \sqrt{\left(r_i^2 - r_o^2\right)} \tag{2.2}$$

where r_i and r_o are the radii of the riser and the rod respectively (Figure 2-3b). The value of r_{eq} used by the simulator was 0.00772 m.

The outer boundary of the model, represented by a fixed head, was placed 49.5 m from the source well to avoid interference during the simulated tests (Figure 2-10a). The upper boundary is also a fixed head to approximate the position of the water table of the unconfined aquifer, which did not fluctuate significantly in response to the tests. The impermeable lower boundary has a zero-flux condition. The simulation of the effects of wellbore storage and packer placement in the source well is approximated using a formulation of Darcy's Law (Bohling and Butler, 2001), with the screen of the source interval modeled as a region of high permeability and the packers as essentially impermeable (Figure 2-10b). With this option, a column of model cells is used to represent the region inside the wellbore from the radius of the well, r_w, to the inner radius of the model grid ($< r_w$), with Q from Equation (2.1) placed at the inner radius. Thus, the water balance resulting from the flow rate Q induced by the movement of the rod is the sum of the flow represented by the change in storage related to the change in water level in the well Q_w and the flow exchanged with the aquifer Q_a :

$$Q = Q_w + Q_a = \pi r_{eq}^2 \frac{\partial h}{\partial t} + 2\pi r_w L K_h \frac{\partial h}{\partial r} \tag{2.3}$$

where $\frac{\partial h}{\partial t}$ is the change in water level in the source interval, L is the length of the source interval, and $\frac{\partial h}{\partial r}$ is the radial hydraulic gradient at the interface between the screen and the aquifer. Wellbore properties are given separately for each test to account for the repositioning of the double packer arrangement in the source well. Note that without the wellbore option, Q_a must be used instead of Q because the amplitude of head and lag of responses in the simulated aquifer may not accurately represent field measurements. This exchange flow rate Q_a can be estimated using Equation (2.3) (e.g. Equation 1 in Cheng and Renner, 2018). Wellbore storage in the

observation intervals was neglected as packers were isolating the screens (Sageev, 1986). The average head of the nodes that coincide with the observation intervals represents the head in these intervals (Figure 2-10c).

2.5.3 Inversion strategy

The strategy for inversion of heads from the tomography experiments involved first creating an initial model of hydraulic parameters **p** of the aquifer with preliminary estimates for K_h, K_v/K_h, and S_s. The initial model for each heterogeneous simulation (simulations b in Table 2-4) was obtained from the inversion of a homogeneous model using all tests associated with the simulation (simulations a in Table 2-4). These initial models with different values of K_h, K_v/K_h, and S_s for each model represent the "effective hydraulic properties" of the aquifer. This strategy facilitated the search for the optimal solutions. The groundwater flow simulator was then used to perform a forward simulation to predict the head based on the initial model, and the residuals between the measured heads h_i and the heads predicted by the simulation $f_i(\mathbf{p})$ were calculated.

The Levenberg-Marquardt algorithm was then used to iteratively adjust the hydraulic parameters to minimize the residuals according to the following chi-squared objective function:

$$\chi^2 = \sum_{i=1}^{n} \left(\frac{h_i - f_i(\mathbf{p})}{\sigma_i} \right)^2 \tag{2.4}$$

where σ_i is a scaling factor associated with each measurement. Scaling factors were used to weigh the objective function according to the relative magnitude in head for the source and observation intervals. This is necessary for fitting equally well the heads of the observation intervals, which are up to three orders of magnitude lower than the heads in the source intervals (Table 2-2). The scaling factors were determined by comparing the average variation of the head measured in the source and observation intervals (H_0 and h_0 max in Table 2-2). The same global scaling factors of 0.52 for source intervals and 0.0068 for observation intervals were used for all inversions. The minimization of the objective function was achieved using an implicit row-oriented directional line iteration method.

At each iteration, the sensitivity matrix **J** of the residuals with respect to the hydraulic parameters estimated at the current iteration was first calculated. The sensitivity matrix is an *i*-by-*j* normalized sensitivity matrix of *i* measurements and *j* hydraulic parameters, expressing the head response at each observation point and at each time to a change in each hydraulic parameter value:

$$J_{i,j} = \frac{1}{\sigma_i} \frac{\partial (h_i - f_i(\mathbf{p}))}{\partial p_j \Big/ \widehat{p_j}} \tag{2.5}$$

where $\widehat{p_j}$ represents the estimated value of the *j*th hydraulic parameter. This normalized form of the sensitivities is used to better identify the relative influence of each hydraulic parameter. The elements of the sensitivity matrix were evaluated using the sequential perturbation approach of a groundwater flow model developed with the lr2dinv simulator.

The hydraulic parameters were then updated at each iteration *k* using the Levenberg-Marquardt rule:

$$\mathbf{p}_{k+1} = \mathbf{p}_k - \left(\mathbf{J}^{\mathrm{T}}\mathbf{J} + \lambda \mathbf{I}\right)^{-1} \mathbf{J}^{\mathrm{T}}\mathbf{r} \tag{2.6}$$

where $\mathbf{r}$ is the vector of scaled residuals $\frac{h_i - f_i(\mathbf{p})}{\sigma_i}$ and λ is the damping factor that controls the interpolation between the gradient descent and Gauss-Newton methods. The algorithm dynamically adjusts λ to ensure a slow but stable solution when the hydraulic parameters are far from the optimal solution and faster convergence as they approach the optimal solution. This iterative process continued until convergence criteria were met that is a chi-squared error $<1\times10^{-8}$ or a change in hydraulic parameter values $<1\times10^{-3}$.

For each inversion listed in Table 2-4, all tests and intervals were processed simultaneously for the corresponding source signal period. The static initial condition before each test was simulated with a constant head of 0 m for the entire simulation grid, representing the relative head (change) from to the initial conditions. No model regularization was used in the minimization of the objective function, so that only the information contained in the measured heads is used to estimate the hydraulic properties.

2.6 Results and discussion

2.6.1 Analysis of the residuals

Table 2-5 summarizes the statistics of the residuals between observed and predicted head for the four inversion scenarios listed in Table 2-4. As observed in the analysis of the noise level, the standard deviation of the residuals for the source intervals is larger than for the observation intervals and decreases with the period. In the simulation that combines the three periods, the standard deviation is close to the average of the individual simulations. The standard deviation

for the observation intervals increases slightly with the period, whereby the value for the combined simulation is the highest. Overall, the standard deviation of the residuals is very small, considering that it is only 1.5 to 1.7 times the noise level estimated for the observation intervals (subsampled head data in Table 2-3) and 2.1 to 3.6 times for the source intervals. This difference is the result of cumulative errors or simplifications related to the field operations, data processing, model construction or numerical analysis.

Table 2-5 : Mean and standard deviation (SD) of the residuals for source and observation intervals for the four inversions. The standard deviation, the coefficient of determination (R2) and the slope of the linear regression (m) of the scaled residuals are also shown. The scaling factors for the scaled residuals are described in Section 2.5.3. The runtime is for an ARM-based M1 processor with 16 cores and a clock frequency of 3.2 GHz.

Inversion	Period (s)	Runtime (min)	Residuals				Scaled Residuals		
			Source		Observation		Source and Observation		
			Mean (m)	SD (m)	Mean (m)	SD (m)	SD (m)	R^2 (-)	m (-)
1b	150	102	-3.5×10^{-3}	6.6×10^{-2}	-3.7×10^{-4}	7.2×10^{-4}	3.3×10^{-2}	0.996	0.965
2b	300	80	-5.3×10^{-3}	4.8×10^{-2}	-2.0×10^{-4}	8.0×10^{-4}	2.4×10^{-2}	0.996	0.998
3b	600	91	-4.0×10^{-4}	3.1×10^{-2}	-1.2×10^{-4}	8.8×10^{-4}	1.6×10^{-2}	0.995	1.000
4b	combi	374	-7.0×10^{-4}	5.1×10^{-2}	-1.6×10^{-4}	9.4×10^{-4}	3.5×10^{-2}	0.990	0.980

Figure 2-11a provides additional insight into the effectiveness of the inversion process and shows a strong agreement between the measured and simulated head for the tomography experiment with a period of 300 s (Simulation 2b in Table 2-4). The amplitude and phase of the simulated head responses are also generally in very good agreement with the measurements (Figure 2-12). The coefficient of determination and the slope of the linear regression are above 0.96 for all tomography experiments (Table 2-5).

In addition, Figure 2-11a and Figure 2-11c illustrate the discrepancy in the quality of agreement that can be obtained relative to observations between a heterogeneous and a homogeneous model and thus emphasize the necessity to consider the heterogeneity of the test site to reproduce observations. The importance of using a model explicitly considering anisotropy can also be seen when comparing Figure 2-11a and Figure 2-11b. As shown in Figure 2-2, isotropic conditions cannot be assumed for measurement having a vertical resolution of 0.15 m, and the

range of anisotropy is quite variable. An anisotropic model can therefore better capture the effects of smaller scale heterogeneity on the heads. Figure 2-13 also shows that the contrast in K_h and Ss is stronger in the heterogeneous and isotropic model (Figure 2-13b) than in the heterogeneous and anisotropic model (Figure 2-13a) to compensate for the simplified hydrogeology of an isotropic model. Of course, the cells of the parameter grid could be reduced to a size at which isotropic conditions could be assumed. However, centimetric cell sizes would probably have been necessary for the study area, which would have led to an unacceptable computational effort given the enormous increase in the number of cells.

In summary, the analysis of the residuals shows that the inversion process accurately captured the general behavior of head responses influenced by heterogeneity. This is also remarkable considering the short simulation runtimes of about one and a half hours for the individual simulations (Table 2-5).

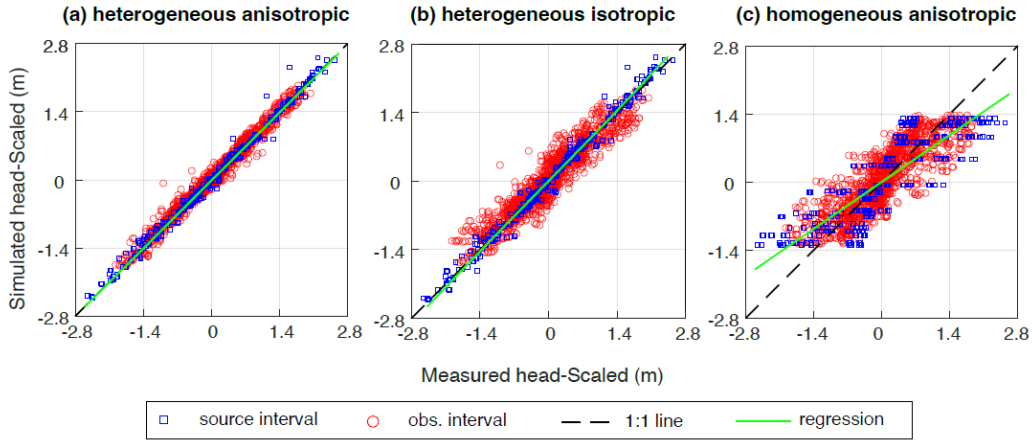

Figure 2-11 : Scatter plots of simulated versus measured heads for all tests of the inversion with the 300-sec period for a (a) heterogeneous and anisotropic model (2b in Table 2-4), (b) heterogeneous and isotropic model and (c) homogeneous and anisotropic model (2a in Table 2-4). The homogeneous model (c) was used to obtain the initial hydraulic properties of the heterogeneous and anisotropic model (a). Heads are scaled according to the scaling factors in Section 2.5.3.

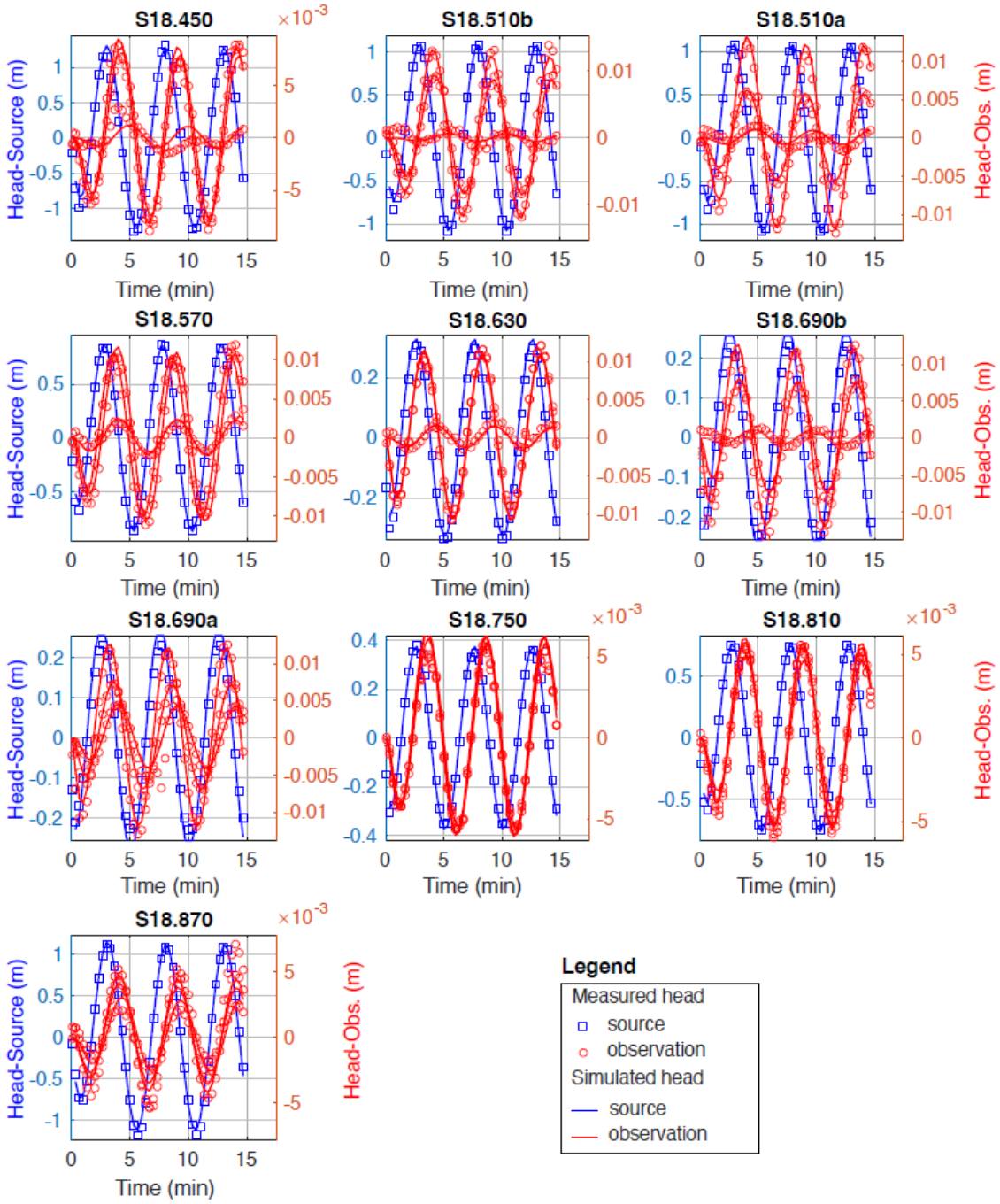

Figure 2-12 : Comparison of the measured and simulated heads for the inversion with the 300-sec period. Data from the intervals of the source (left) and the observation (right) are shown on different scales.

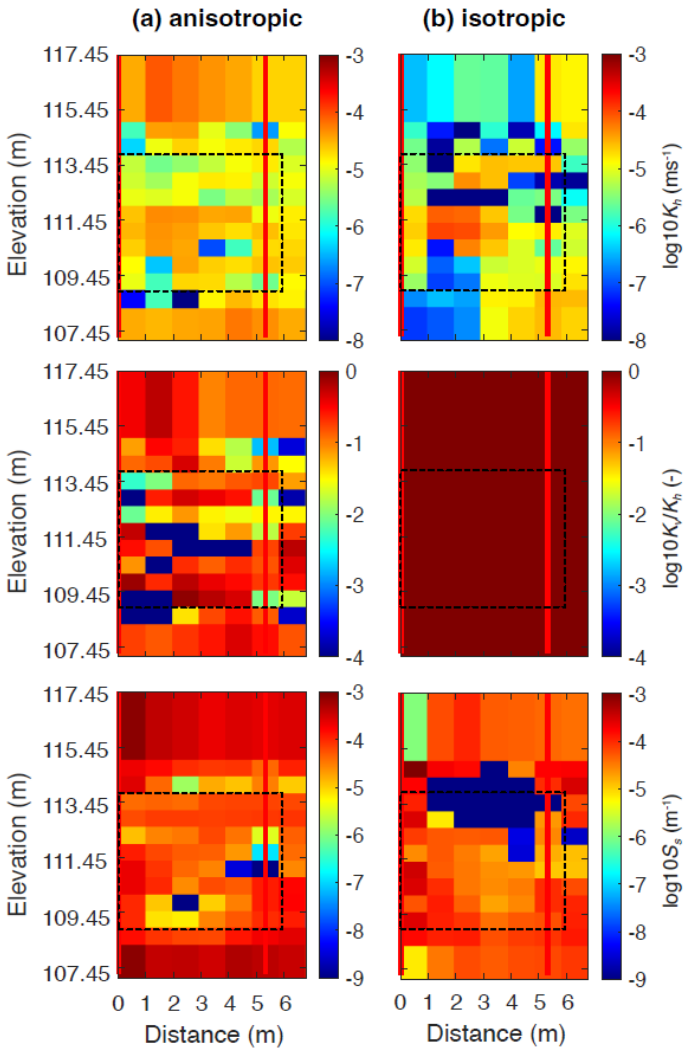

Figure 2-13 : Tomograms for Kh, Kv/Kh and Ss resulting from the inversion of the periodic tests with the 300-sec period under (a) anisotropic and (b) isotropic conditions. The same simulation and parameter grids were used for (a) and (b) (Figure 2-10), but the inversion of (b) was performed by fixing Kv/Kh=1. The rectangle outlined by a black dashed line is the focus area.

2.6.2 Profiles of hydraulic properties

Figure 2-14 shows the profiles of the hydraulic properties estimated by inversion along the source and observation wells for the four heterogeneous models listed in Table 2-4. Overall, the K_h and K_v/K_h profiles are similar for all simulations, with only a few intervals within the focus area showing significant deviations. The S_s profiles along the observation well also show similar trends for the individual periods but differ more significantly at the source well.

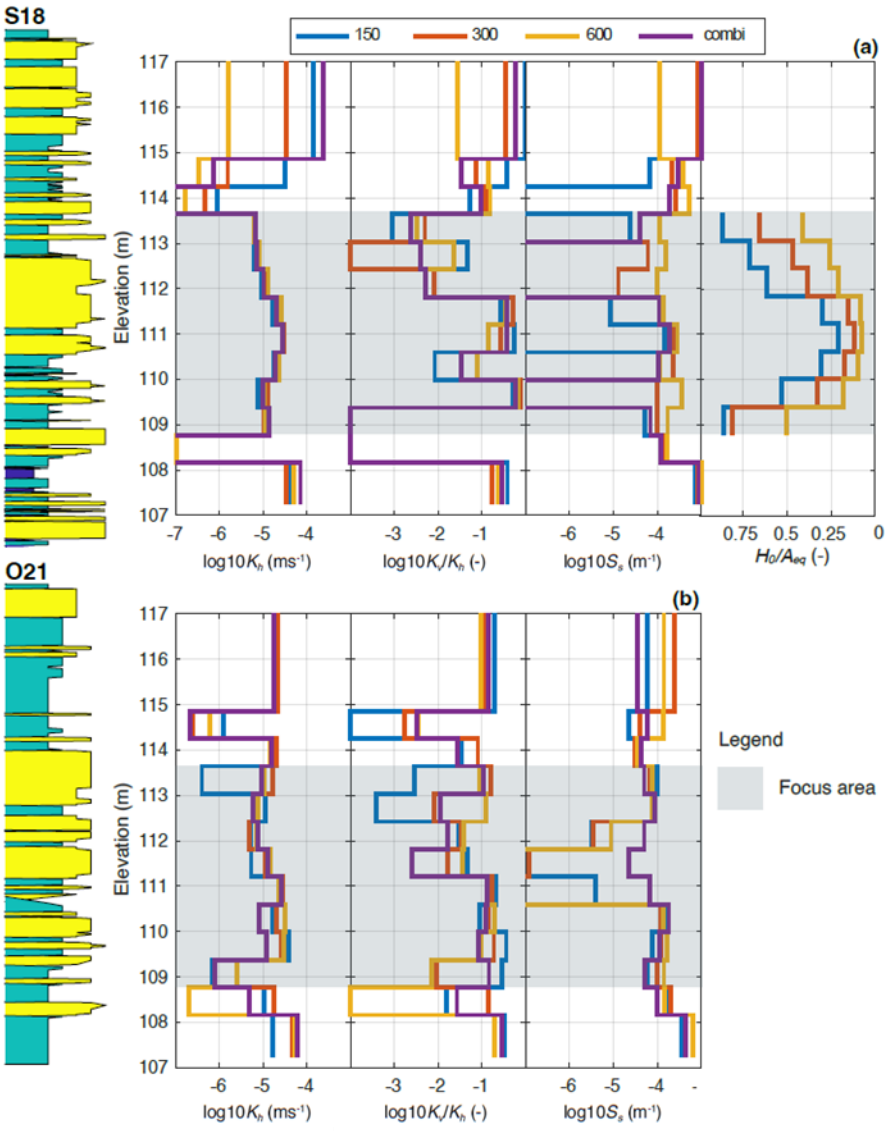

Figure 2-14 : Profiles of hydraulic properties obtained from the inversions of the four heterogeneous simulations in Table 2-4 with the synthetic geologic logs from cone penetrometer tests along the (a) source well and (b) observation well. The ratio of H_0/A_{eq} in Table 2-2 is also plotted along the source well. The legend of the geologic logs can be found in Figure 1. The focus area between the upper and lower intervals is highlighted in gray.

The ratio of H_0/A_{eq} in Table 2-2 is also plotted in Figure 2-14a for comparison. H_0 is the variation of the head measured in the source interval, while A_{eq} is calculated using the following equation:

$$A_{eq} = \frac{A_0 r_o^2}{r_{eq}^2} \tag{2.7}$$

A_{eq} thus represents the maximum variation of the head that could be achieved in the source interval for a given value of A_0 and with the specific radii r_o and r_{eq} of the experimental setup if there were no water exchange with the aquifer. A ratio of H_0/A_{eq} equal to 1 means that there is no water exchange between the well and the aquifer, while a ratio of 0 means all water flows into the aquifer. Figure 2-14a shows that the patterns of H_0/A_{eq} values (with inverted scale) and K_h are similar, but with different magnitudes of the ratios depending on the period of the source signal. This illustrates the control that K_h and the signal period exert on the volume of water that can be exchanged between the well and the aquifer.

Figure 2-14 also shows a limited agreement between the profiles of hydraulic properties and the grain size indications provided by cone penetrometer soundings. Although one might expect the maximum K_h values to occur in the interval where sand units (yellow) are prominent, the higher values are somewhat offset. Such high K_h values are found at the bottom of the thicker sand unit along S18 (about 111 m elevation) and at the bottom of the focus area for O21 (about 110 m), where a mixture of silt and sand is observed. However, the higher K_h values do correspond to intervals where coarser sand predominates. For K_v/K_h, greater anisotropy would have been expected where the silt and sand units alternate (e.g., in the lower part of the focus area). However, the general trend for the two profiles is that stronger anisotropy ($\sim 1\times10^{-2}$) is found in the upper half of the focus area, whereas more isotropic conditions ($>1\times10^{-1}$) are present in the lower half. The isotropic conditions are also found where K_h is higher, which may indicate that sediments deposited under higher energy are less stratified. For S_s, the correlation with geology is more difficult to define. This parameter is primarily influenced by the compressibility of the aquifer matrix and the history of stress changes in the aquifer or during sediment deposition, making it difficult to link directly to the sediment characteristics alone.

This comparison of indicators of sediment size with hydraulic properties illustrates the difficulties often encountered when attempting to quantify hydraulic properties based on geological descriptions of materials. For example, sediments at the study site in the same lithologic units (based on mean sediment grain size) may have differences in K_h and K_v values of up to two orders of magnitude (Paradis et al., 2014). Variations in sediment sorting (from moderately well sorted to very poorly sorted) associated with the littoral depositional environment, which is not fully captured by the mean grain size, explain these variations in permeability for apparently similar sediments. This illustrates the importance of favoring direct estimates of hydraulic properties with

hydraulic tests over indirect estimates based on proxies to effectively capture the specific conditions of a site.

2.6.3 Tomograms of hydraulic properties

Figure 2-15 shows the tomograms for K_h, K_v/K_h, and S_s obtained from the inversion of the periodic test data from the three individual periods and the combination of data from the three periods. Like the profiles, the tomograms for K_h and K_v/K_h show similar general spatial distributions for the four inversions, but they differ slightly for Ss.

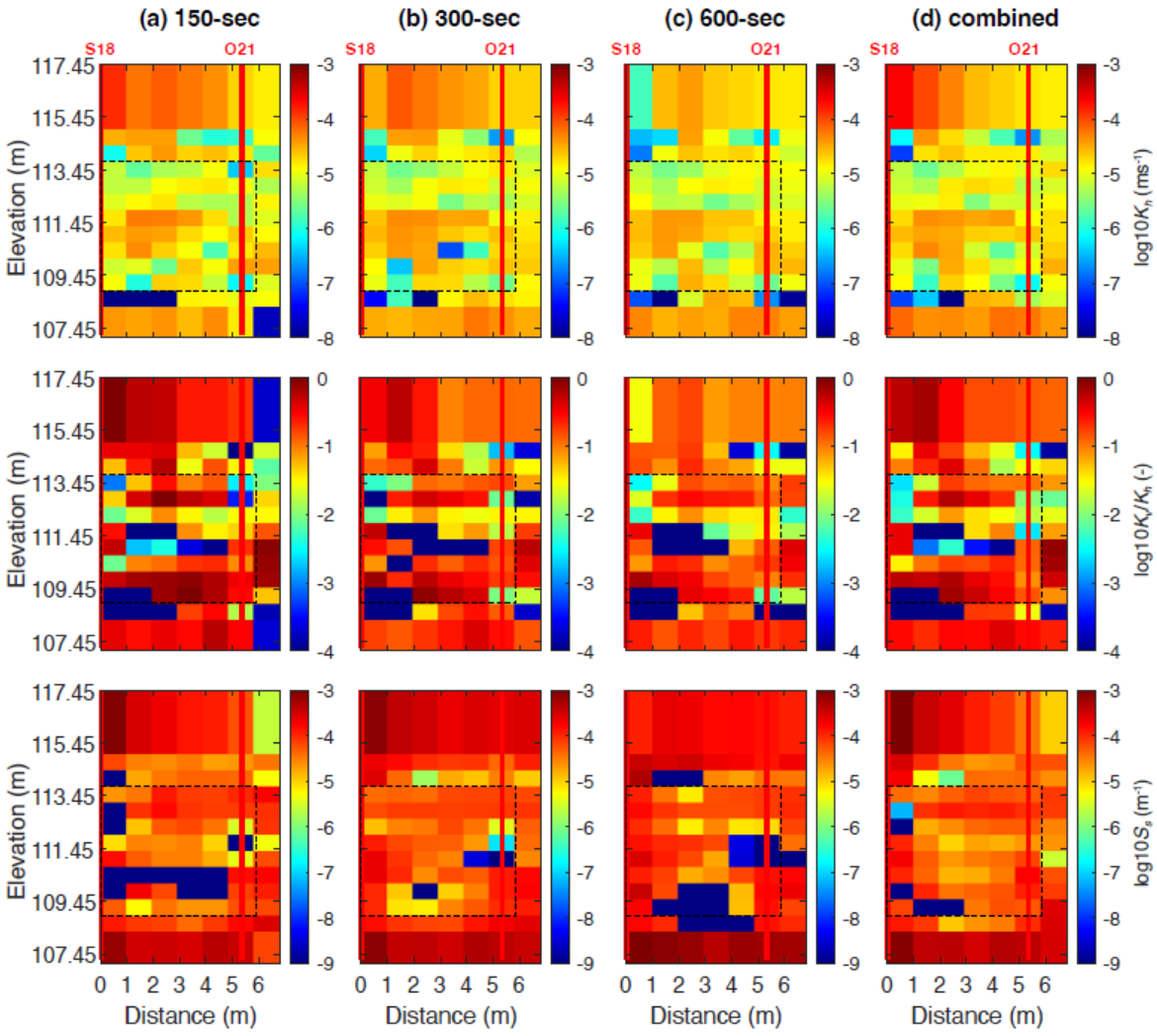

Figure 2-15 : Tomograms for Kh, Kv/Kh, and Ss resulting from the inversion of the periodic tests with the individual period of (a) 150-sec, (b) 300-sec, (c) 600-sec, and (d) the combination of the three periods. The rectangle outlined by a black dashed line is the focus area.

The tomograms for K_h show that the lower part of the focus area is crossed by a layer with higher K_h. Similarly, the tomograms for K_v/K_h show a region of moderate to high anisotropy in the middle of the focus area. The tomograms for S_s are similar in the upper part of the focus area, whereas they differ significantly in the lower part.

These similarities are also apparent in the statistics of hydraulic properties (Figure 2-16). Despite a slight decrease in K_h and a slight increase in K_v/K_h and S_s with period, the median values for each hydraulic property are close for all inversions. The median values for the inversion combining the three periods are intermediate between the values obtained for each individual period. The variability of the hydraulic property values, indicated by the range of 25-75% quantiles, decreases with period for K_h and K_v/K_h. With S_s, the variability is more constant but increases slightly for the period of 600 s. The variability for the combined inversion is also between the values for each period. Note that the increase in variability could be the result of better spatial resolution of the heterogeneity or uncertainties in the estimates due to the lack of information in the heads to constrain the inversion.

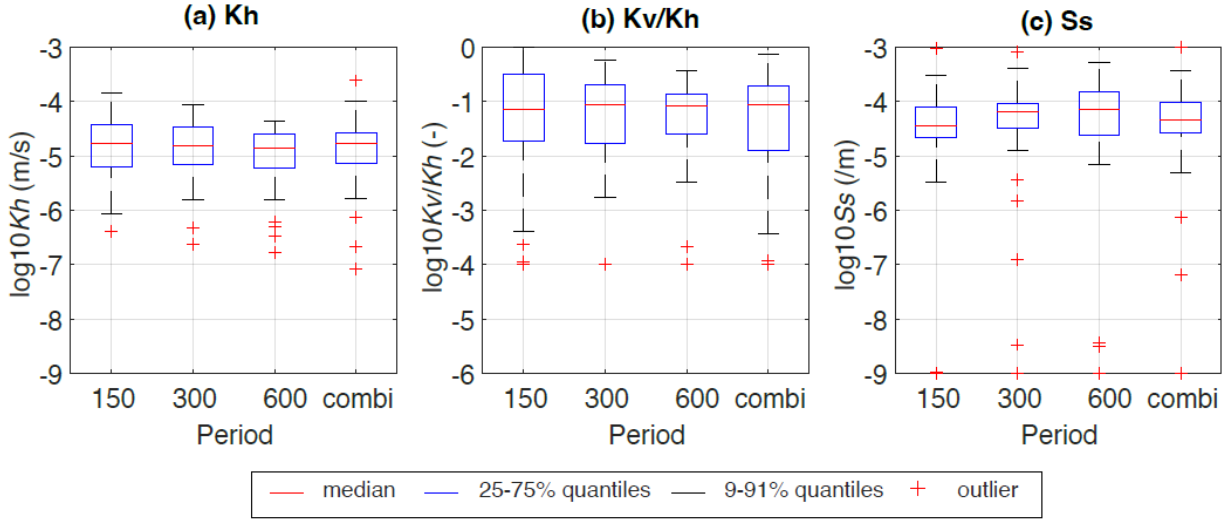

Figure 2-16 : Statistical distribution of the values of (a) Kh, (b) Kv/Kh, and (c) Ss within the focus area resulting from the inversion of the periodic tests with the three individual periods and their combination (combi).

2.6.4 Cross-verification

Since the real hydraulic properties of an aquifer are not known in field-based studies, it is not possible to directly assess the accuracy of a hydraulic property model by comparing it with reality. However, differences in information content between models can be assessed by comparing their

performance in predicting heads using independent hydraulic tests that were not included in the original analysis to produce these models. Models that predict heads equally well from independent tests are assumed to have similar hydraulic properties. In this section, we propose a cross-verification procedure in which each of the three inverted models from one period is used to simulate the heads from another period to evaluate the differences in information content (e.g., the projection of the tests with a period of 150 s to the tomograms obtained from the inversion using the tests with the period of 300 s). The model that combines the three periods is also tested with the three periods individually. A total of nine scenarios are simulated (Table 2-6). This procedure is performed with the numerical model in forward mode.

Table 2-6 : Mean, standard deviation (SD), coefficient of determination (R2) and slope of the linear regression (m) of the scaled residuals for the nine cross-verification simulations. The SD of the original inversion and its difference with the cross-verification simulation are also shown. A negative value of the mean indicates that the simulated head is overestimated compared to the measurements. The color scale for the columns of SD is red for the maximum and green for the minimum. The first number in the simulation name indicates the period for the flow rate and the head used in the simulation, while the last string indicates the model of hydraulic properties.

Simulation	Scaled Residuals					
	Inversion	Cross-Verification				Difference
	SD (m)	Mean (m)	SD (m)	R^2 (-)	m (-)	SD (m)
150-to-300	3.3×10^{-2}	-2.8×10^{-2}	2.3×10^{-1}	0.98	0.80	2.0×10^{-1}
150-to-600	3.3×10^{-2}	-2.2×10^{-2}	3.1×10^{-1}	0.98	0.72	2.7×10^{-1}
300-to-150	2.4×10^{-2}	-4.5×10^{-2}	2.4×10^{-1}	0.98	1.16	2.2×10^{-1}
300-to-600	2.4×10^{-2}	-2.1×10^{-2}	1.5×10^{-1}	0.99	0.91	1.3×10^{-1}
600-to-150	1.6×10^{-2}	-3.3×10^{-2}	2.4×10^{-1}	0.96	1.19	2.2×10^{-1}
600-to-300	1.6×10^{-2}	-1.5×10^{-2}	1.3×10^{-1}	0.98	1.00	1.1×10^{-1}
150-to-combi	3.5×10^{-2}	-3.4×10^{-2}	1.5×10^{-1}	0.99	0.90	1.1×10^{-1}
300-to-combi	3.5×10^{-2}	-3.0×10^{-2}	1.3×10^{-1}	0.99	1.03	1.0×10^{-1}
600-to-combi	3.5×10^{-2}	-1.8×10^{-2}	1.3×10^{-1}	0.98	1.02	1.0×10^{-1}

Figure 2-17 shows the results of the cross-verification procedure for the six scenarios with individual periods. First, it is noticeable that the standard deviation of the projected simulations is consistently greater than that of the original inversions for the same period. This discrepancy indicates that the different periods convey different information about the hydraulic properties. Only identical fields or periodic tests with the same sensitivity to the hydraulic properties would have yielded the same residuals (or very specific combinations of hydraulic property fields contingent on highly specific circumstances or field configurations). This becomes even clearer when comparing the differences in the standard deviation, which are greatest for the two extreme periods (150 s and 600 s). The smallest differences are found in the models that were inverted with the periods of 300 s and 600 s. A similar interpretation was obtained by Fischer et al. (2018) for cross-verification with two periodic signals in a karst aquifer.

Table 2-6 also shows the performance statistics for the scenarios with the combined model. As with the inversions with the single period, the standard deviations of the residuals for the three periods with the combined model are higher than for the original combined inversion. But the differences in the standard deviations are similar for the three periods. This indicates that the combined inversion finds the best compromise to reproduce the head responses of the tests with different periods. These similarities in the differences in the residuals are to be expected since the tests used for the projection with the combined model are not truly independent, as each scenario has the same period as one of the three periods used in the combined inversion. Table 2-6 also shows that the differences in the standard deviations with the combined model are smaller than in the inversions with the single period. This indicates that the combined model is a better "effective model" of the hydraulic properties to reproduce the general flow conditions for the range of aquifer stimulation used in this study.

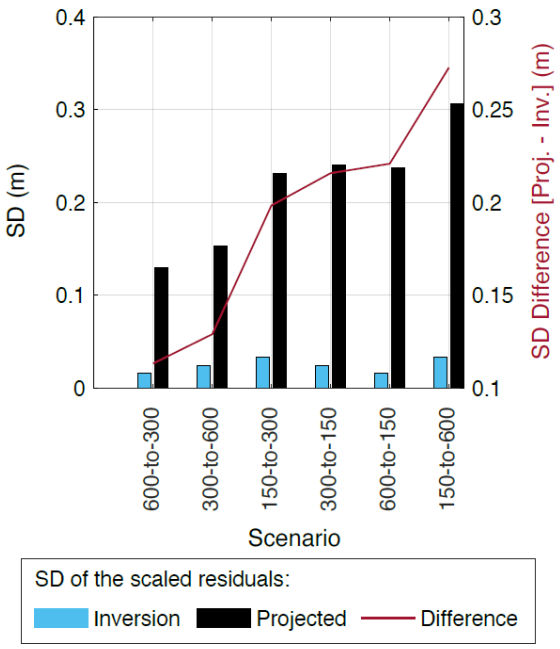

Figure 2-17 : Results of the cross-verification procedure for the six scenarios with individual periods (Table 2-6). The standard deviation (SD) of the scaled residuals between the inverted and projected models is shown along with their difference. The scenarios are ordered by the ascending value of the difference of the standard deviation. The first number in the scenario name indicates the period of flow and the head used in the simulation, while the last string indicates the model of hydraulic properties.

2.6.5 Verification with conventional slug tests

To further evaluate the difference in the information content of the models of hydraulic properties obtained from the inversion of periodic slug tests, conventional slug tests were simulated in forward mode with the four inverted models obtained from single and combined periods. The conventional slug tests were performed in a tomographic arrangement at the same source and observation intervals used for the periodic tests. Six tests were available for the intervals S18.510a to S18.750 (see Figure 2-3 for the location of the intervals). Figure 2-18 shows an example of the good agreement between the measured head and the simulated head for an example related to the inverted parameter field obtained from the tomographic experiment with a period of 300 s. Both the amplitude and the time delay of the maximum head of the response for the observation intervals are generally well reproduced. Table 2-7 describes the statistics of the residuals for the verification simulations and shows that the standard deviation of the scaled residuals for the simulation with a period of 300 s is the smallest. This result is unexpected, as the 150 s period was anticipated to perform better due to its greater similarity to the stresses

induced in the aquifer by the slug tests, compared to the longer periods. However, the higher noise level associated with the 150 s period may have reduced the resolution of the hydraulic properties, potentially explaining these findings (Figure 2-8). As for the cross-verification, the difference in the standard deviation is similar for the periods of 300 s and 600 s and quite different for the period of 150 s. Additionally, the fit for the model with the combination of the three periods lies between those of the experiments with a single period.

Table 2-7 : Descriptive statistics (mean, standard deviation-SD, coefficient of determination-R2 and slope of the linear regression-m) of the scaled residuals for the verification simulations of conventional slug tests with the parameter fields inverted from individual and combined oscillatory tomographic experiments.

Simulation	Scaled Residuals			
	Mean (m)	SD (m)	R^2 (-)	m (-)
150 (s)	-2.5×10^{-2}	9.7×10^{-2}	0.93	1.15
300 (s)	-8.6×10^{-3}	7.2×10^{-2}	0.95	1.02
600 (s)	-8.2×10^{-3}	7.4×10^{-2}	0.94	1.01
Combi	-1.5×10^{-2}	8.3×10^{-2}	0.94	1.09

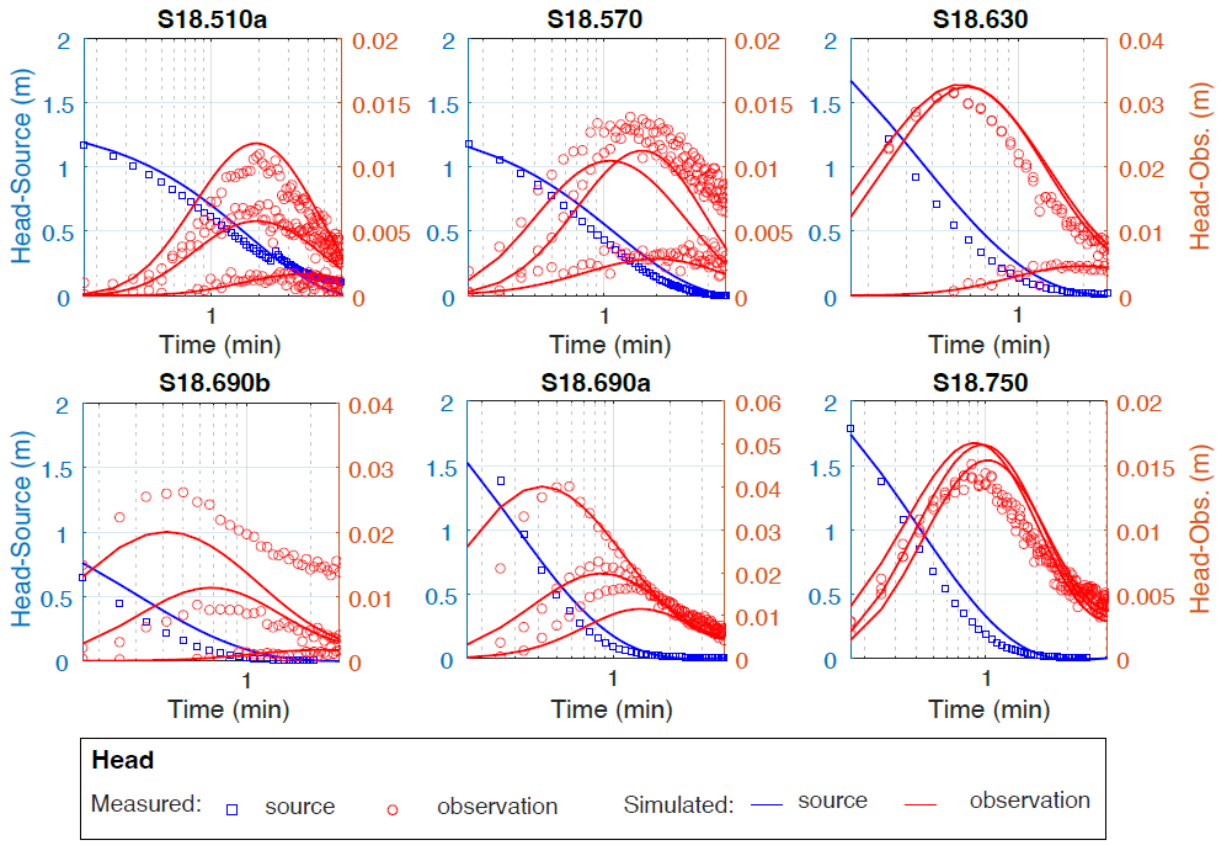

Figure 2-18 : Results of the verification procedure using conventional slug test data that were simulated using the parameter fields obtained from the inversion of measurements with the 300-sec period. (Table 2-7). Observations and simulations of the source (left scale) and observation (right scale) intervals are shown at different scales. The slug tests were performed in the same intervals as the periodic tests, as shown in Figure 2-3.

2.7 Conclusions

This study presented a complete example of the practical application of hydraulic tomography with periodic tests to a littoral aquifer, covering field procedures, data processing and data inversion. The periodic signals of the tomographic tests were obtained mechanically with a rod attached to a computer-controlled winch. This system allowed the generation of a sinusoidal displacement of the rod with adjustable amplitude and period. The field experiment involved 30 periodic tests performed in small intervals isolated by packers in two fully screened wells. Three different periods were used, and for each period a total of 40 head responses were measured in the source interval and in three intervals of an adjacent observation well. The head records were analyzed by numerical inversion to estimate the 2D distribution of hydraulic properties between

the two test wells. Inversion was performed by simulating the radial groundwater flow equation in combination with the Levenberg-Marquardt algorithm. The analysis considered K_h, K_v/K_h, and S_s, as well as wellbore storage in the source well. Periodic tests were inverted individually for each period and for the combination of data from all tests. To the author's knowledge, these are the first tomography experiments with periodic signals that consider the anisotropy of hydraulic conductivity.

The key findings from this field proof-of-concept of periodic slug tests conducted in a tomography configuration between wells are manifold:

Testing devices and procedures. This study shows that the field experiment yielded high quality head measurements despite the challenges of conducting tests at small intervals in a heterogeneous environment where anisotropy strongly attenuates the signal in observation intervals. The experimental setup, with a small equivalent radius (r_{eq}), significantly enhanced signal quality by enabling substantial water level fluctuations in the source intervals (A_{eq}) for the given volume of water displaced by the rod (A_0), effectively acting as an "amplifier" for the head (e.g. $A_{eq}>A_0$). However, the limited volume of water used in each test restricted the experiment to a narrow range of periods. Shorter or longer periods than those reported in this study resulted in lower heads, which were within the noise level. In addition, the rod length used for the tests could not be increased further due to the shallow water table, which limited the amplitude of the generated signal. These limitations highlight the need for developing new testing equipment and procedures that are versatile and capable of generating broader range of periods and higher-amplitude signals. The pneumatic source described by Sayler et al. (2018) shows promise for generating a broader range of periods and offers the advantage of no net removal of water at the surface, which is beneficial for sites where water disposal or mobilization of pollutants could be a concern.

Anisotropy of hydraulic conductivity. Furthermore, this study shows that the anisotropy of hydraulic conductivity (K_v/K_h) can be effectively estimated using tomography experiments with periodic tests. The results agree well with the values of previous studies at the test site. The estimation of K_v/K_h is enabled by the small aspect ratio of the source interval (length of the screen to the radius of the screen), which promotes significant vertical flow in the aquifer (Paradis and Lefebvre, 2013). The comparison of the isotropic and anisotropic scenarios for the analysis of the hydraulic tests has also shown the importance of K_v/K_h. However, it is important to note that the heterogeneities reflected for given degree of anisotropy are often scale-dependent. Variations in experimental setups (e.g., different lengths of source intervals) and numerical configurations (e.g.,

different discretization of model cells) can lead to different estimates of K_v/K_h. While experimental and model scales can be refined to better capture the heterogeneous nature of aquifers, no type of field evidence can definitively confirm whether a particular discretization is fine enough to assume isotropic conditions. Regardless of the discretization chosen, the use of an anisotropic framework for tomographic data analysis increases confidence in the estimated model parameters. Even if the analysis ultimately shows that anisotropy is unnecessary, an isotropic model derived from an anisotropic approach is inherently more robust and reliable; an approach widely accepted for decades in the geophysics community (Babuska and Cara, 1991). The inclusion of K_v/K_h in numerical models then has the potential to significantly improve the accuracy of groundwater flow simulations (Shepley, 2024) and optimize the effectiveness of pump-and-treat systems for contaminant recovery (Bair and Lahm, 1996). Future research should investigate the effects of varying experimental scales and discretization levels on the estimation of anisotropy and examine how these factors influence groundwater flow models and contaminant recovery systems at different scales. Additionally, expanding these findings to other aquifer types with varying degrees of heterogeneity and anisotropy could provide valuable examples from diverse geological environments. This broader understanding of the hydraulic property characteristics of various settings would enhance knowledge and help guide best practices in hydrogeological applications.

Information content of the periods. Finally, the results of this study show that the inversion of individual periods or their combination leads to slightly different models of hydraulic properties, indicating that they convey similar information. These differences are reflected in the spatial and statistical distribution of the hydraulic properties and in the ability of each model to reproduce the heads obtained from independent periodic and conventional slug tests. The relatively narrow range of periods used in this study (150, 300 and 600 s) may explain the small differences in the estimated hydraulic properties, as each period could have examined similar spatial scales within the aquifer. However, the difference in information content is more pronounced for the extreme periods (150 and 600 s), supporting the idea that contrasting periods may carry complementary information (e.g., Rosa and Horne, 1997). Although this is not explicitly demonstrated in this field study, shorter periods could provide more detailed insights into near-field hydraulic responses, while longer periods might capture broader, integrated properties over larger distances (e.g., Ahn and Horne, 2010; Paradis et al., 2024). Although the combined inversion integrated data from multiple periods, the verification with conventional slug tests performed no better than the average of the inversions for individual periods. This is in line with the theoretical analysis proposed by Wang et al. (2021), which suggests that “multifrequency tests do not increase the resolution of

aquifer characterization" because "the sensitivity maps of different frequencies are highly correlated." However, tomography experiments with a wider range of periods could have led to a different conclusion. As shown by Paradis et al. (2024) with synthetic aquifers, the choice of the period is crucial for aquifer resolution. Short periods with significant transient responses, as well as large differences in period lengths (both shorter and longer than those used in this field study), could help reduce the sensitivities of the head to the hydraulic parameters and improve resolution. Future work should prioritize experimenting with a broader range of periods to evaluate how variations, particularly extreme period lengths, affect the resolution and sensitivity of aquifer characterization. These experimental efforts should be complemented by fundamental studies that quantitatively assess the information content of the experiments, providing a stronger theoretical foundation for optimizing and interpreting hydraulic tomography applications.

Acknowledgment

Sincere thanks are extended to F. Huchet and V. Boisvert for their precious contribution during the field investigation. B. Giroux is acknowledged for the parallelization of the simulator lr2dinv. N. Benoit is also thanked for the internal review of the paper. The device brands mentioned in this work are for information purposes only, to document procedures, and do not constitute a recommendation for these specific products. This is a GSC contribution 20230267.

2.8 Bibliographie 1er ARTCILE

Ahn, S., Horne, R.N., 2010. Estimating permeability distributions from pressure pulse testing. In Proceedings - SPE Annual Technical Conference and Exhibition, 3:2388–2403. Florence, 10.2118/134391-MS.

Babuska, V. and M. Cara (1991) Seismic Anisotropy in the Earth. Kluwer Academic Publishers, Boston, 227 pp.

Bair, E.S., Lahm, T.D., 1996. Variations in capture-zone geometry of a partially penetrating pumping well in an unconfined aquifer. Groundwater, 34: 842-852. https://doi.org/10.1111/j.1745-6584.1996.tb02079.x.

Barry, F., Ophori, D., Hoffman, J., Canace, R., 2009. Groundwater flow and capture zone analysis of the Central Passaic River Basin, New Jersey. Environmental Geology 56, 1593–1603.

Becker, M.W., Guiltinan, E., 2010. Cross-hole periodic hydraulic testing of inter-well connectivity. In: Thirty-Fifth Workshop on Geothermal Reservoir Engineering. Stanford University, Stanford, California.

Berg, S.J., Illman, W.A., 2015. Comparison of hydraulic tomography with traditional methods at a highly heterogeneous site. Groundwater 53 (1), 71-89. doi:10.1111/gwat.12159.

Berg, S.J., Illman, W.A., 2011. Three-dimensional transient hydraulic tomography in a highly heterogeneous glaciofluvial aquifer-aquitard system. Water Resour. Res. 47, W10507. doi:10.1029/2011WR010616.

Black, J.H., Kipp, K.L.J., 1981. Determination of hydrogeological parameters using sinusoidal pressure tests: A theoretical appraisal. Water Resour. Res. 17 (3), 686–692. doi:10.1029/WR017i003p00686.

Boggs, J.M., Young, S.C., Beard, L.M., 1992. Field study of dispersion in a heterogeneous aquifer 1: Overview and site description. Water Resour. Res. 28 (12), 3281-3291.

Bohling, G.C., 1993. Hydraulic tomography in two-dimensional, steady-state groundwater flow. Eos Trans. AGU 74, 141.

Bohling, G.C., Butler, J.J., 2001. lr2dinv: A finite-difference model for inverse analysis of two-dimensional linear or radial groundwater flow. Comput. Geosci. 27, 1147-1156. doi.org/10.1016/S0098-3004(01)00036-X.

Bohling, G.C., Butler, Jr.J.J., Zhan, X., Knoll, M.D., 2007. A field assessment of the value of steady shape hydraulic tomography for characterization of aquifer heterogeneities. Water Resour. Res. 43, W05430. doi:10.1029/2006WR004932.

Bolduc, A., 2003. Géologie des formations superficielles, Charny, Québec. Commission Géologique du Canada, Dossier public 1976, échelle 1/50000, Ottawa, Canada.

Brauchler, R., Hu, R., Dietrich, P., Sauter, M., 2011. A field assessment of high-resolution aquifer characterization based on hydraulic travel time and hydraulic attenuation tomography. Water Resour. Res. 47, W03503. http://dx.doi.org/10.1029/2010WR009635.

Brauchler, R., Hu, R., Hu, L., Jimenez, S., Bayer, P., Dietrich, P., Ptak, T., 2013. Rapid field application of hydraulic tomography for resolving aquifer heterogeneity in unconsolidated sediments. Water Resour. Res. 49 (4), 2013–2024.

Butler Jr., J.J., McElwee, C.D., 1995. Well-testing methodologies for characterizing heterogeneities in alluvial-aquifer systems: final technical report. Kansas Geological Survey Open File Report 95-75.

Butler, Jr.J.J., Dietrich, P., Wittig, V., Christy, T., 2007. Characterizing hydraulic conductivity with the direct-push permeameter. Ground Water 45 (4), 409–419.

Cardiff, M., Zhou, Y., Barrash, W., Kitanidis, P.K., 2020. Aquifer imaging with oscillatory hydraulic tomography: Application at the field scale. Groundwater 58 (5), 710–722. doi:10.1111/gwat.12960.

Cardiff, M., Bakhos, T., Kitanidis, P.K., Barrash, W., 2013. Aquifer heterogeneity characterization with oscillatory pumping: Sensitivity analysis and imaging potential. Water Resour. Res. 49 (9), 5395–5410. doi.org/10.1002/wrcr.20356.

Cardiff, M., Barrash, W., Kitanidis, P.K., Malama, B., Revil, A., Straface, S., Rizzo, E., 2009. A potential-based inversion of unconfined steady state hydraulic tomography. Ground Water 47 (2), 259–270.

Cheng, Y., Renner, J., 2018. Exploratory use of periodic pumping tests for hydraulic characterization of faults. Geophys. J. Int. 212 (1), 543–565, 10.1093/gji/ggx390.

Crisman, S.A., Molz, F.J., Dunn, D.L., Sappington, F.C., 2001. Application procedures for the electromagnetic borehole flowmeter in shallow unconfined aquifers. Ground Water Monit. R. 21 (4), 96-100.

de Marsily, G., Delay, F., Gonçavès, J., Renard, P., Teles, V., Violette, S., 2005. Dealing with spatial heterogeneity. Hydrogeol. J. 13, 161–183.

Dubreuil-Boisclair, C., Gloaguen, E., Marcotte, D., Giroux, B., 2011. Heterogeneous aquifer characterization from ground-penetrating radar tomography and borehole hydrogeophysical data using nonlinear Bayesian simulations. Geophysics 76 (4), 1–13. doi.org/10.1190/1.3571273.

Falta, R.W., Basu, N., Rao, P.S., 2005. Assessing impacts of partial mass depletion in DNAPL source zones: II. Coupling sources strength functions to plume evolution. Journal of Contaminant Hydrology 79, 45–66.

Ferris, J.G., 1952. Cyclic fluctuations of water level as a basis for determining aquifer transmissibility. United States Geological Survey, Washington, D.C. 16 pp. doi.org/10.3133/70133368.

Fischer P., Jardani, A., Jourde, H., Cardiff, M., Wang, X., Chedeville, S., Lecoq, N., 2018. Harmonic pumping tomography applied to image the hydraulic properties and interpret the connectivity of a karstic and fractured aquifer (Lez aquifer, France). Adv. Water Resour. 119, 227-244. https://doi.org/10.1016/j.advwatres.2018.07.002.

Fischer, P., De Clercq, T., Jardani, A., Massei, N., Abbas, M., 2020. Imaging the hydraulic properties of a contaminated alluvial aquifer perturbed with periodic signals. Hydrogeol. J. 28, 2713–2726. doi.org/10.1007/s10040-020-02233-8.

Frei, S., Fleckenstein, J.H., Kollet, S.J., Maxwell, R.M., 2009. Patterns and dynamics of river–aquifer exchange with variably-saturated flow using a fully-coupled model. J. Hydrol. 375, 383-393. doi.org/10.1016/j.jhydrol.2009.06.038.

Gernez S., Bouchedda, A., Gloaguen, E., Paradis, D., 2019. Comparison between hydraulic conductivity anisotropy and electrical resistivity anisotropy from tomography inverse modeling. Front. Environ. Sci. 7, 67. doi: 10.3389/fenvs.2019.00067.

Gloaguen, E., Lefebvre, R., Ballard, J.M., Paradis, D., Tremblay, L., Michaud, Y., 2012. Inference of the two-dimensional GPR velocity field using collocated cokriging of direct push permittivity and conductivity logs and GPR profiles. J. Appl. Geophys. 78, 94-101. doi.org/10.1016/j.jappgeo.2011.10.015.

Gottlieb, J., Dietrich, P., 1995. Identification of the permeability distribution in soil by hydraulic tomography. Inverse Probl. 11, 353–360. http://dx.doi.org/10.1088/0266-5611/11/2/005.

Guiltinan, E., Becker, M.W., 2015. Measuring well hydraulic connectivity in fractured bedrock using periodic slug tests. J. Hydrol. 521, 100-107. 10.1016/j.jhydrol.2014.11.066.

Hanson, R.T., Nishikawa, T., 1996. Combined use of flowmeter and time-drawdown data to estimate hydraulic conductivities in layered aquifer systems. Ground Water 34 (1), 84-94.

Hart, D.J., Bradbury, K.R., Feinstein, D.T., 2006. The vertical hydraulic conductivity of an aquitard at two spatial scales. Ground Water 44 (2), 201–211.

Hochstetler, D.L., Barrash, W., Leven, C., Cardiff, M., Chidichimo, F., Kitanidis, P.K., 2016. Hydraulic Tomography: Continuity and Discontinuity of High-K and Low-K Zones. Groundwater 54, 171-185. https://doi.org/10.1111/gwat.12344.

Hoque, M.A., Burgess, W.G., 2020. Representing heterogeneity of fluvio-deltaic aquifers in models of groundwater flow and solute transport: A multi-model investigation in the Bengal Basin. J. Hydrol. 590, 125507. doi.org/10.1016/j.jhy.

Hommersen, J.D., Quinn, P.M., Parker, B.L., 2021. Evaluating friction and inertial losses from slug tests conducted in a multilevel system. Water Resour. Res. 57, e2021WR029794. doi.org/10.1029/2021WR029794.

Illman, W. A., Liu, X., Takeuchi, S., Yeh, T. J., Ando, K., Saegusa, H., 2009. Hydraulic tomography in fractured granite: Mizunami Underground Research site, Japan. Water Resour. Res. 45, W01406. doi:10.1029/2007WR006715.

Keller, C.E., Cherry, J.A., Parker, B.L., 2014. New method for continuous transmissivity profiling in fractured rock. Groundwater 52 (3), 352–367.

Kruseman, G.P., de Ridder, N.A., 2000. Analysis and Evaluation of Pumping Test Data. 2nd Edition, International Institute for Land Reclamation and Improvement, 372.

Lancaster-Jones, P.F.F., 1975. The interpretation of the Lugeon water-test. Q. J. Eng. Geol. Vol. 8 (2), 151-154.

Lavenue, M., de Marsily, G., 2001. Three-dimensional interference test interpretation in a fractured aquifer using the Pilot Point Inverse Method. Water Resour. Res. 37 (11), 2659–2675. https://doi.org/10.1029/2000WR000289.

LeBlanc, D.R., Garabedian, S.P., Hess, K.M., Gelhar, L.W., Quadri, R.D., Stollenwerk, K.G., Wood, W.W., 1991. Large-scale natural gradient tracer test in sand and gravel, Cape Cod, Massachusetts, 1: Experimental design and observed tracer movement. Water Resour. Res. 27, 895-910.

Li, W., Englert, A., Cirpka, O. A., Vereecken, H., 2008. Three-dimensional geostatistical inversion of flowmeter and pumping test data. Ground Water 46 (2), 193-201.

Liu, Q., Hu, L., Hu, R., Brauchler, R., Xing, Y., Qi, J., Ptak, T., 2023. Characterization of aquifer heterogeneity by tomographic slug test responses considering wellbore effects. J. Hydrol. 627, 130472. doi:10.1016/j.jhydrol.2023.130472.

Liu, G., Butler Jr. J. J., Bohling, G.C., Reboulet, E., Knobbe, S., Hyndman, D.W., 2009. A new method for high-resolution characterization of hydraulic conductivity. Water Resour. Res. 45, W08202. doi:10.1029/2009WR008319.

Lochbühler, T., Doetsch, J., Brauchler, R., Linde, N., 2013. Structure-coupled joint inversion of geophysical and hydrological data. Geophysics 78 (3), ID1–ID14. doi:10.1190/GEO2012---0460.1.

Marquardt, D.W., 1963. An algorithm for least squares estimation of nonlinear parameters. Journal of the Society for Industrial and Applied Mathematics 11, 431–441.

Molz, F.J., Morin, R.H., Hess, A.E., Melville, J.G., Guven, O., 1989. The impeller meter for measuring aquifer permeability variations - evaluation and comparison with other tests. Water Resour. Res. 25 (7), 1677-1683.

Morin, R.H., Hess, A.E., Paillet, F.L., 1988. Determining the distribution of hydraulic conductivity in a fractured limestone aquifer by simultaneous injection and geophysical logging. Ground Water 2 (6), 587-595.

Paillet, F.L., 1998. Flow modeling and permeability estimation using borehole flow logs in heterogeneous fractured formations. Water Resour. Res. 34 (5), 997-1010.

Paradis, D., Lefebvre, R., Morin, R.H., Gloaguen, E., 2011. Permeability profiles in granular aquifers using flowmeters in direct-push wells. Ground Water 49, 534–547. doi:10.1111/j.1745-6584.2010.00761.x.

Paradis, D., Lefebvre, R., 2013. Single-well interference slug tests to assess the vertical hydraulic conductivity of unconsolidated aquifers. J. Hydrol. 478 (25), 102–118. doi:10.1016/j.jhydrol.2012.11.047.

Paradis, D., Tremblay, L., Lefebvre, R., Gloaguen, E., Rivera, A., Parent, M., Ballard, J.-M., Michaud, Y., Brunet, P., 2014. Field characterization and data integration to define the hydraulic heterogeneity of a shallow granular aquifer at a sub-watershed scale. Environ. Earth Sci. 72, 1325-1348. doi.org/10.1007/s12665-014-3318-2.

Paradis, D., Lefebvre, R., Gloaguen, E., Rivera, A., 2015. Predicting hydrofacies and hydraulic conductivity from direct-push data using a data-driven relevance vector machine approach: Motivations, algorithms, and application. Water Resour. Res. 51, 481-505. doi.org/10.1002/2014WR015452.

Paradis, D., Gloaguen, E., Lefebvre, R., Giroux, B., 2016. A field proof-of-concept of tomographic slug tests in an anisotropic littoral aquifer. J. Hydrol. 536, 61-73. doi.org/10.1016/j.jhydrol.2016.02.041.

Paradis, D., Lefebvre, Nefzi, A., 2024. Parameter resolution of simulated responses to periodic hydraulic tomography signals in aquifers. Adv. Water Resour. 190, 104734. doi.org/10.1016/j.advwatres.2024.104734.

Parent, M., Occhietti, S., 1988. Late Wisconsinan Deglaciation and Champlain Sea Invasion in the St. Lawrence Valley, Québec. Geogr. Phy. Quatern. 42, 215. doi.org/10.7202/032734ar

Press, W.H., Teukolsky, S.A., Vetterling, W.T., Flannery, B.P., 1992. Numerical recipes in FORTRAN: The Art of Scientific Computing, 2nd Edition. Cambridge University Press, Cambridge, 963pp.

Price, M., Morris, B., Robertson, A., 1982. A study of intergranular and fissure permeability in Chalk and Permian aquifers, using double-packer injection testing. J. Hydrol. 54 (4), 401-423. doi.org/10.1016/0022-1694(82)90165-2.

Quinn, P.M., Parker, B.L., Cherry, J.A., 2011. Using constant head step tests to determine hydraulic apertures in fractured rock. J. Hydrol. 126 (1-2), 85-99. doi.org/10.1016/j.jconhyd.2011.07.002.

Quinn, P., Cherry, J.A., Parker, B.L., 2015. Combined use of straddle packer testing and FLUTe profiling for hydraulic testing in fractured rock boreholes. J. Hydrol. 524, 439-454. doi.org/10.1016/j.jhydrol.2015.03.008.

Quinn, P., Cherry, J.A., Parker, B.L., 2011. Using constant head step tests to determine hydraulic apertures in fractured rock. J. Hydrol. 126 (1-2), 85-99. doi.org/10.1016/j.jconhyd.2011.07.002.

Rehfeldt, K.R., Boggs, J.M., Gelhar, L.W., 1992. Field study of dispersion in a heterogeneous aquifer, 3. Geostatistical analysis of hydraulic conductivity. Water Resour. Res. 28 (12), 3309–3324. doi:10.1029/92WR01758.

Rosa, A.J., Horne, R.N., 1997. Reservoir description by well-test analysis by use of cyclic flow-rate variation. SPE Formation Evaluation 12 (04), 247–254. doi:10.2118/22698-PA.

Ross, H.C., McElwee, C.D., 2007. Multi-Level Slug Tests to Measure 3-D Hydraulic Conductivity Distributions. Nat. Resour. Res. 16, 67–79. doi.org/10.1007/s11053-007-9034-9.

Ruggeri, P., Gloaguen, E., Lefebvre, R., Irving, J., Holliger, K., 2014. Integration of hydrological and geophysical data beyond the local scale: Application of Bayesian sequential simulation to field data from the Saint-Lambert-de-Lauzon site, Québec, Canada. J. Hydrol. 514, 271-280. doi.org/10.1016/j.jhydrol.2014.04.031.

Sageev, A., 1986. Slug test analysis. Water Resour. Res. 22, 1323–1333.

Sayler, C., M. Cardiff, and M.D. Fort. 2018. Understanding the geometry of connected fracture flow through multiperiod oscillatory hydraulic testing. Ground Water 56(2), 276–287. doi.org/10.1111/gwat.12580.

Shepley, M.G., 2024. Vertical hydraulic conductivity and layered heterogeneity: from measurements to models. Hydrogeol. J. 32, 1017–1042. doi.org/10.1007/s10040-024-02773-3.

Sudicky, E.A., Illman, W.A., 2011. Lessons Learned from a Suite of CFB Borden Experiments. Groundwater 49, 630-648. doi.org/10.1111/j.1745-6584.2011.00843.x.

Tiedeman, C.R., Barrash, W., 2020. Hydraulic Tomography: 3D Hydraulic Conductivity, Fracture Network, and Connectivity in Mudstone. Groundwater 58, 238-257. https://doi.org/10.1111/gwat.12915.

Tosaka, H., Masumoto, K., Kojima, K., 1993. Hydropulse tomography for identifying 3-D permeability distribution in high level radioactive waste management. In: Proceedings of the Fourth Annual International Conference of the ASCE. Am. Soc. Civ. Eng., Reston, VA, pp. 955–959.

Tremblay, L., Lefebvre, R., Paradis, D., Gloaguen, E., 2014. Conceptual model of leachate migration in a granular aquifer derived from the integration of multi-source characterization data (St-Lambert, Canada). Hydrogeol. J. 22, 587-608. doi.org/10.1007/s10040-013-1065.

Wang, Y.-L., Yeh, T.-C.J., Xu, D., Li, K., Wen, J.-C., Huang, S.-Y., Wang, W., Hao, Y., 2021. Stochastic analysis of oscillatory hydraulic tomography. Journal of Hydrology, 596, 10.1016/j.jhydrol.2021.126105.

Yin, M., Ma, R., Zhang, Y., Lin, J., Guo, Z., Zheng, C., 2023. Competitive control of multiscale aquifer heterogeneity on solute transport in an alluvial aquifer. J. Hydrol. 616, 128819. doi.org/10.1016/j.jhydrol.2022.128819.

Zha, Y., Yeh, T.-C.J., Mao, D., Yang, J., Lu, W., 2014. Usefulness of flux measurements during hydraulic tomographic survey for mapping hydraulic conductivity distribution in a fractured medium. Adv. Water Resour. 71, 162-176. doi.org/10.1016/j.advwatres.2014.06.008.

Zeyrek, C., Mittelstet, A.R., Gilmore, T.E., Zlotnik, V., Solomon, D.K., Genereux, D.P., Humphrey, C.E., Shrestha, N., 2023. Modeling groundwater transit time distributions and means across a Nebraska watershed: Effects of heterogeneity in the aquifer, riverbed, and recharge parameters. J. Hydrol. 617, 128891. doi.org/10.1016/j.jhydrol.2022.128891.

3 RESPONSES AND RESOLUTION OF OSCILLATORY HYDRAULIC TOMOGRAPHY UNDER A WIDE RANGE OF SINGLE AND COMBINED SIGNAL PERIODS

Titre de l'article : Réponses et résolution de la tomographie hydraulique oscillatoire sous une large gamme de périodes de signaux simples et combinés

Auteurs :

Aymen Nefzi[1], Daniel Paradis[1,2], René Lefebvre[1], Olivier Bour[3]

[1] Centre Eau Terre Environnement (INRS-ETE) - Institut national de la recherche scientifique, Québec, Canada

[2] Ressources Naturelles Canada - Commission géologique du Canada, Québec, Canada

[3] Université Rennes, CNRS, Géosciences Rennes, UMR 6118, 35000 Rennes, France

En préparation pour soumission à Water Resources Research

Abstract

Oscillatory Hydraulic Tomography (OHT) can image the heterogeneous distribution of subsurface hydraulic properties. However, there are remaining issues regarding the choice of optimal signal periods and the improvement in resolution obtained from using multiple signal periods. This study investigated these issues through a detailed sensitivity analysis of simulated OHT experiments using a wide range of signal periods for a homogeneous and a heterogeneous model. Hydraulic properties in the 2D radial models were based on the inversion of an actual OHT experiment. Numerical simulations of OHT were performed with a wide range of signal periods and different

signal amplitudes that could not practically be implemented in the field. Using L-curve analysis, optimal parameter resolution was assessed, and information content was calculated for single periods and combinations of two and three periods. OHT signal propagation was found to depend on period and hydraulic conductivity heterogeneity and anisotropy. For the heterogeneous model, combining short and long periods significantly enhances the information content by capturing both fast and slow hydraulic responses. However, combination of two long periods leads to a reduction in information content, suggesting that overlapping sensitivity ranges may diminish the added value of their combinations. Field results support simulation findings by showing similar trends. Results provide insights to optimize field test durations and select the most effective period combinations to improve data acquisition efficiency without sacrificing the resolution of hydraulic parameters. Results thus offer a better understanding of OHT responses and can improve its application to subsurface imaging.

3.1 Introduction

The characterization of hydraulic properties of aquifers, including horizontal and vertical components of hydraulic conductivity (K) and specific storage (S_s), is needed to quantitatively represent numerical groundwater flow and mass transfer in aquifer systems. This understanding is needed to manage groundwater resources and contaminated sites. Conventionally, hydraulic properties are estimated by hydraulic tests (slug tests and pumping tests) whose interpretation assumes homogeneous hydraulic parameter distribution (Quinn et al., 2015). However, it has long been recognized that modeling of representative groundwater flow and especially contaminant transport requires the definition of subsurface heterogeneity (Zheng and Gorelick, 2003; Maier et al., 2009).

Nonetheless, predicting subsurface flow and transport presents significant challenges due to the complex heterogeneity found in most geologic environments. The hydraulic properties within the subsurface can vary by several orders of magnitude, and this spatial variability fundamentally influences the dynamics of groundwater movement and solute dispersion (Dagan, 1989). The spatial connectivity of different geological facies is critically important. Highly permeable, interconnected structures serve as preferential pathways, facilitating water fluxes and faster solute transfer. Conversely, interconnected regions of low permeability represent barriers, reducing water flow and slowing solute movement (Zinn and Harvey, 2003; Knudby and Carrera, 2006; Huysmans and Dassargues, 2009; Bianchi et al., 2011; Renard and Allard, 2013).

Therefore, the understanding and modeling of subsurface flow and mass transport hinges on thorough characterization of the spatial distribution of subsurface facies.

Over the past few decades, hydraulic tomography (HT) was developed to better characterize subsurface heterogeneity by the estimation of the spatial distribution of hydraulic properties. HT involves the production of a hydraulic signal at a source well and recordings in intervals of a single or multiple observation wells. Cardiff and Barrash (2011) provide a literature review of hydraulic tomography and discuss its advantages and shortcomings. More recently, oscillatory hydraulic tomography (OHT), a variant of HT, has used periodic pressure signals at source wells that create oscillations of water levels that are recorded in intervals of observation wells. Oscillatory aquifer tests have similarly been used to provide information about aquifer heterogeneity (Zhou et al., 2016; Cardiff et al., 2020; Nefzi et al., 2025; Paradis et al., 2024). In a refinement of the analysis of oscillatory pumping tests, Cardiff et al. (2013b) proposed multi-period oscillatory hydraulic imaging. This approach utilizes multiple signals with different periods to obtain more information on the heterogeneity of aquifer hydraulic properties.

Only a few field applications of hydraulic tomography with periodic or oscillatory signals have been published, demonstrating the method's potential to enhance aquifer characterization. Lavenue and de Marsily (2001) conducted sinusoidal pumping tests in a dolomite aquifer, using a two-step inversion approach that combined lithology simulation and K estimation via pilot points. They successfully delineated the boundary between fractured and unfractured rock, demonstrating the effectiveness of periodic testing in complex geological environments. Fischer et al. (2018; 2020) applied harmonic pumping tests in karst and alluvial aquifers, respectively, using two different periods to map the structures and properties of these environments. They employed a deterministic nonlinear optimization algorithm combined with a groundwater flow model in the frequency domain to estimate T and S. Their results highlighted structural differences and were consistent with the site geology and contamination history. Cardiff et al. (2020) utilized oscillatory hydraulic tomography with periods between 5 and 70 seconds in a fluvial aquifer. They applied geostatistical inversion to obtain the 3D hydraulic conductivity field, demonstrating a moderate to strong correlation with previous hydraulic profiles and showing the robustness of oscillatory signals in resolving hydraulic properties across various scales. Nefzi et al. (2025) applied hydraulic tomography with periodic slug tests in an unconsolidated littoral aquifer. By generating periodic signals with adjustable amplitude and period, they inverted the head responses to estimate Kh, K_v/K_h, and S_s, specifically focusing on anisotropy. The inversion of single and combined periods was consistent with previous studies and showed slight spatial and statistical

variations in hydraulic properties. Their study marked the first field application of periodic signals to account for hydraulic conductivity anisotropy, advancing the field by demonstrating the ability of periodic testing to provide reliable data for characterizing complex aquifer systems, despite the challenges of working in small, isolated intervals in heterogeneous environments.

Recently, Zhou et al. (2016) reported that head collected from OHT with single-period excitations provide worse estimates than those from multi-period excitations when the number of pumping tests and observation locations is limited. On the contrary, Wang et al. (2019) concluded from a Monte Carlo experiment of OHT aquifer characterization that the performance of the estimated transmissivity field average is not period-dependent. They suggested that previously reported improvements of estimates using different periods based on a single realization of heterogeneity are not warranted for all possible realizations.

It thus appears that questions remain about the capability of OHT to provide head measurements that resolve heterogeneous aquifer properties and on the potential resolution improvement obtained from the combination of heads obtained with different signal periods. The objective of this study is thus to assess the information content of OHT head responses for a wide range of periodic signals and their resolution of heterogeneous aquifer properties. This assessment covers single tests with different signal periods and the combination of tests with different periods. The study is carried out with numerical simulations that can test a wide range of signal periods and because such an assessment requires the a priori knowledge of hydraulic properties.

The numerical model is developed to be representative of an actual OHT field test (Nefzi et al., 2025). By covering a wider range of periodic signals than the field test, the present study thus allows a posteriori evaluation of the suitability of field test conditions compared to the conditions and signal periods that lead to better resolution based on numerical simulation results. The study also looked at the factors influencing the propagation of periodic signals having different periods. Improvements to test conditions and suitable range of signal periods can also be assessed. Results of this study should provide a better understanding of OHT and support the design of its optimal field applications to the characterization of aquifer heterogeneity.

3.2 Description of the tomography field experiments of St-Lambert

The study utilizes numerical simulations of OHT head responses generated from signals spanning a wide range of periods. To ensure realistic conditions, these simulations are grounded in data from an actual field experiment (Nefzi et al., 2025). The spatial distribution of hydraulic properties

in the model reflects those derived from the inversion of the field data. For comparison, a homogeneous model, representing average hydraulic properties, is also incorporated into the analysis.

The test site is located at Saint-Lambert-de-Lauzon, 40 km south of Quebec City (Canada). The aquifer is made up of unconsolidated Late Quaternary sediments deposited in the Champlain Sea, an arm of the Atlantic Ocean that invaded the St. Lawrence Valley at the end of the last glaciation. The aquifer is under semi-confined conditions and is composed of a 10–20 m thick accumulation of highly heterogeneous sand interbedded with silt and clayey silt lenses (Paradis et al., 2016; Tremblay et al., 2014).

The field experiments at the St-Lambert Test Site investigated the use of periodic hydraulic tomography to characterize a littoral aquifer with significant contrasts between vertical and horizontal hydraulic conductivity (K_v and K_h), as determined by previous studies (Paradis et al., 2016; Paradis et al., 2015a; Paradis and Lefebvre, 2013). These tests highlighted the effectiveness of periodic signals in capturing the heterogeneity and anisotropy of the aquifer (Nefzi et al., 2025). Over a series of 10 periodic slug tests, with varying periods of 2.5, 5, and 10 min, head responses were recorded at multiple intervals in both source and observation wells.

For the field experiments, the wells are screened over the entire saturated thickness of the aquifer. Wells were installed without sand packs (screens in direct contact with the natural sediments) using direct-push equipment according to the protected screen method (Paradis et al., 2011). The diameter of each well is 0.051m with a screen length of 7.6 m. The periodic stimulation was performed with a 2.8 m long aluminum rod immersed in the riser tube. The diameter of the rod was chosen to maximize the volume of water displaced for the tests while ensuring that the water could move freely between the rod and the inside of the riser tube (Figure 3-1). Significant differences in head amplitude and phase shift between test intervals at different locations highlighted the heterogeneity of the aquifer (Nefzi et al., 2025).

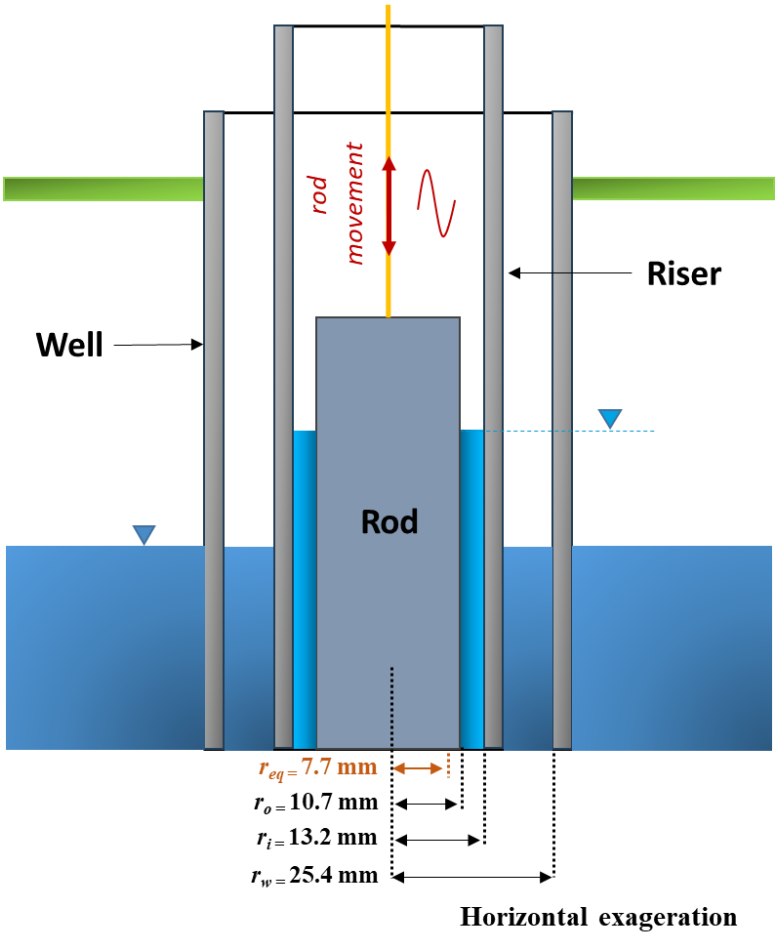

Figure 3-1 : Cross-section of the source well, riser tube and rod arrangement with their corresponding radius.

Numerical inversion in the time domain used the rod-induced flow rates and associated heads to estimate the heterogeneous fields. The heterogeneous fields of K_h, K_v/K_h and S_s were estimated by inversion using the Levenberg-Marquardt algorithm in combination with a groundwater flow model accounting for wellbore storage. The tomography experiments with different period were analyzed individually and together. This work marked a significant step in the application of periodic tomography for understanding aquifer anisotropy, offering valuable insights into the groundwater flow properties of heterogeneous systems (Nefzi et al., 2025).

This study aims to elucidate key findings from the periodic hydraulic tomography experiments conducted at the St-Lambert Test Site. Despite the relatively small head variations observed in the monitoring intervals, the data quality was excellent, characterized by a high signal-to-noise ratio. This underscores the effectiveness of the field experiment, even within the constraints of small intervals in a heterogeneous environment. The specific experimental configuration,

particularly the small equivalent radius (r_{eq}), contributed to significant head variations in both the source well and the observation intervals, enhancing the signal quality.

In terms of the optimal test conditions, the study explored the impact of different signal periods on resolution. While the inversion of each period (2.5, 5, and 10 min) produced slightly different tomograms of the hydraulic properties, the combination of periods resulted in a model that reflects a balance between them. However, this combined inversion did not necessarily represent the "best information" from each period, as it produced a model that was a compromise rather than an optimal solution for accurately reproducing all head responses.

The study also reveals that the slight differences in tomograms for individual periods and their combination may be linked to better spatial resolution of aquifer heterogeneity or uncertainties arising from a lack of information in the head data. The cross-validation procedure showed that multi-period inversions yielded models that did not necessarily extract the finest details from each signal, suggesting that further fundamental research is needed to better explain these outcomes and improve the interpretation of periodic signals in hydraulic tomography.

3.3 Methods

The synthetic oscillatory tomographic experiments include both homogeneous and heterogeneous models, with source signals generated to simulate head responses at one source and three observation intervals. These simulated heads serve to investigate how different periods influence the resolution of hydraulic properties derived from oscillatory hydraulic tomography data. The results from these synthetic experiments will be compared to a real field case experiment, which shares similar aquifer characteristics and experimental setup, providing a basis for understanding the impact of varying signal periods on the resolution of subsurface properties.

A numerical groundwater flow model is used to gain insights into the principles of periodic hydraulic testing in a tomographic configuration. For a series of periodic tests, this model generates the heads and sensitivities on which the resolution analysis is based. A resolution matrix expresses the degree of parameter resolution that can be achieved given the physics and geometry of a particular hydraulic experiment (Aster et al., 2005). Thus, resolution is a tool that can be used to compare the information content of hydraulic tests carried out with different experimental designs.

3.3.1 Groundwater flow numerical model

The tomographic periodic tests are simulated with the radial groundwater flow model lr2dinv (Bohling and Butler, 2001). This model has been used in several peer-reviewed publications to simulate hydraulic tests in wells (Paradis et al., 2016; Bohling et al., 2002; Bohling et al., 2007; Liu et al., 2008; Bohling, 2009; Liu et al., 2009; Bohling et al., 2012; Zschornack et al., 2013; Paradis and Lefebvre, 2013; Paradis et al., 2015b; Bohling et al., 2016). The hydraulic head h (m) generated in an aquifer by a hydraulic test in a well is described by the radial groundwater flow equation:

$$\frac{1}{r}\frac{\partial}{\partial r}\left(rK_r\frac{\partial h}{\partial r}\right)+\frac{\partial}{\partial z}\left(K_z\frac{\partial h}{\partial z}\right)=S_s\frac{\partial h}{\partial t} \tag{3.1}$$

where r (m) is the radial coordinate from the center of the well, z (m) is the vertical coordinate, t (s) is the time, S_s (m^{-1}) is the specific storage, and K_r (or K_h) and K_z (ms^{-1}) are the hydraulic conductivities in the radial (or horizontal) and vertical directions, respectively. Equation (3.1) is solved using a block-centered finite-difference formulation after a logarithmic transformation of the radial flow equation into an equivalent equation in Cartesian coordinates (Butler and McElwee, 1990; Bohling and Butler, 2001).

The homogeneous and heterogeneous models replicate the experimental setup of oscillatory hydraulic tomography tests reported by Nefzi et al. (2025). The hydraulic property field of the heterogeneous model has similar values and spatial distributions as those obtained from the inversion of the actual field tests in the granular aquifer in St-Lambert, Québec. This inversion combined the heads measured for three OHT field tests using different source periods of 2.5 min, 5 min, and 10 min.

In the test configuration represented in the models, two wells with a diameter of 0.0762 m and separated by 5.35 m are considered. The tomographic configuration consists of seven periodic tests performed sequentially at eight source intervals isolated with packers in the source well. For each test, heads are monitored at four locations: the source interval itself and three intervals in the observation well. This test configuration is based on previous studies at a test site, so it offers a basis of comparison with actual tomographic field tests (Paradis et al., 2015a; Paradis et al., 2016)

The length of each source interval is 0.60 m. Simulation of the effects of wellbore storage and packer placement in the source well is achieved by using the inner boundary of the model to represent the region within the wellbore. A Darcy's Law formulation is used to approximate the

processes, with the screened interval represented as a region of high permeability and the packers as impermeable.

A periodic flow rate Q (m^3s^{-1}) is imposed in the screened interval to induce water exchange with the aquifer at the screen of the well having a radius r_w (m):

$$Q = \pi r_c^2 \frac{\partial(A_0 \sin(2\pi/T_0 t))}{\partial t} = 2\pi r_w L K_h \frac{\partial h}{\partial r} \quad (3.2)$$

where r_c (m) is the radius of the casing or riser, L (m) is the length of the source interval, and $A0sin(2\pi/T0t)$ (m) is the sinusoidal hydraulic stress, where A_0 (m) and T_0 (s) are the peak amplitude and period of the periodic stress, respectively. For the simulations, the periodic flow rate is approximated as a series of steps, with each step modeled as a constant flow boundary condition with a start and end time.

A simulation grid with an exponential increase in horizontal cell size from the source is used. Along the vertical axis, there were 66 rows of cells, each with a fixed vertical dimension of 0.1524 m. The parameter grid covers the extent of the aquifer, and its cells coincide with the radial and vertical positions of the source and observation intervals. The model used a simulation grid with 66 cells of logarithmically increasing dimension along the radial axis up to a radial distance of 36 m. The simulation grid was divided into 187 cells of 0.61 m in height which corresponds to the length of the source interval.

Figure 3-2 illustrates the parameter grid from the field test data for interval 2.5 min, which is vertically divided into 17 layers and further subdivided into 11 columns of cells horizontally. Six of these columns are placed between the source and observation wells, while the remaining five columns are present in the region extending beyond the observation well. This same discretization of the parameter grid was applied for K_h, K_v/K_h, and S_s. Figure 3-2 shows the importance of heterogeneity and anisotropy of the heterogeneous model. The focus zone is subdivided in three domains that exhibited different responses in observation wells (Groups 1 to 3).

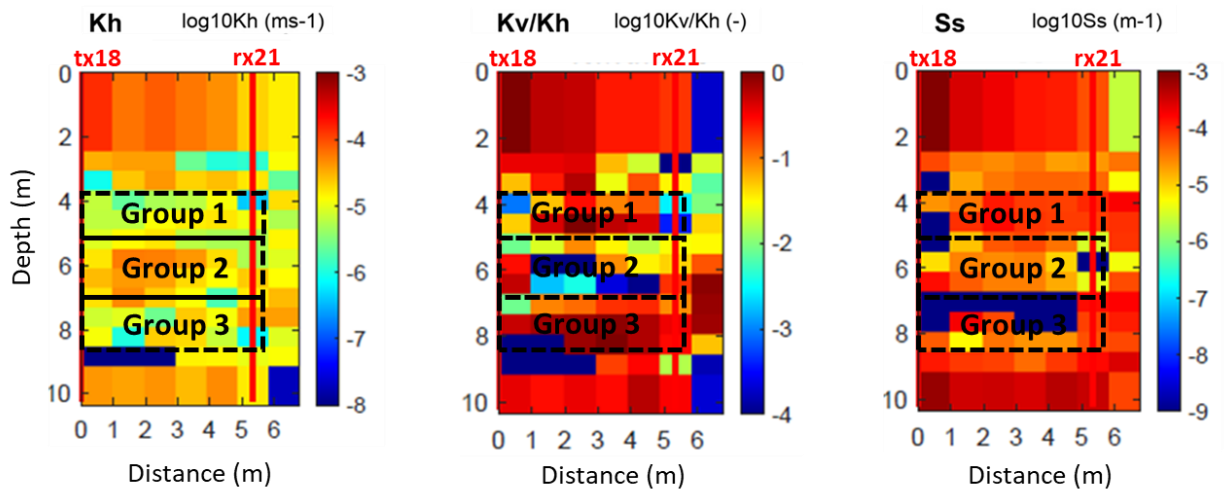

Figure 3-2 : Part of the model parameter grid showing the tomograms for Kh, Kv/Kh, and Ss obtained from the inversion of the periodic tests for the field test with the individual period of 2.5 min. The focus area covering the tested source and observation intervals is divided into three groups intervals based on the relative amplitudes observed in receiver intervals (Figure 3-4). The parameter grid extends over the position of the observation well.

The outer model boundary condition beyond the observation well is defined as a fixed head, and the upper boundary is also a fixed head to approximate the position of the water table of the unconfined aquifer. The impermeable lower boundary has a zero-flux condition. The simulation of the effects of wellbore storage and packer placement in the source well is approximated using a formulation of Darcy's Law (Bohling and Butler, 2001), with the screen of the source interval modeled as a region of high permeability and the packers as essentially impermeable. For the initial conditions, a confined flow is established with zero-flux conditions at both the upper and lower boundaries. Before each simulation, a static condition is used, characterized by a constant head across the entire model. The "focus zone" between the source well and the observation well refers to the area covered by head measurements taken at the source and observation intervals during the tomographic tests. This focus zone encompasses 48 parameter grid cells and represents the zone in which representative hydraulic parameters of the aquifer should be defined. Through trial and error, the number of cells in the parameter grid was determined to ensure that the distinctive characteristics of the L-curve, were revealed for each period tested. Section 3.3.2.5 explains the use of the L-curve to identify the optimal solution.

3.3.2 Resolution analysis

Following a hydraulic test inducing changes in hydraulic heads in an aquifer, the ability to resolve different hydraulic parameters of the aquifer depends on the relative magnitude and correlation between the sensitivities of the heads to those hydraulic parameters (Vasco et al., 1997; Bohling, 2009; Paradis et al., 2015b). Sensitivity expresses the response of the head to a change in the value of a hydraulic parameter. To be resolved, a parameter must have a nontrivial sensitivity value. The greater the difference in the magnitude of the sensitivity of a parameter relative to its surrounding parameters, the better will be its resolution. Moreover, a parameter is better resolved if its sensitivity pattern differs from that of other parameters over time as heads vary following an imposed hydraulic stress.

Although the inverse problem of groundwater flow is nonlinear, the resolution analysis presented in this paper and summarized below is based on a linear approximation of the model behavior in the vicinity of the assumed hydraulic parameters. That is, the sensitivity matrix serves as an approximate linear representation of the nonlinear flow. It is also expected that a resolution analysis based on a radial 2D model is a valid approximation that can be generalized to planar 2D or 3D models. It is shown also that the resolution for wells in a planar 2D confined aquifer is mainly centered in the plane enclosing the wells with similar patterns to those obtained with a radial model (Paradis et al., 2024). Nevertheless, the use of a radial model must be carefully considered when dealing with an aquifer characterized by significant heterogeneities that may cause significant lateral flow outside the plane of the wells. The resolution analysis presented in this paper is performed using the MATLAB (MathWorks, 2023) Regularization Toolbox (Hansen, 2023).

3.3.2.1 Inverse problem

The resolution analysis is based on the study of the inverse problem associated with a specific tomographic experiment. An inverse hydraulic problem involves finding a model for the spatial distribution of the hydraulic parameters of an aquifer for which head data have been measured in wells at different times and locations following an imposed hydraulic stress (Aster et al., 2005):

$$\mathrm{m} = \mathrm{F}^{-1}\,(\mathrm{d}) \tag{3.3}$$

where m is a vector of n hydraulic parameters that we try to estimate from the head data vector d with m observations. F^{-1} is the inverse process of the forward operator F, which represents the non-linear behavior of groundwater flow, as described in Section 3.3.1. However, the process of

finding an inverse solution is challenging and involves important issues such as the existence of the solution (e.g., no model that fits the observations), the uniqueness of the solution (e.g., rank deficiency where many models equally fit the observations) and the instability of the solution process (e.g., ill-conditioning where small changes in the observations lead to very different models) (Aster et al., 2005).

3.3.2.2 Generalized inverse

To facilitate the search for an inverse solution m, the generalized inverse J† of the sensitivity matrix **J** is used as the inverse operator F^{-1} (Moore, 1920; Penrose, 1955):

$$\mathrm{m}_{\dagger} = \mathrm{J}^{\dagger}\mathrm{d} \tag{3.4}$$

The sensitivity matrix **J** is an *m*-by-*n* normalized sensitivity matrix of *m* observations and n parameters, expressing the head response at each observation point and at each time to a change in each hydraulic parameter value:

$$J_{m,n} = \frac{\partial d_m}{\partial m_n / m_n} \tag{3.5}$$

This normalized form of the sensitivities is used to better identify the relative influence of each hydraulic parameter (Bohling and Butler, 2001). The elements of the sensitivity matrix were evaluated using the sequential perturbation approach of a groundwater flow model developed with the lr2dinv numerical simulator.

The generalized inverse J† is a decomposition of the sensitivity matrix J into its singular values (SVD):

$$\mathrm{J}\dagger = \mathrm{V}\mathrm{S}^{-1}\mathrm{U}^{T}\mathrm{d} \tag{3.6}$$

where U and V form two sets of orthonormal matrices of size m-by-m and n-by-n, respectively, and S is an *m*-by-*n* diagonal matrix consisting of the singular values s_i of J arranged in decreasing size. The generalized inverse always produces the least squares inverse solution with minimum length and ensures that an inverse solution always exists for ill-conditioned and rank deficient hydraulic inverse problems.

3.3.2.3 Tikhonov regularization

The presence of very small singular values in S of Eq. (3.6) can however cause the generalized inverse solution to become extremely unstable (Aster et al., 2005). Therefore, regularization of

the solution is necessary. One of the most widely used regularization methods is the Tikhonov technique (Tikhonov and Goncharsky, 1987):

$$\mathrm{m}_{\lambda} = \mathrm{VFS}^{\dagger}\mathrm{U}^{T}\mathrm{d} \tag{3.7}$$

where an *n*-by-*n* diagonal matrix F with diagonal elements given by the filter factors:

$$f_i = \frac{s_i^2}{s_i^2+\lambda^2} \tag{3.8}$$

is introduced to reduce the influence of smaller singular values s_i. The weighting of the singular values is determined by λ. If the value of λ is much higher than s_i, the value of f_i approaches zero, which leads to a lower weighting. Conversely, a much lower value of λ leads to a higher weighting. The choice of λ is explained in Section 3.3.2.5. The matrix S† is the generalized inverse of S, S† = VΣ†UT, in which Σ† is a diagonal matrix where each non-zero diagonal element is the reciprocal of the corresponding non-zero singular value of the original matrix S. The zeros on the diagonal of S† correspond to the zero singular values of S.

3.3.2.4 Resolution matrix

The concept of resolution is a way to evaluate the properties of the generalized inverse solution of a specific hydraulic experiment. A resolution matrix reflects the physics and geometry of the experiment. In the Tikhonov regularization method, the resolution matrix of the hydraulic parameter is given by:

$$\mathrm{R}_{m,\lambda} = \mathrm{VFV}^{T} \tag{3.9}$$

where the elements of $\mathbf{R}_{m,\lambda}$ indicate the relative magnitude and correlation between the sensitivities of the heads to the hydraulic parameters. Thus, if $\mathbf{R}_{m,\lambda}$ = I, the identity matrix, the resolution is perfect, and the true hydraulic parameters are recovered exactly. At the opposite extreme, a resolution value approaching zero means that a parameter cannot be resolved based on the measured heads.

3.3.2.5 Selecting the best solution

Since the model resolution matrix depends on the value of λ, for consistency among the comparisons of the different simulations, the λ value is selected according to the L-curve criterion (Hansen, 1992). A L-curve is constructed from the minimization of the damped least squares equation for a range of λ values:

$$min \, \|\mathrm{Jm}_\lambda - \mathrm{d}\|_2^2 + \lambda^2 \|\mathrm{m}_\lambda\|_2^2 \tag{3.10}$$

where the left side is the squared norm of the residual of the head data and the right side is the squared norm of the model parameter vector. Plotted on a logarithmic scale, the curve of the optimal values of the residual and model norms often takes the form of a L (Figure 3-3). For the horizontal segment of the curve, the solution is dominated by the regularization error. Very large λ values lead to an over-smoothing of the solutions with a large residual norm. On the other hand, the vertical segment is characterized by very small λ values, which results in over-fitting of the head data. Thus, the optimal solution between sensitivity to noise and parameter resolution corresponds to the value of λ that lies at the corner of the L-curve. The adaptative pruning algorithm by (Hansen et al., 2007) was used to locate the corner of the L-curve for each set of simulations and for all periods described in Table 3-2. Thus, by employing an L-curve analysis of the simulated heads and sensitivities, this study identifies the optimal parameter resolution, offering a foundation for comparing the different experimental configurations (Paradis et al., 2024).

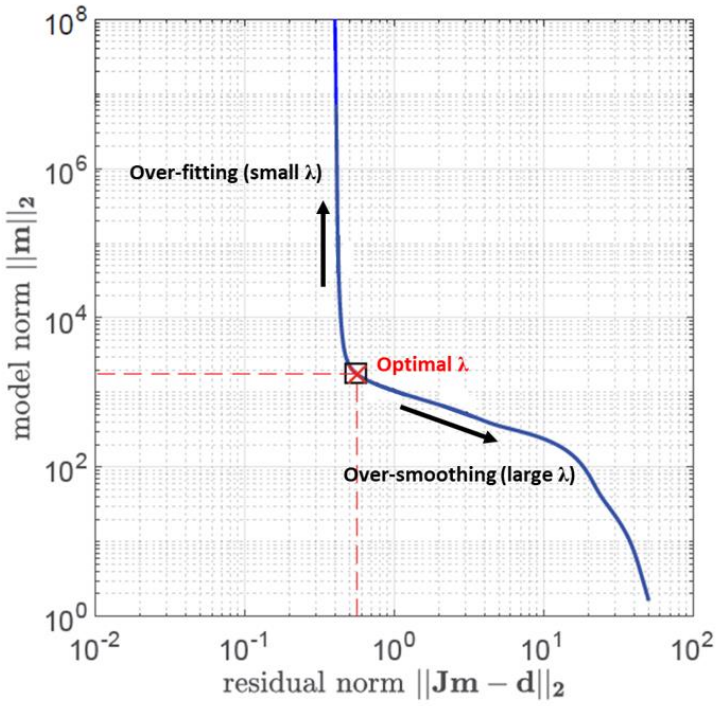

Figure 3-3 : An example of L-curve for the tomographic experiment with tests using a period of 1.25 min in Figure 3-4. The optimal λ value at the corner of the L-curve is a balance between over-fitting the head data and over-smoothing the estimated hydraulic parameter.

3.3.2.6 Noise level

To obtain a realistic evaluation of the resolutions, the heads generated by the groundwater flow model must be perturbed by a noise level consistent with field measurements. The noise level is based on a field application of periodic slug tests carried out by the authors (Nefzi et al., 2025). This noise is estimated as normally distributed with an expected 0 mean and a standard deviation of 8.5×10^{-3} and 1.8×10^{-4} m for the source and observation intervals, respectively. A higher noise is applied to the heads of the source intervals to account for the turbulent flow created by the motion of the rod used to generate the periodic signal.

3.3.2.7 Metrics

Two different metrics are used to compare the resolution associated to each simulation (Günther, 2004). First, the total information content (IC) of the experiment is assessed by summing all diagonal elements of the model resolution matrix:

$$IC = \sum_i^N R_{m,\lambda,ii}^N \tag{3.11}$$

where N is the total number of parameters within the focus area. The higher IC is, the better the resolution of the parameter obtained for a given hydraulic experiment.

Then, for each hydraulic property (K_h, K_v/K_h and S_s), the information content IC_j associated with each property (j) is divided by the corresponding number of parameters Nj to obtain the resolution degree (*RD*):

$$RD_j = {IC_j}/{N_j} \tag{3.12}$$

where j = 1 to 3 and corresponds to K_h, K_v/K_h and S_s, respectively. *RD* is a measure of the average resolution achieved for each hydraulic property, varying between 0 (not resolved) and 1 (perfectly resolved).

3.3.3 Groundwater flow simulation program

A key shortcoming of prior studies is the limited examination of the relative benefits and the informational content obtained from single, multiple, or combined periods. This research aims to fill that gap by providing a detailed a posteriori analysis of periodic test experiments conducted in a hydraulic tomography configuration. In this study, different scenarios are thus rigorously tested and compared with the original periodic hydraulic tomography experiments to provide valuable insights into the factors that contributed to the success of the original tests and the aspects that can be further optimized. Additionally, the effectiveness of combining multiple periods is explored, with the goal of determining whether a multi-period approach provides more comprehensive and reliable data compared to single-period tests.

The simulated OHT experiments included ten tests involving a periodic signal in one source interval and measurements of heads in that source interval as well as three intervals in the observation well. The combinations of stress and observation intervals considered for these 10 tests are listed in Table 3-1. The maximum head of the oscillatory signals simulated in observation intervals ranged from 0.011 to 0.041 m. Within that focus zones, three groups of observation intervals having distinct responses were identified. The first interval spans from test tx.450 to test tx.510b, corresponding to the Group 1 of the focus zone; the second interval extends from test tx.570 to test tx.690b, representing the Group 2 of the focus zone; and the third interval ranges from test tx.750 to test tx.870, which correlates with the Group 3 of the focus zone (Figure 3-2).

Table 3-1 : Summary of simulated oscillatory hydraulic tomography experiments. Prefix ‘‘tx” is for ‘‘transmitter” (stressed interval) whereas ‘‘rx” is for ‘‘receiver” (observation interval).

Stressed interval*	Observation intervals for each stressed interval			Interval of maximum head	Maximum head(m)
tx450	rx330	rx420	rx510	rx420	0.018
tx510b	rx330	rx420	rx510	rx330	0.024
tx510a	rx510	rx600	rx690	rx510	0.022
tx570	rx510	rx600	rx690	rx690	0.041
tx630	rx510	rx600	rx690	rx690	0.031
tx690b	rx510	rx600	rx690	rx690	0.039
tx690a	rx690	rx780	rx870	rx690	0.039
tx750	rx700	rx790	rx880	rx880	0.014
tx810	rx700	rx790	rx880	rx880	0.011
tx870	rx690	rx780	rx870	rx870	0.008

*: the names of stressed intervals refer to their depth relative to soil surface.

Table 3-2 summarizes the simulation program whose purpose is to fully explore the effect of test conditions on the hydraulic response, information content and resolution of individual and combined periodic signals. The eight sets of simulations that were caried out that involved a series of experiments using twelve different periodic signals. The simulated heads were recorded in the source interval itself and in 3 observation intervals in the observation well. The eight (8) periods range from 0.312 to 40 min are applied across all scenarios. The selection of these periods is based on those used in hydraulic tomography experiments with periodic slug tests in an anisotropic littoral aquifer at Saint-Lambert (Nefzi et al., 2025). Consequently, periods were chosen both below and above those used in the field test.

Table 3-2 : Simulated tomography experiment scenarios. The radii are defined and illustrated in Figure 3-1 (section 3.2). A0 = 1.25 m for all tests. Scenarios 5 to 10 use the same conditions as previous scenarios, but inversions were done with data from two or three periods.

Scenario	Variable considered	Hydraulic properties	Periods (min)	Radius (m)			Displaced volume (L) per half cycle
				r_o	r_{eq} or r_i	r_w	
1	Hydraulic properties	Heterogeneous	0.312, 0.625, 1.25, 2.5, 5, 10, 20, 40	0.0107	0.0077	0.0254	4.5
2		Homogeneous: $Kh=2.3x10^{-5}$ ms^{-1} $Kv/Kh=1.6x10^{-1}$ $Ss=6.0x10^{-5}$ m^{-1}	0.312, 0.625, 1.25, 2.5, 5, 10, 20, 40	0.0107	0.0077	0.0254	4.5
3	Radius	Heterogeneous	0.312, 0.625, 1.25, 2.5, 5, 10, 20, 40	0. 0127	0.0127	0.0254	6.9
4		Heterogeneous	0.312, 0.625, 1.25, 2.5, 5, 10, 20, 40	0. 0254	0.0254	0.0254	25.5
5	Period combination (pair)	Heterogeneous	0.312, 0.625, 1.25, 2.5, 5,	0.0107	0.0077	0.0254	4.5

			10, 20, 40				
6		Heterogeneous	0.312, 0.625, 1.25, 2.5, 5, 10, 20, 40	0. 0127	0.0127	0.0254	6.9
7		Heterogeneous	0.312, 0.625, 1.25, 2.5, 5, 10, 20, 40	0. 0254	0.0254	0.0254	25.5
8	Period combination (triplet)	Heterogeneous	0.312, 0.625, 1.25, 2.5, 5, 10, 20, 40	0.0107	0.0077	0.0254	4.5
9		Heterogeneous	0.312, 0.625, 1.25, 2.5, 5, 10, 20, 40	0. 0127	0.0127	0.0254	6.9
10		Heterogeneous	0.312, 0.625, 1.25, 2.5, 5, 10, 20, 40	0. 0254	0.0254	0.0254	25.5

The first set of simulations investigates the influence of heterogeneity in the aquifer, providing a baseline for comparison. Figure 3-2 illustrates the spatially heterogeneous model, which was defined using average hydraulic properties fron the three periods (2.5 min, 5 min, and 10 min) as the reference condition for scenario evaluation. The second scenario for the first set includes a homogeneous aquifer model with specified values for hydraulic conductivity (Table 3-2). This homogeneous case helps isolate the effects of test configurations on the response by using consistent hydraulic properties across the entire model domain.

The second set of simulations assesses the impact of altering the effective well radius for heterogeneous conditions, with values adjusted to 0.0127 m (larger than in Set 1) and a corresponding volume increase to 6.9 liters per half cycle. The second scenario for this set explores an even larger radius (0.0254 m), which significantly increases the volume to 25.5 liters per half cycle. This scenario tests how larger radii affect the simulated heads and resolution responses within the heterogeneous aquifer model.

The third set of simulations introduces a paired combination of periods across a range from 0.312 to 40 min, maintaining the initial radius settings to observe how various period pairs influence head changes and resolution. Two additional scenarios with different radii are included: one with a radius of 0.0127 m and another with a radius of 0.0254 m. This simulation set emphasizes the effect of larger radius conditions on the paired period results.

Finally, the fourth set of simulations is similar to set 3 but uses a triplet combination of periods instead of paired periods. This configuration allows for an extended evaluation of head response and parameter resolution under a triplet period setup, while keeping the other conditions consistent with those in Set 3.

3.3.4 Period combinations

This part of the study focused on combining hydraulic heads obtained from tests with different source signal periods. By analyzing combinations of heads from multiple tests, the aim was to improve the resolution and capture finer details of the hydraulic properties. This analysis incorporated both dual and triple period combinations, examining their potential to enhance the information content (IC) and resolution degree (RD).

For the dual-period combination analysis, pairs of periods were selected from the range of 0.312 to 40 min. In total, there are 28 unique combinations possible from this set of eight periods. Each combination was assessed by calculating the IC and RD from the composite sensitivity matrix

formed by combining the sensitivities obtained from tomographic experiments using the two selected periods. The goal was to determine whether combining these periods could provide a higher IC and better parameter resolution than individual tests.

Similarly, for the triple-period combinations, the potential of combining three different periods from the same set was explored. With eight available periods, a total of 56 unique triple-period combinations were analyzed. As with the dual-period combinations, the IC and RD were computed for each triple-period composite matrix, allowing an assessment of the resolution gain and information captured from combining three different signal periods.

3.4 Results and discussion

3.4.1 Signal propagation under heterogeneous conditions

Figure 3-4 shows the variability in simulated head amplitudes for all receiver intervals (3) related to one transmitter interval for all eight (8) signal periods used in the heterogeneous model. To facilitate comparison, Figure 3-4 shows the relative amplitude, which is the ratio of the variation of the head at each receiver to the maximum variation of the head measured for all receiver intervals and periods. The figure also highlights the ranges of relative amplitude behaviors across different receiver intervals, which involve significant variations in relative amplitudes 1) among the three receivers related to one transmitter, 2) between groups of receivers related to different transmitters, 3) according to the transmitter signal periods, and 4) in relation to the period at which the maximum amplitudes occur.

The patterns of the relative amplitudes shown in Figure 3-4 are distinct for three groups of tests, from top to bottom of the focus zone: (1) tx.450 to tx.510b; (2) tx.570 to tx.690b; and (3) tx.750 to tx.870.

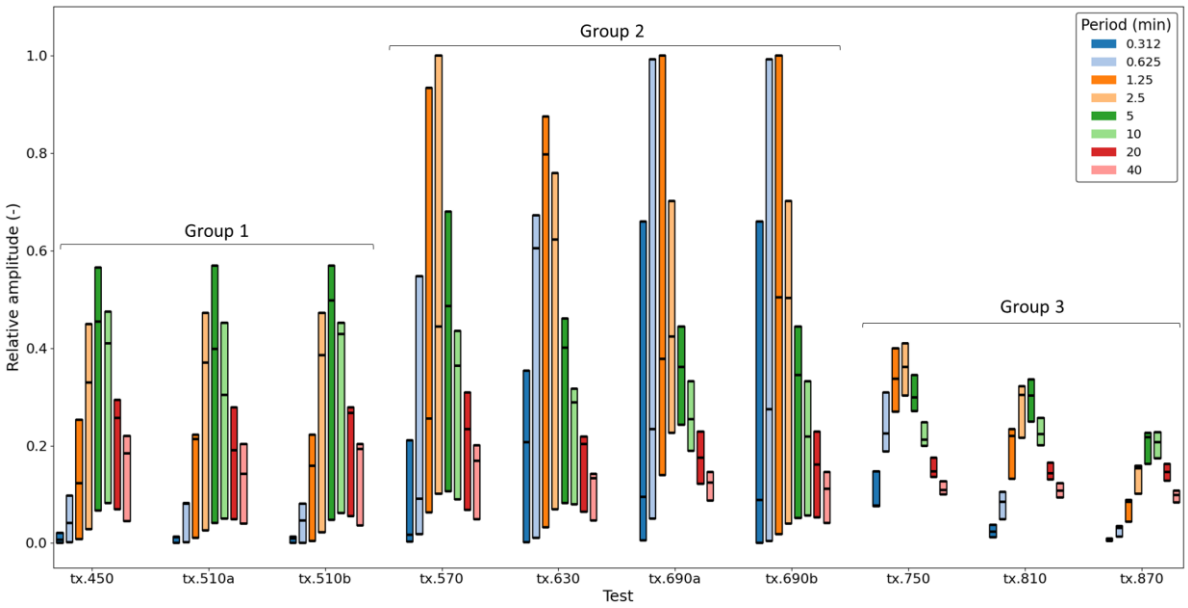

Figure 3-4 : Comparison of relative amplitudes for the three receiver intervals related to the source intervals for the ten signal periods simulated for the heterogeneous model. The relative amplitude in an observation interval for a given period is the ratio of the variation of the head to the maximum variation of the head measured for all observation intervals and periods. The black lines at the extent of the bars and within the bars represent the three values recorded at the three receiver intervals.

For the Group 1, the magnitude of the relative amplitudes has intermediate values relative to the other two groups, and peak values are obtained for the 5-min period. Group 2 exhibits the largest magnitudes among the groups, and their maximum values are obtained for the 1.25-min or 2.5-min periods. Group 3 shows the smallest magnitudes of amplitudes among the groups, with peak amplitudes for periods ranging from 2.5-min to 10-min. For all groups, the variability of amplitudes between the observation intervals (the difference between the minimum and maximum variation of the head) is generally proportional to the magnitude of the relative amplitude.

Moreover, these three groups have different responses to varying periods, indicating differences in how the aquifer material affects the relative amplitude. In Group 1, shorter periods (0.312 to 1.25 min) result in smaller amplitude variations, suggesting that the aquifer material here may dampen the effects of shorter period signals. In contrast, Group 2 shows a broader range of amplitude variation across periods, hinting at more heterogeneous material properties. Group 3 displays lower amplitudes overall, and the periods corresponding to maximum amplitudes are similar to those observed in Group 1 or Group 2. These observations highlight the differing sensitivity of aquifer materials to the applied periods whose signals are transmitted differently.

Referring to the hydraulic properties within the three groups illustrated in Figure 3-2 helps understand their incidence on the distinct signal propagation behavior for these groups as shown in Figure 3-4. Also, Figure 3-5 presents the statistics of hydraulic properties between the source and observation intervals for the three groups identified in Figure 3-4, along with head measurements in the observation intervals associated with these groups. These statistics highlight how variations in hydraulic conductivity K_h, anisotropy K_v/K_h, and specific storage S_s influence the observed head responses.

First, in terms of horizontal hydraulic conductivity (K_h), Group 1 (tests from tx.450 to tx.510b) has the lowest median value, Group 2 (tests from tx.570 to tx.690b) the highest, and Group 3 (tests from tx.750 to tx.870) an intermediate value. Although the lowest individual Kh value is found in Group 3, this group is generally associated with higher median Kh values compared to Group 1. These relative values of K_h thus clearly explain the relative magnitudes of the signal amplitudes between the three groups, as larger values of K_h favor signal propagation from the transmitter to the receivers. Furthermore, for Group 2 having largest K_h values, shorter period signals (0.625 to 2.5 min) propagate better, whereas longer period signals (2.5 to 10 min) lead to the highest amplitudes in lower- K_h Groups 1 and 3.

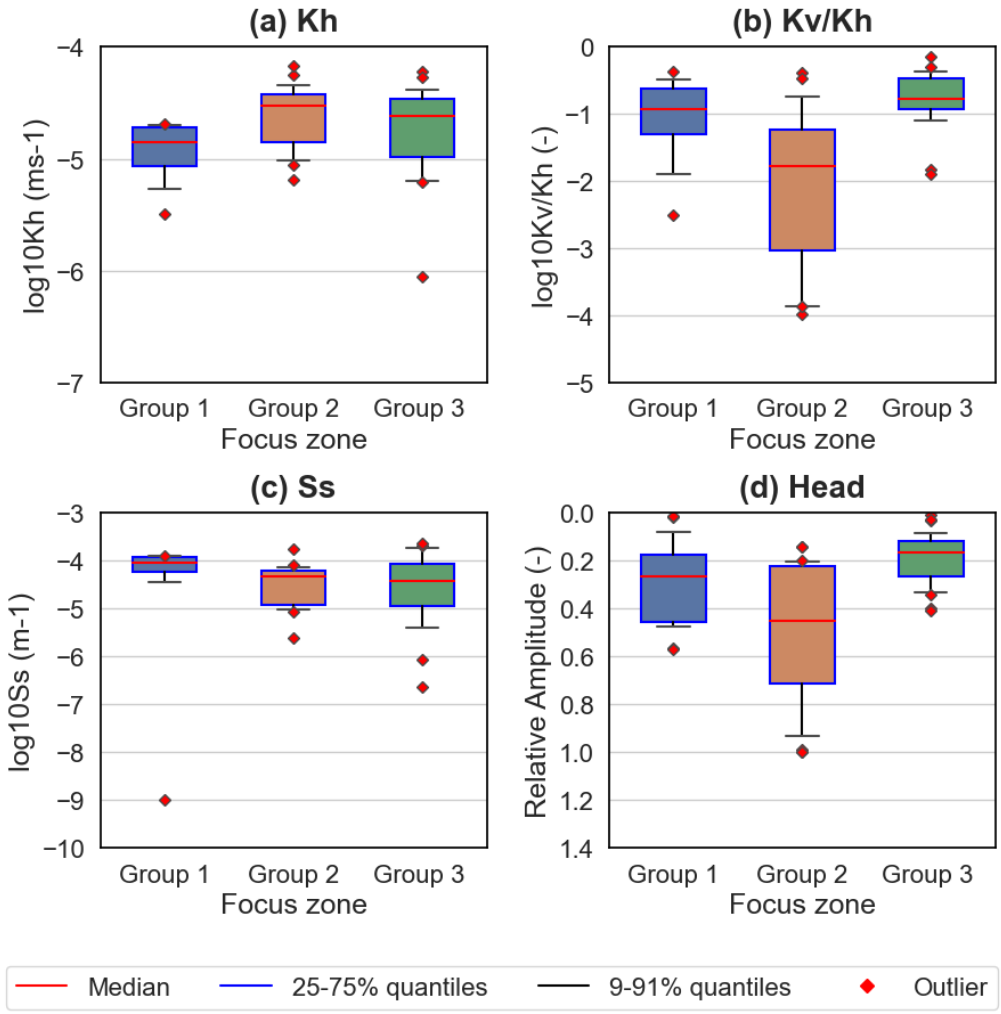

Figure 3-5 : Statistical distributions of (a) Kh, (b) Kv/Kh, (c) Ss and (d) head simulated in the observation intervals for the three zones identified in Figure 3-4 and drawn in Figure 3-2. Note that the y-axis of (d) is reversed to better illustrate its correlation with (b).

Then, in terms of hydraulic conductivity anisotropy (K_v/K_h), the patterns are inverse of those for K_h, as it is Group 3 that shows nearly isotropic conditions, whereas Group 2 exhibits more anisotropic and more variable conditions, and Group 1 has intermediate anisotropy. These distinct anisotropy conditions explain well the level of variability among the three receivers related to a transmitter. When conditions are nearly isotropic, the signal from the transmitter reaches the three receivers with a similar amplitude, leading to low variability in amplitudes, as is the case for Group 3. On the contrary, when conditions are highly anisotropic, the signal amplitude reaching the two receivers with a diagonal path is much smaller than for the receiver in a direct horizontal path. More anisotropy thus involves more variability in receiver amplitudes, as is the case for Group 2.

In summary, the comparison of Figure 3-4 and Figure 3-5 shows that the maximum values of heads are related to the magnitude of K_h (comparing Figure 3-5a and Figure 3-5d); Group 2 showing the largest heads, followed by Groups 1 and 3. On the other hand, the variability of the heads is controlled by anisotropy (K_v/K_h) (comparing Figure 3-5b and Figure 3-5d), with Group 2 exhibiting more variability, followed by Group 2 and then Group 3. The specific storage S_s plays a secondary role by influencing how much water is stored and released from the aquifer during the tests. Although S_s shows minimal variation across the intervals, its consistent influence helps stabilize the amplitude variations, particularly in the group 3, where lower anisotropy leads to a more subdued response. Globally, the differences in K_h, K_v/K_h and S_s across the focus zone directly affect the observed head responses, with K_h influencing the peak period, anisotropy affecting head variability, and both anisotropy and S_s impacting the magnitude of head amplitudes.

The comparison of Figure 3-5a with the period in which the relative peak amplitude is reached in Figure 3-4 shows an inverse relationship. For example, the shorter peak periods (1.25 to 2.5 min) are observed for the second group of tests with the higher K_h. The relationship for the third group is less clear, as the distribution of K_h is less homogeneous for this region than for the other two, especially at the location of the source interval (Figure 3-2). The inverse relationship between peak period and K_h is consistent with the results of Paradis et al. (2024) with a homogeneous model. Figure 3-5b shows that the higher is the anisotropy (smaller K_v/K_h values) the larger is the variability of the head (defined as the range of the 25-75% quantiles). This is to be expected, because the higher the anisotropy, the more concentrated the flow is in the horizontal plane of the source interval, which leads to an increased head within this plane and a lower head outside it (Paradis et al., 2024). Thus, the higher anisotropy for the second group identified in Figure 3-4 explains the greater variability of responses in the observation interval. Finally, it is known that both anisotropy and S_s influence the magnitude of the head (Paradis et al., 2024). For a fixed value of K_v/K_h, the magnitude of the head response at an observation interval increases with decreasing Ss. This is observed for the first two groups identified in Figure 3-4.

3.4.2 The effect of signal period on its propagation under heterogeneous conditions

Figure 3-6 illustrates how relative amplitude varies across different periods for all tests, providing a complementary perspective to Figure 3-4. While Figure 3-4 focuses on amplitude variability by test, Figure 3-6 emphasizes the effect of the signal period on relative amplitude across the entire dataset. Figure 3-6 shows that shorter periods (0.625, 1.25, and 2.5 min) are associated with a

larger variability in relative amplitude, particularly for Group 2 of the focus zone. This variability can be explained by two main mechanisms: (1) the higher heterogeneity of hydraulic properties in Group 2 (Kh, Kv/Kh, Ss), which amplifies contrasts between observation intervals; and (2) the stronger attenuation of short-period signals during propagation, especially for observation intervals located farther from the source.

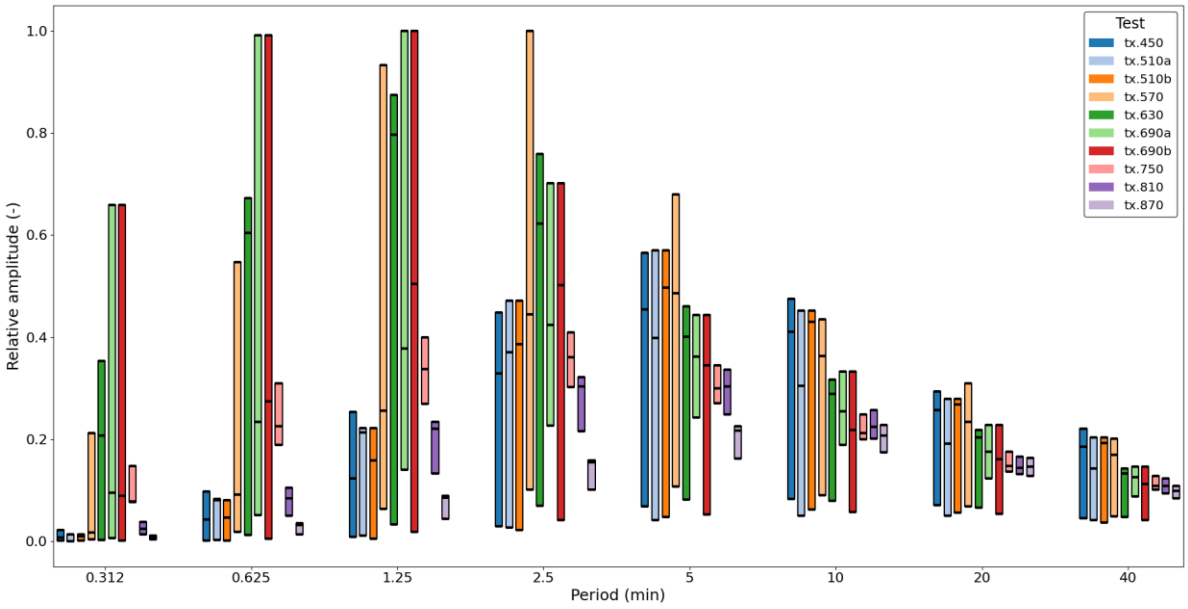

Figure 3-6 : Comparison of relative amplitudes at the three receivers over eight of the simulated signal periods for the heterogeneous model. The extent of the bars represents the minimum and maximum values at two receiver intervals and the black line shows the intermediate value of the third interval.

By comparing both figures, it becomes evident that Figure 3-6 helps to isolate the effect of period length on amplitude responses, whereas Figure 3-4 is more focused on the test-specific variability across periods. Thus, Figure 3-6 provides insights into how the choice of period influences the overall amplitude pattern across the observation intervals, reinforcing the importance of selecting the appropriate period regarding specific geological conditions.

Regarding the maximum responses of the head, the choice of periods for the field experiment was optimal for Group 1 to obtain the best signal-to-noise ratio for the tomography experiments. However, using shorter periods for Group 2 could have generated higher heads, resulting in higher amplitude signals, and a potential improvement of the resolution of hydraulic properties. For Group 3, the choice is mixed as some periods resulted in higher heads, while others yielded less distinct signals.

From a practical perspective, these results suggest that, during field experiments, selecting the optimal period in real-time can be challenging due to the unknown hydraulic properties at the start

of testing. Based on the results for Group 2, shorter periods (e.g., 0.625 or 1.25 min) might be tested first in areas suspected to have higher permeability, as they generate higher heads. For Group 3, where the material is less permeable, longer periods might be initially tested but should be adjusted dynamically depending on real-time data to avoid low head responses.

While the selection of test periods used during the field experiment was generally effective, the results shown here indicate that an adaptive approach, where periods are adjusted in real time based on preliminary and real-time data, would optimize head responses. By employing shorter periods for higher permeability zones and longer periods for less permeable areas, future tomography experiments can ensure higher head responses, improving the overall quality of the data collected. Considering the varied responses to signal periods, an OHT field test should thus involve the use of a range of periods, so that some of the periods could be better adapted to different intervals of the test site.

3.4.3 Parameter resolution under heterogeneous conditions

The resolution analysis for the simulated tomographic experiments, based on the sensitivity matrix, utilized the L-curve criteria to clearly distinguish between noise amplification and parameter resolution. This method allowed for a consistent comparison of tomographic experiments across different periods. The inflection point (marked with "x" on each curve) represents the optimal trade-off between over-fitting the head data and over-smoothing the estimated hydraulic parameters. Figure 3-7 shows the inflection point that was selected on the L-curve related to the simulated tomographic experiments with different signal periods using the heterogeneous model (Scenarios 1 in Table 3-2). The L-curves are well defined, and their optimal point can generally be selected without ambiguity. This figure shows the global behavior but does not indicate how the resolution varies spatially between the transmitter well and the receiver well, or the resolution obtained for the hydraulic parameters.

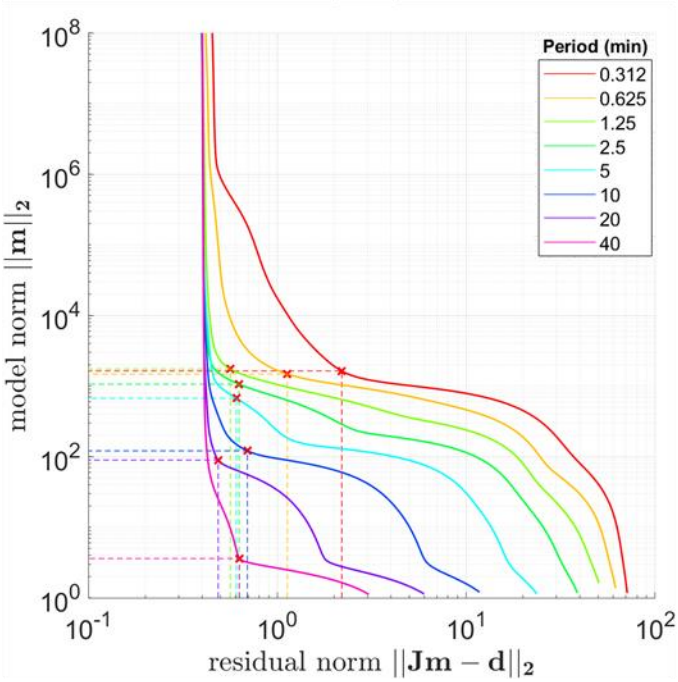

Figure 3-7 : The L-curve plot for the simulated tomographic experiments with different signal periods using heterogeneous conditions (Scenarios 1 in Table 3-2). The inflexion point of each L-curve is marked by a "x" symbol.

For the heterogeneous model, Figure 3-8 shows the spatial resolution of hydraulic parameters (K_h, K_v/K_h, and S_s) for four selected periods (0.312, 1.25, 5, and 20 min) spanning the range of tested periods. Figure 3-8 was obtained by assigning the diagonal elements of the resolution matrix to the corresponding cells of the parameter grid. The higher resolutions for all hydraulic properties and periods are centered on the source well. The resolution is markedly higher at the site of the observation well for K_h and S_s, which also have higher resolutions than K_v/K_h, consistently exhibiting lower resolutions across all periods. Notably, the 1.25 min period provides the highest overall resolution for all parameters.

The lack of significant variation in resolution across the three regions can be explained by the relatively homogeneous sensitivity of the tomography experiments across different periods. The resolution is more influenced by the period length itself, rather than localized changes in head amplitude seen in different regions. While the 1.25 min period is effective for both head response and resolution, longer or shorter periods may optimize head response in certain regions (as discussed in relation to Figure 3-4), but do not result in a significant improvement in resolution. Figure 3-8 shows that the effects of heterogeneous and anisotropic conditions on signal propagation illustrated previously (Figure 3-4 and Figure 3-6) also lead to different global and local resolutions of hydraulic parameters.

In our previous field experiments, the selected periods were 2.5, 5, and 10 min. However, the current analysis suggests that these periods might have been longer than necessary to achieve the highest resolution of hydraulic parameters, particularly K_h and S_s. Simulations indicate that shorter periods, especially around 1.25 min, could provide better spatial resolution across the entire focus area. While the periods of 2.5 to 10 min were effective in generating sufficient head variations for tomographic inversion, they may have missed finer details in the heterogeneity of the subsurface, particularly in regions with more complex anisotropy K_v/K_h. The low resolution for K_v/K_h in Figure 3-8 at 6 m, although close to the source well, likely results from sparse or less sensitive tests in that zone. These limitations can reduce the ability to resolve anisotropy, even in areas near the source. This suggests that while the chosen periods were practical for the field setup, shorter periods could have improved resolution, especially in more heterogeneous zones.

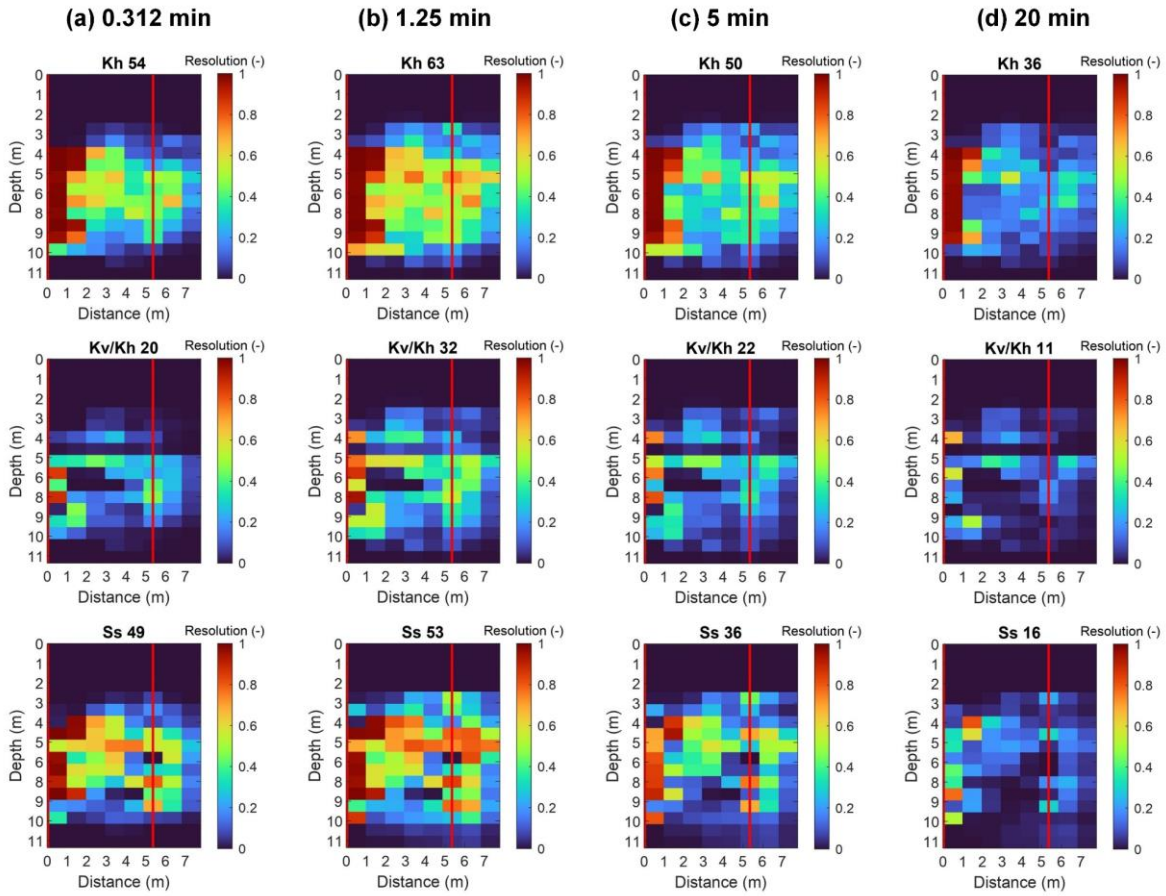

Figure 3-8 : Spatial resolution for the heterogenous case of hydraulic parameters for hydraulic properties Kh, Kv/Kh, and Ss for four selected source signal periods: (a) 0.312 min; (b) 1.25 min; (c) 5 min; and (d) 20 min. The number next to the hydraulic property name is the mean resolution degree within the focus area encompassing the intervals of Groups 1, 2 and 3 shown in Figure 3-2.

3.4.4 Parameter resolution under homogeneous conditions

Figure 3-9 presents the spatial resolution distribution for the homogeneous model for the three hydraulic parameters, evaluated at the same four source periods used for the heterogeneous model (Figure 3-8). This distribution was obtained by assigning the diagonal elements of the resolution matrix to their respective cells within the parameter grid. For the homogeneous model, the spatial patterns of the highest and lowest resolutions remain consistent across the four periods, showing a general decline in the overall resolutions for longer periods, the 20-min period having almost no resolution, except for K_h near the source well.

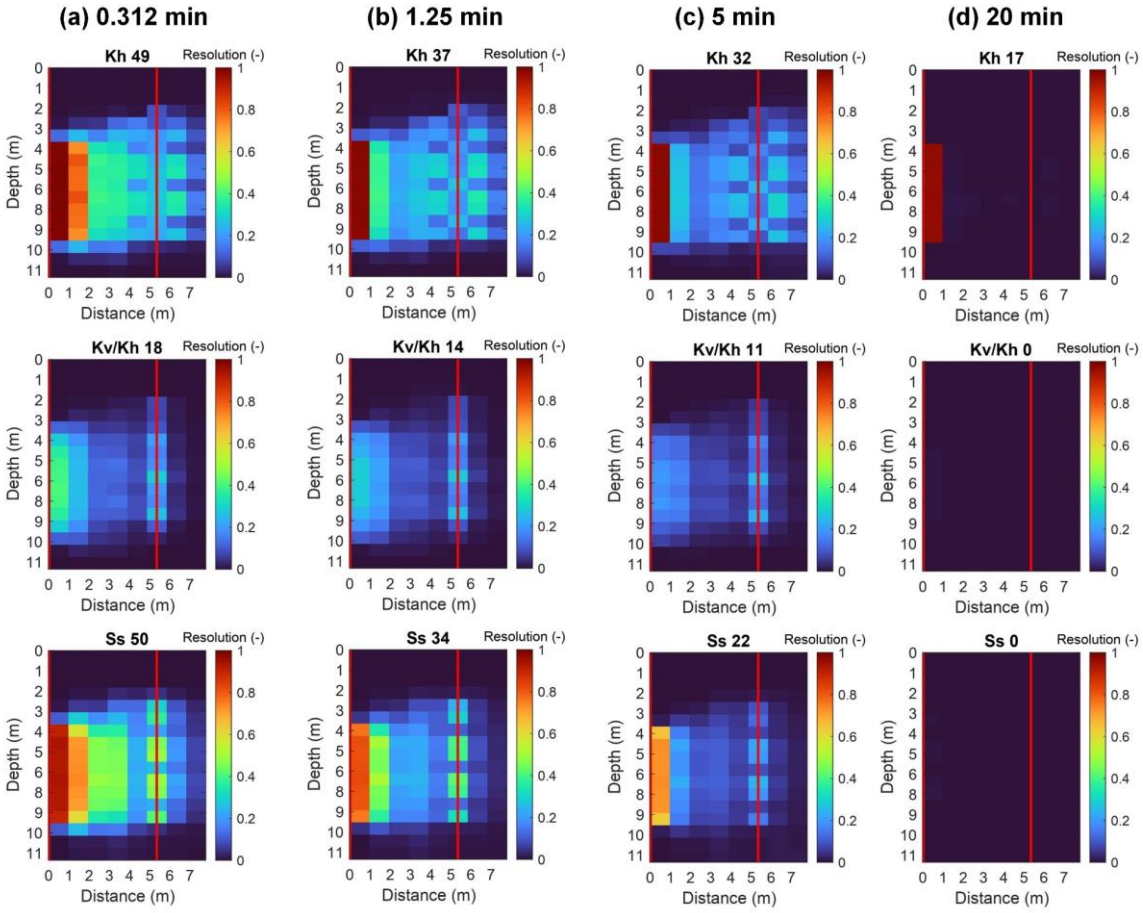

Figure 3-9 : Spatial resolution for the homogeneous model for hydraulic properties Kh, Kv/Kh, and Ss for four selected source signal periods: (a) 0.312 min; (b) 1.25 min; (c) 5 min; and (d) 20 min. The number next to the hydraulic property name is the mean resolution degree within the focus area encompassing the intervals of Groups 1, 2 and 3 shown in Figure 3-2.

For all parameters and periods, the cells near the source well have the highest resolutions. In other regions of the parameter grid, K_h displays enhanced resolution in cells directly upstream and downstream of the observation well. Conversely, K_v/K_h and S_s have better resolutions in cells situated at the observation well itself, which corroborates the results obtained by (Paradis et al., 2024) (Figure 3-9).

3.4.5 Information content

A resolution analysis was carried out to assess the capability of simulated heads (with noise) to resolve the hydraulic properties of the heterogeneous and homogeneous models (referenced as Simulations 1 and 2 in Table 3-2). Figure 3-10 shows the analysis of the diagonal elements of the resolution matrix across the tomographic experiments in terms of information content (IC) and resolution degree (RD) of the three hydraulic parameters (K_h, K_v/K_h and S_s) for the range of source signal periods considered. That analysis was carried out for the heterogeneous model (Figure 3-10a) and the homogeneous model (Figure 3-10b).

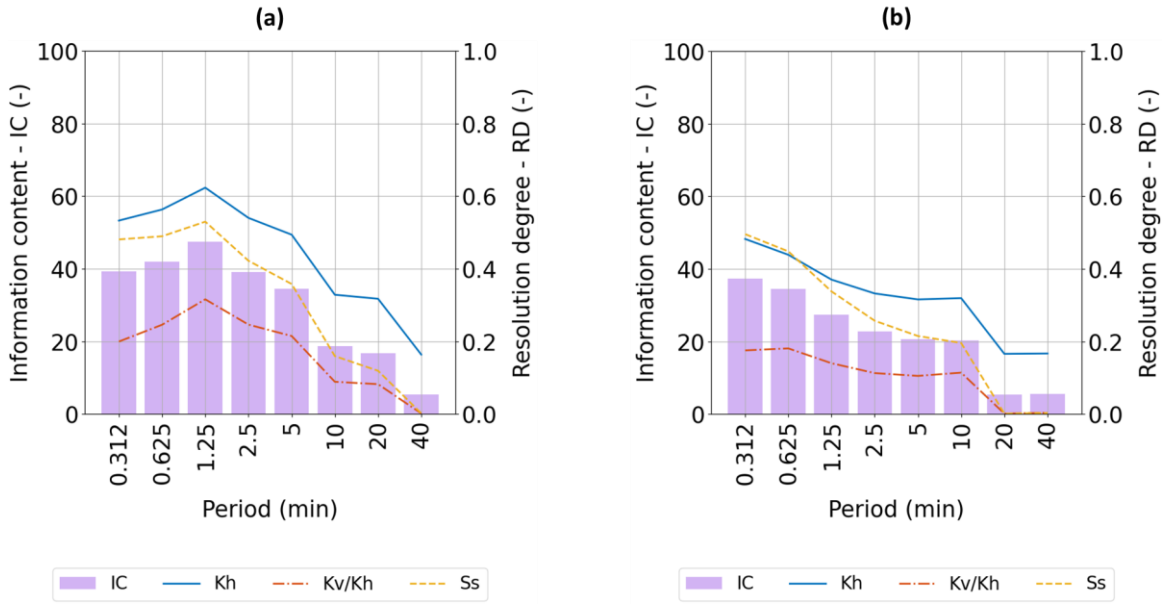

Figure 3-10 : Total information content (IC) and resolution degree (RD) for each hydraulic property (Kh, Kv/Kh and Ss) for eight selected signal periods. The statistics pertain to the cells located within the focus area encompassing the intervals of Groups 1, 2 and 3 shown in Figure 3-2. (a) Heterogeneous model with r_c = 0.0077 m; (b) Homogeneous model with r_c = 0.0077 m.

Although the head is highest in the observation intervals for the 5 min period in Group 1 and for most of the tests in Group 2 (Figure 3-4), the maximum information content and resolution degree are associated with the shorter period (1.25 min) when compared to the other seven periods.

While shorter periods had quite small head variations, their IC and RD remain high, although lower than for the 1.25 min period. For periods longer that 1.25 min, there is a consistent decline in the resolution of all hydraulic properties as the period lengthens.

The resolution of hydraulic parameters improves as the period decreases because shorter periods allow the signals to capture finer-scale heterogeneities. This is why the 1.25 min period yields the highest IC and RD (Paradis et al., 2024). However, when the period becomes too short, such as 0.312 or 0.625 min, the head variations in the observation intervals become very small, approaching the level of noise. This results in a lower signal-to-noise ratio, which limits the ability to resolve hydraulic parameters accurately. Consequently, even though shorter periods still maintain relatively high IC and RD, their resolution is slightly reduced compared to the 1.25 min period.

For longer periods (5, 10, 20, and 40 min), the resolution consistently declines. This is because longer periods lead to spatial averaging, where the signal is spread over a larger area, and finer details of subsurface heterogeneities are lost. The longer periods smooth out the variations in the head data, resulting in lower sensitivity to local changes in the hydraulic properties and, thus, reduced IC and RD.

The comparison between the head variations (relative amplitudes) and the resolution patterns supports this observation. As shown in Figure 3-6, the relative amplitudes follow the same trends as the resolution degree seen in Figure 3-10. Specifically, shorter periods, such as 0.625 and 1.25 min, show higher relative amplitudes, which correspond to higher resolution values for the hydraulic parameters. This indicates that periods generating stronger head variations (larger amplitudes) also yield better resolution. Conversely, longer periods, which produce lower head variations, result in reduced resolution. This pattern suggests that the changes in resolution are indeed linked to the signal-to-noise ratio, where larger head variations provide a clearer signal, enabling more accurate resolution of subsurface heterogeneities. Therefore, the resolution degree appears to be directly influenced by the magnitude of the head variations, reinforcing the importance of selecting periods that maximize the signal strength for improved resolution. Since the amplitude of the signal is constrained by the experimental setup involving the injection rod, we focused on adjusting the signal period instead of increasing the amplitude. Additionally, Figure 3-7 exhibits the same trend across periods from 0.312 to 40 min, mirroring the shape of the resolution curves, further confirming the consistency between head variations and resolution patterns.

The field tests using the three periods (2.5, 5, and 10 min) yielded the best head responses, providing strong signal variations while ensuring adequate signal penetration across the observation intervals. However, our posteriori evaluation, as shown in Figure 3-8, suggests that the 1.25 min period would have provided better resolution of hydraulic parameters, particularly K_h and S_s, across the focus area.

While the periods used in the field test were effective in capturing overall trends, the simulations demonstrate that shorter periods, like 1.25 min, could have improved the resolution of finer-scale heterogeneities, especially in regions with higher anisotropy. The 2.5 min period performed well, but it did not achieve the same level of spatial resolution as 1.25 min. Similarly, the 5 and 10 min periods, although practical for ensuring signal propagation at greater depths, resulted in smoother parameter estimates, as they averaged out smaller subsurface variations. Given the results, under the field test conditions, incorporating the 1.25 min period could be particularly effective when used in combination with longer periods such as 2.5, 5, and 10 min.

In contrast, the homogeneous model (Figure 3-10b) presents a different narrative. First, for the homogeneous model, the IC and RD are systematically lower for the same source period than for the heterogeneous model. Furthermore, maximum IC and RD values are obtained for the shortest signal period and decline as periods become longer. Since previous results showed various responses related to hydraulic properties (Figure 3-4 and Figure 3-6), it can be expected that the "optimal" signal period would depend on specific site conditions. Surprisingly, it was more difficult to resolve the homogeneous model properties compared to the heterogeneous model. Perhaps the wide variability of responses for heterogeneous and anisotropic conditions favors higher resolutions.

3.4.6 Increased well radius to obtain higher heads and better resolutions

In this section, the specific configuration of the source used to generate the periodic tests is evaluated (Scenarios 1, 3 and 4 in Table 3-2). Figure 3-11 shows two examples (for tests 630 and 810) of the amplitudes of head variations in a source interval and its corresponding three observation intervals for the range of signal periods simulated with the heterogeneous model. Several observations can be made from this figure.

First, for Scenario 1 (Figure 3-11a and Figure 3-11b), while $2*H_0$ remains constant for all signal periods, the head variation within the source interval diminishes for longer periods. This occurs because the long signal periods allow more water to be exchanged between the well and the

aquifer, which results in lower head in the source interval (Paradis et al., 2024). In addition, while the head variation for the source interval decreases with the period, the head in the observation intervals reach a peak at intermediate periods. The explanation is that for the shorter periods, even though the head variation is large in the source interval, the volume of water exchanged between the well and the aquifer is small, which does not allow the periodic signal to propagate far within the aquifer. For the longer periods, the volume of water exchanged is larger, but it is the small head variation at the source interval that leads to small head in observation intervals (Paradis et al., 2024). Intermediate periods with maximum head variation in the observation intervals benefit from optimal combination of fluxes and head variation in the source intervals. Figure 3-11 also shows that head variation in the source interval is lower for test tx.630 (Figure 3-11a) than test tx.810 (Figure 3-11b). This is an indication that K_h around the source interval is higher for test tx.630 (Figure 3-2). Higher K_h allows a better exchange of the water between the well and the aquifer, similar to the effects of long periods.

Although the volumes of water exchanged in the riser are larger in scenarios 3 and 4 (as shown in Table 3-1), the head variation in the source interval is smaller due to the larger radii of the riser in these scenarios. For a given volume, the head variation decreases as the riser radius increases. This illustrates that the specific source configuration which was applied in the original period slug test serves as an "amplifier" for the head, with the head varying in the smaller annular space between the riser and the rod. Consequently, a smaller radius leads to greater head variation. Even though scenario 3 displaces around 52% more water than scenario 1, the head variation in the observation intervals remains similar, indicating that the two scenarios provide equivalent signal-to-noise ratios. This demonstrates that the "periodic slug test" configuration is highly effective in generating substantial head variations with a relatively small volume of water.

In contrast, the head variation in the observation intervals for scenario 4 is considerably greater than in the other two scenarios with smaller radii. Not only does the head double, but the period at which the maximum head is observed (the peak period) also increases by a factor of two. This can be attributed to the larger volume of water exchanged with the increased radius, which requires a longer peak period to compensate (Paradis et al., 2024). Overall, these findings highlight the importance of the test configuration in controlling head variation, with the smaller annular space in the original tests amplifying head response, while larger radii necessitate longer periods to achieve similar peak effects. This suggests that the improved resolution at longer periods may not only be due to the period itself, but also to the increased amplitude of the source signal when a larger volume is displaced.

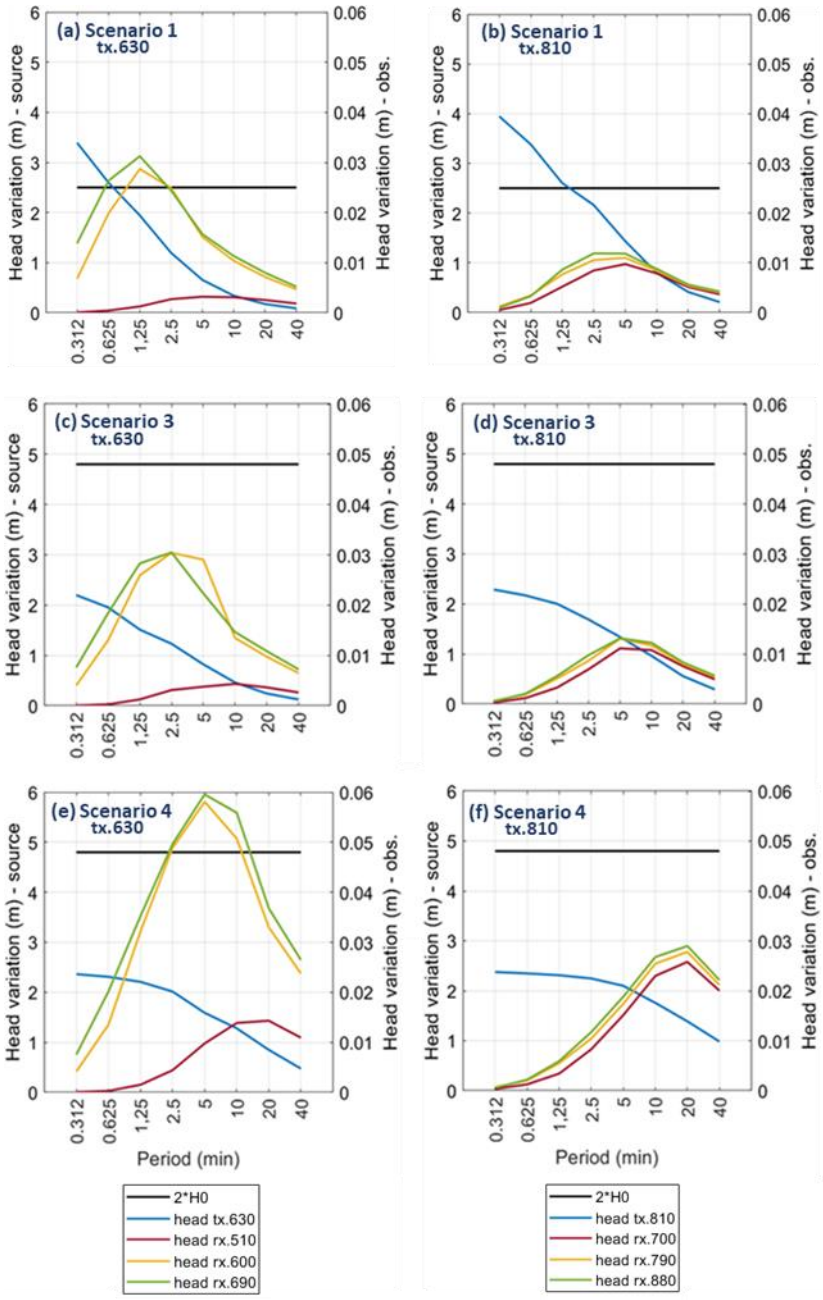

Figure 3-11 : Examples of simulated variation of heads in a source and in three observation intervals for eight selected periods for the heterogeneous case with rc = 0.0077; rc = 0.0127 and rc = 0.0254 m. Head variation is the difference between maximum and minimum head over a cycle when steady state is reached. (a) Test tx.630 and (b) test tx.810 for r_c = 0.0077 m; (c) Test tx.630 and (d) test tx.810 for r_c = 0.0127 m; (e) Test tx.630 and (f) test tx.810 for r_c = 0.0254 m. The positions of tx and rx are shown in Figure 3-2.

Figure 3-12 shows the information content (IC) and resolution degree (RD) for scenarios 3 and 4. A comparison with Figure 8a shows that the period of maximum resolution generally decreases with increasing radius. The greater the volume of water exchanged between the well and the aquifer, the better the signal-to-noise ratio for the shorter periods. As the shorter periods have a better resolution than longer periods (Paradis et al., 2024), a shift towards short periods can be observed. This also leads to a larger overall resolution for the scenarios with the larger radii. Therefore, larger head responses uncover the resolution potential of the shorter periods and lead to a better characterization of the hydraulic properties.

In summary, for the aquifer under investigation, it is therefore to be expected that the use of a different source with a larger diameter of the riser would have led to a better resolution of the hydraulic parameters. It would also have been possible to reduce the fieldwork considerably by using much shorter periods (0.312 to 1.25 min instead of 2.5 to 10 min).

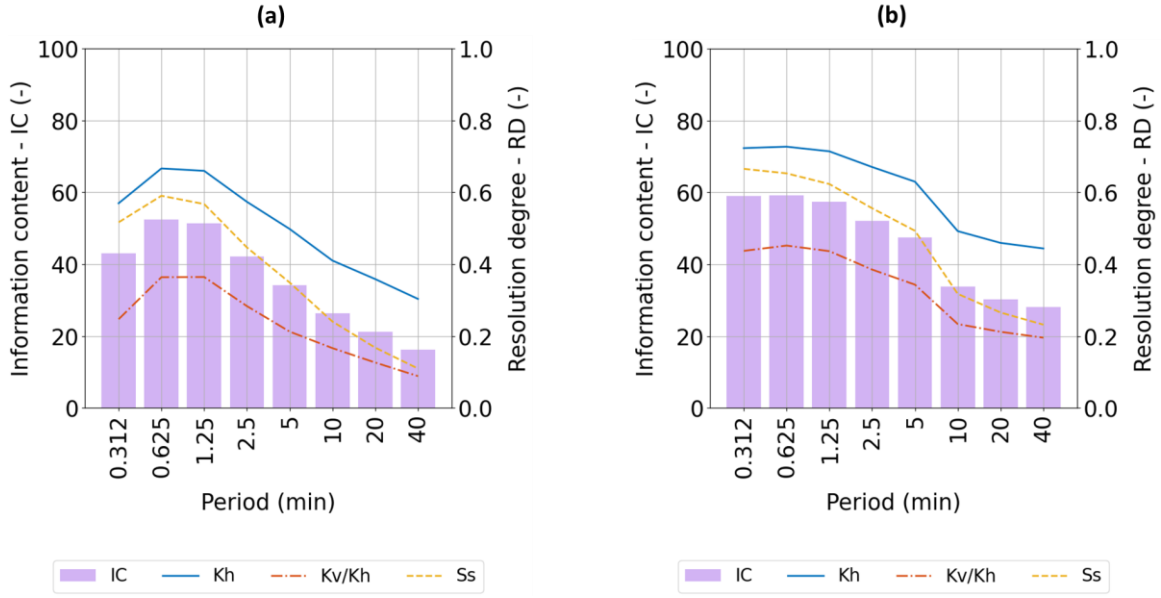

Figure 3-12 : Information content (IC) and resolution degree (RD) for Kh, Kv/Kh and Ss with the periods for the heterogeneous model with (a) rc = 0.0127 m (Scenario 3 in Table 3-2); and (b) rc = 0.0254 m (Scenario 4 in table 3-2). The IC and RD metrics are for the cells of the focus area (Figure 3-2).

Figure 3-13 illustrates the L-curve plots for different modeling scenarios with varying effective radii. The shape of the L-curve generally sharpens as the effective radius increases, indicating that larger radii provide clearer distinctions between model norms and residual norms. Specifically, for shorter periods (0.312 to 1.25 min), the L-curves exhibit a more distinct "L" shape across all radii, implying better regularization and parameter resolution. However, as the periods

increase (5 to 40 min), the optimal model norm tends to decrease, particularly for smaller radii, reflecting a loss in sensitivity with longer periods.

In contrast, as the radius increases (Figure 3-13c and Figure 3-13d), the L-curves maintain a more defined "L" shape even at longer periods, demonstrating that a larger source radius can compensate for the longer period by maintaining higher signal strength and parameter resolution. This trend indicates that using a larger source well (with greater r_c) could improve the overall resolution of the hydraulic parameters, even for extended signal periods, as the volume of water exchanged becomes more significant.

The comparison of the L-curve patterns across these scenarios emphasizes that while shorter periods generally yield better resolution, the amplitude of the source signal and also the choice of the source radius plays a critical role in maintaining sensitivity across a range of periods. Larger radii lead to better-defined L-curves, indicating more robust regularization outcomes, even when using longer signal periods.

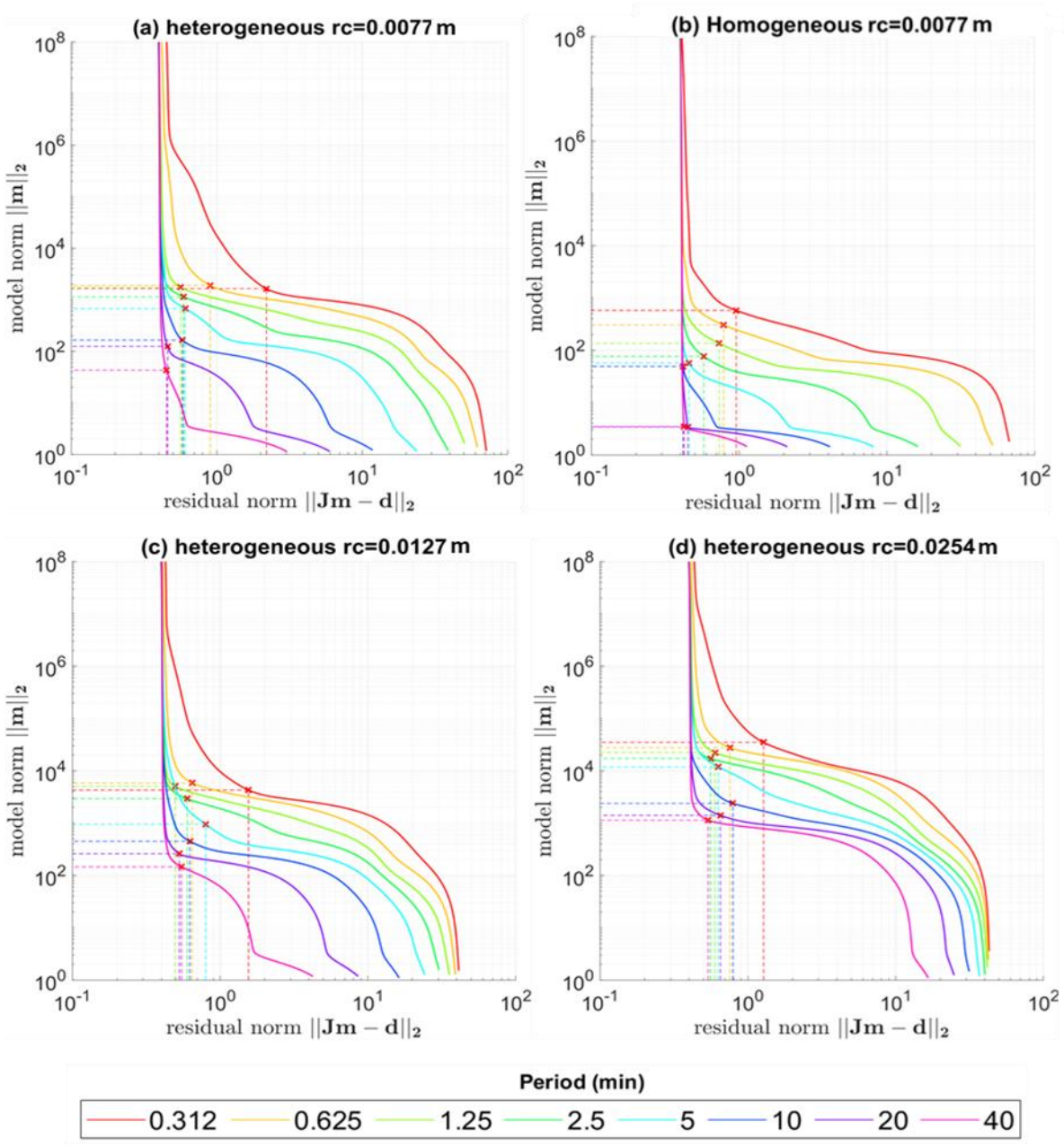

Figure 3-13 : The L-curve plot for different scenarios with different periods. rc is the effective radius. (a) Heterogeneous model (Scenarios 1 in Table 3-2) with rc = 0.0077 m; (b) Homogenous model (Scenarios 2 in Table 3-2) with rc = 0.0077 m; (c) Heterogeneous model (Scenarios 3 in Table 3-2) with rc = 0.0127 m (d) Heterogeneous model (Scenarios 4 in Table 3-2) with r_c = 0.0254 m.

3.4.7 Benefits of combining periods

3.4.7.1 Period combination for the heterogeneous model

Figure 3-14 presents a comparison of information content (IC) derived from various period combinations for three different radii for the heterogeneous model. The results indicate that combining multiple periods slightly improves resolution compared to using a single period.

For all three examples of different radii, the optimal combination typically includes a short period (e.g., 0.612 min) paired with a medium period (e.g., 2.5 min). However, in the first case (scenarios 1, 5 and 8), we observe that using multiple periods together, especially combinations including the 40 min period leads to a significant improvement in information content. For example, combinations such as 0.625 - 1.25 – 40 min, which is a surprising result considering the 40 min period on its own typically yields little information. This enhanced performance likely arises from the interaction between long and short periods. The 40 min period may be more sensitive to deeper or slower processes within the system, while the shorter periods (0.625 and 1.25 min) capture more rapid or shallow features. These complementary sensitivities likely improve the ability to resolve different hydraulic parameters within the heterogeneous model, as demonstrated by recent findings (Ahn and Horne, 2010; Cardiff et al., 2013b; Paradis et al., 2024). Thus, the combination of periods provides better parameter estimation, showing that even longer periods can be valuable when used together with shorter ones (Figure 3-14a). In the second case (scenarios 4, 7 and 10), the information content distribution becomes more uniform across different period combinations. Interestingly, no specific combination, including those with longer periods like 40 min, offers a distinct advantage over others (Figure 3-14b).

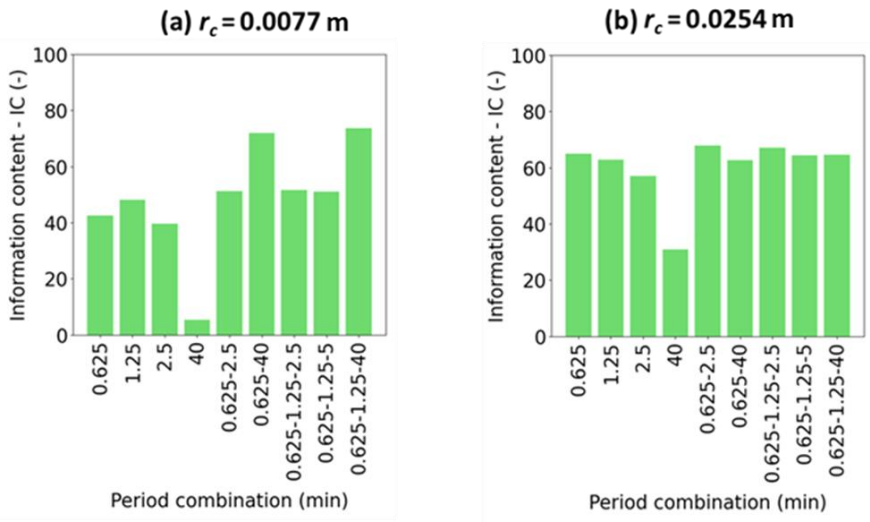

Figure 3-14 : Information content (IC) for different combinations of signal periods for periodic tests for the heterogeneous model with (a) rc = 0.0077 m (Scenario 1,5 and 8 in Table 3-2); (b) rc = 0.0254 m (Scenario 4, 7 and 10 in Table 3-2).

Figure 3-15 compares the information content for the St-Lambert field test inversion results and scenario 1 with the same periods and their combination. Both examples present similar trends, which indicates that both the synthetic and field results follow the same overall pattern. For the scenario 1, combining short and long periods (2.5 and 10 min) appears to significantly increase the information content. The result is a more balanced and comprehensive dataset, which improves the overall resolution and depth of the analysis. This is why combinations involving short periods, even with long ones, provide a more informative signal than combinations of only longer periods.

In contrast, longer periods, such as10 min, generally tend to capture slower processes within the system, but they can be less sensitive to higher-frequency variations or fast responses. This insensitivity can explain the observed reduction in information content when combining two long periods (5 and 10 min). In such cases, the response from the system is dominated by slower dynamics, which may cause the system to miss critical details, ultimately lowering the overall information captured. The lack of finer resolution is reflected in the reduced information content when these two long periods are combined.

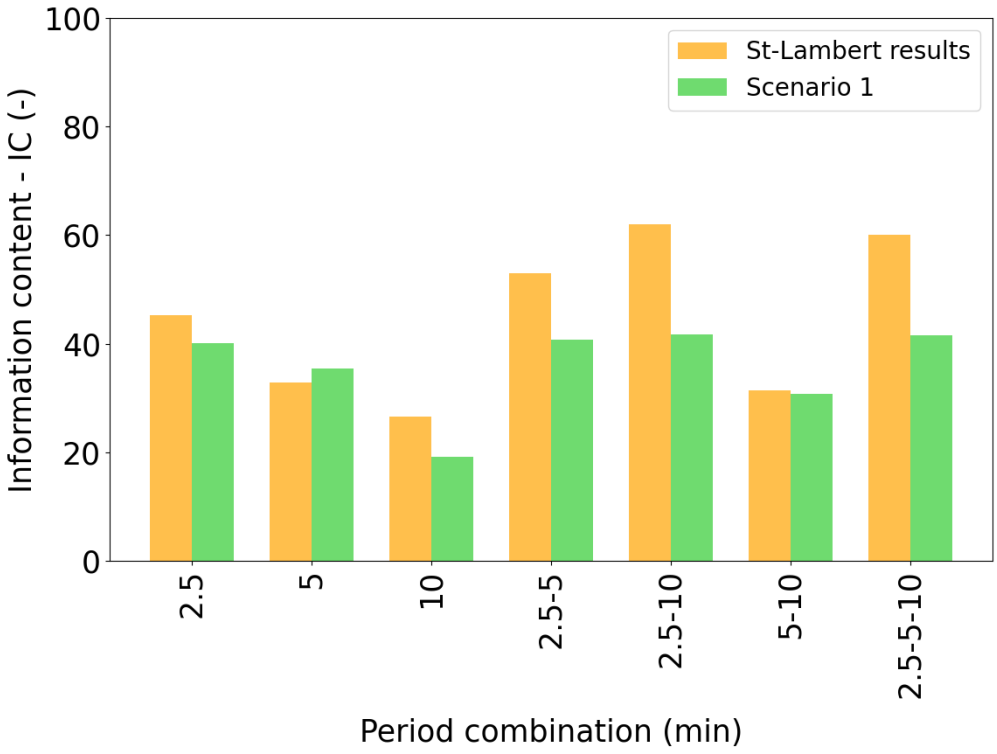

Figure 3-15 : Comparison of information content (IC) for different combinations of signal periods in periodic tests for the heterogeneous model with rc=0.0077 m (Scenario 1 in Table 3-2) and the field periods along with their combinations used in Nefzi et al. (2025).

The decrease in information content when combining two long periods (5 and 10 min) may also be due to overlapping sensitivities. The 5 min period might already capture most of the dynamics that the 10 min period could provide, meaning that adding the longer period does not contribute significant new information. Additionally, longer periods typically have a lower signal-to-noise ratio, meaning that the measured response can become more prone to noise over time. When combining two long periods, the cumulative effect of noise can become more pronounced, further reducing the clarity and value of the information. Thus, rather than reinforcing each other, the two long periods may both suffer from noise and overlapping sensitivity, ultimately reducing the total information gained. In fact, this overlap of sensitivities, combined with the influence of noise, can explain why combining two long periods does not yield the additive or complementary benefit that one might expect. Instead, it leads to a decrease in the total information content, as seen in the example of combining 5 and 10 min in our analysis.

This slight difference between scenario 1 and the St-Lambert application is caused by the difference in rod amplitude used in each case, as well as variations in noise level and the hydraulic properties considered. From a practical standpoint, these findings are valuable for field

operations. The results show that there is little to no benefit in combining two long periods, as this can lead to diminished returns in terms of information.

3.4.7.2 Period combination for the homogenous model

Figure 3-16 shows that for this homogeneous case, the information content (IC) appears more uniformly distributed across the different period combinations compared to the heterogeneous model. The shorter periods, such as 0.625 and 1.25 min, seem to provide a relatively consistent level of information, which suggests that the homogeneous model does not exhibit the same variability that longer periods could exploit, unlike in a heterogeneous context.

Notably, the combination with a 40-minute period, which typically adds more information in heterogeneous cases, does not perform well here. This may be due to the fact that in a homogeneous system, the amplitude of the source signal tends to decrease with longer periods, making it more susceptible to noise and thus reducing its effectiveness in improving resolution. The single period 0.625 min provides a higher level of information than the combination 0.625-2.5 min, indicating that adding the 2.5 min period reduces the total information content in this homogeneous model. This suggests that combining these two periods does not improve the resolution and might even introduce redundancy or less effective sensitivity at this scale. On the other hand, the combination 0.625-1.25-5 min shows the highest information content, demonstrating that adding the 1.25 and 5 min periods to the 0.625 min period leads to a significant increase in information. This implies that these periods, when used together, are complementary and enhance the sensitivity of the inversion process for the homogeneous model. it seems that not all period combinations are equally effective in this homogeneous case. While some combinations, like 0.625-1.25-5 min, capture more useful information, others like 0.625-2.5 min may not be as beneficial, likely because the homogeneous system does not have enough variability for longer periods to add value or resolve additional features. This highlights the importance of selecting appropriate period combinations even in simpler systems.

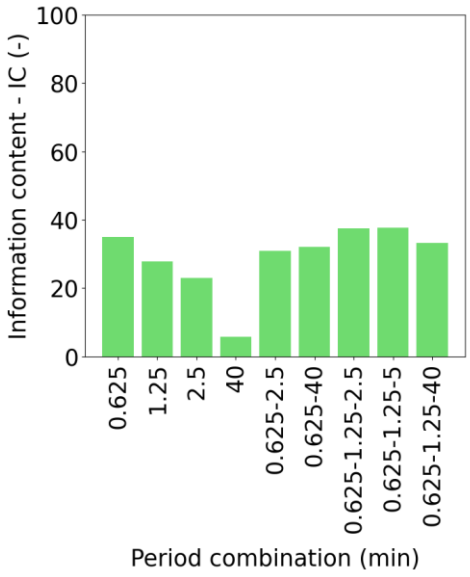

Figure 3-16 : Information content (IC) for different combinations of signal periods for periodic tests for the homogeneous model with rc=0.0077 m (Scenario 2 in Table 3-2).

3.5 Conclusions

In this study, a posteriori evaluation of oscillatory hydraulic tomography (OHT) experiments was conducted using numerical modeling to assess the information content and resolution degree of OHT head responses across a wide range of periodic signals for both heterogeneous and homogeneous hydraulic properties. The evaluation focused on single tests with varying signal periods as well as combinations of tests with different periods, aiming to deepen the understanding of parameter resolution in OHT experiments. Eight simulation scenarios were conducted, including three heterogeneous model scenarios with varying effective source well radii r_c, one homogeneous model scenario, and four scenarios using different period combinations (pairs and triplets).

The field experiments were conducted without prior knowledge of the specific hydraulic properties, making the period selection a critical challenge. The choice of 2.5, 5, and 10 min was made to ensure adequate signal-to-noise ratio and coverage of deeper subsurface areas. However, the current study indicates that incorporating shorter periods (e.g., 0.625 or 1.25 min) during field experiments could have enhanced the resolution, particularly in the middle interval where head responses were most sensitive to shorter signals. The posteriori analysis shows that while the chosen periods were reasonable, they likely resulted in some loss of resolution, especially for

capturing smaller-scale heterogeneities. Shorter periods may have better captured the localized variability of hydraulic properties without sacrificing signal quality.

In general, OHT data obtained with shorter signal periods contain better information, especially for the homogeneous model. However, heterogeneous conditions can have more variable behaviors, with higher information content related to short period signals but not the shortest. It is crucial to distinguish between signal periods that yield optimal observation interval responses and those that lead to superior resolutions. While certain periods might excel in producing discernible responses in observation wells, they might not necessarily equate to periods that provide the highest resolution. This dichotomy underscores the importance of multifaceted analysis in period selection, ensuring that chosen intervals serve the intended scientific objectives comprehensively.

A clear pattern becomes evident when examining the timeframe in which the peak head amplitude occurs: as the diameter increases, the receivers will experience higher maximum amplitudes at longer periods. Specifically, as the source signal amplitude increases (that is, as r_c increases) there is a corresponding enhancement in parameter resolution, and the period of maximum resolution shifts toward shorter periods. This direct relationship between the source signal amplitude and parameter resolution accentuates the pivotal role that head amplitude plays in controlling the clarity and accuracy of results. As r_c increases, the displaced volume grows, leading to stronger source signals and improved resolution.

This research reaffirms the significance of short signal periods, providing crucial insights that will guide the selection of periods in subsequent studies. Extended periods in field investigations may not be indispensable, given their limited contribution to new information. A pragmatic approach suggests that amalgamating a brief period with one or two intermediate-length periods optimizes results, effectively diminishing the correlation amongst hydraulic parameters.

To demonstrate the potential influence of combining multiple periods on parameter resolution, our investigation adopted a rigorous approach by examining combinations of both two and three periods. A primary objective of this study was to discern the differential impacts of these period combinations on heterogeneous and homogeneous scenarios. Such a nuanced exploration sought to determine whether both cases would be similarly modulated by the period combinations. It is noteworthy that the practice of integrating multiple periods, as highlighted by (Cardiff et al., 2013b), has been previously underscored to obtain marked enhancements in parameter resolution. Our results show the underlying causes of these previous findings, but also show that the information content and resolution can widely vary depending on the source signal period, whose optimal range of value is site specific.

Finally, heterogeneity plays a pivotal role in introducing significant variability in the amplitude of responses in observation intervals. This characteristic variability, attributed to the complex and diverse nature of the medium, accentuates the need for meticulous analysis to more thoroughly comprehend the effects of heterogeneity on the response of periodic tests.

3.6 Bibliographie 2e ARTCILE

Ahn, S., Horne, R.N., 2010. Estimating permeability distributions from pressure pulse testing. In: Proceedings of the SPE Annual Technical Conference and Exhibition, 3, pp. 2388–2403. https://doi.org/10.2118/134391-MS.

Aster, R.C., Borchers, B., Thurber, C., 2005. Parameter Estimation and Inverse Problems Elsevier, Amsterdam, p. 301.

Bianchi, M., Zheng, C., Wilson, C., Tick, G.R., Liu, G., Gorelick, S.M., 2011. Spatial connectivity in a highly heterogeneous aquifer: From cores to preferential flow paths. Water Resources Research 47. https://doi.org/10.1029/2009WR008966.

Bohling, G.C., 2009. Sensitivity and resolution of tomographic pumping tests in an alluvial aquifer. Water Resour. Res. 45. https://doi.org/10.1029/2008WR007249.

Bohling, G.C., Butler, J.J., 2001. lr2dinv: A finite-difference model for inverse analysis of two-dimensional linear or radial groundwater flow. Computers & Geosciences 27, 1147–1156. https://doi.org/10.1016/S0098-3004(01)00036-X.

Bohling, G.C., Butler, J.J., Zhan, X., Knoll, M.D., 2007. A field assessment of the value of steady shape hydraulic tomography for characterization of aquifer heterogeneities. Water Resour. Res. 43. https://doi.org/10.1029/2006WR004932.

Bohling, G.C., Liu, G., Dietrich, P., Butler Jr., J.J., 2016. Reassessing the MADE direct-push hydraulic conductivity data using a revised calibration procedure. Water Resources Research 52, 8970–8985. https://doi.org/10.1002/2016WR019008.

Bohling, G.C., Liu, G., Knobbe, S.J., Reboulet, E.C., Hyndman, D.W., Dietrich, P., Butler Jr, J.J., 2012. Geostatistical analysis of centimeter-scale hydraulic conductivity variations at the MADE site. Water Resources Research 48. https://doi.org/10.1029/2011WR010791.

Bohling, G.C., Zhan, X., Butler, J.J., Zheng, L., 2002. Steady shape analysis of tomographic pumping tests for characterization of aquifer heterogeneities. Water Resour. Res. 38, 60-1-60–15. https://doi.org/10.1029/2001WR001176.

Butler, J.J., McElwee, C.D., 1990. Variable-rate pumping tests for radially symmetric nonuniform aquifers. Water Resour. Res. 26, 291–306. https://doi.org/10.1029/WR026i002p00291.

Cardiff, M., Bakhos, T., Kitanidis, P.K., Barrash, W., 2013b. Aquifer heterogeneity characterization with oscillatory pumping: Sensitivity analysis and imaging potential. Water Resour. Res. 49, 5395–5410. https://doi.org/10.1002/wrcr.20356.

Cardiff, M., Barrash, W., 2011. 3-D transient hydraulic tomography in unconfined aquifers with fast drainage response. Water Resources Research 47. https://doi.org/10.1029/2010WR010367.

Cardiff, M., Zhou, Y., Barrash, W., Kitanidis, P.K., 2020. Aquifer imaging with oscillatory hydraulic tomography: application at the field scale. Groundwater 58, 710–722. https://doi.org/10.1111/gwat.12960.

Dagan, G., 1989. Flow and Transport in Porous Formations. Springer-Verlag.

Fischer, P., De Clercq, T., Jardani, A., Thannberger, L., Massei, N., Abbas, M., 2020. Imaging the hydraulic properties of a contaminated alluvial aquifer perturbed with periodic signals. Hydrogeol J 28, 2713–2726. https://doi.org/10.1007/s10040-020-02233-8.

Günther, T., 2004. Inversion Methods and Resolution Analysis For the 2D/3D Reconstruction of Resistivity Structures from DC Measurements. Technische Universit¨at Bergakademie Freiberg, p. 160. Ph.D. Thesis.

Hansen, P.C., 2023. Regularization tools: A MATLAB Package For Analysis and Solution of Discrete Ill-Posed Problems. Version 4.1. regtools (https://www.mathworks.com /matlabcentral/fileexchange/52-regtools), MATLAB Central File Exchange. Retrieved February 6, 2023.

Hansen, P.C., 1992. Analysis of discrete Ill-posed problems by means of the L-curve. SIAM Rev. 34, 561–580. https://doi.org/10.1137/1034115.

Hansen, P.C., Jensen, T.K., Rodriguez, G., 2007. An adaptive pruning algorithm for the discrete L-curve criterion. Journal of Computational and Applied Mathematics, Special Issue: Applied Computational Inverse Problems 198, 483–492. https://doi.org/10.1016/j.cam.2005.09.026.

Huysmans, M., Dassargues, A., 2009. Application of multiple-point geostatistics on modelling groundwater flow and transport in a cross-bedded aquifer (Belgium). Hydrogeol J 17, 1901–1911. https://doi.org/10.1007/s10040-009-0495-2.

Knudby, C., Carrera, J., 2006. On the use of apparent hydraulic diffusivity as an indicator of connectivity. Journal of Hydrology 329, 377–389. https://doi.org/10.1016/j.jhydrol.2006.02.026.

Lavenue, M., de Marsily, G., 2001. Three-dimensional interference test interpretation in a fractured aquifer using the Pilot Point Inverse Method. Water Resour. Res. 37, 2659–2675. https://doi.org/10.1029/2000WR000289.

Liu, G., Bohling, G.C., Butler Jr., J.J., 2008. Simulation assessment of the direct-push permeameter for characterizing vertical variations in hydraulic conductivity. Water Resources Research 44. https://doi.org/10.1029/2007WR006078.

Liu, G., Butler Jr., J.J., Bohling, G.C., Reboulet, E., Knobbe, S., Hyndman, D.W., 2009. A new method for high-resolution characterization of hydraulic conductivity. Water Resources Research 45. https://doi.org/10.1029/2009WR008319.

Maier, U., DeBiase, C., Baeder-Bederski, O., Bayer, P., 2009. Calibration of hydraulic parameters for large-scale vertical flow constructed wetlands. Journal of Hydrology, Transfer of pollutants in soils, sediments and water systems: From small to large scale (AquaTerra) 369, 260–273. https://doi.org/10.1016/j.jhydrol.2009.02.032.

Moore, E.H, 1920. On the reciprocal of the general algebraic matrix. Bull. Am. Math. Soc. 26, 394–395.

Nefzi, A., Paradis, D., Lefebvre, R., Bour, O., Lavenant, N., 2025. Field deployment and analysis of hydraulic tomography experiments with periodic slug tests in an anisotropic littoral aquifer. Journal of Hydrology 653, 132747. https://doi.org/10.1016/j.jhydrol.2025.132747.

Paradis, D., Gloaguen, E., Lefebvre, R., Giroux, B., 2016. A field proof-of-concept of tomographic slug tests in an anisotropic littoral aquifer. Journal of Hydrology 536, 61–73. https://doi.org/10.1016/j.jhydrol.2016.02.041.

Paradis, D., Gloaguen, E., Lefebvre, R., Giroux, B., 2015b. Resolution analysis of tomographic slug test head data: Two-dimensional radial case. Water Resour. Res. 51, 2356–2376. https://doi.org/10.1002/2013WR014785.

Paradis, D., Lefebvre, R., 2013. Single-well interference slug tests to assess the vertical hydraulic conductivity of unconsolidated aquifers. Journal of Hydrology 478, 102–118. https://doi.org/10.1016/j.jhydrol.2012.11.047.

Paradis, D., Lefebvre, R., Gloaguen, E., Rivera, A., 2015a. Predicting hydrofacies and hydraulic conductivity from direct-push data using a data-driven relevance vector machine approach: Motivations, algorithms, and application. Water Resour. Res. 51, 481–505. https://doi.org/10.1002/2014WR015452.

Paradis, D., Lefebvre, R., Morin, R.H., Gloaguen, E., 2011. Permeability Profiles in Granular Aquifers Using Flowmeters in Direct-Push Wells. Ground Water 49, 534–547. https://doi.org/10.1111/j.1745-6584.2010.00761.x.

Paradis, D., Lefebvre, R., Nefzi, A., 2024. Parameter resolution of simulated responses to periodic hydraulic tomography signals in aquifers. Advances in Water Resources 190, 104734. https://doi.org/10.1016/j.advwatres.2024.104734.

Penrose, R., 1955. A generalized inverse for matrices. Proc. Camb. Philos. Soc. 51, 406–413.

Quinn, P., Cherry, J.A., Parker, B.L., 2015. Combined use of straddle packer testing and FLUTe profiling for hydraulic testing in fractured rock boreholes. Journal of Hydrology 524, 439–454. https://doi.org/10.1016/j.jhydrol.2015.03.008.

Renard, P., Allard, D., 2013. Connectivity metrics for subsurface flow and transport. Advances in Water Resources, 35th Year Anniversary Issue 51, 168–196. https://doi.org/10.1016/j.advwatres.2011.12.001.

Tikhonov, A.N.,, Goncharsky, A.V., 1987. Ill-posed problems in the natural sciences. [WWW Document]. URL MIR Publishers, Moscow. (accessed 1.15.25).

Tremblay, L., Lefebvre, R., Paradis, D., Gloaguen, E., 2014. Conceptual model of leachate migration in a granular aquifer derived from the integration of multi-source characterization data (St-Lambert, Canada). Hydrogeol J 22, 587–608. https://doi.org/10.1007/s10040-013-1065-1.

Vasco, D.W., Datta-Gupta, A., Long, J.C.S., 1997. Resolution and uncertainty in hydrologic characterization. Water Resources Research 33, 379–397. https://doi.org/10.1029/96WR03301.

Wang, Y., Yeh, T.J., Wen, J., Gao, X., Zhang, Z., Huang, S., 2019. Resolution and Ergodicity Issues of River Stage Tomography With Different Excitations. Water Resources Research 55, 4974–4993. https://doi.org/10.1029/2018WR023204.

Zheng, C., Gorelick, S.M., 2003. Analysis of Solute Transport in Flow Fields Influenced by Preferential Flowpaths at the Decimeter Scale. Groundwater 41, 142–155. https://doi.org/10.1111/j.1745-6584.2003.tb02578.x.

Zhou, Y., Lim, D., Cupola, F., Cardiff, M., 2016. Aquifer imaging with pressure waves—Evaluation of low-impact characterization through sandbox experiments. Water Resour. Res. 52, 2141–2156. https://doi.org/10.1002/2015WR017751.

Zinn, B., Harvey, C.F., 2003. When good statistical models of aquifer heterogeneity go bad: A comparison of flow, dispersion, and mass transfer in connected and multivariate Gaussian hydraulic conductivity fields. Water Resources Research 39. https://doi.org/10.1029/2001WR001146.

Zschornack, L., Bohling, G.C., Butler, J.J., Dietrich, P., 2013. Hydraulic profiling with the direct-push permeameter: Assessment of probe configuration and analysis methodology. Journal of Hydrology 496, 195–204. https://doi.org/10.1016/j.jhydrol.2013.05.036.

4 EVALUATION OF THE INFORMATIONAL CONTENT AND PRACTICAL EFFECTIVENESS OF PERIODIC AND CONVENTIONAL SLUG TEST HYDRAULIC TOMOGRAPHY

Titre de l'article : Évaluation du contenu informationnel et de l'efficacité pratique de la tomographie hydraulique par essais périodiques et essais à choc hydraulique conventionnels

Auteurs :

Aymen Nefzi[1], Daniel Paradis[2], René Lefebvre[1], Olivier Bour[3]

[1] Centre Eau Terre Environnement (INRS-ETE) - Institut national de la recherche scientifique, Québec, Canada

[2] Ressources Naturelles Canada - Commission géologique du Canada, Québec, Canada

[3] Université Rennes, CNRS, Géosciences Rennes, UMR 6118, 35000 Rennes, France

En préparation pour soumission à Hydrogeology Journal

Abstract

This study compares Oscillatory Hydraulic Tomography (OHT) with conventional slug-test-based hydraulic tomography to image subsurface heterogeneity at the Saint-Lambert experimental site, a highly heterogeneous and anisotropic granular aquifer. The research aims to assess the informational content, spatial resolution, and practical implementation of these methods. OHT experiments employed three distinct signal periods (150, 300, and 600 seconds), with hydraulic heads measured at stress and observation intervals 5.35 m apart. Numerical inversions were

conducted for individual periods and their combinations, followed by sensitivity and resolution analyses to evaluate the relative performance of OHT and slug tests.

Results demonstrate that both methods effectively capture the distribution of K_h, K_v/K_h and S_s within the aquifer. However, OHT shows a slight advantage in processing hydraulic head data due to the periodic nature of its signal, which is easier to isolate from ambient noise. Despite this advantage, OHT requires more sophisticated equipment to generate and control oscillatory signals, and the tests are generally longer due to the need to apply multiple signals over different cycles. The resolution analysis reveals that both methods yield comparable results overall, with slug tests providing robust resolution for Ss near the observation well. For OHT, the choice of periods proves to be a critical factor in enhancing resolution. While a single period may not always outperform slug tests in resolution, the combination of multiple carefully selected periods significantly improves the ability to resolve heterogeneities. This comparative study advances the understanding of hydraulic tomography techniques and their applications in heterogeneous aquifers.

Keywords Oscillatory hydraulic tomography, periodic tests, slug test, numerical inversion, information content, resolution analysis, sensitivity analysis

4.1 Introduction

The quantitative representation of groundwater dynamics necessitates the measurement of hydraulic properties, primarily hydraulic conductivity (K) and specific storage (S_s) and the definition of their heterogeneous spatial distribution. These parameters have significant controls on transient groundwater flow and solute transport. Therefore, accurately characterizing subsurface heterogeneity in K and S_s is essential for improving groundwater resource evaluation and management, as well as for the prevention and remediation of contamination.

Hydraulic tomography, which involves the simultaneous analysis of inter-well responses at multiple observation points during various hydraulic tests such as pumping tests (Bohling, 1993; Gottlieb et Dietrich, 1995; Yeh and Liu, 2000; Bohling et al., 2002, 2007; Illman et al., 2008; Cardiff et al., 2009; Illman et al., 2009; Berg and Illman, 2011; Cardiff and Barrash, 2011; Cardiff et al., 2012; Sun et al., 2013; Hochstetler et al., 2016), slug tests (Brauchler et al., 2003, 2007, 2011; Paradis et al., 2015b; Liu et al., 2023), and oscillatory tests (Cardiff et al., 2013b; Zhou et al., 2016; Wang et al., 2021; Paradis et al., 2024; Nefzi et al., 2025; Nefzi et al., En préparation “a”)

offers a promising alternative to traditional hydraulic testing methods for imaging the heterogeneity of hydraulic properties, particularly hydraulic conductivity (K), in aquifer systems at the field scale.

Most methods used to define the anisotropic transmissivity tensor are based on pumping tests. However, slug tests, which are faster and simpler to carry out, have become widely used to assess aquifer transmissivity, especially in potentially contaminated sites where water production during a test is undesirable. Multiple slug tests can also provide better Indications of the statistical and spatial distribution of hydraulic conductivity (Ouellon et al., 2008). The use of modern equipment allows for the generation of larger and more distinct perturbations, enabling the accurate detection of stronger signals at observation points distant from the source well.

Slug tests offer an efficient approach for characterizing the spatial heterogeneity of a study site. When combined with the imaging method of hydraulic tomography, they hold significant potential for applications in aquifer reconstruction. The resolution of parameters in tomographic slug tests is influenced by various factors, including the signal-to-noise ratio, the experimental setup, and the range of hydraulic properties. These tests have shown considerable potential for providing detailed insights into aquifer heterogeneity, particularly in terms of horizontal hydraulic conductivity (K_h), hydraulic anisotropy (K_v/K_h), and specific storage (S_s) (Paradis et al., 2015b).

Oscillatory hydraulic tomography (OHT) is a relatively recent hydraulic testing method used for subsurface imaging that utilizes tomographic analysis of oscillatory signals. During these tests, a periodic pressure signal is generated at one or multiple stimulation points in a stressed well, and the subsequent effects of this signal transmission through the aquifer are captured at multiple intervals in observation wells. The concept of multi-frequency oscillatory hydraulic imaging, as introduced by Cardiff et al. (2013b) in their seminal work, involves the use of multiple signals of varying frequencies as a stimulant. This approach is designed to extract detailed information about the heterogeneity of the aquifer (Nefzi et al., 2025; Cardiff et al., 2020; Fischer et al., 2018; Zhou et al., 2016).

The primary aim of this study is to evaluate the informational content and practical effectiveness of OHT in comparison to conventional hydraulic tomography based on slug tests, applied to a highly heterogeneous and anisotropic littoral aquifer. By leveraging data from both OHT and slug test experiments, this research examines their respective abilities to resolve hydraulic parameters and capture spatial variability in aquifer properties. This work represents a novel contribution by providing a detailed assessment of tomographic resolution across multiple signal periods, highlighting the advantages of a multi-period approach in enhancing parameter estimation.

Additionally, the study compares the efficiency of the two methods, highlighting their respective strengths, limitations, and applicability to subsurface characterization.

4.2 Materials and methods

In the summer of 2018, a comprehensive tomographic experiment was conducted in Saint-Lambert, located 40 km south of Quebec City, Canada. The experimental methodology was meticulously designed to ensure the accurate and complete acquisition of data necessary for characterizing aquifer heterogeneity through tomographic analysis. This section provides a general overview of the test site, the equipment used, and the procedures employed, as well as a broad description of the dataset processing workflow. The objective is to present the foundational aspects of the experiment without delving into intricate technical details.

For a more in-depth understanding of the experimental setup, including the specifics of the test equipment and procedures, hydraulic head data collection, simulation grids, periodic flow rate calculations, boundary and wellbore conditions, and inversion strategies, readers are encouraged to refer to the detailed documentation by Nefzi et al. (2025). This additional reference provides a comprehensive breakdown of the methodologies used to support the tomographic imaging of aquifer heterogeneity.

4.2.1 Site description and experimental setup

The test site has been extensively studied for its unique hydrogeological characteristics and has been the focus of multiple investigations aimed at advancing aquifer characterization techniques (Dubreuil-Boisclair et al., 2011; Paradis and Lefebvre, 2013; Paradis et al., 2016; Nefzi et al., 2025). The granular semi-confined aquifer reaches a thickness of up to 20 m, with a thickness of 12 m at the test site. Its base is composed of an impermeable glaciomarine diamicton. The water table is shallow, lying less than 1 m below the surface.

This site designated for tomographic analysis was equipped with five wells strategically positioned in a diamond configuration. This arrangement included a well at each vertex and one centrally located. The longest axis spanned 15.92 meters while the shorter axis measured 10.79 meters (Figure 4-1) (Paradis et al., 2016). The wells are screened across the full saturated thickness of the aquifer. They were installed without the use of sand packs, with the screens placed in direct contact with the natural sediments, utilizing direct-push equipment following the protected screen method outlined by Paradis et al. (2011).

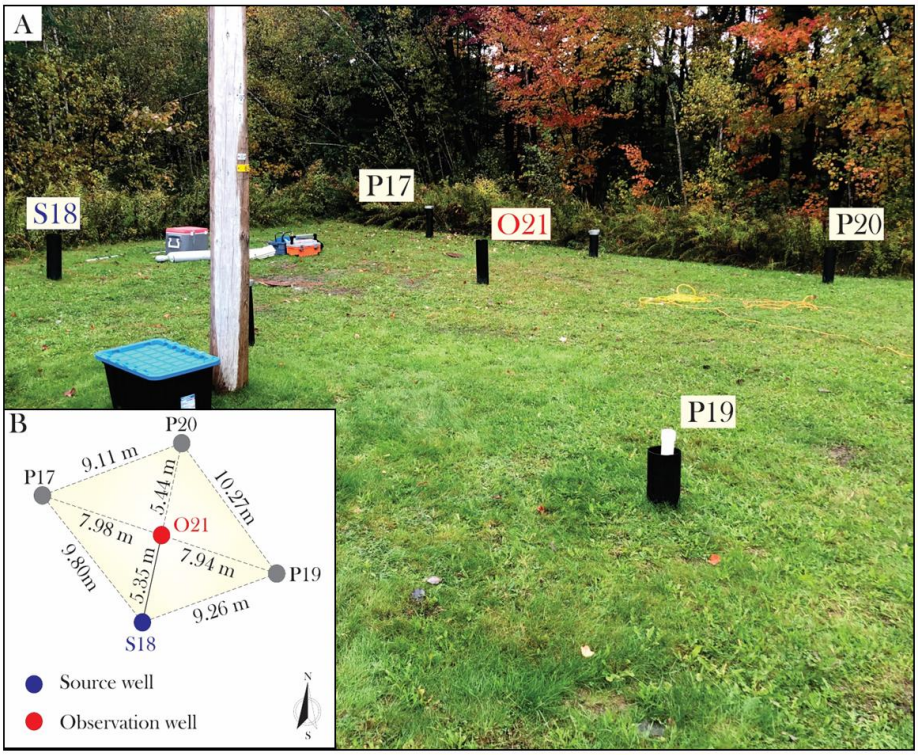

Figure 4-1 : Overview of wells S18 (stressed) and O21 (observation) used for tomographic experiment S18O21 B: relative position of the wells used for the tomographic experiment.

For this study, the experimental setup consisted of two wells (S18 and O21) spaced 5.35 m apart, screened over the saturated thickness of the aquifer. To increase flexibility in the design of the experiment, inflatable low-pressure packers and screens with threaded tubes were made. A double-packer system was utilized in the source well (S18) to isolate 0.61 m long source intervals. In the observation well (O21), four packers were used to isolate three observation intervals, each measuring 0.30 m in length and spaced 0.91 m apart. To streamline data collection, the packer arrangement in O21 was adjusted after every three tests conducted in S18, with a stabilization period allowed after each adjustment to ensure reliable head measurements.

The periodic stimulation was conducted using a 2.8 m long aluminum rod, controlled through a numerically operated winch. Moving the rod upward simulated pumping, while lowering it simulated water injection. The diameter of the rod was optimized to maximize water displacement during the tests while maintaining free water flow within the riser tube. Before each test, the rod was partially submerged, and a computer program regulated the amplitude and period of its vertical movement. Three signal periods (150, 300, and 600 seconds) were applied sequentially for each source interval to achieve maximum head variations in the observation intervals. A minimum of three cycles were conducted for each period, with rest periods in between to ensure

stability. This setup provided precise control of periodic signals, facilitating high-quality data collection for analysis. Figure 4-2 summarizes the overall approach for the test equipment and procedures presented in this paper for OHT method.

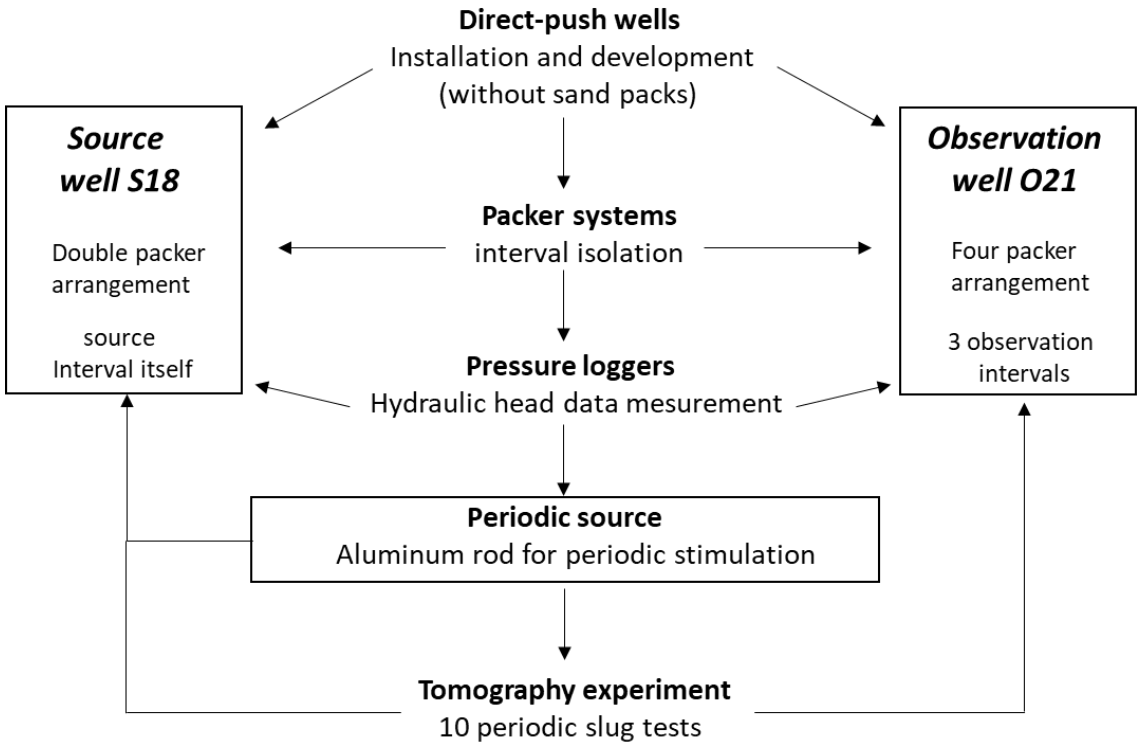

Figure 4-2: Field Data Acquisition Workflow

After completing the oscillatory tests with three distinct signal periods (150, 300, and 600 seconds), a rest period followed, after which a conventional slug test was conducted using the rod. In these tests, the rod was initially submerged and then rapidly withdrawn, inducing an abrupt change in water level and generating a transient response used to evaluate the aquifer properties.

4.2.2 Data analysis

4.2.2.1 Head data

The head data from both the periodic slug tests and the conventional hydraulic tomography based on slug tests, comprising 120 and 40 responses respectively, were standardized relative to the static head prior to each test and referenced to the start time of the corresponding experiment. Periodic and hydraulic tomography based on slug tests signals were filtered to address minor

stabilization issues observed in a few observation intervals within less permeable materials, though no such corrections were required for the source intervals.

The analysis revealed significant differences between the head variations in the source and observation intervals. In the source intervals, head variation ranged from 0.126 to 1.386 m, whereas in the observation intervals, variations were between 0.001 and 0.0189 m (Nefzi et al., 2025). This contrast reflects a strong attenuation of the signal as it propagates through the aquifer, which is more pronounced for shorter periods.

To improve computational efficiency during numerical inversions, the head data initially sampled at 1 Hz were resampled to 15 points per cycle. This was achieved by applying a moving average with window sizes of 10, 20, and 40 seconds for the 150, 300, and 600-second periods, respectively. Similarly, for the head data from the conventional hydraulic tomography based on slug tests, a moving average with a window size of 5 seconds was applied. This approach retained the essential characteristics of the head responses while significantly reducing the computational load for subsequent analysis.

4.2.2.2 Numerical groundwater flow

The tomographic periodic tests are simulated with the radial groundwater flow model lr2dinv (Bohling and Butler, 2001). This model has been used in several peer-reviewed publications to simulate hydraulic tests in wells (Bohling et al., 2002, 2007; Liu et al., 2008; Bohling, 2009; Liu et al., 2009; Bohling et al., 2012; Zschornack et al., 2013; Paradis and Lefebvre, 2013; Paradis et al., 2015b; Paradis et al., 2016; Bohling et al., 2016). The hydraulic head h (m) generated in an aquifer by a hydraulic test in a well is described by the radial groundwater flow equation:

$$\frac{1}{r}\frac{\partial}{\partial r}\left(rK_r\frac{\partial h}{\partial r}\right)+\frac{\partial}{\partial z}\left(K_z\frac{\partial h}{\partial z}\right)=S_s\frac{\partial h}{\partial t} \tag{4.1}$$

where r (m) is the radial coordinate from the center of the well, z (m) is the vertical coordinate, t (s) is the time, S_s (m^{-1}) is the specific storage, and K_r (or K_h) and K_z (ms^{-1}) are the hydraulic conductivities in the radial (or horizontal) and vertical directions, respectively.

In the test configuration represented by the models, two wells with a diameter of 0.0762 m and separated by 5.35 m are considered. The tomographic configuration consists of seven periodic tests performed sequentially at eight source intervals isolated with packers in the source well. The length of each source interval is 0.60 m. Simulation of the effects of wellbore storage and packer

placement in the source well is achieved by using the inner boundary of the model to represent the region within the wellbore.

A periodic flow rate Q (m^3s^{-1}) is imposed in the screened interval to induce water exchange with the aquifer at the screen of the well having a radius r_w (m):

$$Q = \pi r_c^2 \frac{\partial(A_0 \sin(2\pi/T_0 t))}{\partial t} = 2\pi r_w L K_h \frac{\partial h}{\partial r} \quad (4.2)$$

where r_c (m) is the radius of the casing or riser, L (m) is the length of the source interval, and $A0sin(2\pi/T0t)$ (m) is the sinusoidal hydraulic stress, where A_0 (m) and T_0 (s) are the peak amplitude and period of the periodic stress, respectively.

The simulation grid used for inversions consists of 43 radial cells with exponentially increasing widths and 34 vertical cells with a constant height of 0.30 m. Smaller radial cells near the source well improve the representation of higher hydraulic gradients, while the grid aligns with the packers and screens used in the field experiment. The observation well, located 5.35 m from the source, is positioned directly on the grid nodes.

A parameter grid overlays the simulation grid and includes 13 layers and 8 columns. Layers within the tested zone are 0.61 m thick to match the source intervals, while layers outside this zone are thicker. Horizontally, seven columns with an average width of 1.0 m span the source and observation wells, with a larger column of 54.85 m beyond the observation well to account for hydraulic properties outside the tested zone. The same parameter grid discretization is applied for K_h, K_v/K_h, and S_s. The outer boundary of the model, represented by a fixed head, was placed 49.5 m from the source well to avoid interference with tests. The upper boundary is also a fixed head to approximate unconfined condition. The impermeable lower boundary has a zero-flux condition (Nefzi et al., 2025).

The heads generated by the groundwater flow model must be perturbed by a noise level consistent with field measurements. The noise level is based on a field application of periodic slug tests carried out by the authors (Nefzi et al., 2025).

4.2.2.3 Resolution analysis

The resolution analysis provides a quantitative evaluation of the ability of hydraulic experiments to resolve subsurface parameters, reflecting both the physics and geometry of the experimental setup. The resolution matrix is a key metric that describes the relationship between the measured hydraulic responses and the estimated parameters.

In the context of Tikhonov regularization, the resolution matrix is expressed as:

$$\mathrm{R}_{m,\lambda} = \mathrm{VFV}^T \tag{4.3}$$

where $R_{m,\lambda}$ elements indicate the degree of correlation and sensitivity between hydraulic head data and the corresponding parameters. A perfect resolution $(\mathbf{R}_{m,\lambda} = \mathrm{I})$ implies that the true hydraulic parameters are fully recovered, while values near zero indicate unresolved parameters.

To ensure consistency in comparisons across different simulations, the regularization parameter λ is selected using the L-curve criterion (Hansen, 1992). This approach balances the trade-off between fitting the head data and over-smoothing the solution. The optimal λ corresponds to the corner of the L-curve, where the residual norm and model norm achieve equilibrium, minimizing noise sensitivity while maximizing parameter resolution. The adaptive pruning algorithm (Hansen et al., 2007) is applied to accurately locate the L-curve corner for each simulation.

Two metrics are employed to quantify and compare resolution across simulations. The first is the information content (IC), defined as the sum of the diagonal elements of the resolution matrix:

$$IC = \sum_i^N R_{m,\lambda,ii}^N \tag{4.4}$$

where *N* is the total number of parameters in the focus area. A higher IC indicates greater overall resolution for the parameters.

The second metric is the resolution degree (RD), which normalizes the information content of each hydraulic property by the corresponding number of parameters:

$$RD_j = {IC_j}\Big/{N_j} \tag{4.5}$$

Where j represents the hydraulic properties K_h, K_v/K_h and S_s. RD values range from 0 (not resolved) to 1 (perfectly resolved) and provide insight into the average resolution achieved for each property.

4.2.2.4 Simulation strategy

The numerical inversion of each tomography experiment was performed using a parallelized version of the lr2dinv model (Bohling and Butler, 2001), modified by the authors. In the lr2dinv model, a forward radial groundwater flow model is coupled with the Levenberg–Marquardt algorithm to simultaneously estimates the spatial distribution of K_h, K_v/K_h, and S_s.

In this study, various scenarios are rigorously evaluated to investigate the information content of periodic hydraulic tomography experiments and to compare their performance with conventional hydraulic tomography based on slug tests. Particular attention is given to the effectiveness of combining multiple testing periods, aiming to determine whether a multi-period approach offers more comprehensive and reliable insights into subsurface hydraulic properties compared to single-period tests.

The simulated OHT experiments included ten tests involving a periodic signal in one source interval and measurements of heads in that source interval as well as three intervals in the observation well. The combinations of stress and observation intervals considered for these 10 tests are listed in (Nefzi et al., 2025). The maximum head of the oscillatory signals simulated in observation intervals ranged from 0.011 to 0.041 m. Slug tests were conducted within the same source intervals as the hydraulic oscillatory tomography experiments; however, due to poor data quality in some tests, we decided to retain only six tests for analysis.

For each inversion listed in Table 4-1, all tests and intervals were processed simultaneously for the corresponding source signal period. The initial K_h, K_v/K_h, and S_s values for each heterogeneous simulation (simulations b in Table 4-1), were obtained from a preliminary inversion (simulations a in Table 4-1) using all tests associated with the simulation but with a homogeneous model. Therefore, slightly different initial conditions were used for each inversion to facilitate the search for the best solutions. The static condition before each test was simulated with a constant head of 0 m for the entire simulation grid. For the simulations of tomography based on slug tests, the same principle was applied as for OHT.

Table 4-1 : Overview of Simulation Programs for Tomography Inversions Across Different Periods and Slug Tests.

Inversion	Period (sec)	Number of test (interval)	a-Homogeneous model for all tests (1 zone)		b-Heterogeneous model for all tests (104 zones)	
			Hydraulic parameters			
			Initial	Final	Initial	Final
1a-b	150	10 (40)	K_h 1.10x10^{-5} ms^{-1} K_v/K$_h$ 1.23x10^{-1} S_s 4.74x10^{-5} m^{-1}			Figure 4-6a
2a-b	300	10 (40)		K_h 1.19x10^{-5} ms^{-1} K_v/K$_h$ 8.15x10^{-2} S_s 6.88x10^{-5} m^{-1}		Annexe III Figure 8-1a
3a-b	600	10 (39)		K_h 1.18x10^{-5} ms^{-1} K_v/K$_h$ 6.09x10^{-2} S_s 8.00x10^{-5} m^{-1}		Annexe III Figure 8-1b
4a-b	combi: 150,300	20 (80)		K_h 1.16x10^{-5} ms^{-1} K_v/K$_h$ 9.98x10^{-2} S_s 5.74x10^{-5} m^{-1}		Annexe III Figure 8-1c
5a-b	combi: 150,600	20 (79)		K_h 1.17x10^{-5} ms^{-1} K_v/K$_h$ 9.30x10^{-2} S_s 5.58x10^{-5} m^{-1}		Figure 4-6b
6a-b	combi: 300,600	20 (79)		K_h 1.20x10^{-5} ms^{-1} K_v/K$_h$ 7.28x10^{-2} S_s 7.21x10^{-5} m^{-1}		Annexe III Figure 8-1d
7a-b	combi: 150, 300 and 600	30 (119)		K_h 1.18x10^{-5} ms^{-1} K_v/K$_h$ 8.80x10^{-2} S_s 6.12x10^{-5} m^{-1}		Figure 4-6c
8a-b	Slug	6 (24)		K_h 2.22x10^{-5} ms^{-1} K_v/K$_h$ 3.5x10^{-2} S_s 6.6x10^{-5} m^{-1}		Figure 4-6d
			K_h 1x10^{-5} ms^{-1} K_v/K_h 1x10^{-1} S_s 1x10^{-5} m^{-1} -			

4.3 Analysis of inversion results

4.3.1 Hydraulic head

Comparison of simulated and observed heads for the tomography experiment with a combination of 150, 300 and 600 second (Simulation 7b in Table 4-2) and slug tests (Simulation 8b in Table 4-2) in Figure 4-3a and b reveals that the inversion captures well the general behavior of head responses obtained during the tests. The correlation coefficient (r) and the slope of the linear regression (m) between measured and simulated heads indicate a strong agreement for both the OHT (combi 150-300-600 sec) and the slug tests (Table 4-2).

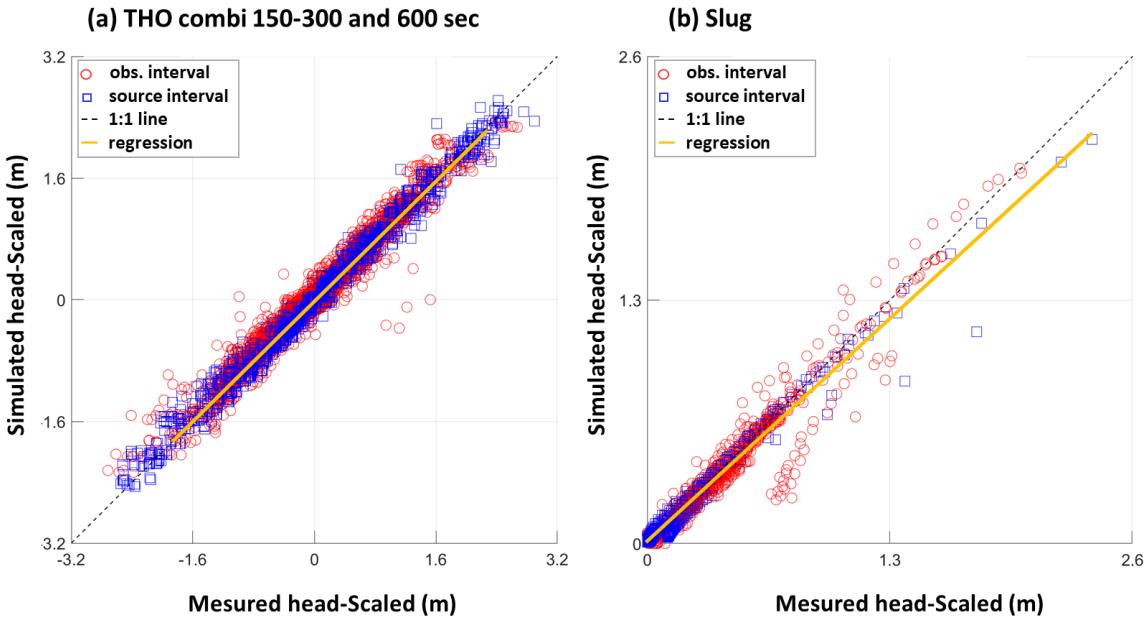

Figure 4-3 : Comparison between observed and simulated head data for the stressed (blue squares) and observation (red circles) intervals for (a) combination of 150-300-600 sec OHT and (b) slug test.

Specifically, for the OHT test (Figure 4-3a), the data points are closely aligned with the 1:1 line, reflecting minimal scattering and a high consistency between measured and simulated values. Similarly, for the slug tests (Figure 4-3b), the slope and correlation are close to unity, although slightly more dispersion is observed in comparison to the OHT configuration. Table 4-2 presents the statistical analysis of the residuals between observed and predicted heads for the eight inversion scenarios detailed in Table 4-1.

Table 4-2 : Statistics for observed and simulated heads for periodic and slug test used in the inversion of tomographic experiments: ‘‘r” is the coefficient of correlation, ‘‘m” is the slope of the linear regression between observed and simulated heads.

Inversion	Period (sec)	Runtime (min)	Residual							
			Source interval				Observation interval			
			r	m	Mean (m)	SD (m)	r	m	Mean (m)	SD (m)
1b	150	102	1	0.97	-3.5×10^{-3}	6.6×10^{-2}	0.99	0.97	-3.7×10^{-4}	7.2×10^{-4}
2b	300	80	1	1	-5.3×10^{-3}	4.8×10^{-2}	0.99	0.97	-2.0×10^{-4}	8.0×10^{-4}
3b	600	91	1	1	-4.0×10^{-4}	3.1×10^{-2}	0.98	0.95	-1.2×10^{-4}	8.8×10^{-4}
4b	150-300	214	0.99	1	-7×10^{-3}	6.9×10^{-2}	0.99	1	-2.6×10^{-4}	9.3×10^{-4}
5b	150-600	274	0.99	1.1	-9×10^{-4}	5.7×10^{-2}	0.97	1	-1.7×10^{-4}	9.8×10^{-4}
6b	300-600	155	1	1	-5×10^{-4}	3.5×10^{-2}	0.98	0.97	-1.4×10^{-4}	8.9×10^{-4}
7b	combi	374	0.99	1	-7.0×10^{-4}	5.1×10^{-2}	0.97	0.99	-1.6×10^{-4}	9.4×10^{-4}
8b	Slug	23	0.95	0.89	-1.9×10^{-3}	1.1×10^{-1}	0.97	0.96	-3.1×10^{-4}	1.6×10^{-3}

All 10 OHT of tomography experiment were analyzed with different periods to produce heterogeneous distributions of K_h, K_v/K_h, and S_s in the panel between wells S18 and O21. It should be noted that four slug test responses (test S18-450, S18-510b, S18-810 and S18-870) were excluded from the dataset due to poor data quality. For the OHT experiments, a total of 10 stressed interval responses and 30 observation interval responses were available and subsequently analyzed. In contrast, for the slug test experiments, 6 stressed interval responses and 18 observation interval responses were retained for analysis after excluding unreliable tests. While the slug tests involved a smaller dataset, they still allowed for meaningful comparisons of the resolution and accuracy of hydraulic property estimations between the two methodologies (Figure 4-4). To ensure fairness, we tested both configurations: comparing six OHT tests with six

slug tests, and ten OHT tests with six slug tests. The results were consistent across both setups, confirming that limiting the slug test dataset does not introduce bias. Moreover, the resolution comparison focuses on the same area covered by the six tests in both methods, ensuring an equivalent spatial basis for evaluation. Figure 4-5 reveal that for OHT, the shape of the simulated responses (e.g., first arrival times and maximum amplitudes) generally aligns well with field observations. This is especially evident in Figure 4-5, where the 600-second period example was selected to illustrate the strong agreement between simulated and observed responses. This consistency underscores the effectiveness of the OHT methodology in capturing the key characteristics of hydraulic responses.

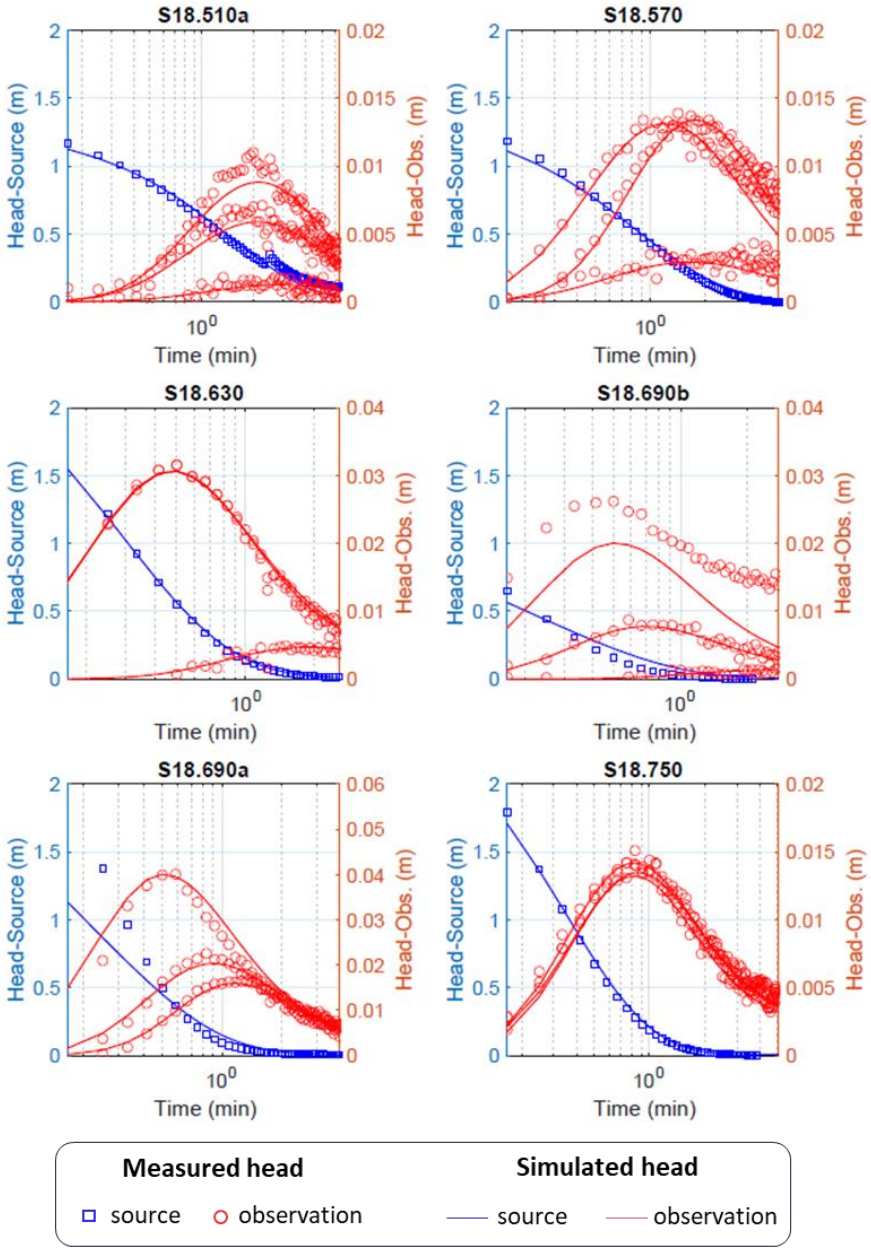

Figure 4-4 : Comparison between simulated (blue curves) head and observed responses for each of the 6 stressed interval (black squares) and the 18 observation intervals used for tomographic experiment S18O21. The slug tests were performed at the same intervals as the periodic tests.

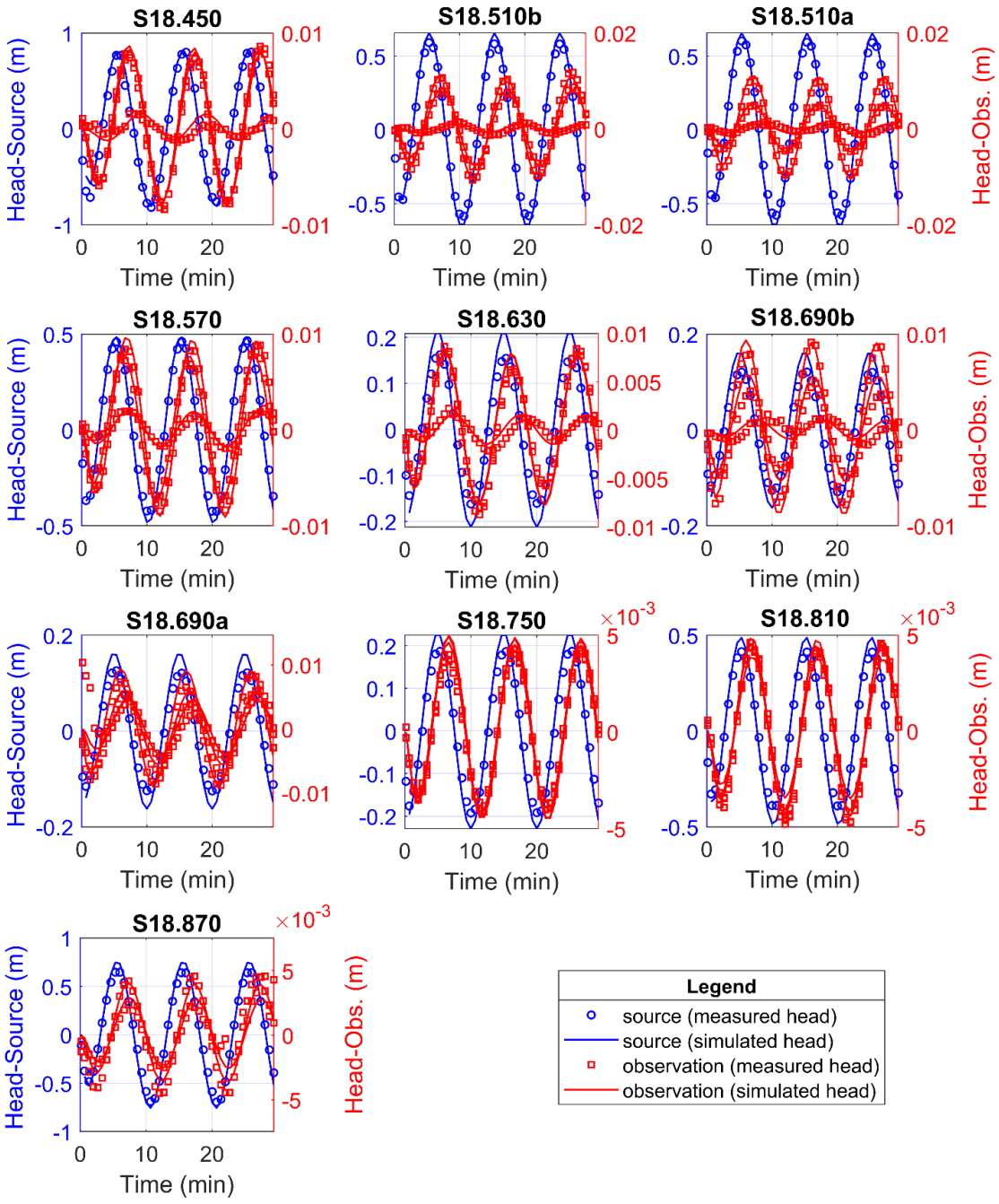

Figure 4-5 : Comparison of the measured and simulated head for the inversion with the 600-sec period. The intervals of the source (left) and the observation (right) are shown on different scales.

4.3.2 Hydraulic properties distribution

Figure 4-6 presents tomograms for K_h, K_v/K_h, and S_s derived from the inversion of the periodic test data for an individual period (150 sec), the combination of two (150-600 sec) and three (150-300-600 sec) periods, and the slug test. While the tomograms for the periodic tests exhibit consistent spatial patterns, the tomograms from the slug test data reveal distinct differences.

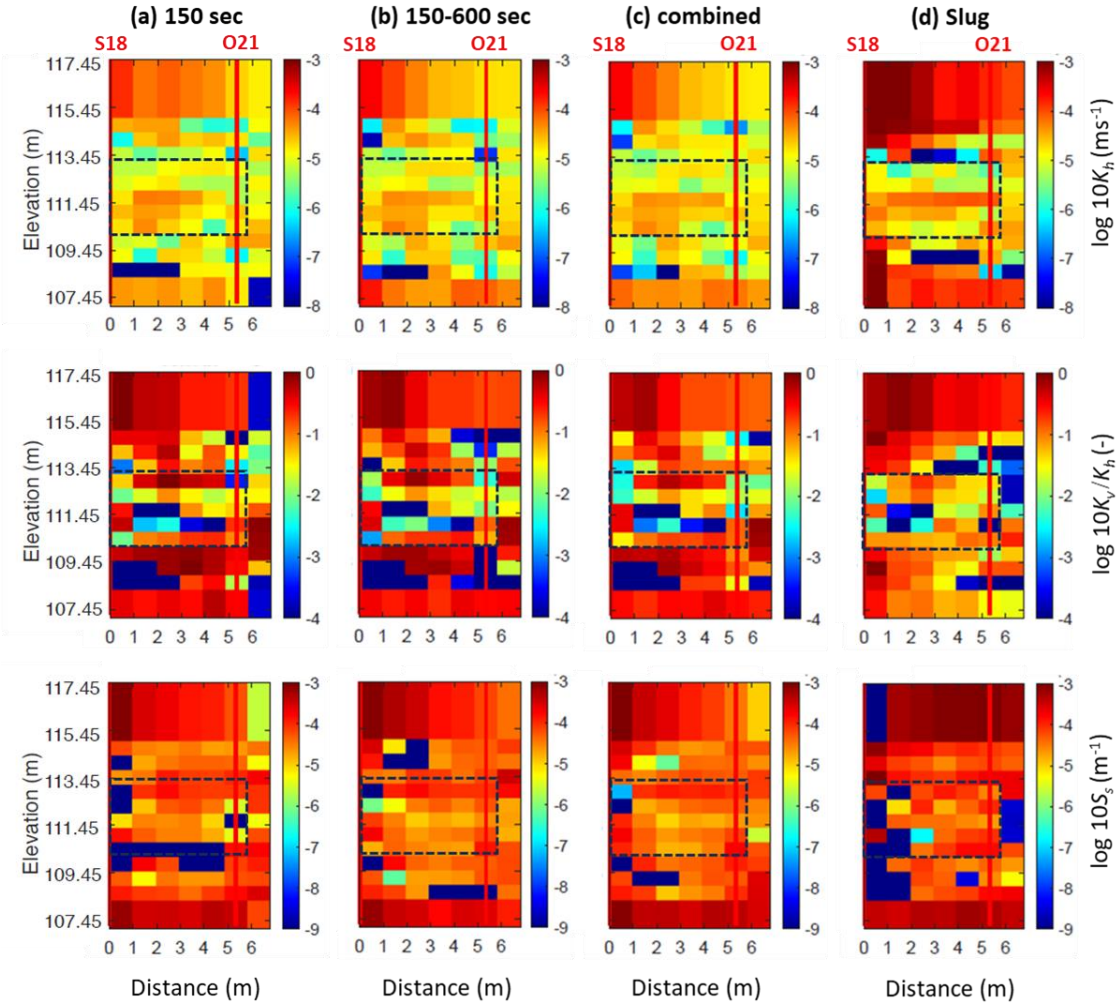

Figure 4-6 : Tomograms for Kh, Kv/Kh, and Ss resulting from the inversion of the periodic and slug tests with the (a) 150 sec, (b) 150-600 sec, (c) the combination of the three periods, and (d) slug test. The rectangle outlined by a black dashed line is the focus area for the periodic and slug tests.

For K_h, the periodic test inversions (150 sec, 150-600 sec, and the combination of three periods) consistently highlight a high-conductivity layer crossing the lower part of the focus area. This layer appears more distinct pronounced in the slug test tomograms. Additionally, both within the focus zone and outside it, the values of K_h are noticeably higher in the slug test tomograms compared

to those derived from the periodic test inversions. For K_v/K_h, the periodic test tomograms are nearly identical, consistently showing a zone of elevated anisotropy in the central part of the focus area. The combination of periods does not introduce any significant differences compared to the individual periodic inversions. In contrast, the slug test tomogram displays a more fragmented anisotropy distribution with distinct regions of lower anisotropy appearing both within and outside the focus zone. The spatial distribution of S_s generally more homogeneous compared to K_h and K_v/K_h with scattered very low values predominantly in the lower part of the focus area specially for 150 sec. The slug test tomogram reveals a more heterogeneous distribution of S_s particularly near the source well.

Figure 4-7 illustrates the statistical distribution of the values of hydraulic proprieties within the focus area for 6 tests derived from the inversion of the periodic and slug test data. The distributions of K_h are consistent across the periodic tests (150 sec, 150-600 sec, and combi) with a median near -5. However, the interquartile range (25-75% quantiles) is slightly higher for the combination (150-300-600 sec) compared to the two periods (150-600 sec) and single period (150 sec). This indicates that the combination of three periods captures a slightly broader variability in hydraulic conductivity values, suggesting potential contributions from more heterogeneous zones compared to the single period. In contrast, the slug test displays a wider interquartile range and a comparable median value near -5, but with a larger spread towards higher values. For K_v/K_h, the periodic tests (150 sec, 150-600 sec, and combi) display similar distributions of anisotropy ratios, with medians around -1.5 and broad interquartile ranges. The slug test reveals a narrower interquartile range while maintaining a median value similar to that of the periodic tests. Finally, for of Ss, the periodic tests (150-600 sec and combi) exhibit consistent distributions with relatively narrow interquartile ranges (25-75% quantiles) and median values clustered around -4.5. In contrast, the 150 sec period test shows a much broader interquartile range, extending to lower Ss values, with a median also closer to -4.5. This highlights a greater variability and the presence of significantly lower S_s values, suggesting that the shorter period may be less effective at stabilizing specific storage estimates. The slug test, on the other hand, demonstrates a similar median value to the periodic tests (around -4.5) but maintains a slightly narrower interquartile range, indicating a more constrained and stable estimation of Ss.

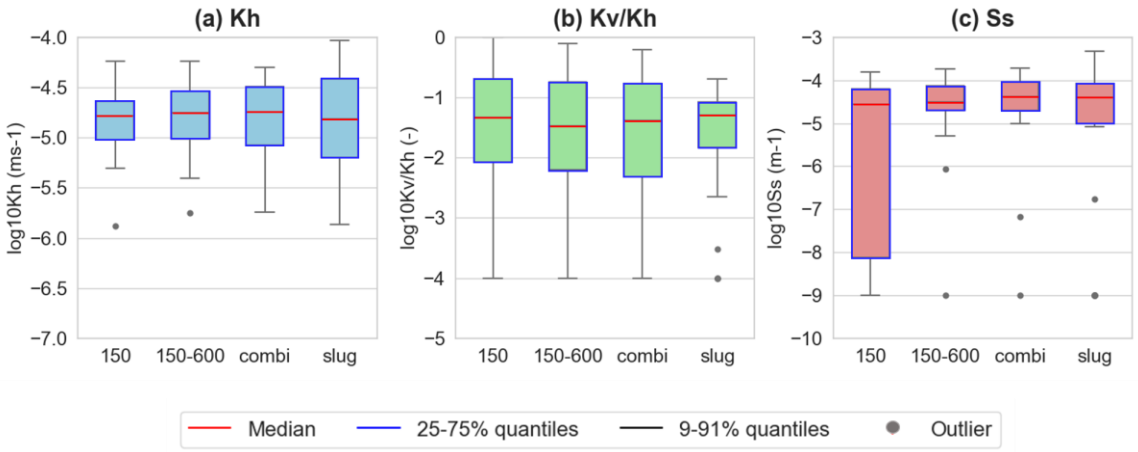

Figure 4-7 : Statistical distribution of the values of (a) Kh, (b) Kv/Kh, and (c) Ss within the focus area resulting from the inversion of the periodic and slug tests.

The sensitivity of HT methods is well known to be strongest in the vicinity of source and observation wells. Accordingly, we analyzed the correspondence between hydraulic property profiles obtained using both OHT and slug tests at these well locations (Figure 4-8).

For the source well, the K_h profile derived from the 150 sec period follows a similar overall trend to the profiles obtained from the combined 150-600 sec periods and the combination of three periods. The K_h profile from the slug test aligns well with the periodic test profiles, exhibiting comparable trends. Then, the K_v/K_h profiles obtained from both single and combined periods in the periodic tests, as well as from the slug tests, consistently show similar trends throughout most of the well depth. In contrast, for S_s, defining the correlation between periodic and slug tests proves more challenging. This discrepancy likely arises because S_s is primarily governed by the compressibility of the aquifer matrix and the history of stress changes within the aquifer, including those during sediment deposition. Consequently, S_s cannot be easily attributed solely to sediment characteristics. For the observation well, the K_h and K_v/K_h profiles exhibit poor correlation. The K_v/K_h profile derived from the slug test appears to oppose the general trends observed in the periodic tests, highlighting significant discrepancies between the methods. Conversely, for S_s, there is a notable agreement between the two methods.

For a quantitative comparison, we evaluated the correlation coefficients between the combined periods and the slug test results. At the source well, the results revealed a wide range of correlations: from poor correlation for specific storage (S_s; correlation coefficient > 0.1), to moderate correlation for anisotropy (K_v/K_h; correlation coefficient > 0.4), and strong correlation for hydraulic conductivity (K_h; correlation coefficient > 0.9).

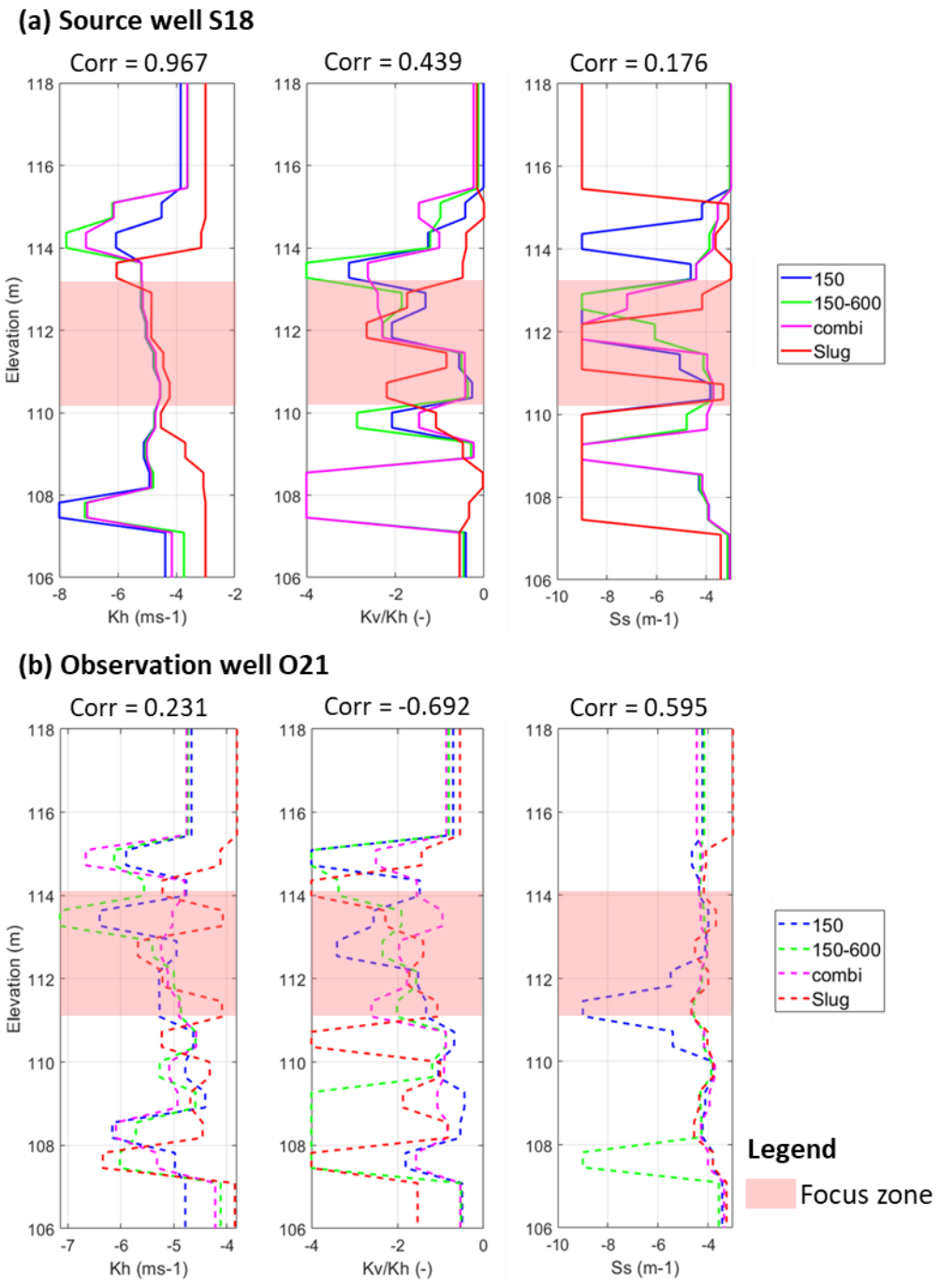

Figure 4-8 : Comparison between profiles of hydraulic properties obtained from the inversions of the four simulations (1, 5, 7 and 8) in Table 4-1 along the (a) source well S18 and (b) observation well O21.

These results indicate that the K_h profiles derived from both methods exhibit a strong consistency, while K_v/K_h and S_s show a weaker correspondence. In contrast, the observation well demonstrated poorer agreement overall. Specifically, the K_h profiles exhibited weak correlations (correlation coefficient > 0.2), while the K_v/K_h profiles showed negative correlation values,

indicating significant discrepancies between the two methods. However, for specific storage (S_s), a moderate correlation (correlation coefficient > 0.5) was observed, suggesting a better agreement for this parameter compared to hydraulic conductivity and anisotropy (Figure 4-8).

4.3.3 Parameter resolution

Figure 4-9 illustrates that the sensitivities for K_h, K_v/K_h, and S_s reach their maximum values within the focus area when combining the three periods.

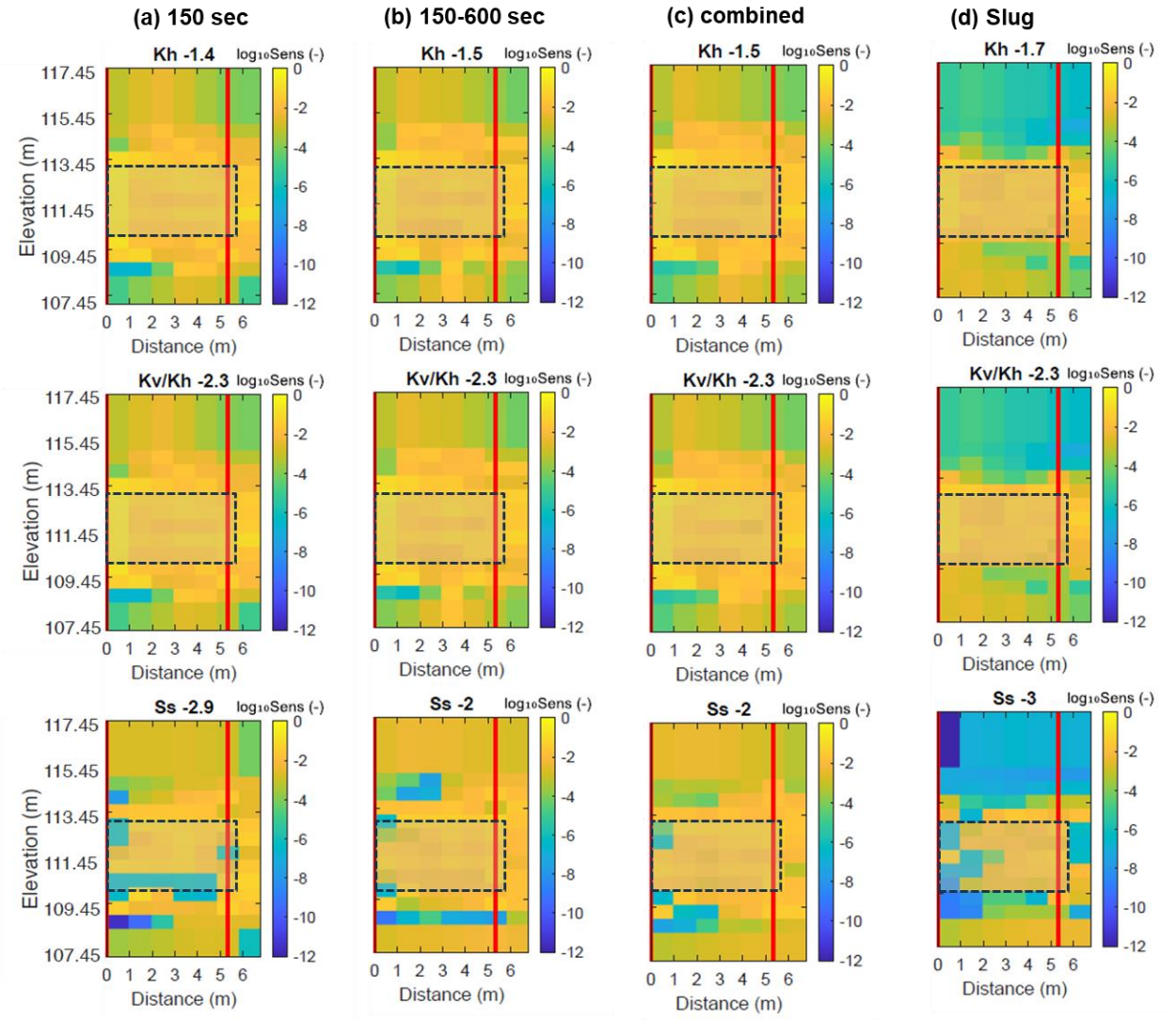

Figure 4-9 : Spatial distribution of RMS (root-mean-square) normalized sensitivities for Kh, Kv/Kh and Ss for (a) 150 sec, (b) 150-300 sec, (c) the combination of the three periods, and (d) slug test. The number next to the name of the hydraulic property is the average RMS sensitivity within the focus area.

Additionally, it is observed that the sensitivity for S_s increases steadily with the inclusion of additional periods. However, the sensitivity transition from slug tests to periodic tests for K_h, K_v/K_h, and S_s exhibits a notable decrease. Furthermore, Figure 4-9 (a, b, and c) reveals that the sensitivity across the three inversion scenarios does not show significant variation for the three hydraulic properties.

The L-curve analysis illustrated in Figure 4-10 offers a comprehensive comparison of the regularization strategies applied to simulated periodic and conventional slug test experiments. Each plot highlights the inflection point, marked with an "x" representing the optimal balance between minimizing data misfit and avoiding over-smoothing of the hydraulic parameters.

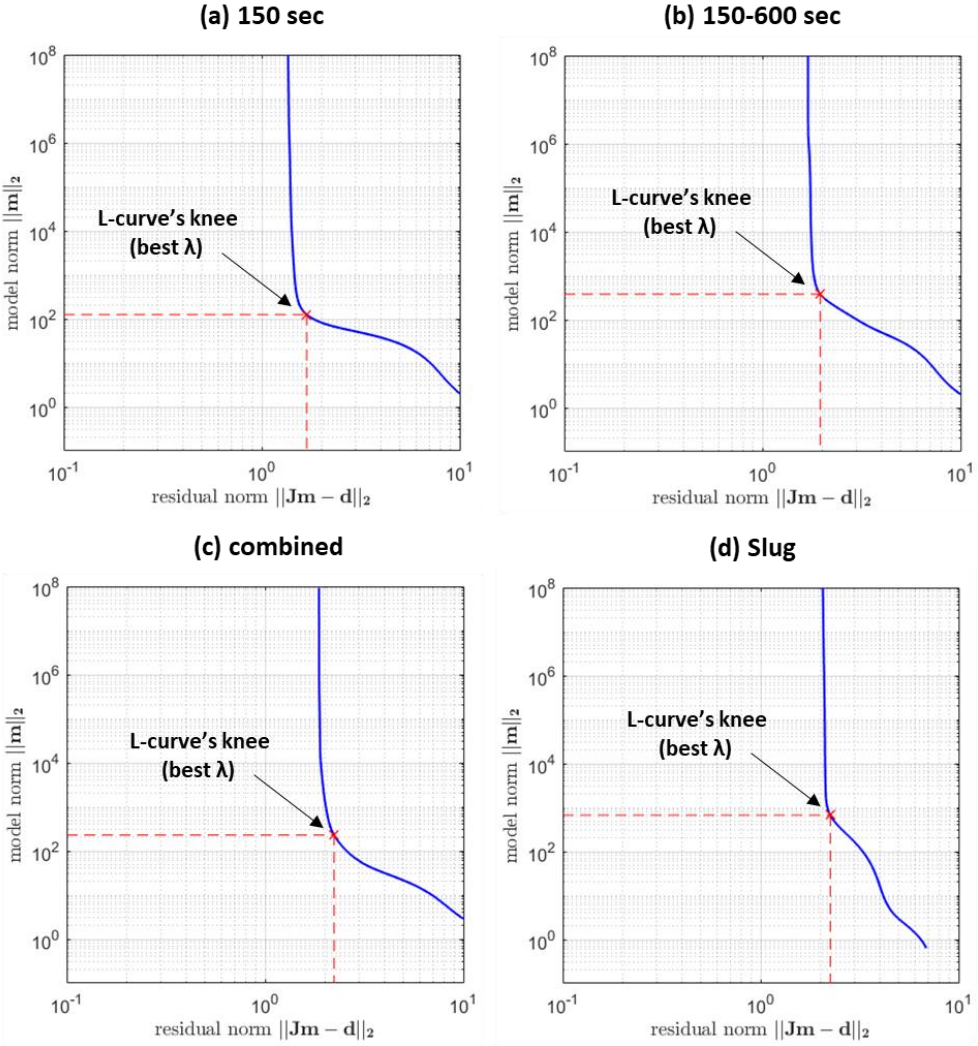

Figure 4-10 : Comparison of L-curve plots for simulated tomographic and slug tests: (a) 150 sec, (b) 150-300 sec, (c) combination of three periods, and (d) slug test. The inflexion point of each L-curve is marked by a "x" symbol.

These results reveal notable differences in the definition of the L-curves for the various test configurations. Contrary to the assumption that period combinations would provide better stability, the L-curve for the single 150-sec period (Figure 4-10a) appears to be the most well-defined, allowing for a clear and precise selection of the inflection point. In contrast, the period combinations (Figure 4-10b and Figure 4-10c) and the slug test (Figure 4-10d) produce less well-defined L-curves, occasionally making the selection of the optimal point more uncertain. These findings highlight that while period combinations may offer advantages in terms of spatial resolution, they do not always ensure better-defined L-curves. Even in cases where the L-curve is less well-defined, this approach provides a systematic and consistent means of determining the optimal point.

Figure 4-11 presents the diagonal elements of the resolution matrix at the corresponding parameter grid cells for K_h, K_v/K_h, and S_s estimates depicted in Figure 4-6a–d, respectively. The noise level was assessed through a residual analysis of head data recorded during the field implementation. Each diagonal element of the resolution matrix represents the degree to which the K_h, K_v/K_h, and S_s values are resolved within a specific model cell, with values ranging from 0, indicating a completely unresolved parameter, to 1, signifying a perfectly resolved parameter (Aster et al., 2005; Menke, 2012). Resolution values below 0.5 suggest that the parameter estimate for the cell is more strongly influenced by other parameters than by the cell's corresponding parameter.

For OHT, the combination of two or three periods provides improved resolution for all three hydraulic properties compared to a single-period test. However, the overall resolution patterns for the three scenarios remain broadly similar. The tomograms generated using combined periods for OHT are also highly comparable to those derived from the slug tests. Across the parameter grid, the resolution of K_h is notably higher for cells located at the source and observation wells in both OHT and slug tests. In contrast, K_v/K_h, and S_s parameters are better resolved at the source well in OHT. Slug tests, on the other hand, exhibit superior resolution at the center of the focus zone, particularly for K_v/K_h, and achieve better S_s resolution at the observation well. This highlights the complementary nature of the two approaches in resolving different hydraulic properties across the domain.

Indeed, no clear correlation can be observed between Figure 4-9 and Figure 4-11. While all three OHT scenarios display sensitivities of about –2.3 in the focus area, similar to the slug test, the latter still provides the highest resolution. This highlights that sensitivity alone does not guarantee

better parameter resolution, as illustrated by the consistently lower resolution of Kv/Kh across all OHT scenarios."

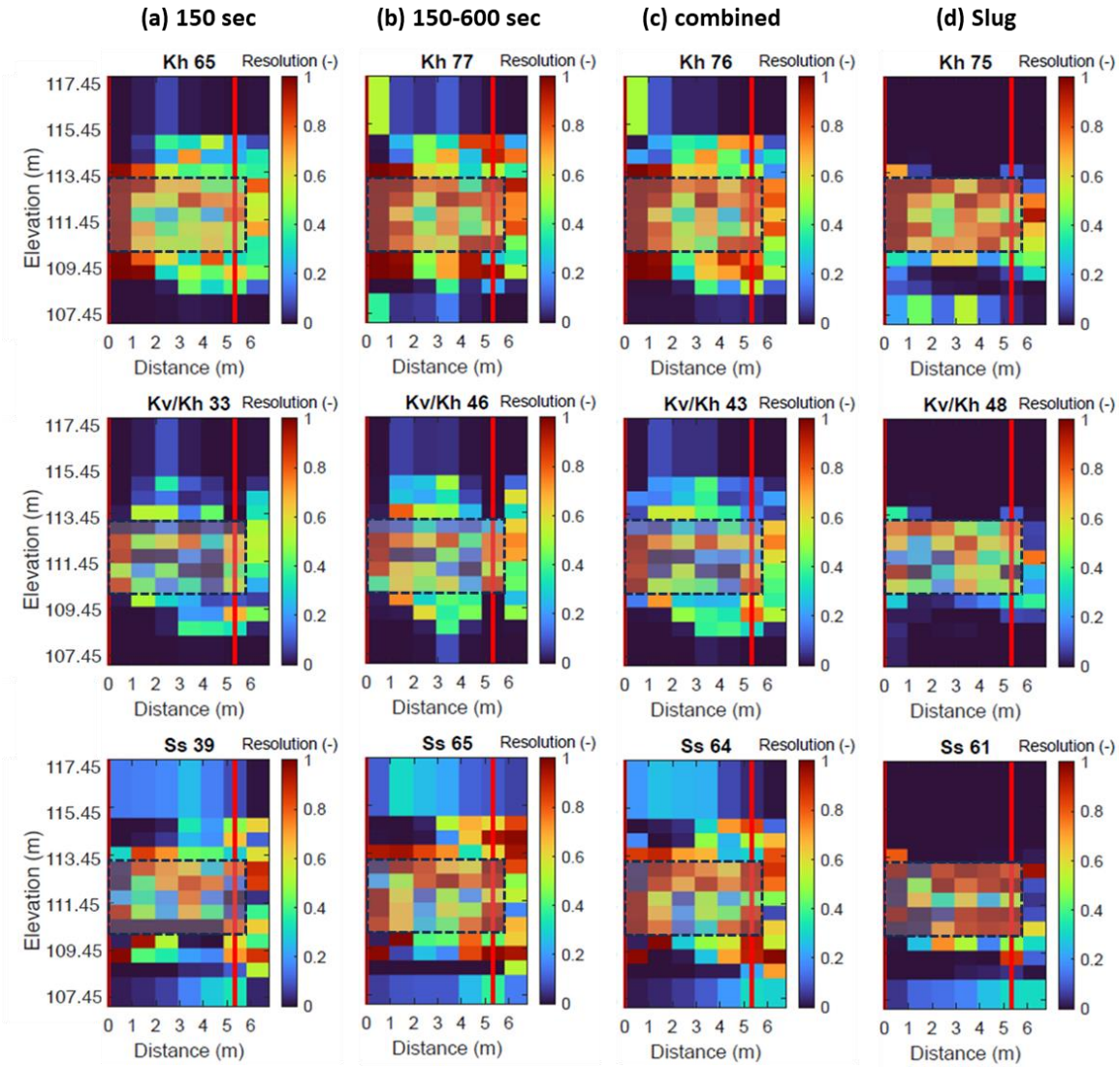

Figure 4-11 : Spatial distribution of the resolution for the hydraulic properties Kh, Kv/Kh and Ss for (a) 150 sec, (b) 150-300 sec, (c) the combination of the three periods, and (d) slug test. The number next to the name of the hydraulic property is the resolution degree (RD) within the focus area.

Figure 4-12 presents a comparison of the information content (*IC*) and resolution degree (*RD*) derived from various period combinations in periodic tests and slug tests. The findings suggest that combining multiple periods generally enhances resolution compared to using a single period. However, this improvement is not consistent across all period combinations, highlighting the importance of selecting appropriate periods. For the analysis of individual periods (150, 300, and 600 sec), the results indicate that the shortest period (150 sec) provides the highest resolution.

Additionally, combining two periods, such as 150 and 600 sec, enhances resolution, whereas the combination of 300 and 600 sec does not lead to a significant improvement. It is also noteworthy that the combination of 150 and 600 sec offers a slight improvement in resolution compared to the combination of all three periods together. The key insight from this figure is that the greatest information content in periodic tests is obtained either from the combination of all three periods or from the combination of 150 and 600 sec. Meanwhile, the slug test exhibits a resolution comparable to the best-performing combinations from the periodic test approach.

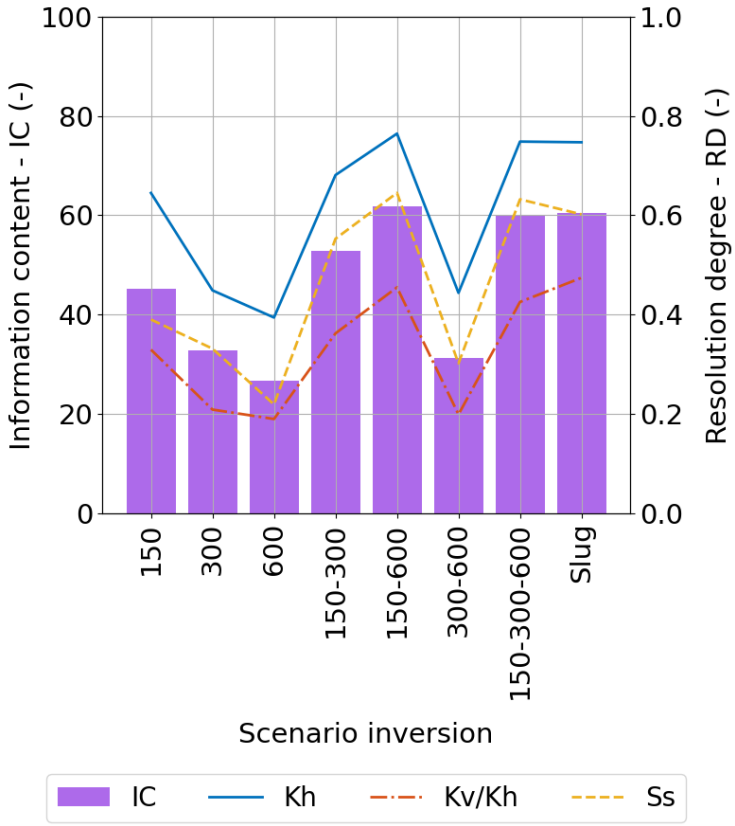

Figure 4-12 : Information content (IC) and resolution degree (RD) for different combinations of signal periods for periodic tests and slug test within the focus area.

4.4 Conclusions

The primary aim of this study was to evaluate the capabilities of Oscillatory Hydraulic Tomography (OHT) and Tomographic Slug Test methodologies in estimating the hydraulic parameters of the St-Lambert aquifer, including horizontal hydraulic conductivity (K_h), anisotropy (K_v/K_h), and specific storage (S_s). Using the L-curve criterion as a comparative tool, we analyzed the resolution and sensitivity of various tomographic scenarios, highlighting the importance of methodological choices in improving subsurface characterization.

The findings demonstrate that both OHT and slug tests provide valuable insights into aquifer heterogeneity, but their effectiveness varies depending on the parameter of interest, the spatial location within the aquifer, and the experimental design. The OHT approach shows a clear advantage in processing hydraulic head data, as its periodic signal structure is more resilient to ambient noise. However, the slug test remains a robust method, offering comparable resolution, particularly for Ss near observation wells, with the added benefit of a simpler field implementation.

From a fundamental perspective, this study emphasizes the critical role of period selection in OHT. By combining three distinct periods (150, 300, and 600 seconds), we achieved a resolution comparable to that of the slug test. This highlights the importance of leveraging a multi-period strategy to maximize information content and capture the spatial variability of hydraulic properties. Moreover, the results indicate that shorter periods, such as 150 seconds, could potentially enhance parameter resolution, particularly for properties like Ss, which are sensitive to time-dependent stress changes. These findings provide a deeper understanding of the mechanisms driving hydraulic responses and their relation to signal properties, offering a theoretical basis for optimizing future OHT designs.

The choice of periods should be tailored to the specific objectives of the study, balancing the need for resolution against logistical constraints, such as test duration and equipment requirements. While periodic slug tests requires more sophisticated instrumentation and longer test durations, its ability to isolate and interpret head responses with high precision makes it a valuable tool for challenging field conditions, particularly in highly heterogeneous aquifers. In contrast, slug tests, with their simplicity and efficiency, remain a reliable alternative for scenarios where resources or time are limited. Lastly, the study highlights the broader implications of period selection and testing strategies on subsurface characterization. By systematically analyzing the influence of time scales on parameter resolution, this work provides a framework for future studies to refine hydraulic tomography methodologies. This is particularly relevant for aquifers with complex

hydrogeological settings, where the interplay of heterogeneity, anisotropy, and storage properties requires nuanced experimental designs.

In conclusion, this study advances the understanding of hydraulic tomography techniques by demonstrating the importance of methodological choices, particularly in OHT. The insights gained from this work have both theoretical and practical relevance, offering a roadmap for optimizing field testing strategies and improving the resolution of hydraulic parameters in complex aquifer systems.

4.5 Bibilographie 3e ARTICLE

Aster, R.C., Borchers, B., Thurber, C., 2005. Parameter Estimation and Inverse Problems Elsevier, Amsterdam, p. 301.

Berg, S.J., Illman, W.A., 2011. Three-dimensional transient hydraulic tomography in a highly heterogeneous glaciofluvial aquifer-aquitard system. Water Resour. Res. 47. https://doi.org/10.1029/2011WR010616.

Bohling, G.C., 2009. Sensitivity and resolution of tomographic pumping tests in an alluvial aquifer. Water Resour. Res. 45. https://doi.org/10.1029/2008WR007249.

Bohling, G.C., 1993. Hydraulic tomography in two-dimensional, steady-state groundwater flow. Eos Trans. AGU 74, 141.

Bohling, G.C., Butler, J.J., 2001. lr2dinv: A finite-difference model for inverse analysis of two-dimensional linear or radial groundwater flow. Computers & Geosciences 27, 1147–1156. https://doi.org/10.1016/S0098-3004(01)00036-X.

Bohling, G.C., Butler, J.J., Zhan, X., Knoll, M.D., 2007. A field assessment of the value of steady shape hydraulic tomography for characterization of aquifer heterogeneities. Water Resour. Res. 43. https://doi.org/10.1029/2006WR004932.

Bohling, G.C., Liu, G., Dietrich, P., Butler Jr., J.J., 2016. Reassessing the MADE direct-push hydraulic conductivity data using a revised calibration procedure. Water Resources Research 52, 8970–8985. https://doi.org/10.1002/2016WR019008.

Bohling, G.C., Liu, G., Knobbe, S.J., Reboulet, E.C., Hyndman, D.W., Dietrich, P., Butler Jr, J.J., 2012. Geostatistical analysis of centimeter-scale hydraulic conductivity variations at the MADE site. Water Resources Research 48. https://doi.org/10.1029/2011WR010791.

Bohling, G.C., Zhan, X., Butler, J.J., Zheng, L., 2002. Steady shape analysis of tomographic pumping tests for characterization of aquifer heterogeneities. Water Resour. Res. 38, 60-1-60–15. https://doi.org/10.1029/2001WR001176.

Brauchler, R., Cheng, J.-T., Dietrich, P., Everett, M., Johnson, B., Liedl, R., Sauter, M., 2007. An inversion strategy for hydraulic tomography: Coupling travel time and amplitude inversion. Journal of Hydrology 345, 184–198. https://doi.org/10.1016/j.jhydrol.2007.08.011.

Brauchler, R., Hu, R., Dietrich, P., Sauter, M., 2011. A field assessment of high-resolution aquifer characterization based on hydraulic travel time and hydraulic attenuation tomography. Water Resour. Res. 47. https://doi.org/10.1029/2010WR009635.

Brauchler, R., Liedl, R., Dietrich, P., 2003. A travel time based hydraulic tomographic approach. Water Resour. Res. 39. https://doi.org/10.1029/2003WR002262.

Cardiff, M., Bakhos, T., Kitanidis, P.K., Barrash, W., 2013b. Aquifer heterogeneity characterization with oscillatory pumping: Sensitivity analysis and imaging potential. Water Resour. Res. 49, 5395–5410. https://doi.org/10.1002/wrcr.20356.

Cardiff, M., Barrash, W., 2011. 3-D transient hydraulic tomography in unconfined aquifers with fast drainage response. Water Resources Research 47. https://doi.org/10.1029/2010WR010367.

Cardiff, M., Barrash, W., Kitanidis, P. k., Malama, B., Revil, A., Straface, S., Rizzo, E., 2009. A Potential-Based Inversion of Unconfined Steady-State Hydraulic Tomography. Groundwater 47, 259–270. https://doi.org/10.1111/j.1745-6584.2008.00541.x.

Cardiff, M., Barrash, W., Kitanidis, P.K., 2012. A field proof-of-concept of aquifer imaging using 3-D transient hydraulic tomography with modular, temporarily-emplaced equipment. Water Resour. Res. 48. https://doi.org/10.1029/2011WR011704.

Cardiff, M., Zhou, Y., Barrash, W., Kitanidis, P.K., 2020. Aquifer imaging with oscillatory hydraulic tomography: application at the field scale. Groundwater 58, 710–722. https://doi.org/10.1111/gwat.12960.

Dubreuil-Boisclair, C., Gloaguen, E., Marcotte, D., Giroux, B., 2011. Heterogeneous aquifer characterization from ground-penetrating radar tomography and borehole hydrogeophysical data using nonlinear Bayesian simulations. GEOPHYSICS 76, J13–J25. https://doi.org/10.1190/1.3571273.

Fischer, P., Jardani, A., Jourde, H., Cardiff, M., Wang, X., Chedeville, S., Lecoq, N., 2018. Harmonic pumping tomography applied to image the hydraulic properties and interpret the connectivity of a karstic and fractured aquifer (Lez aquifer, France). Advances in Water Resources 119, 227–244. https://doi.org/10.1016/j.advwatres.2018.07.002.

Gottlieb, J., Dietrich, P., 1995. Identification of the permeability distribution in soil by hydraulic tomography. Inverse Problems 11, 353–360. https://doi.org/10.1088/0266-5611/11/2/005.

Hansen, P.C., 1992. Analysis of discrete Ill-posed problems by means of the L-curve. SIAM Rev. 34, 561–580. https://doi.org/10.1137/1034115.

Hansen, P.C., Jensen, T.K., Rodriguez, G., 2007. An adaptive pruning algorithm for the discrete L-curve criterion. Journal of Computational and Applied Mathematics, Special Issue: Applied Computational Inverse Problems 198, 483–492. https://doi.org/10.1016/j.cam.2005.09.026.

Hochstetler, D.L., Barrash, W., Leven, C., Cardiff, M., Chidichimo, F., Kitanidis, P.K., 2016. Hydraulic tomography: continuity and discontinuity of high-K and low-K zones. Groundwater 54, 171–185. https://doi.org/10.1111/gwat.12344.

Illman, W.A., Craig, A.J., Liu, X., 2008. Practical Issues in Imaging Hydraulic Conductivity through Hydraulic Tomography. Groundwater 46, 120–132. https://doi.org/10.1111/j.1745-6584.2007.00374.x.

Illman, W.A., Liu, X., Takeuchi, S., Yeh, T.-C.J., Ando, K., Saegusa, H., 2009. Hydraulic tomography in fractured granite: Mizunami Underground Research site, Japan. Water Resour. Res. 45. https://doi.org/10.1029/2007WR006715.

Liu, G., Bohling, G.C., Butler Jr., J.J., 2008. Simulation assessment of the direct-push permeameter for characterizing vertical variations in hydraulic conductivity. Water Resources Research 44. https://doi.org/10.1029/2007WR006078.

Liu, G., Butler Jr., J.J., Bohling, G.C., Reboulet, E., Knobbe, S., Hyndman, D.W., 2009. A new method for high-resolution characterization of hydraulic conductivity. Water Resources Research 45. https://doi.org/10.1029/2009WR008319.

Liu, Q., Hu, L., Hu, R., Brauchler, R., Xing, Y., Qi, J., Ptak, T., 2023. Characterization of aquifer heterogeneity by tomographic slug test responses considering wellbore effects. Journal of Hydrology 627, 130472. https://doi.org/10.1016/j.jhydrol.2023.130472.

Menke, W., 2012. Geophysical Data Analysis: Discrete Inverse Theory, 3rd ed., 293 pp., Acedemic Press, Elsevier.

Nefzi, A., Paradis, D., Lefebvre, R., En préparation “a.” Responses and resolution of oscillatory hydraulic tomography under a wide range of single and combined signal periods. Article en préparation.

Nefzi, A., Paradis, D., Lefebvre, R., Bour, O., Lavenant, N., 2025. Field deployment and analysis of hydraulic tomography experiments with periodic slug tests in an anisotropic littoral aquifer. Journal of Hydrology 653, 132747. https://doi.org/10.1016/j.jhydrol.2025.132747.

Ouellon, T., Lefebvre, R., Marcotte, D., Boutin, A., Blais, V., Parent, M., 2008. Hydraulic conductivity heterogeneity of a local deltaic aquifer system from the kriged 3D distribution of hydrofacies from borehole logs, Valcartier, Canada. Journal of Hydrology 351, 71–86. https://doi.org/10.1016/j.jhydrol.2007.11.040.

Paradis, D., Gloaguen, E., Lefebvre, R., Giroux, B., 2016. A field proof-of-concept of tomographic slug tests in an anisotropic littoral aquifer. Journal of Hydrology 536, 61–73. https://doi.org/10.1016/j.jhydrol.2016.02.041.

Paradis, D., Gloaguen, E., Lefebvre, R., Giroux, B., 2015b. Resolution analysis of tomographic slug test head data: Two-dimensional radial case. Water Resour. Res. 51, 2356–2376. https://doi.org/10.1002/2013WR014785.

Paradis, D., Lefebvre, R., 2013. Single-well interference slug tests to assess the vertical hydraulic conductivity of unconsolidated aquifers. Journal of Hydrology 478, 102–118. https://doi.org/10.1016/j.jhydrol.2012.11.047.

Paradis, D., Lefebvre, R., Morin, R.H., Gloaguen, E., 2011. Permeability Profiles in Granular Aquifers Using Flowmeters in Direct-Push Wells. Ground Water 49, 534–547. https://doi.org/10.1111/j.1745-6584.2010.00761.x.

Paradis, D., Lefebvre, R., Nefzi, A., 2024. Parameter resolution of simulated responses to periodic hydraulic tomography signals in aquifers. Advances in Water Resources 190, 104734. https://doi.org/10.1016/j.advwatres.2024.104734.

Sun, R., Yeh, T.-C.J., Mao, D., Jin, M., Lu, W., Hao, Y., 2013. A temporal sampling strategy for hydraulic tomography analysis. Water Resources Research 49, 3881–3896. https://doi.org/10.1002/wrcr.20337.

Wang, Y.-L., Yeh, T.-C.J., Xu, D., Li, K., Wen, J.-C., Huang, S.-Y., Wang, W., Hao, Y., 2021. Stochastic analysis of oscillatory hydraulic tomography. Journal of Hydrology 596, 126105. https://doi.org/10.1016/j.jhydrol.2021.126105.

Yeh, T.-C.J., Liu, S., 2000. Hydraulic tomography: Development of a new aquifer test method. Water Resour. Res. 36, 2095–2105. https://doi.org/10.1029/2000WR900114.

Zhou, Y., Lim, D., Cupola, F., Cardiff, M., 2016. Aquifer imaging with pressure waves—Evaluation of low-impact characterization through sandbox experiments. Water Resour. Res. 52, 2141–2156. https://doi.org/10.1002/2015WR017751.

Zschornack, L., Bohling, G.C., Butler, J.J., Dietrich, P., 2013. Hydraulic profiling with the direct-push permeameter: Assessment of probe configuration and analysis methodology. Journal of Hydrology 496, 195–204. https://doi.org/10.1016/j.jhydrol.2013.05.036.

5 DISCUSSION GÉNÉRALE ET CONCLUSION

L'objectif principal de ce doctorat était d'explorer en détail le potentiel de la tomographie hydraulique oscillatoire (THO) pour la caractérisation détaillée de la distribution spatiale des propriétés hydrauliques à l'échelle locale. La connaissance de l'hétérogénéité de ces propriétés est nécessaire à la compréhension des processus d'écoulement et de migration des contaminants, ainsi qu'à l'amélioration de la représentation de ces phénomènes à l'aide de modèles numériques. Ce projet de recherche a impliqué l'usage de diverses méthodes : un volet expérimental, du traitement de données et de la modélisation numérique. Au niveau expérimental, les essais hydrauliques se sont déroulés sur un site d'essai de 400 m² situé à l'intérieur du site d'enfouissement de Saint-Lambert-de-Lauzon. Une caractérisation de l'hétérogénéité et de l'anisotropie de l'aquifère granulaire du site expérimental a été faite par THO. Ces essais ont servi de base à l'exploration complète du potentiel de la THO, incluant l'acquisition des mesures, le traitement des données, l'inversion des données avec un modèle numérique pour estimer les propriétés hydrauliques et l'utilisation de la modélisation numérique pour généraliser les résultats expérimentaux obtenus. Les chapitres de mise en contexte de la thèse ont documenté comment les travaux antérieurs ont montré que la THO peut être exploitée pour révéler l'hétérogénéité et l'anisotropie des aquifères.

Dans le premier article, nous avons exploré l'application pratique des tests périodiques dans un aquifère littoral, englobant les procédures sur le terrain, le traitement des données et leur inversion numérique, offrant une preuve de concept complète pour cette approche. Cette étude a mis en évidence la capacité des signaux périodiques à fournir des données de haute qualité malgré les défis liés à l'hétérogénéité et à l'anisotropie de l'aquifère. Les tests ont montré que l'anisotropie de la conductivité hydraulique peut être estimée avec précision grâce à des intervalles de source courts et une configuration adaptée. Pour la THO, les travaux montrent pour la première fois l'importance de la représentation explicite de l'anisotropie de K dans le modèle numérique utilisé pour l'inversion des données obtenues des essais. En résumé, ce premier manuscrit constitue une avancée importante dans l'application des tests périodiques pour la tomographie hydraulique en conditions réelles. Il s'inscrit parmi les rares exemples pratiques documentés dans la littérature scientifique. Il fournit une base solide pour améliorer la caractérisation des hétérogénéités et de l'anisotropie des aquifères, tout en identifiant les défis technologiques et méthodologiques à relever pour optimiser cette approche.

Le deuxième article a réalisé une évaluation a posteriori des expériences de THO pour analyser la résolution et le contenu informationnel des réponses hydrauliques à travers une large gamme de signaux périodiques. Cela constitue la première étude sur la résolution des mesures obtenues des expériences de THO. En combinant des modèles homogènes et hétérogènes, cette étude a mené des simulations numériques rigoureuses pour évaluer les effets des périodes sur la sensibilité et la résolution des paramètres hydrauliques. Les résultats ont révélé que l'utilisation de périodes courtes améliore significativement la résolution des hétérogénéités locales, tandis que les périodes longues permettent de capturer les réponses hydrauliques globales. L'analyse a également montré que la combinaison stratégique de périodes courtes et intermédiaires maximise le contenu informationnel en exploitant des réponses hydrauliques rapides et lentes. Toutefois, combiner des périodes longues aux sensibilités fortement corrélées peut réduire leur efficacité. Cette recherche souligne que le choix des périodes est déterminant pour la qualité des résultats et offre une stratégie pragmatique pour optimiser les durées de tests sur le terrain tout en améliorant l'efficacité de l'acquisition des données. Elle fournit ainsi des orientations claires pour affiner l'application de l'OHT à l'imagerie du sous-sol.

Dans le troisième article, une comparaison entre la THO et la TH par choc hydraulique a été réalisée dans l'aquifère de St-Lambert. Le cœur de cette étude réside dans l'exploration du contenu informationnel des essais par THO et TH. Les inversions menées avec des périodes distinctes, ainsi que les multiples combinaisons de ces périodes, permettent d'analyser en détail l'apport des THO en termes de résolution des hétérogénéités. Les tests THO, basés sur trois périodes distinctes (150, 300 et 600 secondes), ont montré un léger avantage dans le traitement des données de charge hydrauliques grâce à leur résilience au bruit ambiant, bien que cette méthode exige un équipement plus sophistiqué et des durées de tests plus longues. En revanche, la TH par choc hydraulique, simple à mettre en œuvre, offre une résolution robuste pour des paramètres comme l'emmagasinement spécifique (S_s) près des puits d'observation. L'analyse de résolution a révélé que la stratégie multi-périodes améliore considérablement la capacité à résoudre les hétérogénéités, en particulier lorsque des périodes soigneusement choisies sont combinées. Cette étude met en avant l'importance des choix méthodologiques dans l'amélioration des caractérisations hydrauliques, tout en soulignant l'équilibre à trouver entre résolution et contraintes logistiques pour une application efficace des tests sur le terrain.

Un défi important abordé au cours de la dernière année de cette étude a été l'optimisation du code d'inversion pour améliorer son efficacité et réduire le temps de calcul. Grâce à la collaboration avec le Professeur Bernard Giroux de l'INRS, une avancée significative a été

réalisée en parallélisant la boucle responsable du calcul de la matrice de sensibilité, qui représentait jusqu'à 98 % du temps total de traitement. Cette optimisation a considérablement réduit le temps de calcul et amélioré l'efficacité des inversions, représentant une avancée technique importante pour la poursuite de cette recherche.

Dans le cadre de cette thèse, les expérimentations ont été réalisées en 2D entre une paire de puits. Toutefois, pour améliorer la représentation spatiale de l'hétérogénéité à une échelle plus large, les travaux futurs devraient viser l'intégration de plusieurs puits dans les simulations d'inversions numériques. Cela nécessiterait le développement ou l'adaptation de programmes numériques en 3D. Cependant, la simulation en 3D requiert des ressources matérielles considérablement plus importantes par rapport à la simulation en 2D. C'est pourquoi les avancées en matière de parallélisation offrent des perspectives prometteuses dans cette direction. De plus, d'un point de vue pratique, l'intégration de plusieurs puits nécessiterait le développement d'approches d'acquisition de données sur le terrain beaucoup plus efficaces. La réalisation de multiples essais, avec l'enregistrement des réponses hydrauliques dans plusieurs intervalles d'observation, exige des ressources matérielles importantes ainsi qu'un déploiement optimal des moyens sur le terrain. Cet aspect de la recherche appliquée devrait être davantage encouragé afin d'améliorer les méthodologies et leur mise en œuvre.

Bien que nos travaux aient fourni des avancées significatives dans l'utilisation des techniques tomographiques pour caractériser les propriétés hydrauliques des aquifères complexes, il existe quelques limitations qui devraient être prises en compte pour les études futures. Une des principales limitations identifiées lors des essais de terrain concernait l'ajustement du déplacement de la tige (A_0). Le mouvement de la tige, bien qu'entièrement contrôlé numériquement, a dû être ajusté dans les intervalles moins perméables et pour les périodes courtes afin d'optimiser les charges hydrauliques et d'éviter de dénoyer partiellement la tige. Cet ajustement, efficace pour prévenir des artefacts opérationnels, a entraîné une variation sous-optimale des charges dans certains intervalles d'observation, influençant ainsi la qualité des données obtenues. Aussi, la petite quantité d'eau pouvant être déplacée avec la tige a limité l'amplitude des variations de charge dans le puits source et les intervalles d'observation associés. Cette contrainte a restreint l'expérimentation à une gamme relativement étroite de périodes. Pour les périodes courtes, le faible volume ne permet pas de générer des fluctuations de charge suffisantes pour être mesurées avec un bon rapport signal/bruit, tandis que pour les périodes longues, il limite également la capacité à maintenir des variations de charge significatives. Ces limitations opérationnelles ont réduit la possibilité de capturer une gamme plus variée de

réponses hydrauliques. L'utilisation de sources pneumatiques pour générer des signaux de test, comme présentée par Sayler et al. (2018), pourrait offrir une gamme plus large de périodes avec un meilleur rapport signal/bruit. Le développement de ces outils permettrait d'améliorer les performances des essais sur le terrain et d'élargir les capacités d'investigation de la tomographie hydraulique.

Finalement, Les travaux de recherche documentés dans cette thèse ont permis de répondre aux principaux objectifs initiaux et ont soulevé de nouvelles questions. Ces travaux proposent des pistes pour des travaux futurs en tomographie hydraulique.

ANNEXE I : FIGURES ET TABLEAUX SUPPLÉMENTAIRES POUR L'ARTICLE 1

I.1 Corrected raw head data after accounting for incomplete stabilization with the ambient head

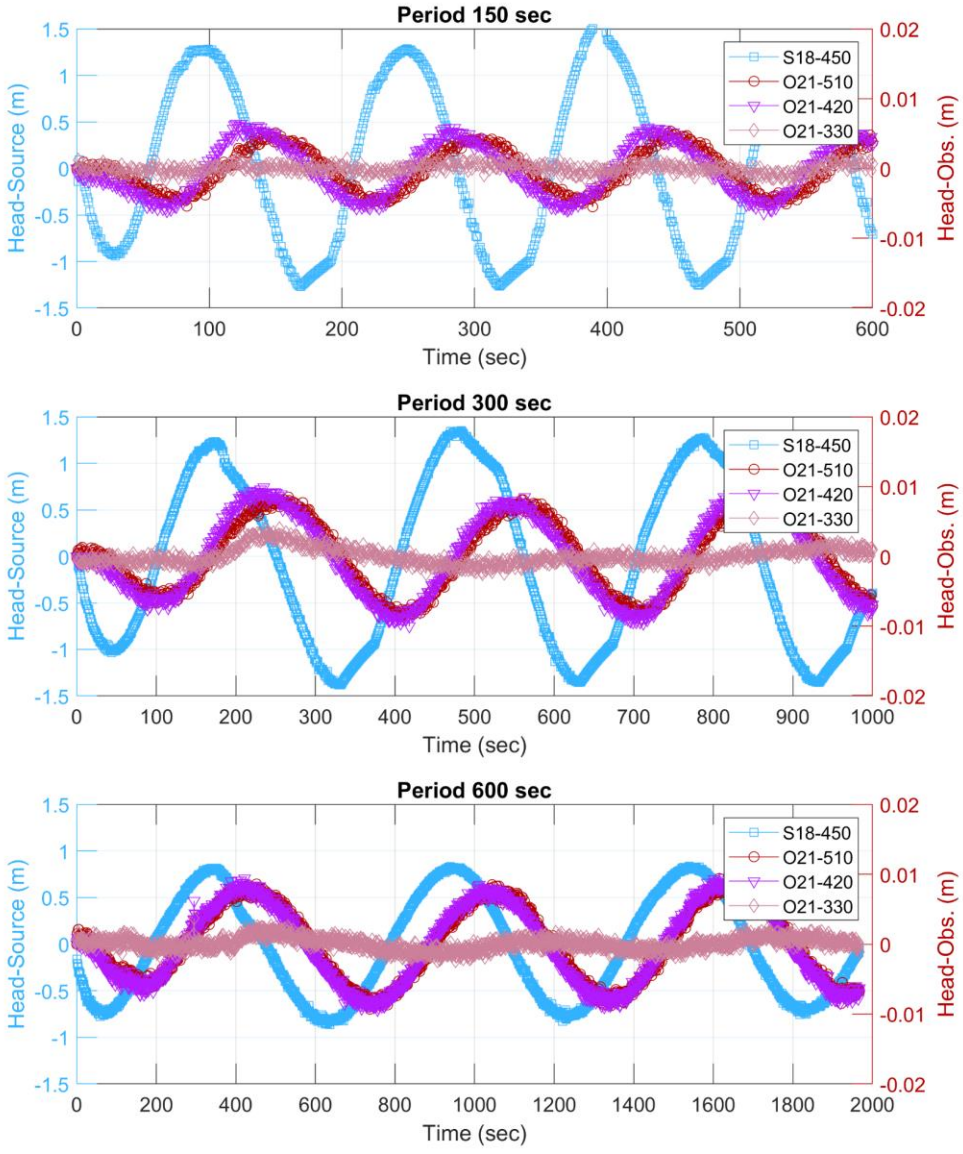

Figure I-1 : Head recordings in the source interval and the three observation intervals for test S18.450 for periods of: (a) 150 s; (b) 300 s; and (c) 600 s. The head represents the variation of the head with respect to the static head measured before each test.

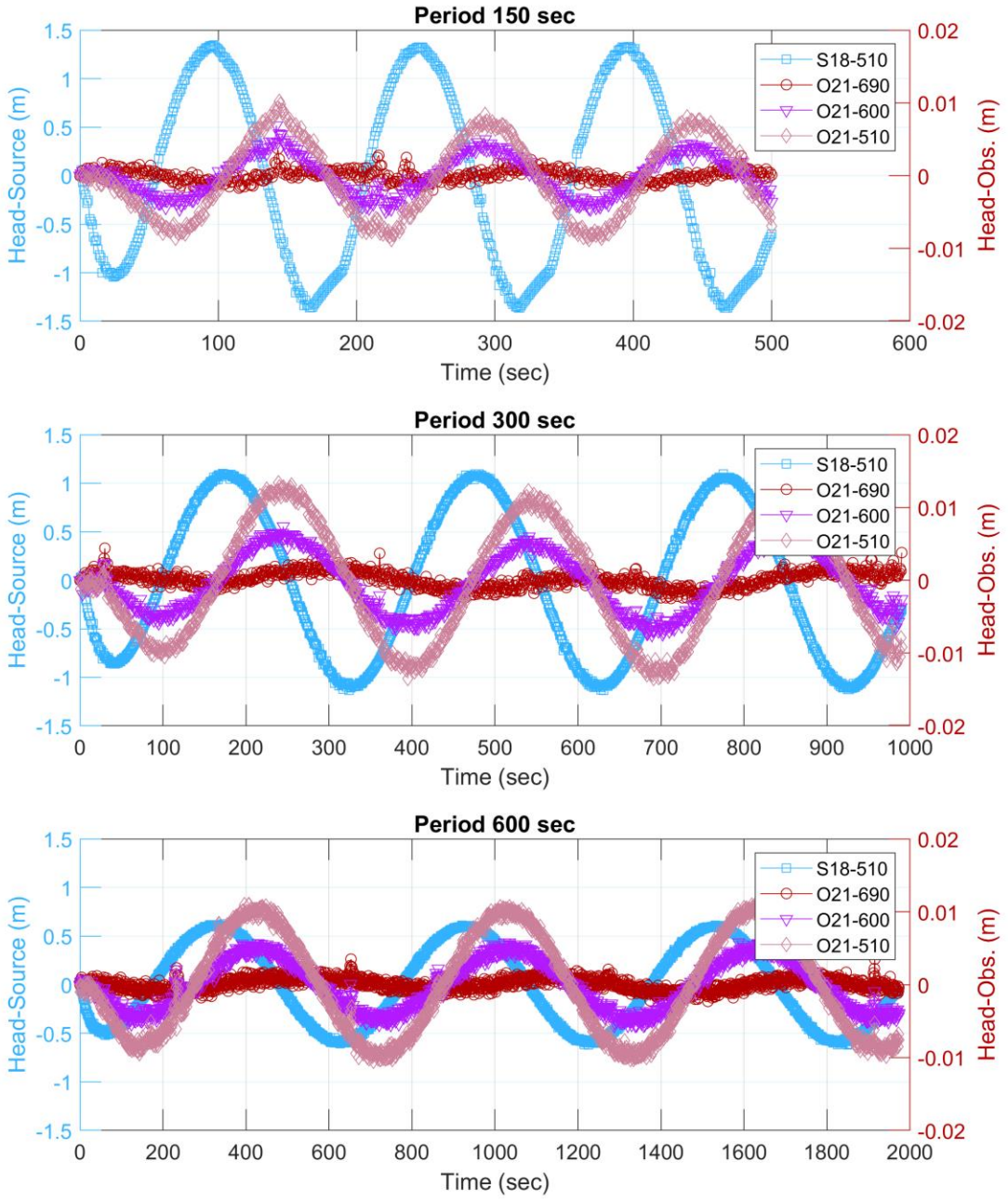

Figure I-2 : Head recordings in the source interval and the three observation intervals for test S18.510a for periods of: (a) 150 s; (b) 300 s; and (c) 600 s. The head represents the variation of the head with respect to the static head measured before each test.

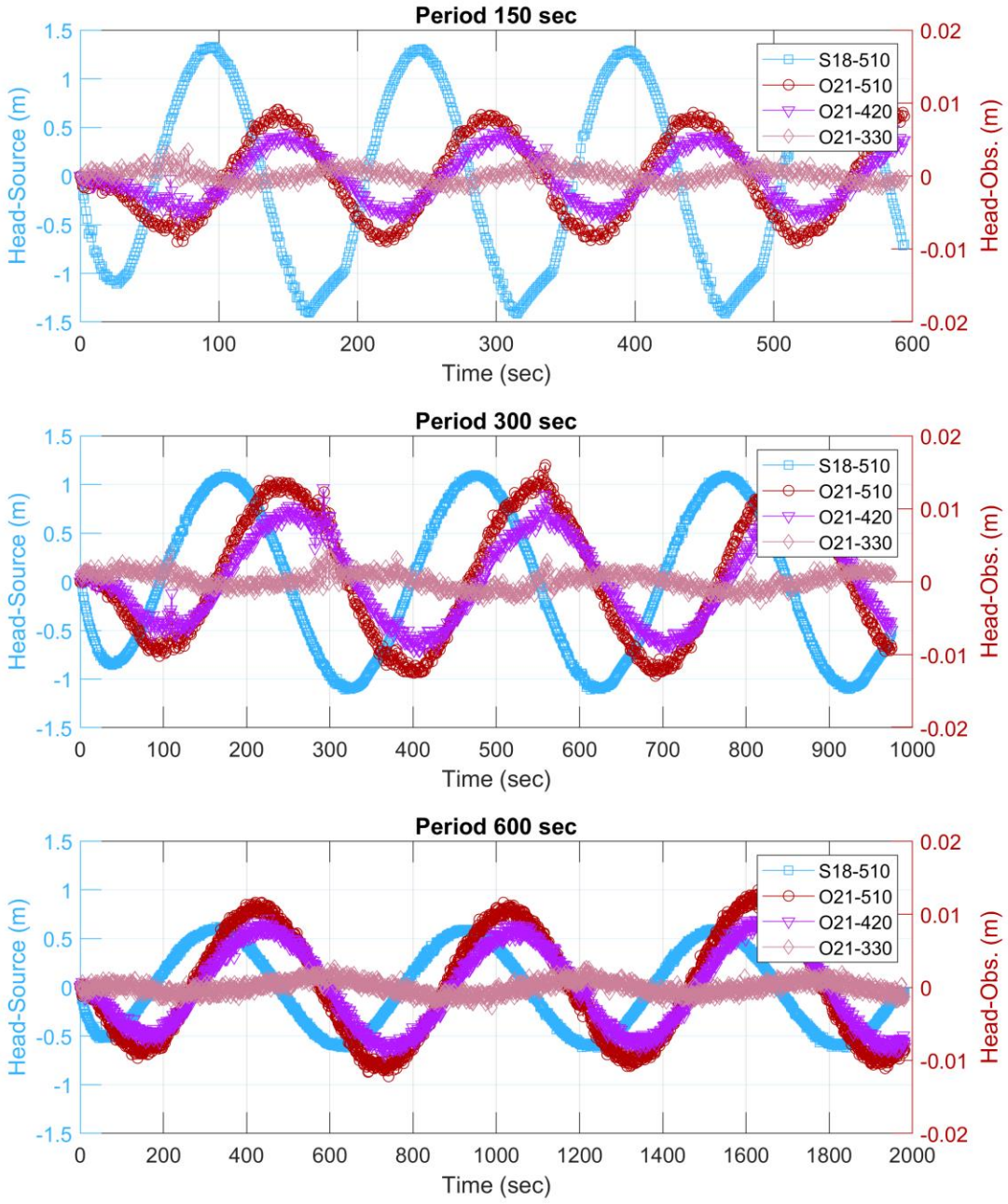

Figure I-3 : Head recordings in the source interval and the three observation intervals for test S18.510b for periods of: (a) 150 s; (b) 300 s; and (c) 600 s. The head represents the variation of the head with respect to the static head measured before each test.

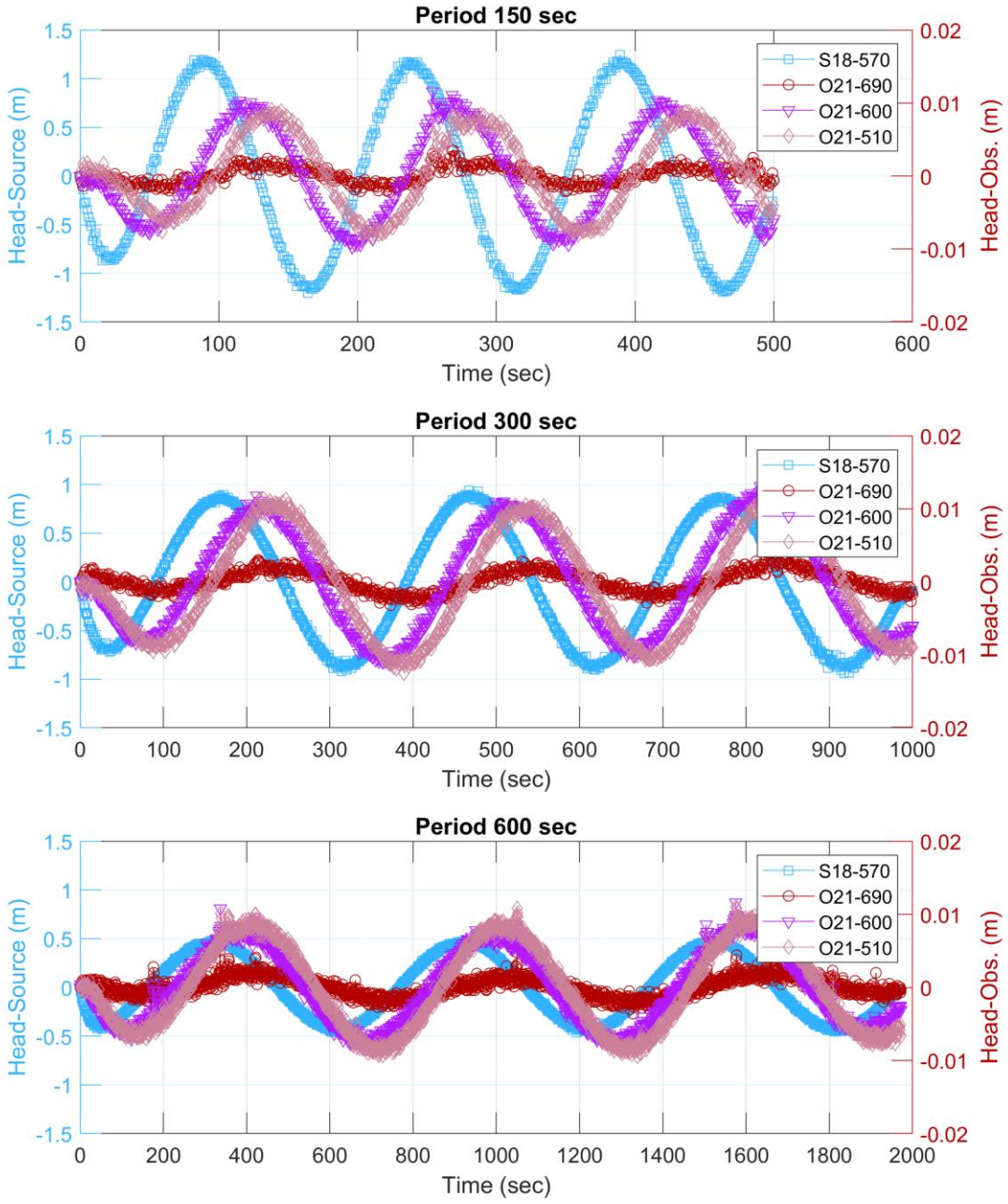

Figure I-4 : Head recordings in the source interval and the three observation intervals for test S18.570 for periods of: (a) 150 s; (b) 300 s; and (c) 600 s. The head represents the variation of the head with respect to the static head measured before each test.

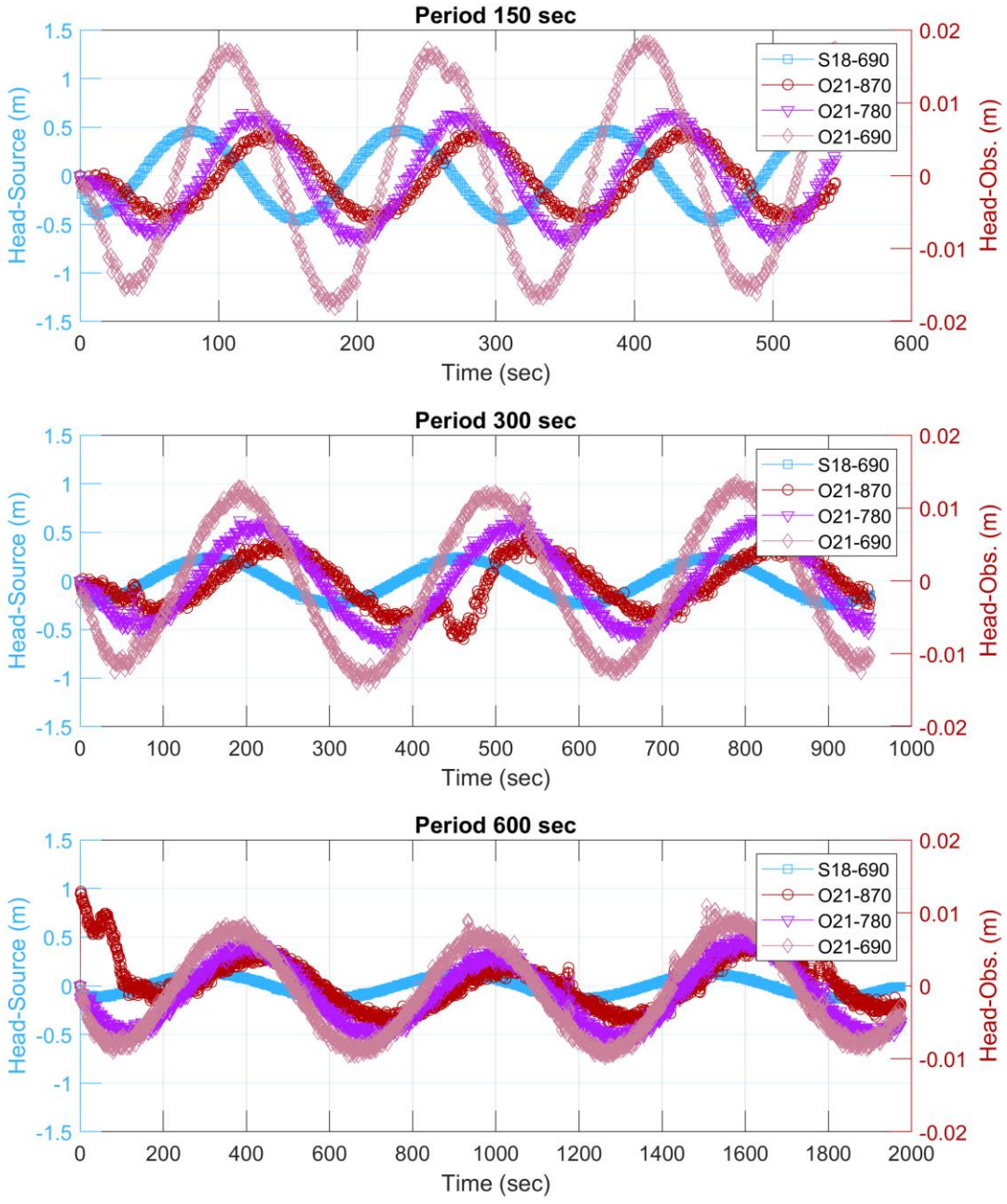

Figure I-5 : Head recordings in the source interval and the three observation intervals for test S18.690a for periods of: (a) 150 s; (b) 300 s; and (c) 600 s. The head represents the variation of the head with respect to the static head measured before each test.

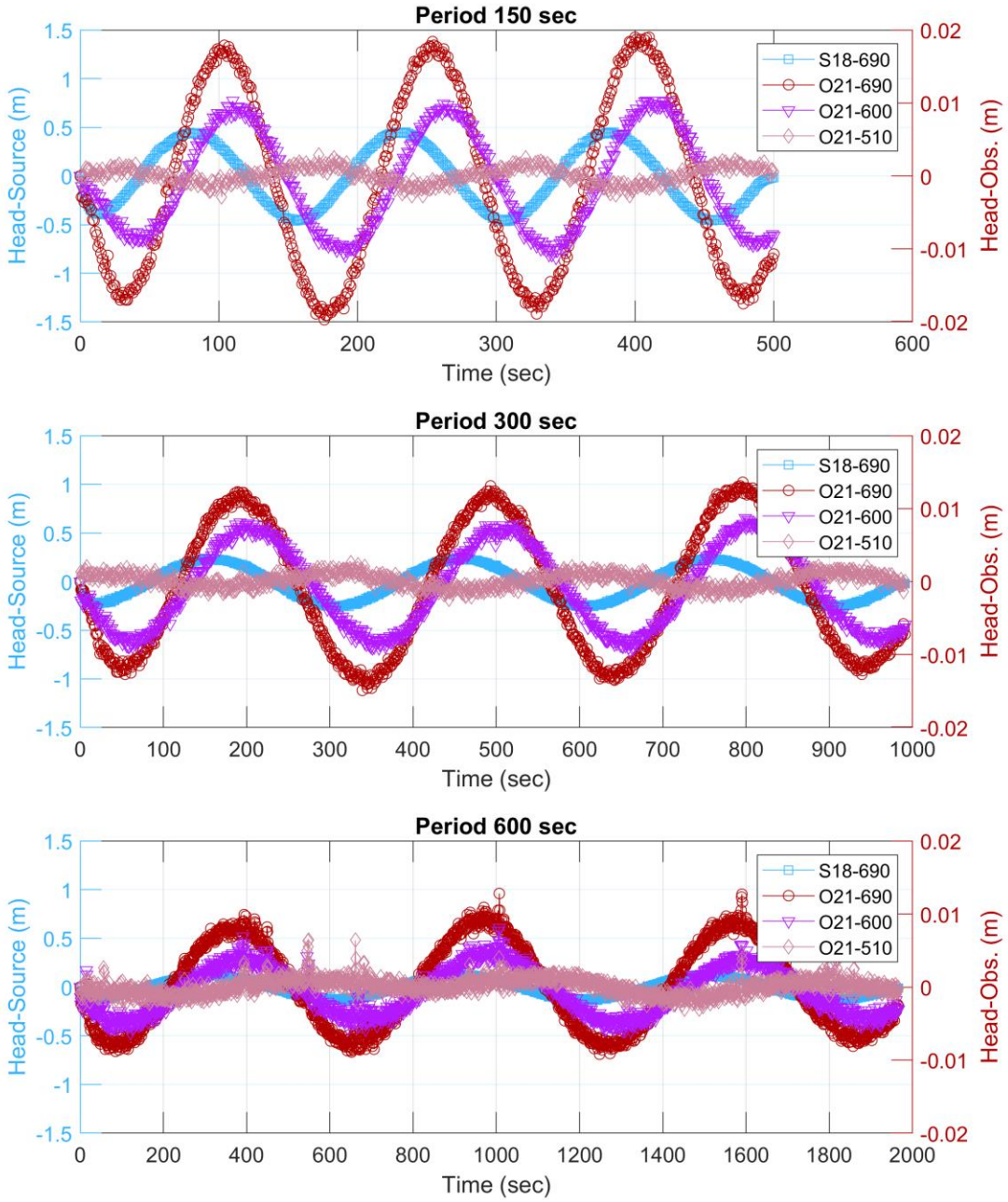

Figure I-6 : Head recordings in the source interval and the three observation intervals for test S18.690b for periods of: (a) 150 s; (b) 300 s; and (c) 600 s. The head represents the variation of the head with respect to the static head measured before each test.

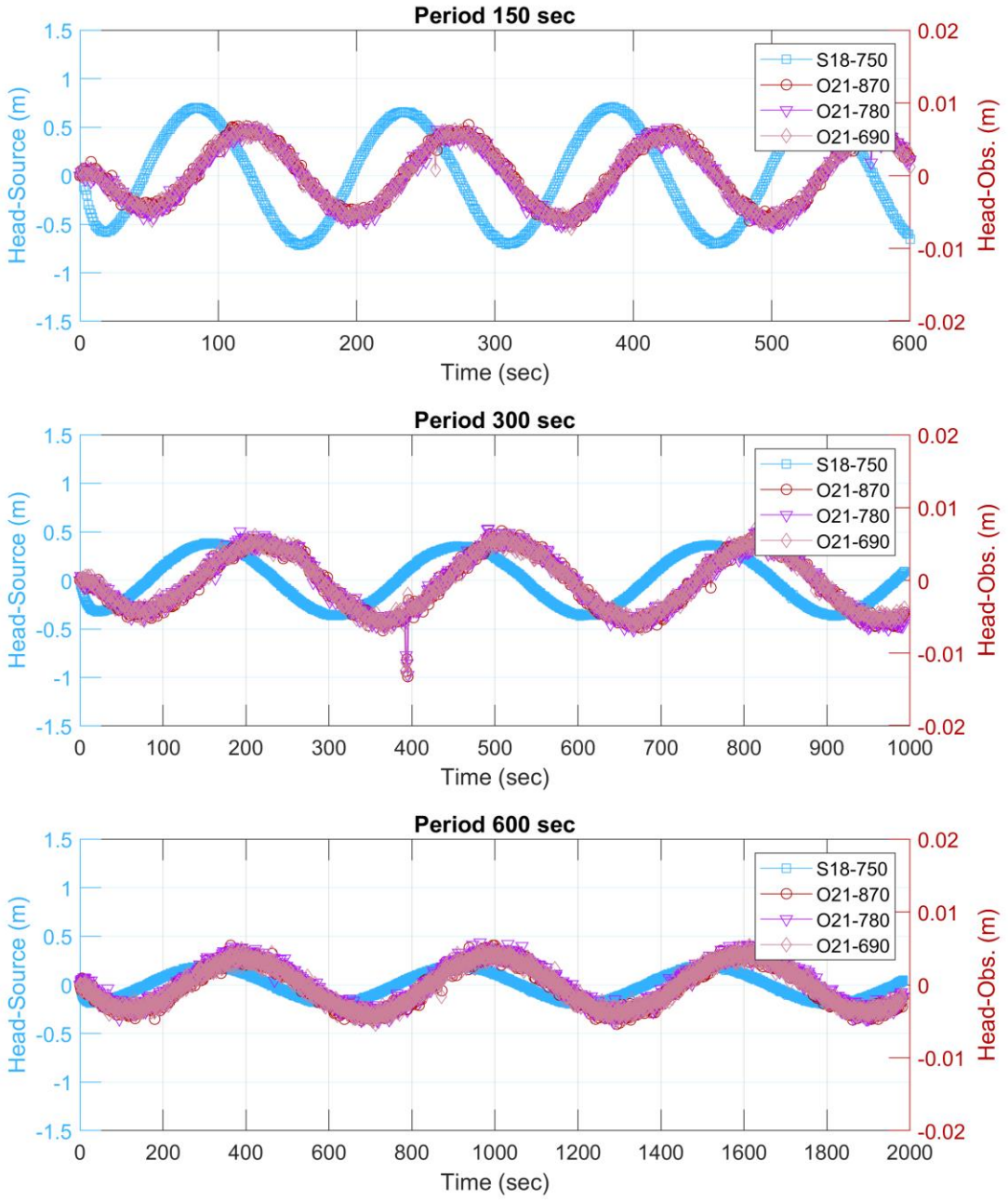

Figure I-7 : Head recordings in the source interval and the three observation intervals for test S18.750 for periods of: (a) 150 s; (b) 300 s; and (c) 600 s. The head represents the variation of the head with respect to the static head measured before each test.

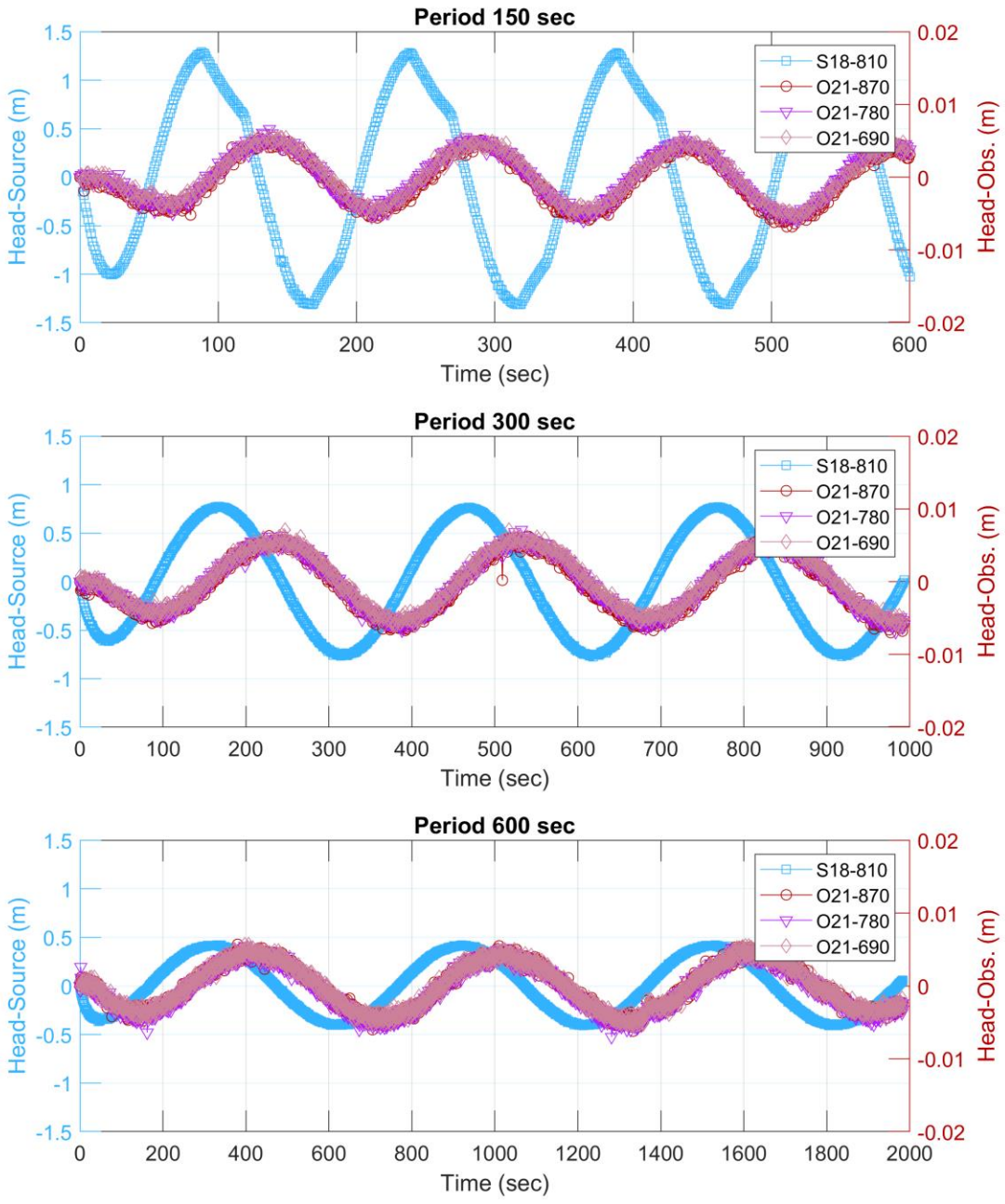

Figure I-8 : Head recordings in the source interval and the three observation intervals for test S18.810 for periods of: (a) 150 s; (b) 300 s; and (c) 600 s. The head represents the variation of the head with respect to the static head measured before each test.

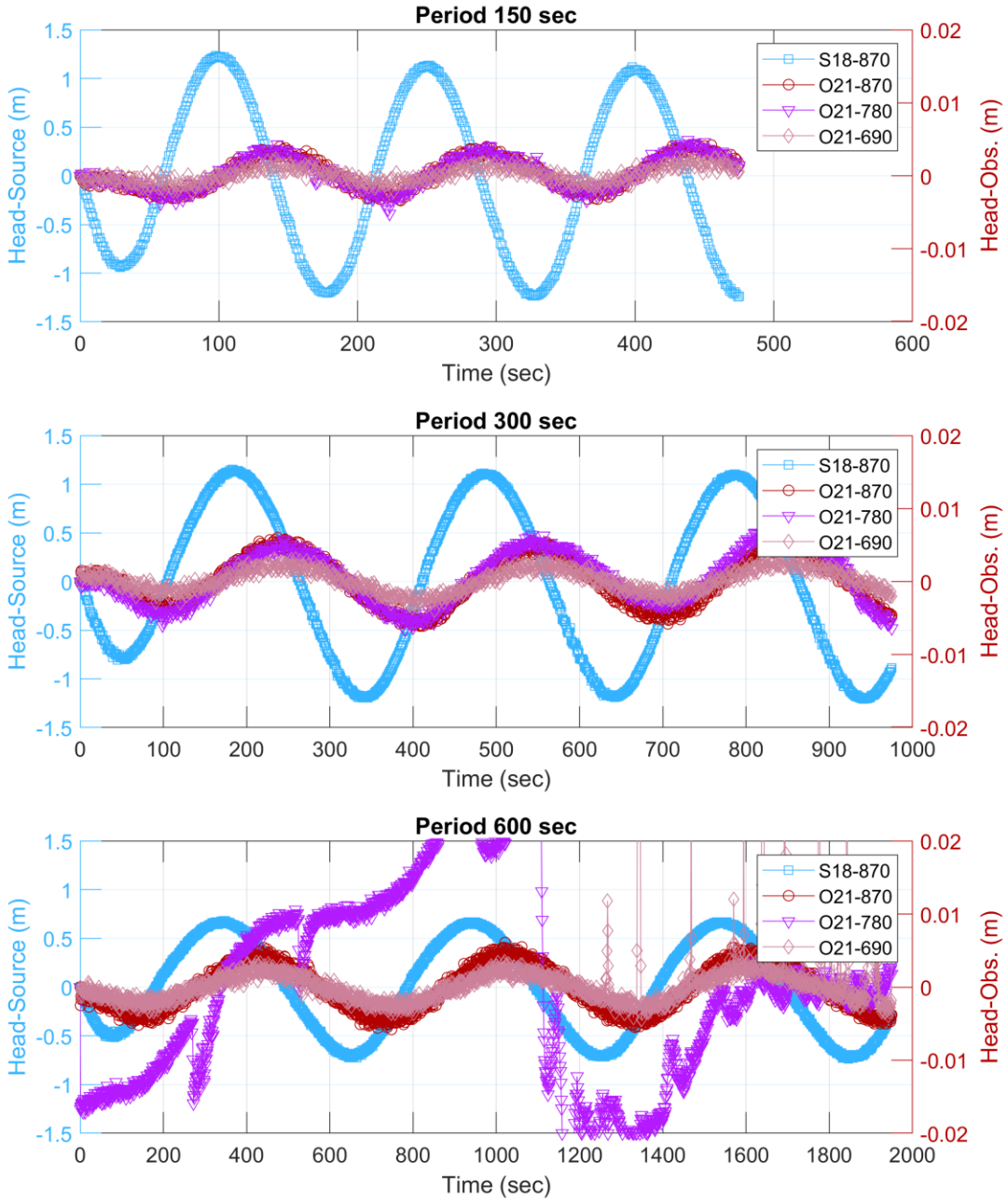

Figure I-9 : Head recordings in the source interval and the three observation intervals for test S18.870 for periods of: (a) 150 s; (b) 300 s; and (c) 600 s. The head represents the variation of the head with respect to the static head measured before each test.

I.2 Comparison of inverted head data from the LR2DInv model with measured head data (scatter plot)

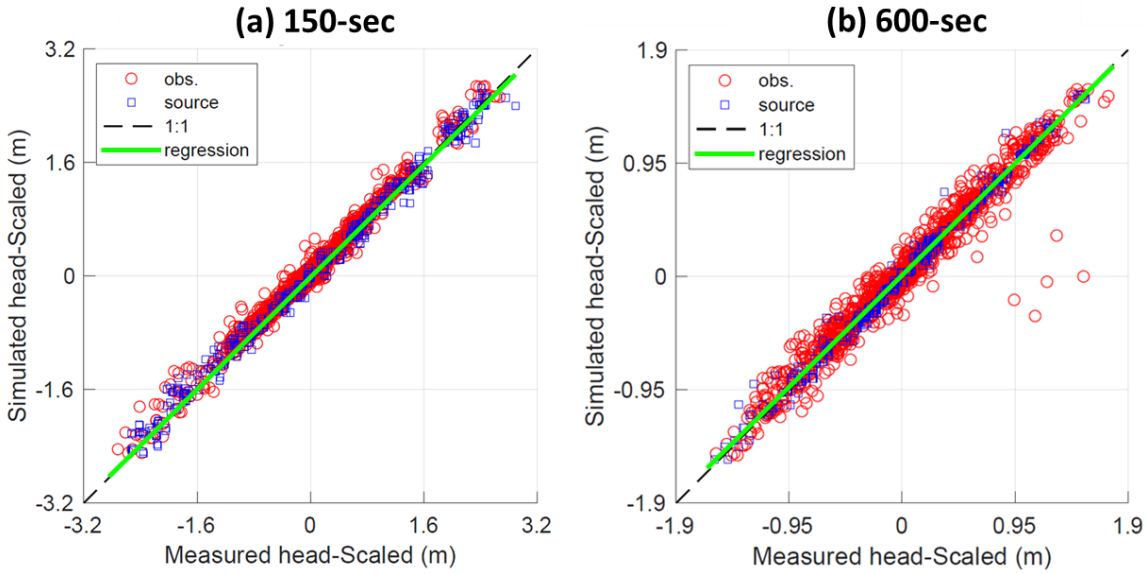

Figure I-10 : Scatter plots of simulated versus measured heads for all tests of the inversion with (a) the 150-sec period and (b) the 600-sec period.

I.3 Comparison of inverted head data from the lr2dinv model with measured head data (temporal plot)

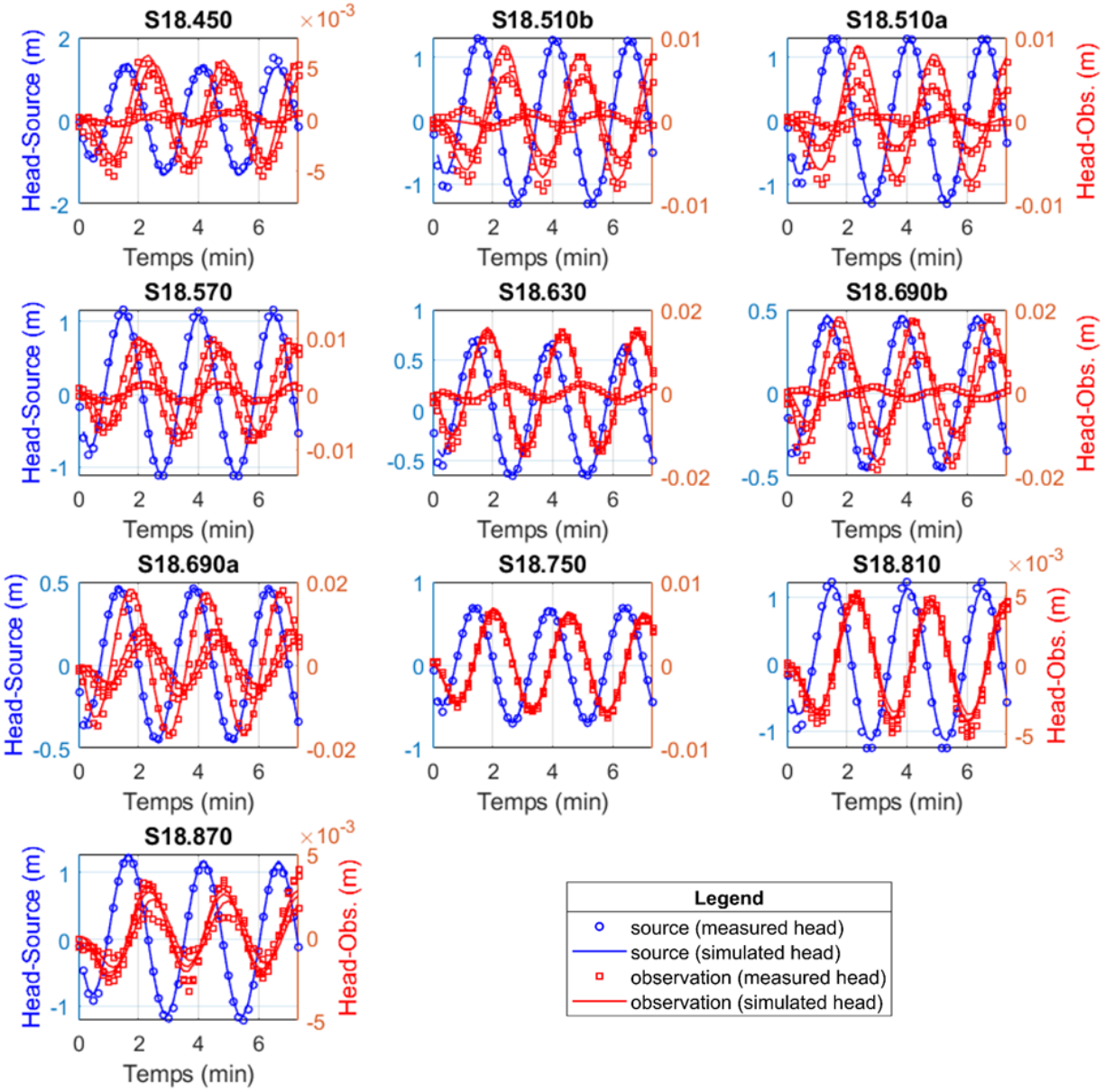

Figure I-11 : Comparison of the measured and simulated head for the inversion with the 150-sec period. The intervals of the source (left) and the observation (right) are shown on different scales.

I.4 Calculated flow for the simulation of periodic tests using the Ir2dinv model, based on the known displacement of the rod used to induce the test

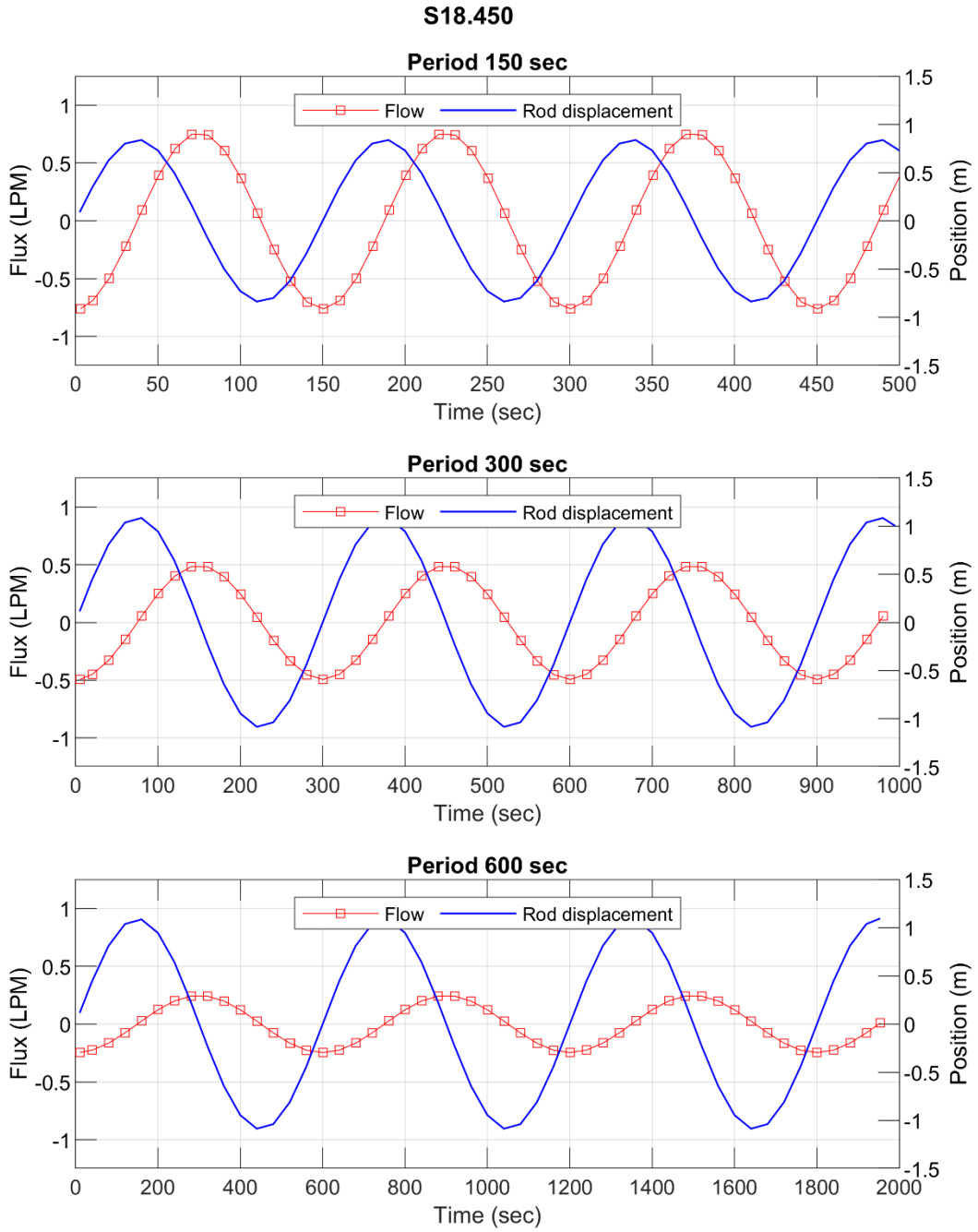

Figure I-12 : Calculated flow and rod displacement for test S18.870 for periods of (a) 150 s, (b) 300 s and (c) 600 s.

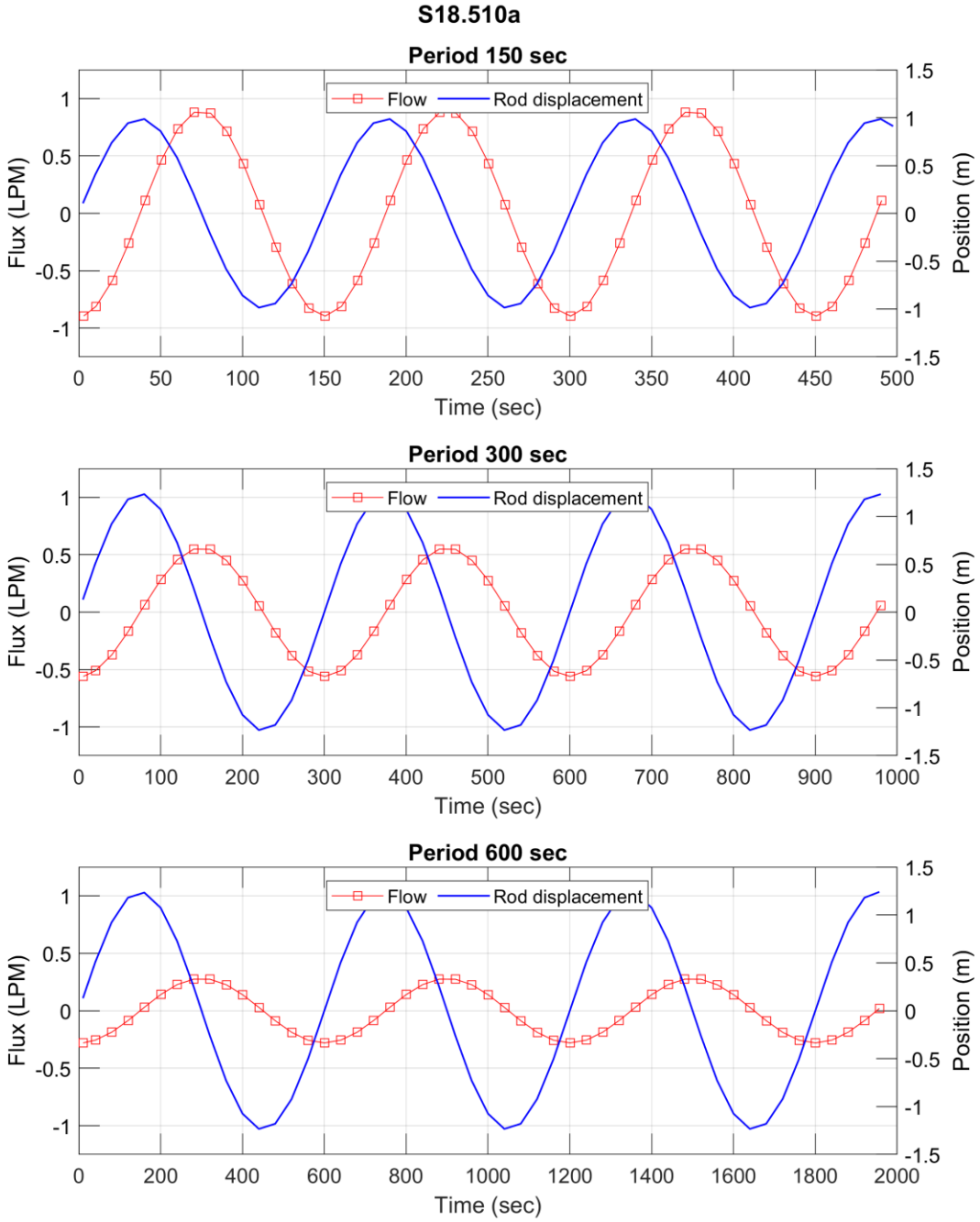

Figure I-13 : Calculated flow and rod displacement for test S18.510a for periods of (a) 150 s, (b) 300 s and (c) 600 s.

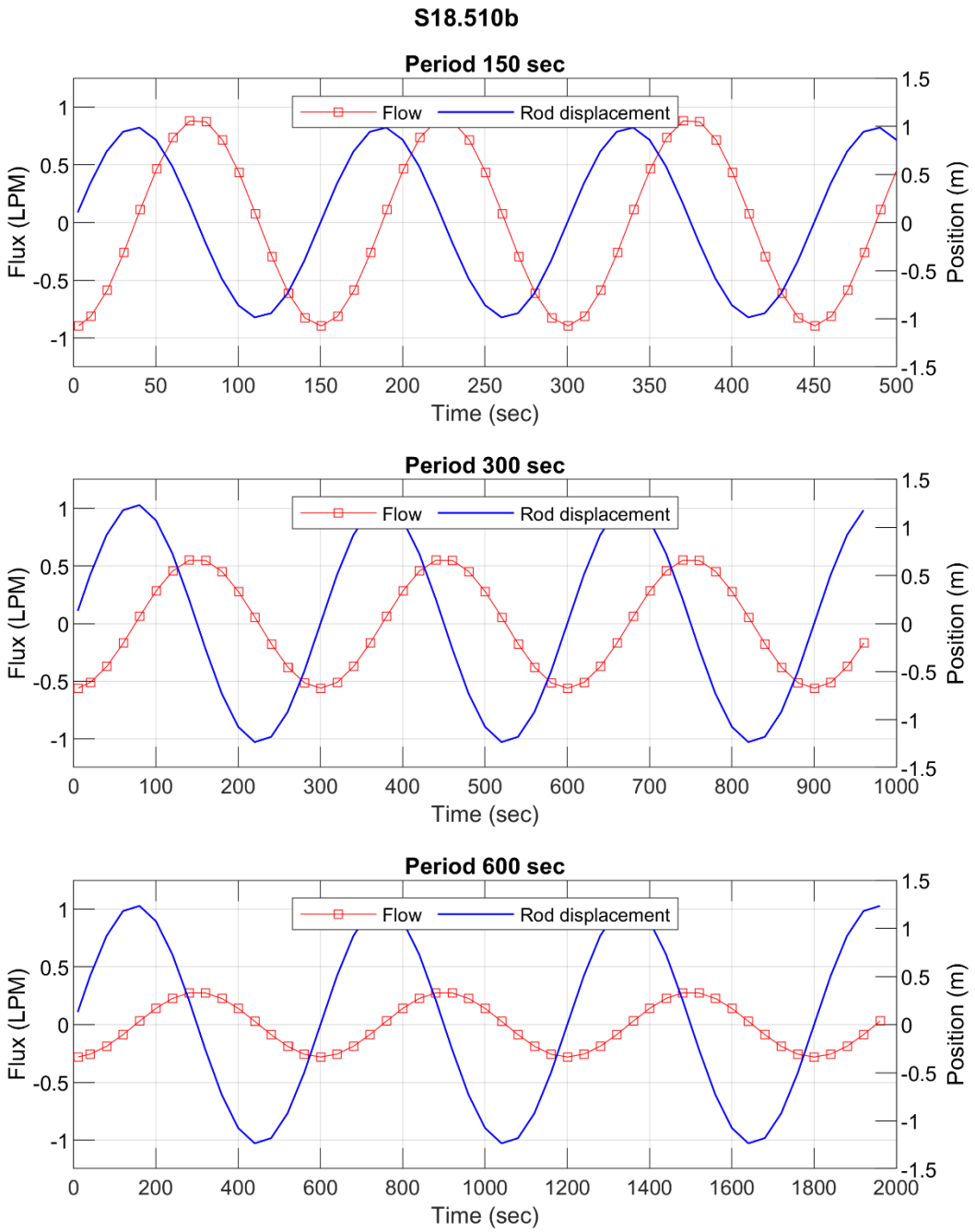

Figure I-14 : Calculated flow and rod displacement for test S18.510b for periods of (a) 150 s, (b) 300 s and (c) 600 s.

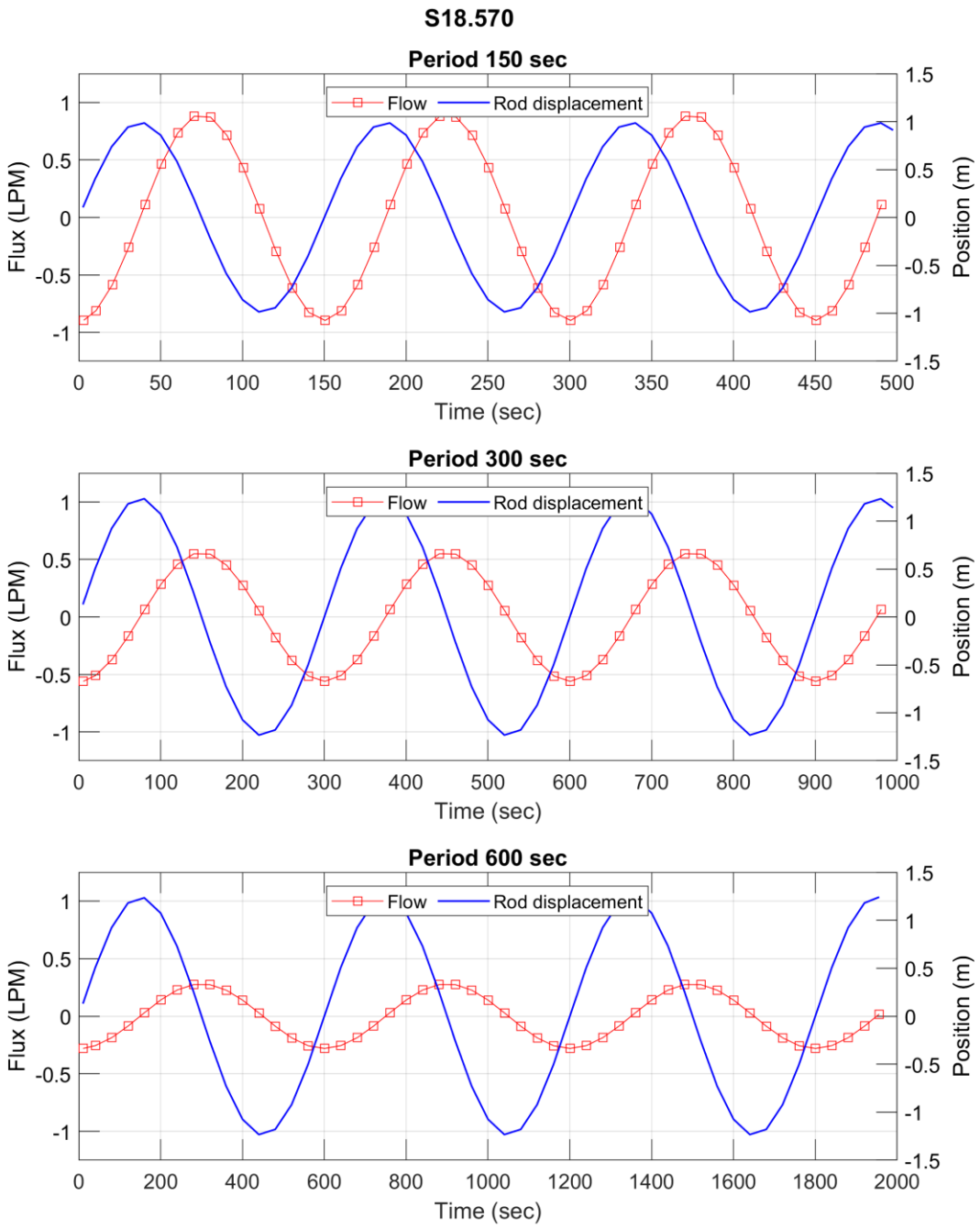

Figure I-15 : Calculated flow and rod displacement for test S18.570 for periods of (a) 150 s, (b) 300 s and (c) 600 s.

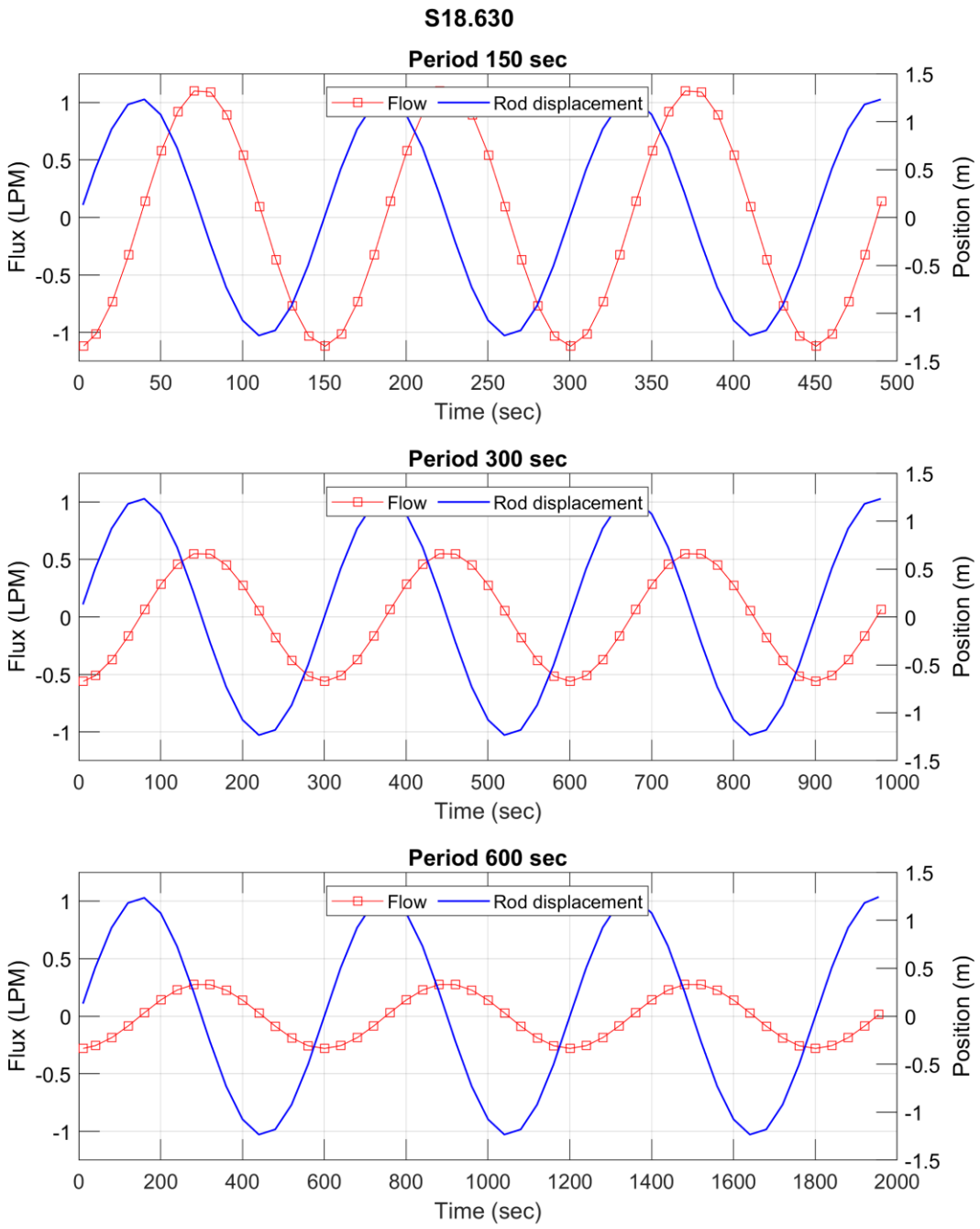

Figure I-16 : Calculated flow and rod displacement for test S18.630 for periods of (a) 150 s, (b) 300 s and (c) 600 s.

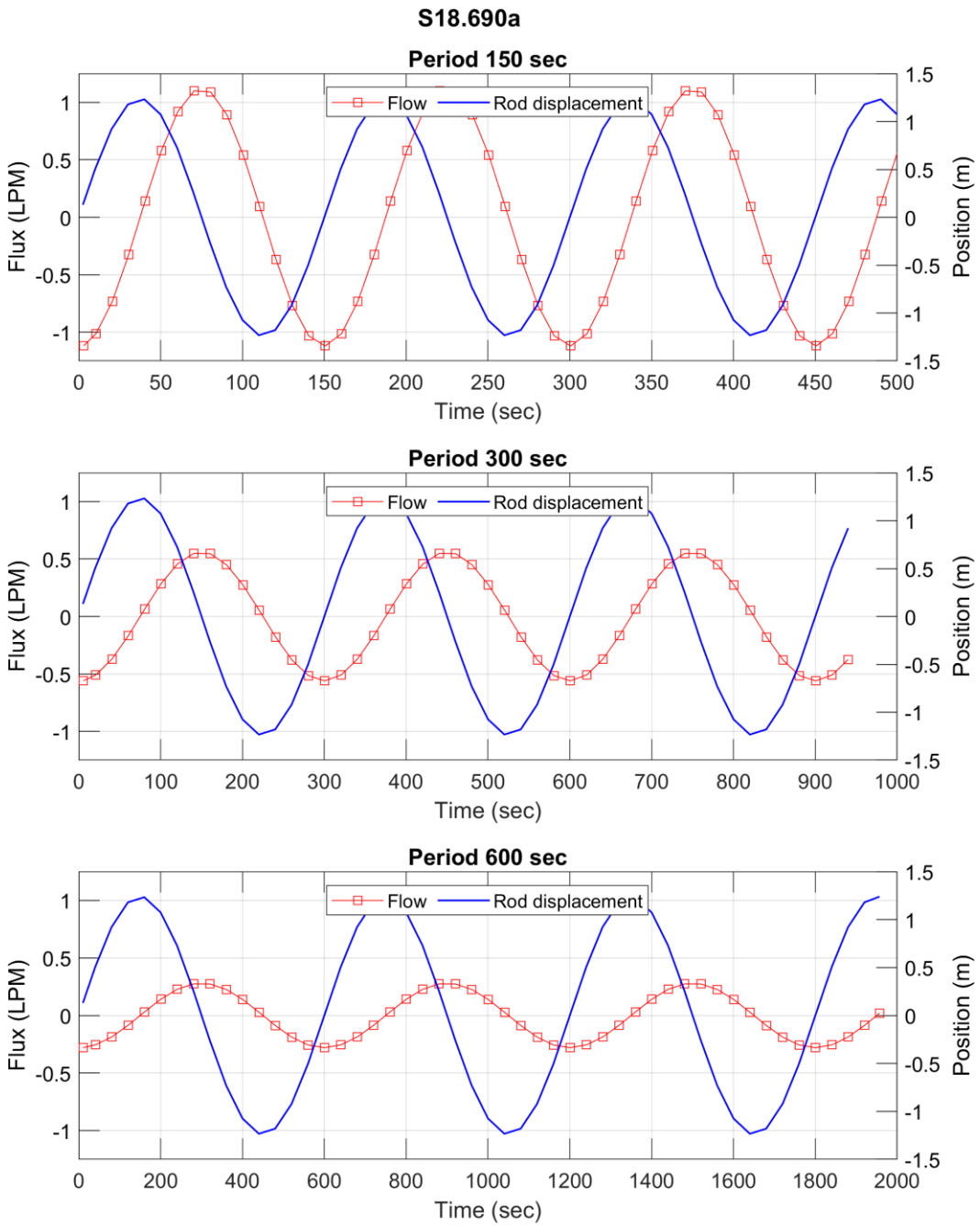

Figure I-17 : Calculated flow and rod displacement for test S18.690a for periods of (a) 150 s, (b) 300 s and (c) 600 s.

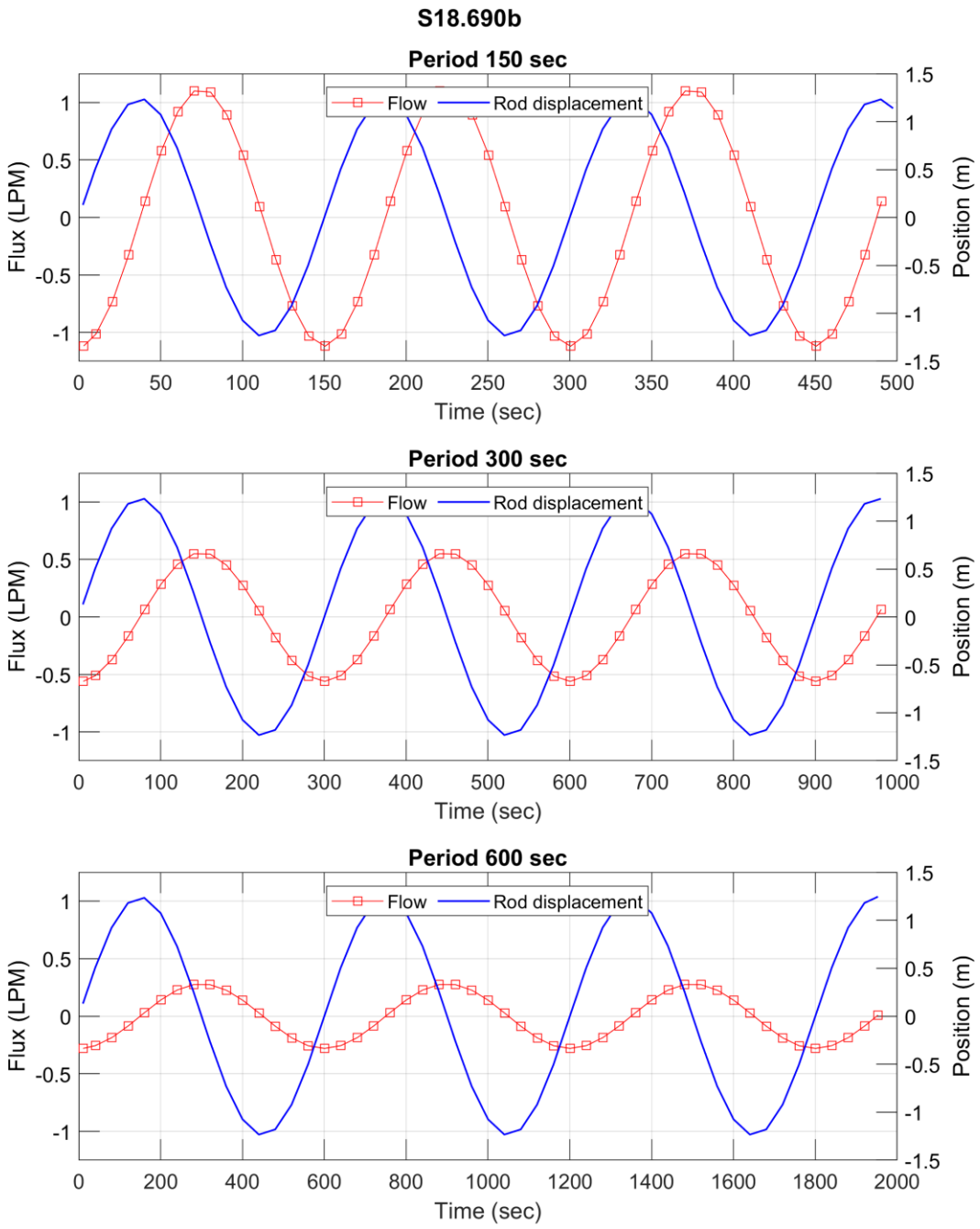

Figure I-18 : Calculated flow and rod displacement for test S18.690b for periods of (a) 150 s, (b) 300 s and (c) 600 s.

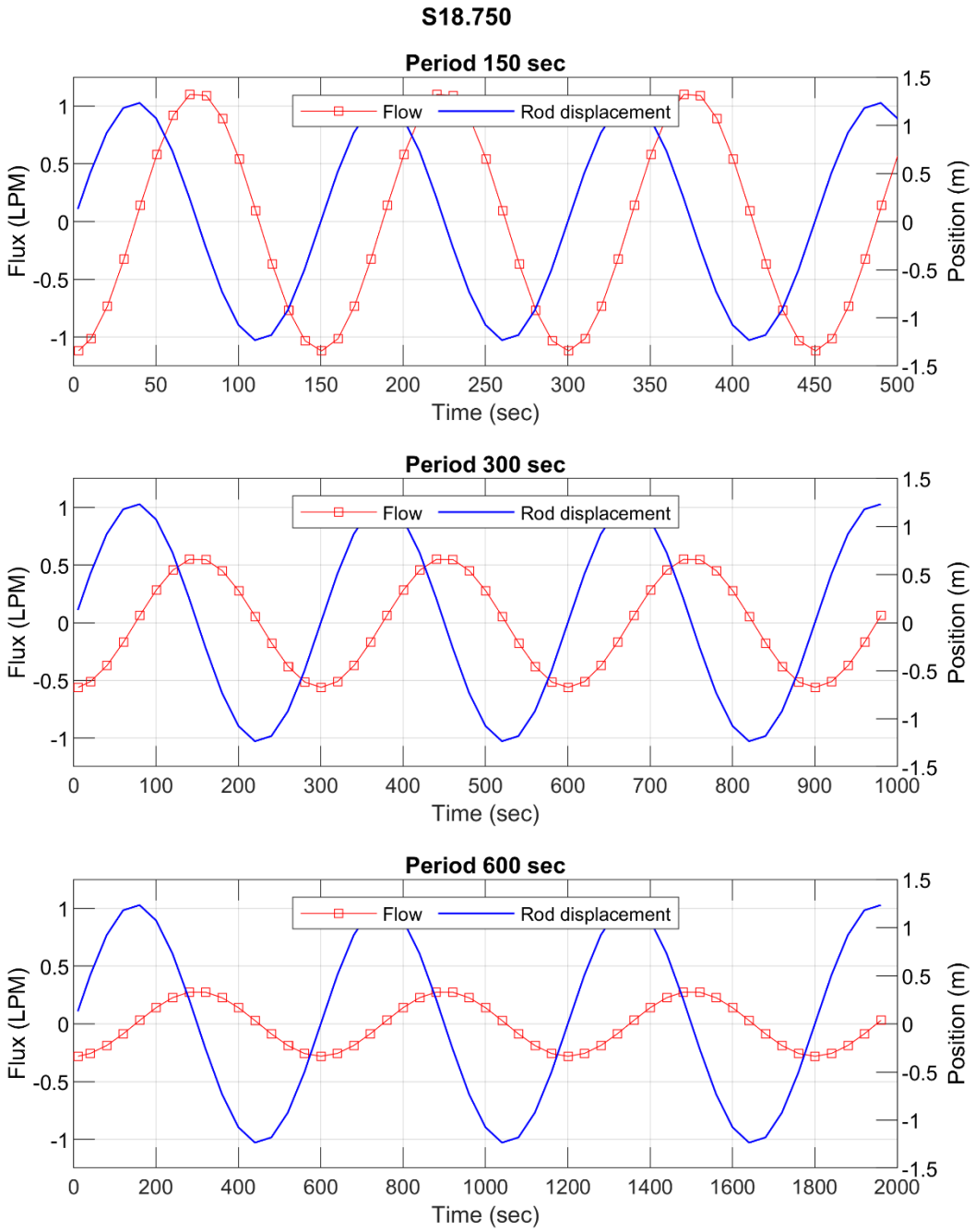

Figure I-19 : Calculated flow and rod displacement for test S18.750 for periods of (a) 150 s, (b) 300 s and (c) 600 s.

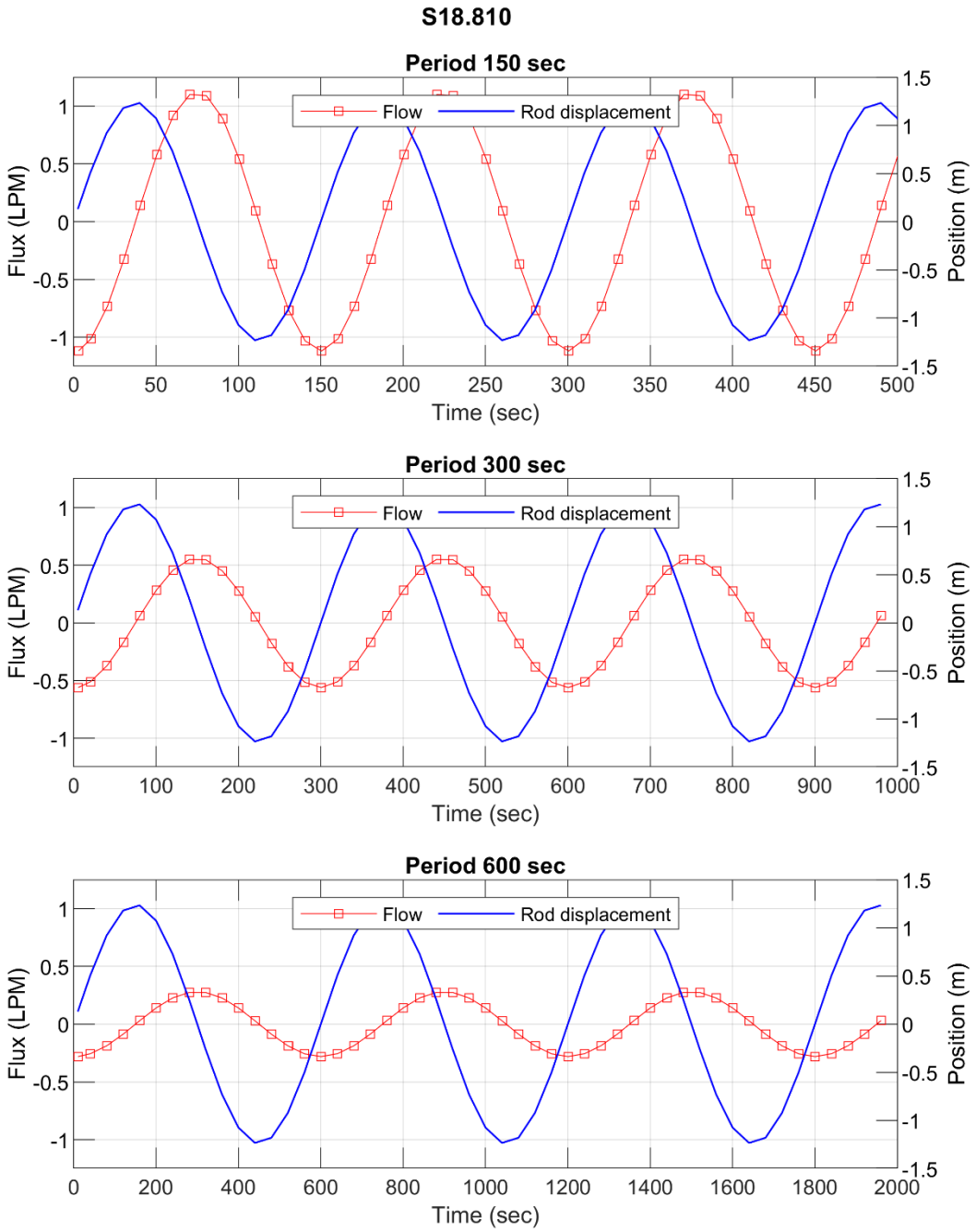

Figure I-20 : Calculated flow and rod displacement for test S18.810 for periods of (a) 150 s, (b) 300 s and (c) 600 s.

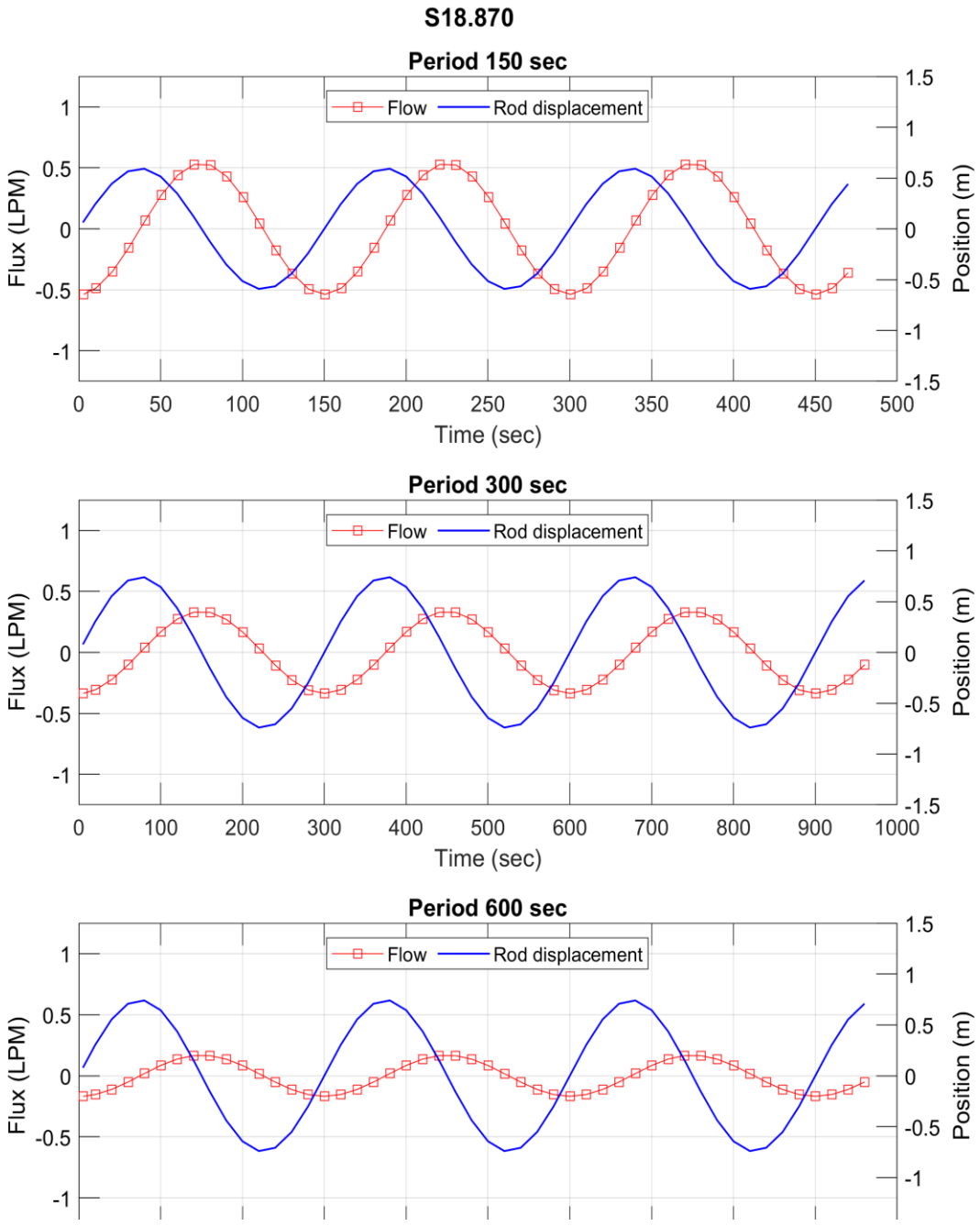

Figure I-21 : Calculated flow and rod displacement for test S18.870 for periods of (a) 150 s, (b) 300 s and (c) 600 s.

I.5 Head noise level estimated from raw head data

Tableau I-1 : Median standard deviation (SD) of the residual between a sinusoid and the original head measurements recorded at 1 sample per second (1 Hz). The median is derived from the SD of the residuals for all individually evaluated source and observation intervals.

Test	Period (sec)	Median SD of the residual (m)			
		Original (1 Hz)			
		Source	Obs1	Obs2	Obs3
S18.450	150	2.33×10^{-3}	-8.13×10^{-7}	4.58×10^{-5}	-1.21×10^{-5}
	300	3.66×10^{-3}	3.10×10^{-5}	8.48×10^{-6}	1.27×10^{-6}
	600	2.26×10^{-3}	-7.33×10^{-6}	2.18×10^{-6}	1.56×10^{-6}
S18.510b	150	1.04×10^{-3}	-1.90×10^{-5}	-1.09×10^{-5}	4.01×10^{-5}
	300	-4.12×10^{-4}	-9.54×10^{-5}	-8.80×10^{-5}	-8.14×10^{-5}
	600	1.92×10^{-4}	-3.22×10^{-7}	-9.37×10^{-6}	-2.82×10^{-5}
S18.510a	150	2.22×10^{-3}	7.62×10^{-6}	-6.13×10^{-5}	-5.87×10^{-5}
	300	-1.36×10^{-3}	1.60×10^{-5}	-4.21×10^{-5}	-4.99×10^{-5}
	600	-1.07×10^{-4}	-7.54×10^{-6}	-1.18×10^{-5}	2.72×10^{-6}
S18.570	150	-1.12×10^{-3}	-2.98×10^{-5}	2.95×10^{-5}	-6.11×10^{-5}
	300	-1.36×10^{-3}	1.34×10^{-5}	7.49×10^{-6}	1.11×10^{-5}
	600	1.25×10^{-4}	-1.14×10^{-5}	-3.63×10^{-5}	-5.16×10^{-5}
S18.630	150	4.19×10^{-3}	-5.70×10^{-5}	2.60×10^{-5}	-1.67×10^{-5}
	300	6.75×10^{-5}	-5.43×10^{-5}	-1.05×10^{-4}	-4.79×10^{-5}
	600	-5.40×10^{-5}	-1.95×10^{-5}	-1.59×10^{-5}	3.70×10^{-5}
S18.690b	150	-6.97×10^{-4}	3.43×10^{-5}	-1.78×10^{-5}	1.41×10^{-5}
	300	2.34×10^{-5}	4.55×10^{-6}	-2.58×10^{-6}	1.18×10^{-5}
	600	4.92×10^{-4}	-4.30×10^{-5}	-3.05×10^{-5}	-5.26×10^{-5}
S18.690a	150	-5.24×10^{-4}	4.09×10^{-5}	2.62×10^{-5}	7.30×10^{-5}
	300	-4.83×10^{-4}	-3.04×10^{-5}	-4.31×10^{-5}	-1.21×10^{-5}
	600	2.15×10^{-4}	-3.07×10^{-5}	-2.19×10^{-5}	-1.63×10^{-5}
S18.750	150	-3.04×10^{-3}	-6.97×10^{-5}	-2.53×10^{-5}	1.37×10^{-5}
	300	-1.76×10^{-3}	6.36×10^{-5}	7.34×10^{-5}	7.93×10^{-5}
	600	-6.23×10^{-5}	3.16×10^{-5}	2.06×10^{-5}	-3.62×10^{-6}
S18.810	150	1.08×10^{-2}	-1.53×10^{-5}	-1.87×10^{-5}	6.16×10^{-7}
	300	-8.17×10^{-4}	4.07×10^{-5}	-1.51×10^{-5}	1.87×10^{-5}
	600	-3.41×10^{-5}	-1.15×10^{-6}	5.91×10^{-6}	1.50×10^{-5}
S18.870	150	-2.73×10^{-3}	-3.19×10^{-5}	7.77×10^{-5}	-9.49×10^{-6}
	300	-6.61×10^{-3}	-7.66×10^{-6}	1.33×10^{-5}	6.47×10^{-5}
	600	9.47×10^{-4}	4.84×10^{-6}	-4.65×10^{-4}	-3.60×10^{-6}

I.6 Head noise level estimated from subsampled head data used for the numerical inversion with the Ir2dinv model

Tableau I-2 : Median standard deviation (SD) of the subsampled head used for the inversion. The amount of data for the subsampled data set is the same for all periods and corresponds to 15 measurements per cycle. The median is obtained from the SD of the residuals for all individually evaluated source and observation intervals.

Test	Period (sec)	Median SD of the residual (m)			
		Subsampled (15/cycle)			
		Source	Obs1	Obs2	Obs3
S18.450	150	4.66×10^{-3}	-3.71×10^{-5}	-1.75×10^{-5}	-1.99×10^{-5}
	300	4.99×10^{-3}	8.59×10^{-6}	-6.11×10-6	1.60×10-5
	600	5.76×10^{-4}	-1.08×10^{-5}	-2.78×10^{-5}	2.78×10^{-5}
S18.510b	150	-5.26×10^{-4}	-8.67×10^{-6}	4.53×10^{-7}	7.66×10^{-6}
	300	2.65×10^{-3}	-2.79×10^{-5}	-5.28×10^{-5}	-8.36×10^{-5}
	600	-9.83×10^{-5}	-7.84×10^{-5}	-3.85×10-5	1.57×10^{-5}
S18.510a	150	8.09×10^{-3}	8.62×10^{-6}	-8.21×10^{-5}	-5.79×10^{-5}
	300	-2.95×10^{-3}	-1.89×10^{-5}	2.13×10^{-5}	-1.89×10^{-5}
	600	-3.57×10^{-4}	-3.10×10^{-5}	-3.02×10^{-5}	-2.08×10^{-5}
S18.570	150	6.36×10^{-4}	-3.93×10^{-5}	-1.68×10^{-5}	-3.11×10^{-5}
	300	1.42×10^{-3}	-8.67×10^{-6}	-1.16×10^{-5}	-3.14×10^{-6}
	600	-4.18×10^{-4}	-1.17×10^{-5}	-1.76×10^{-5}	-1.81×10^{-5}
S18.630	150	-4.34×10^{-3}	3.89×10^{-5}	-1.10×10^{-5}	-3.75×10^{-6}
	300	-5.81×10^{-4}	3.17×10^{-6}	3.15×10^{-5}	-2.83×10^{-5}
	600	-2.79×10^{-5}	-2.99×10^{-5}	2.28×10^{-5}	-1.48×10^{-5}
S18.690b	150	-7.04×10^{-4}	1.91×10^{-5}	-6.02×10^{-5}	-3.15×10^{-5}
	300	2.65×10^{-4}	3.43×10^{-5}	1.75×10^{-5}	-4.53×10^{-5}
	600	4.56×10^{-5}	-1.23×10^{-5}	-4.91×10^{-5}	4.72×10^{-6}
S18.690a	150	-1.78×10^{-3}	-2.32×10^{-5}	-2.32×10^{-5}	4.64×10^{-5}
	300	-1.99×10^{-4}	-8.33×10^{-5}	-3.70×10^{-5}	-1.24×10^{-6}
	600	1.39×10-4	-4.69×10-5	-1.65×10-5	-4.50×10-5
S18.750	150	-4.11×10^{-3}	4.74×10^{-5}	4.48×10^{-6}	1.04×10^{-5}
	300	-1.37×10^{-3}	2.18×10^{-5}	4.51×10^{-5}	5.51×10^{-5}
	600	1.61×10^{-4}	3.26×10^{-5}	-5.47×10^{-5}	6.92×10^{-6}
S18.810	150	1.71×10^{-3}	2.28×10^{-5}	3.71×10^{-5}	7.57×10^{-5}
	300	-1.68×10^{-3}	1.87×10^{-6}	-1.11×10^{-7}	1.34×10^{-5}
	600	-6.67×10^{-4}	-1.85×10^{-5}	-1.09×10^{-5}	-1.91×10^{-6}
S18.870	150	-3.40×10^{-3}	4.12×10^{-5}	2.36×10^{-5}	-3.74×10^{-5}
	300	3.93×10^{-3}	-1.73×10^{-5}	5.41×10^{-5}	-1.36×10^{-5}

	600	8.32×10^{-4}	-7.54×10^{-6}	-1.29×10^{-3}	-5.12×10^{-6}

I.7 Coordinates and construction characteristics of the wells at the St. Lambert experimental site

Tableau I-3 : Coordinates and characteristics of the site wells.

Well	X (m) UTM 19T	Y (m) UTM 19T	Ground elevation (m)	PVC elevation (m)	Top screen elevation (m)	Bottom screen elevation (m)	Screen length (m)	Water table elevation (m)
P17	324586	5163353	117.40	118.09	116.089	106.939	9.15	116.949
S18	324591	5163345	117.791	118.291	116.351	108.731	7.62	117.071
P19	324603	5163348	117.982	118.412	116.572	108.952	7.62	117.172
P20	324598	5163353	117.647	118.142	116.202	108.582	7.62	117.032
O21	324595	5163351	117.753	118.203	116.363	108.743	7.62	117.043

ANNEXES II : FIGURES SUPPLÉMENTAIRES POUR L'ARTICLE 2

II.1 Parameter resolution associated with the numerical inversion of periodic hydraulic tomography using a single period

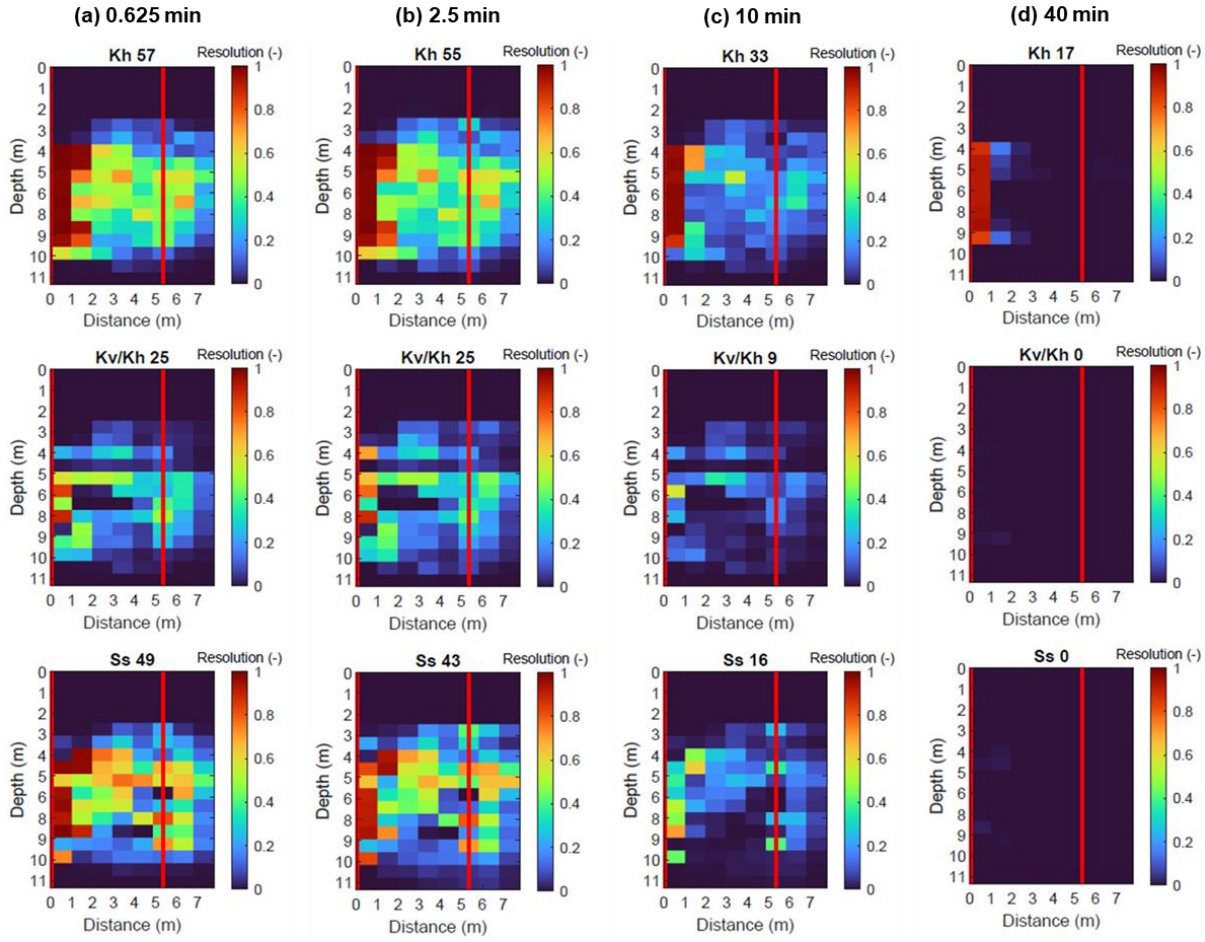

Figure II-1 : Spatial resolution for the heterogenous case of hydraulic parameters for hydraulic properties Kh, Kv/Kh, and Ss for four selected source signal periods: (a) 0.625 min; (b) 2.5 min; (c) 10 min; and (d) 40 min. The number next to the hydraulic property name is the mean resolution degree within the focus area

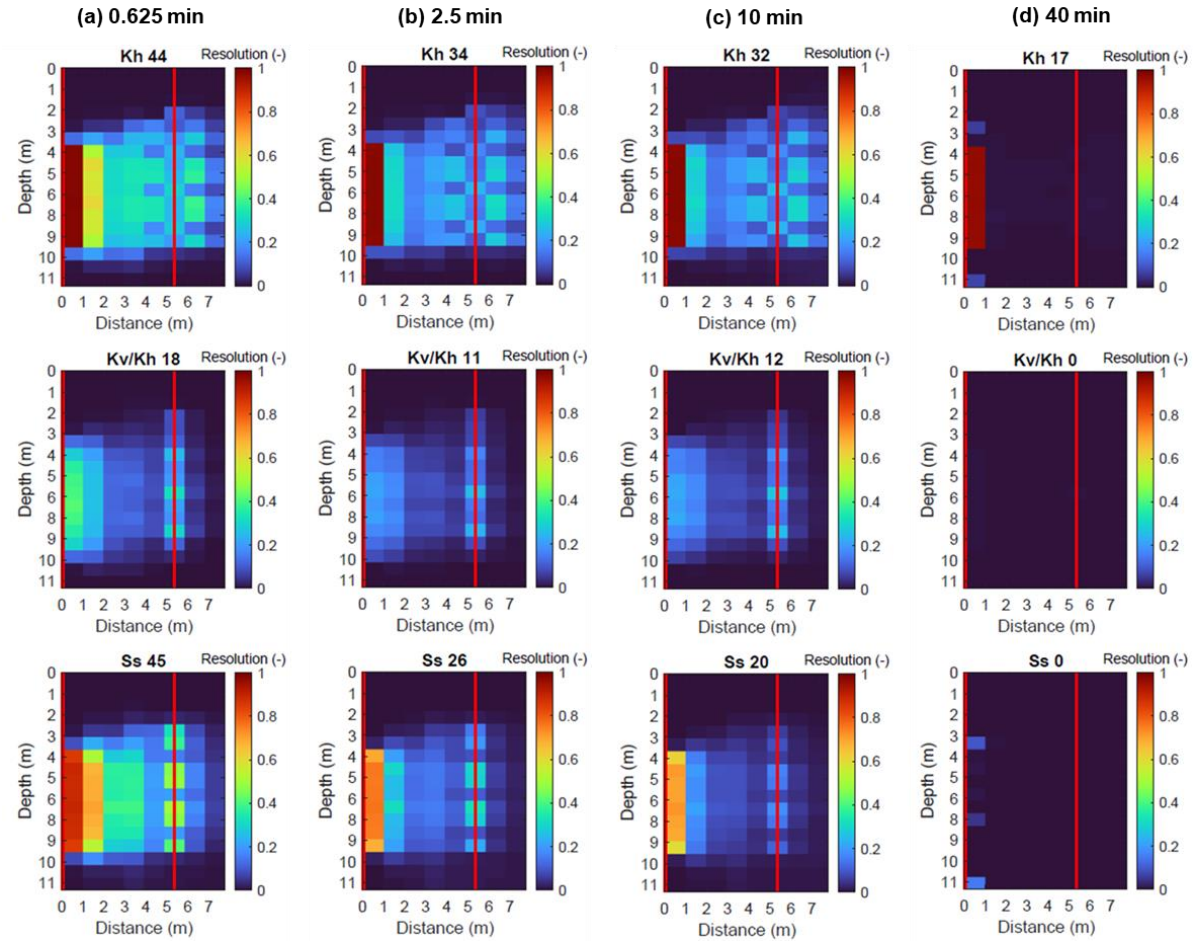

Figure II-2 : Spatial resolution for the homogeneous model for hydraulic properties Kh, Kv/Kh, and Ss for four selected source signal periods: (a) 0.625 min; (b) 2.5 min; (c) 10 min; and (d) 40 min. The number next to the hydraulic property name is the mean resolution degree within the focus area encompassing the intervals of Groups 1, 2 and 3 shown in Figure 3-2.

II.2 Simulated head variations for different experimental configurations of the periodic test

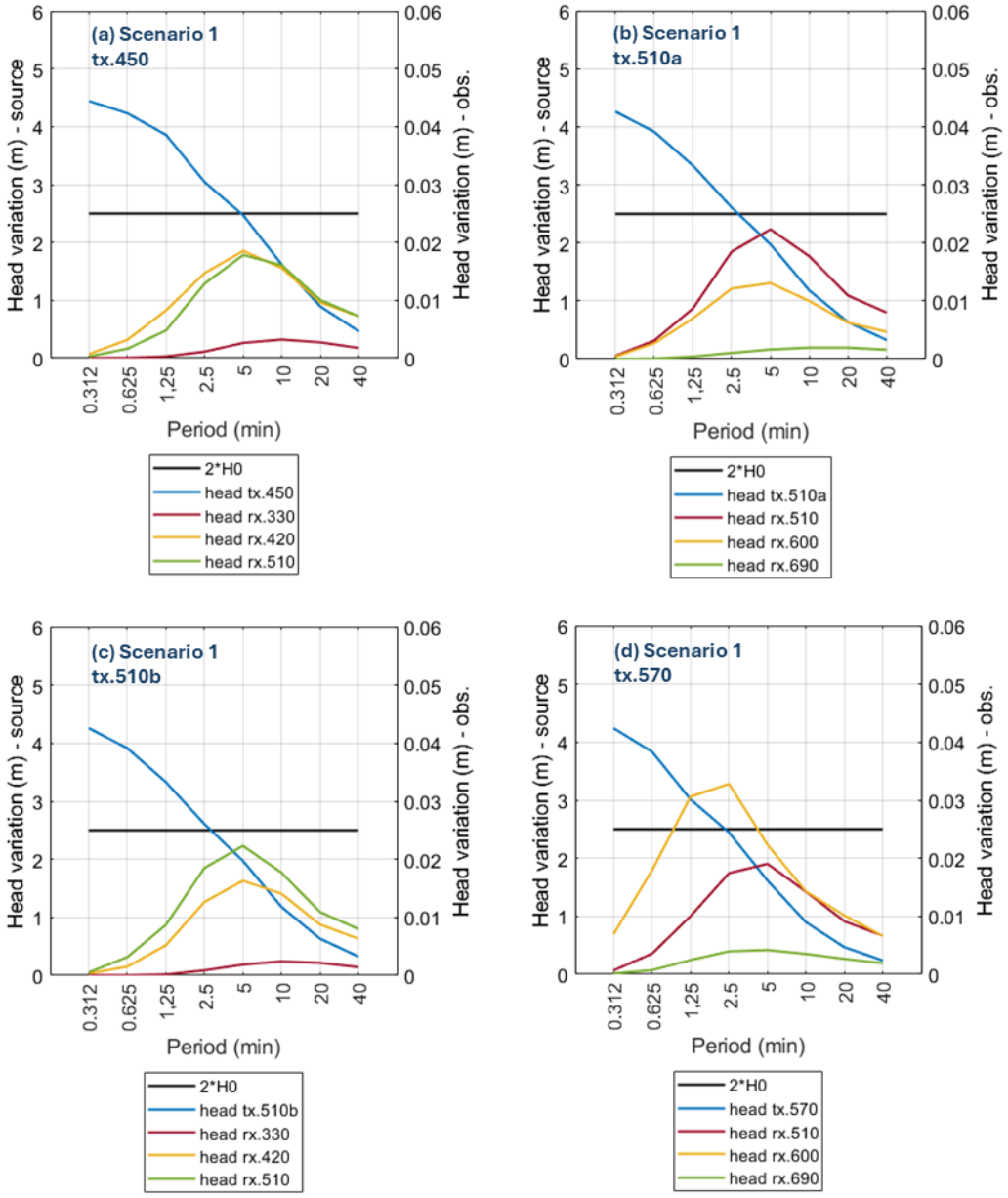

Figure II-3 : Simulated variation of heads in a source and in three observation intervals for eight selected periods for the heterogeneous case with rc = 0.0077. Head variation is the difference between maximum and minimum head over a cycle when steady state is reached. (a) Test tx.450; (b) test tx.510a; (c) test tx.510b and (d) test tx.570.

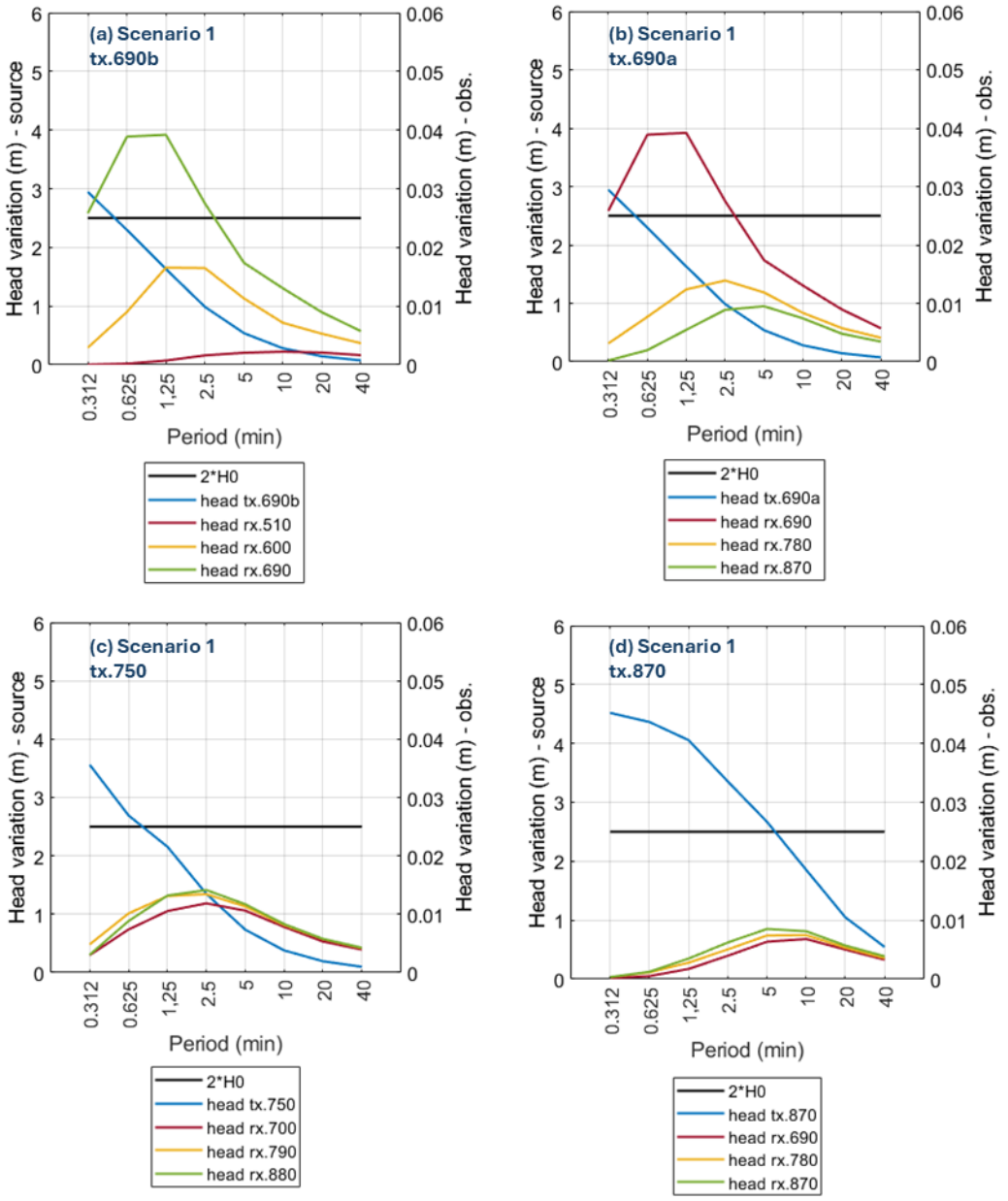

Figure II-4 : Simulated variation of heads in a source and in three observation intervals for eight selected periods for the heterogeneous case with rc = 0.0077. Head variation is the difference between maximum and minimum head over a cycle when steady state is reached. (a) Test tx.690b; (b) test tx.690a; (c) test tx.750 and (d) test tx.870.

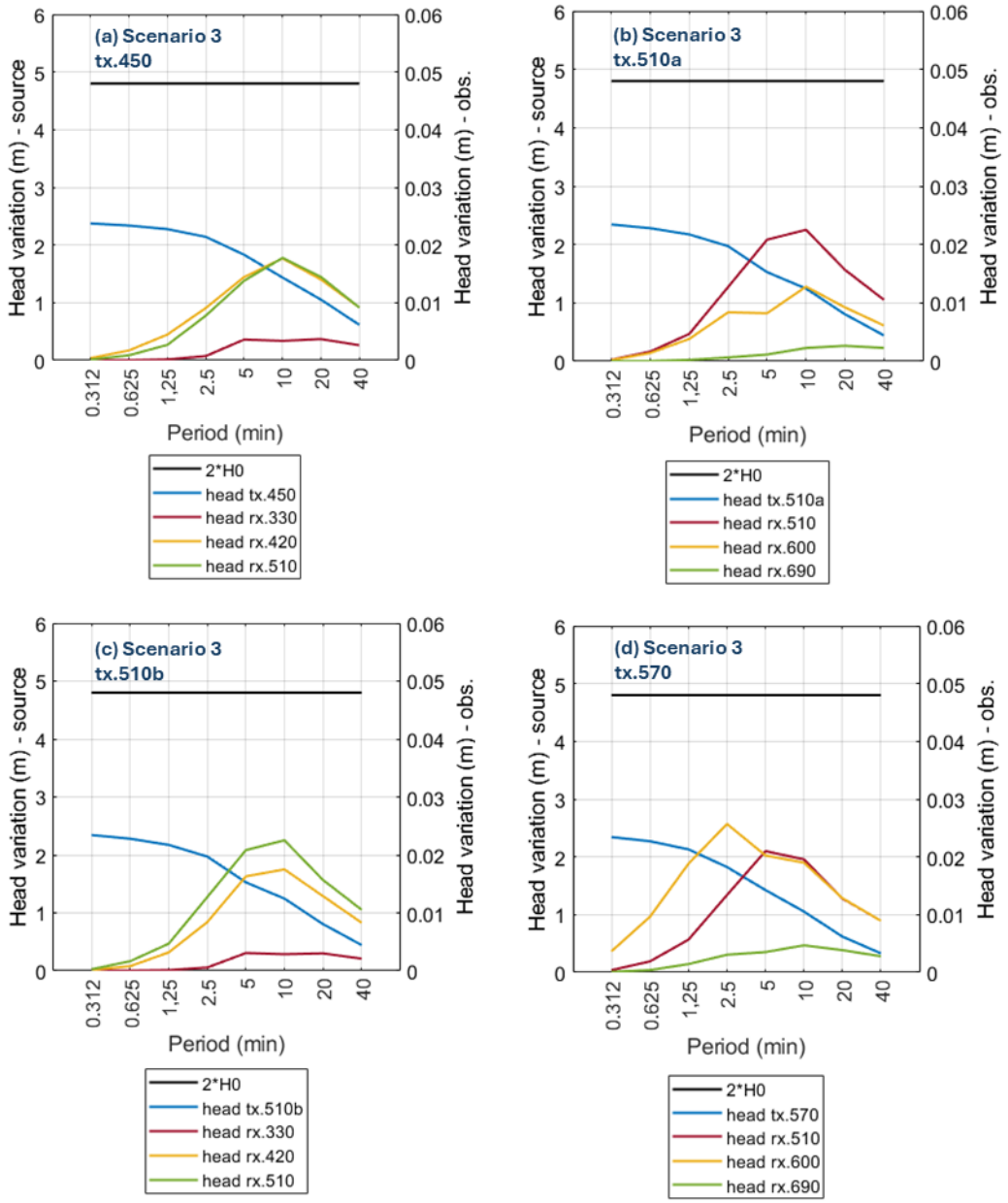

Figure II-5 : Simulated variation of heads in a source and in three observation intervals for eight selected periods for the heterogeneous case with rc = 0.0127. Head variation is the difference between maximum and minimum head over a cycle when steady state is reached. (a) Test tx.450; (b) test tx.510a; (c) test tx.510b and (d) test tx.570.

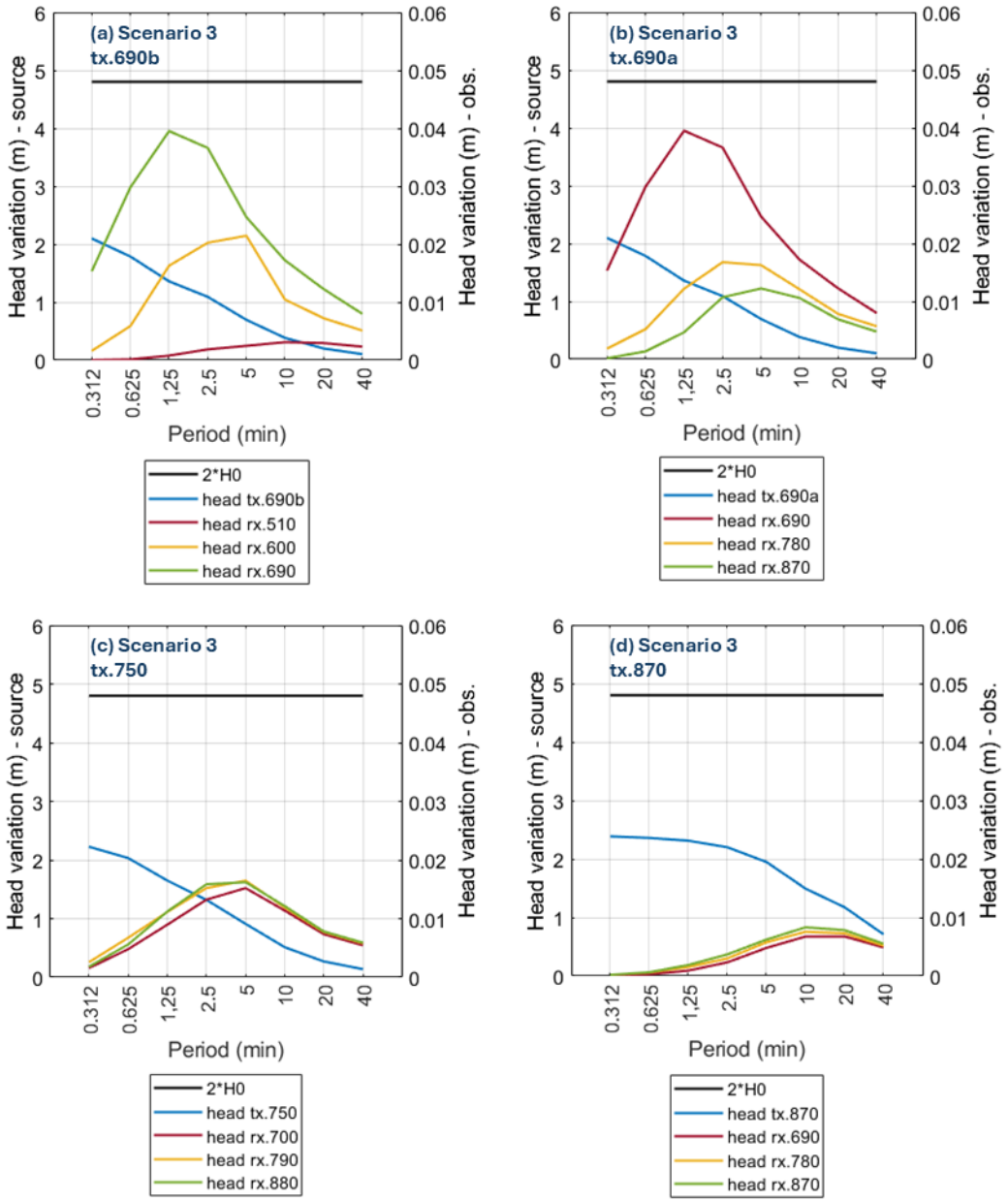

Figure II-6 : Simulated variation of heads in a source and in three observation intervals for eight selected periods for the heterogeneous case with rc = 0.0127. Head variation is the difference between maximum and minimum head over a cycle when steady state is reached. (a) Test tx.690b; (b) test tx.690a; (c) test tx.750 and (d) test tx.870.

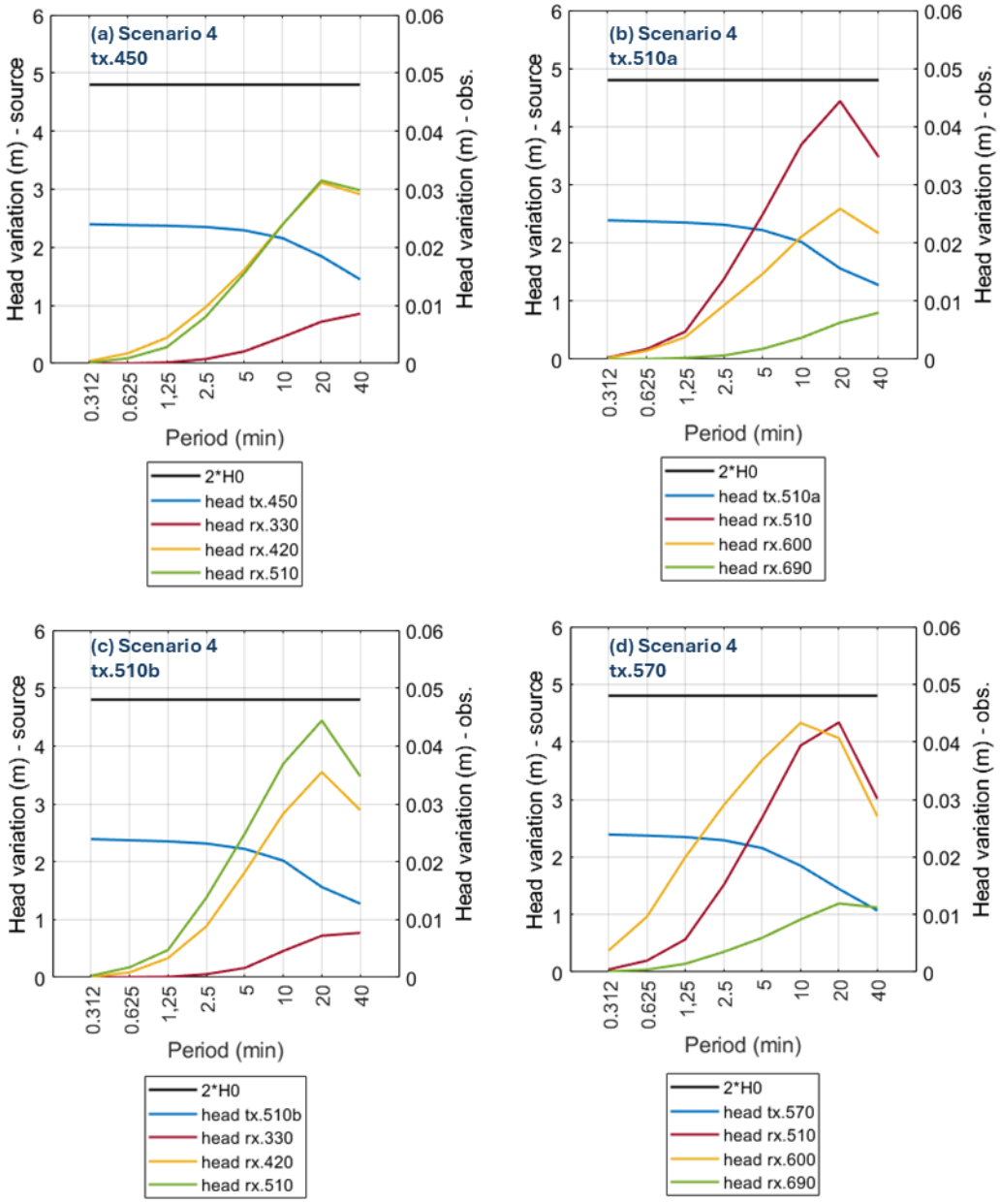

Figure II-7 : Simulated variation of heads in a source and in three observation intervals for eight selected periods for the heterogeneous case with rc = 0.0254. Head variation is the difference between maximum and minimum head over a cycle when steady state is reached. (a) Test tx.450; (b) test tx.510a; (c) test tx.510b and (d) test tx.570.

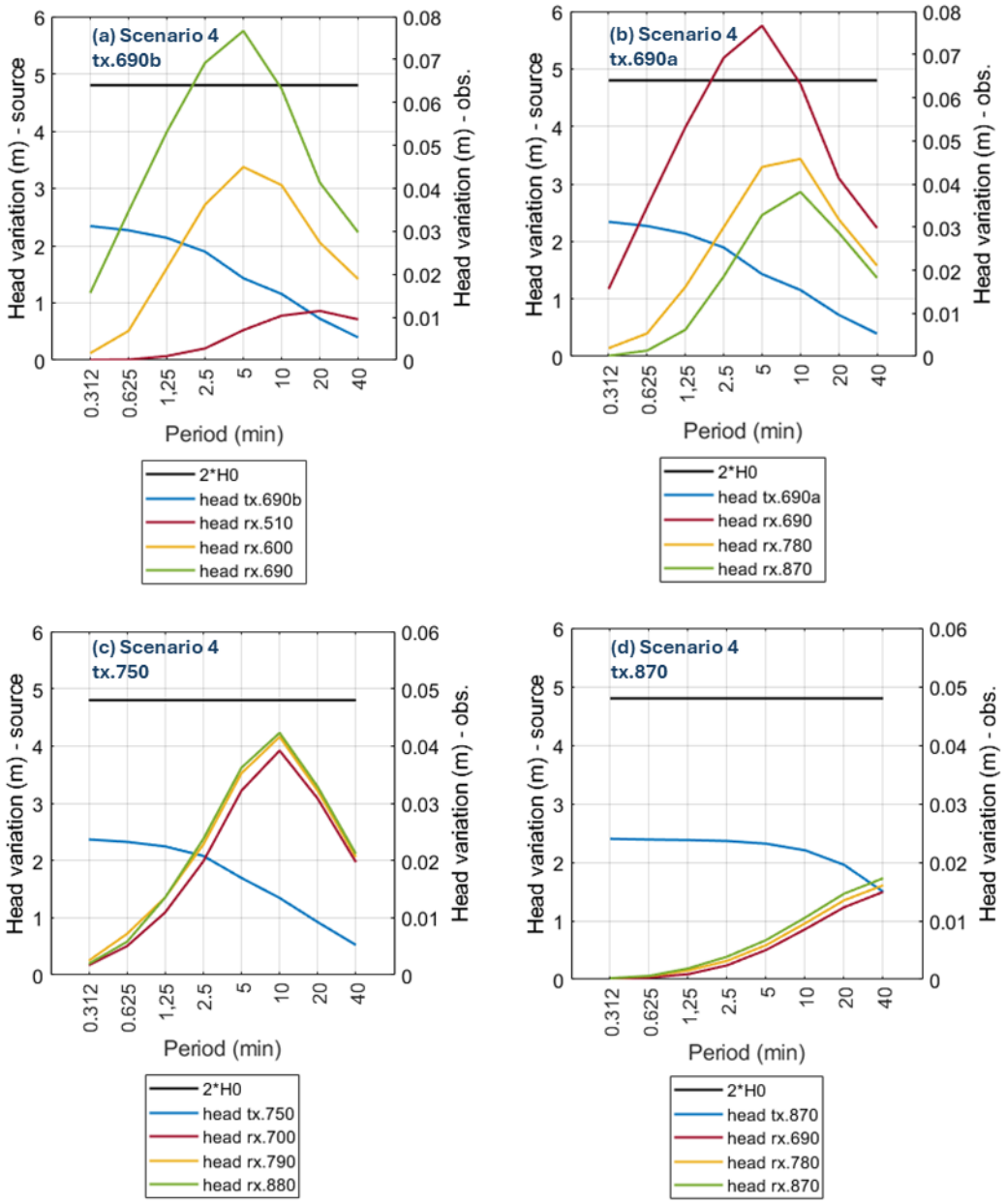

Figure II-8 : Simulated variation of heads in a source and in three observation intervals for eight selected periods for the heterogeneous case with rc = 0.0254. Head variation is the difference between maximum and minimum head over a cycle when steady state is reached. (a) Test tx.690b; (b) test tx.690a; (c) test tx.750 and (d) test tx.870.

II.3 Information content associated with the numerical inversion of periodic hydraulic tomography using different period combinations

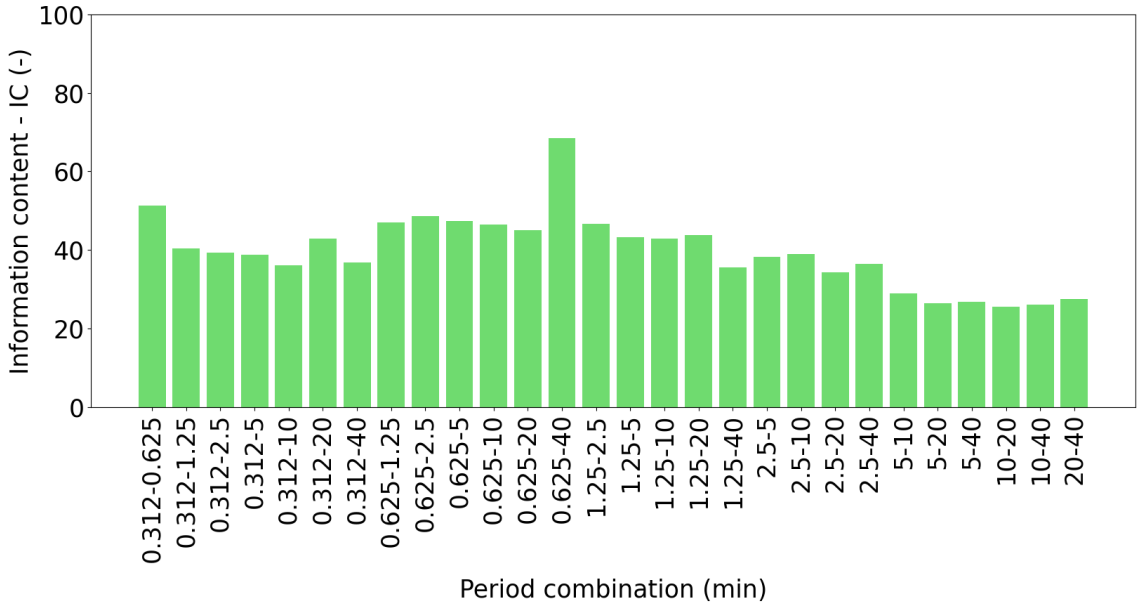

Figure II-9 : Information content (IC) for all different pair combinations of signal periods for periodic tests for the heterogeneous model with rc = 0.0077 m.

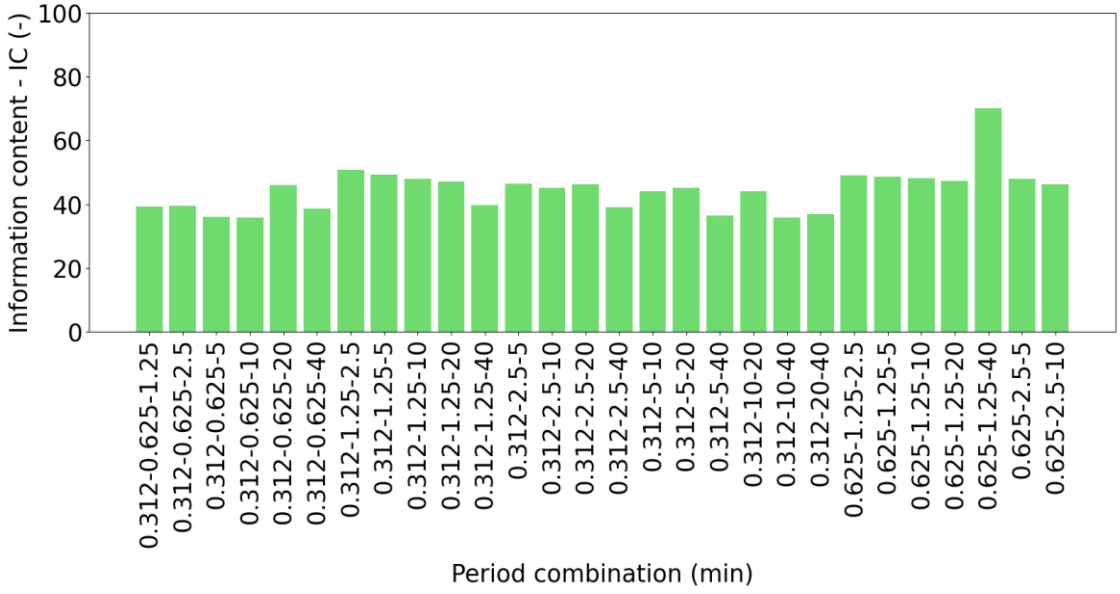

Figure II-10 : Information content (IC) for first part of different triplet combinations of signal periods for periodic tests for the heterogeneous model with rc = 0.0077 m.

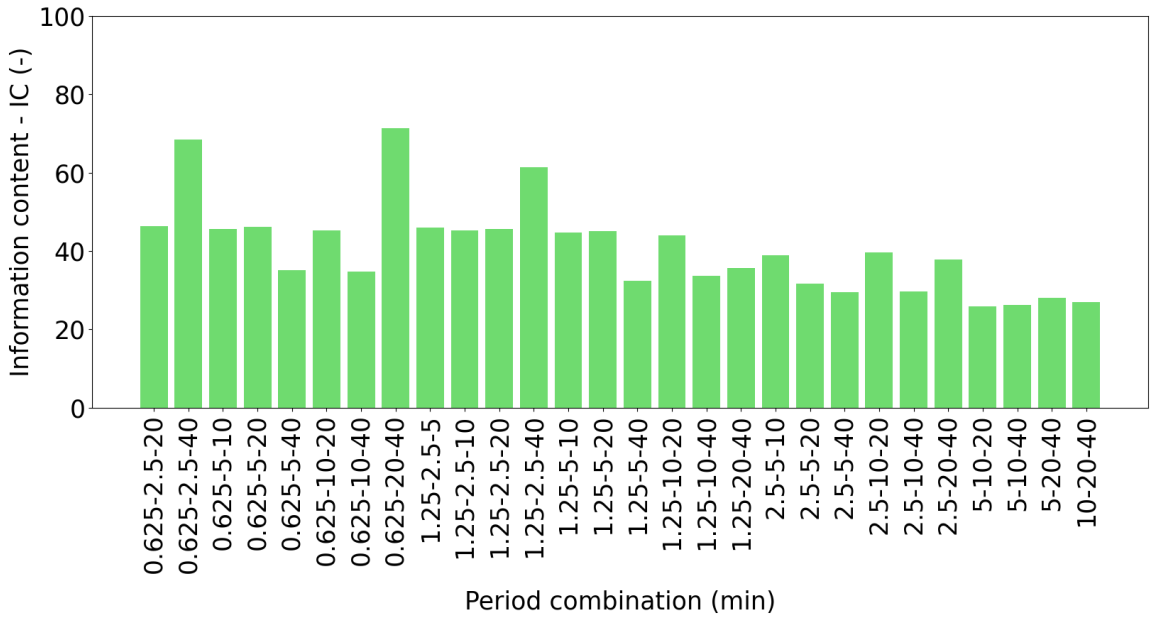

Figure II-11 : Information content (IC) for second part of different triplet combinations of signal periods for periodic tests for the heterogeneous model with rc = 0.0077 m.

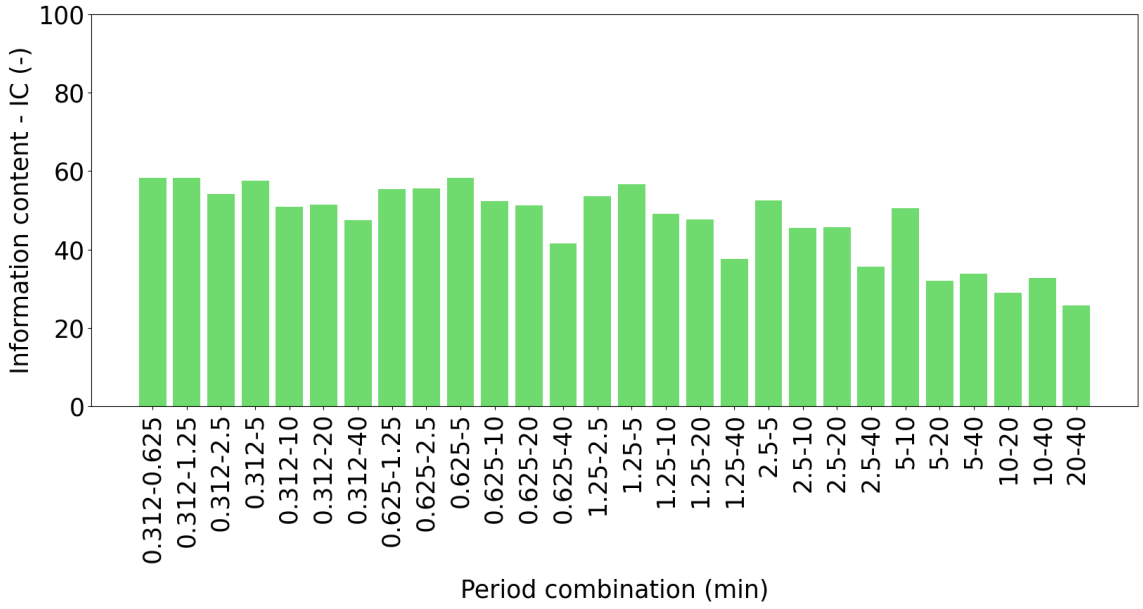

Figure II-12 : Information content (IC) for all different pair combinations of signal periods for periodic tests for the heterogeneous model with rc = 0.0127 m.

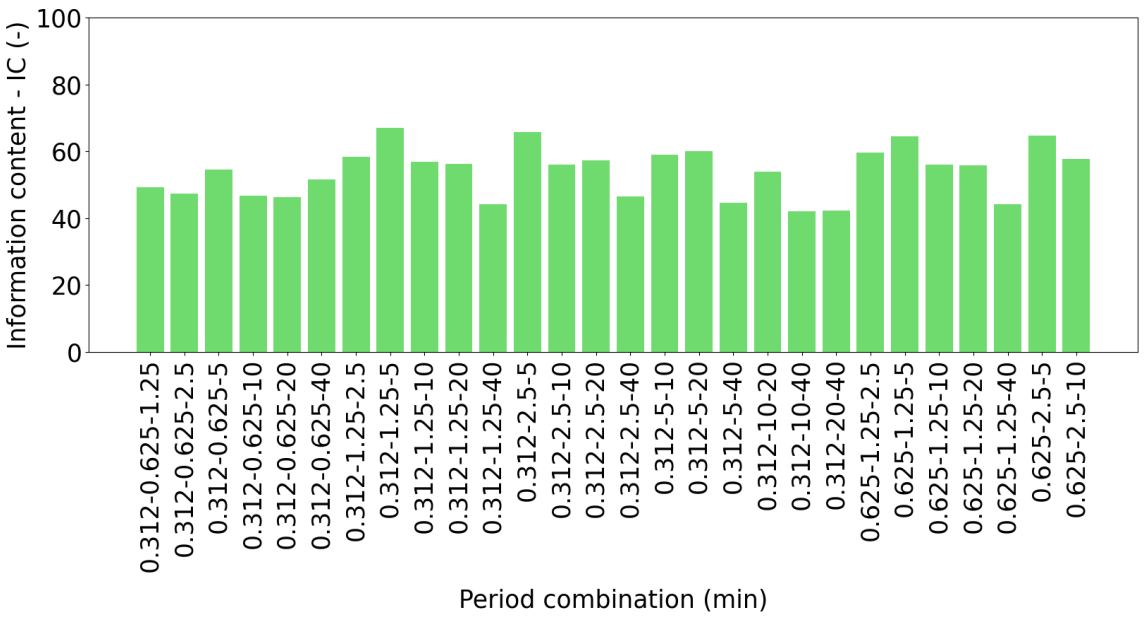

Figure II-13 : Information content (IC) for first part of different triplet combinations of signal periods for periodic tests for the heterogeneous model with rc = 0.0127 m.

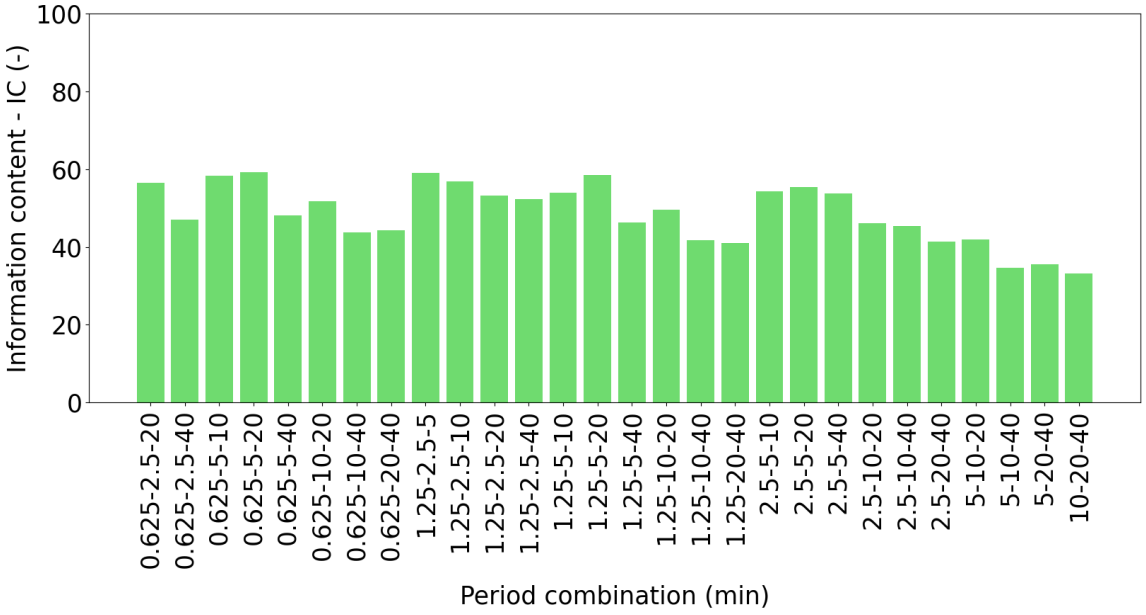

Figure II-14 : Information content (IC) for second part of different triplet combinations of signal periods for periodic tests for the heterogeneous model with rc = 0.0127 m.

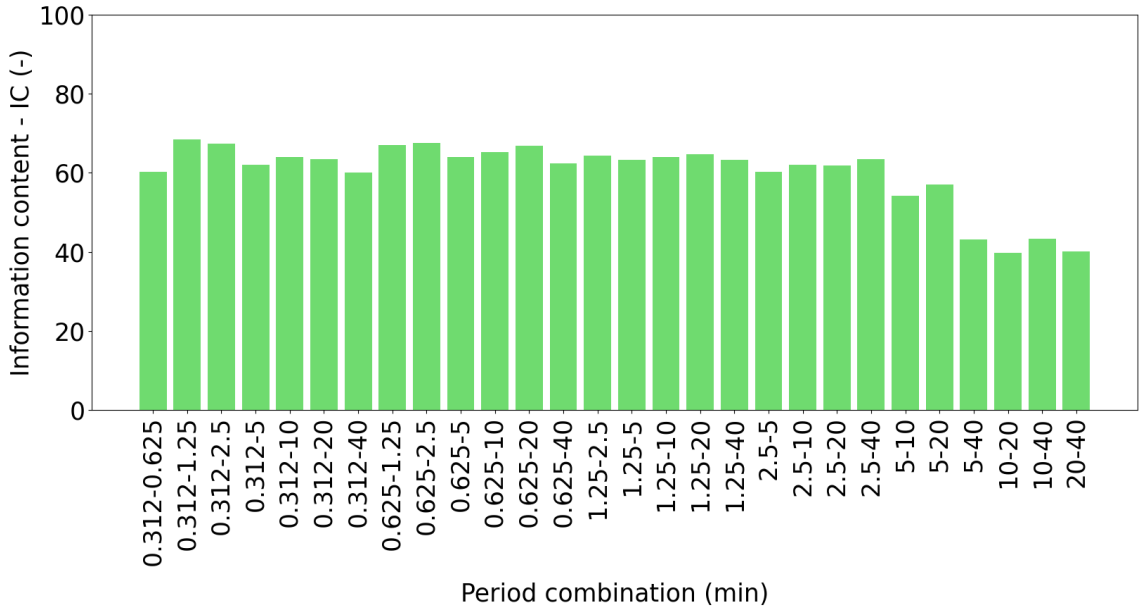

Figure II-15 : Information content (IC) for all different pair combinations of signal periods for periodic tests for the heterogeneous model with rc = 0.0254 m.

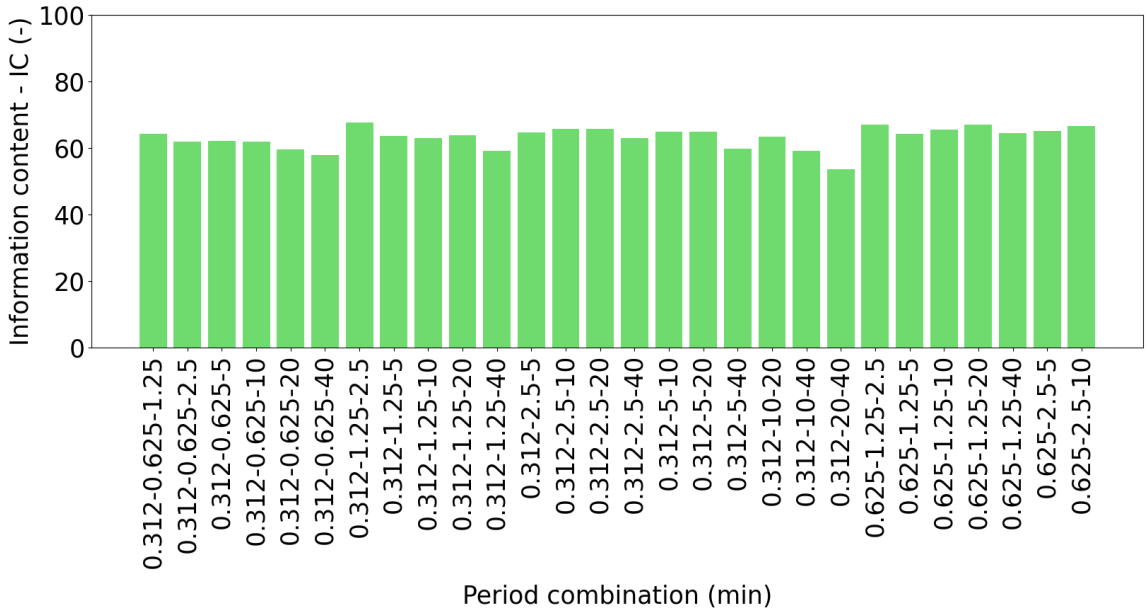

Figure II-16 : Information content (IC) for first part of different triplet combinations of signal periods for periodic tests for the heterogeneous model with rc = 0.0254 m.

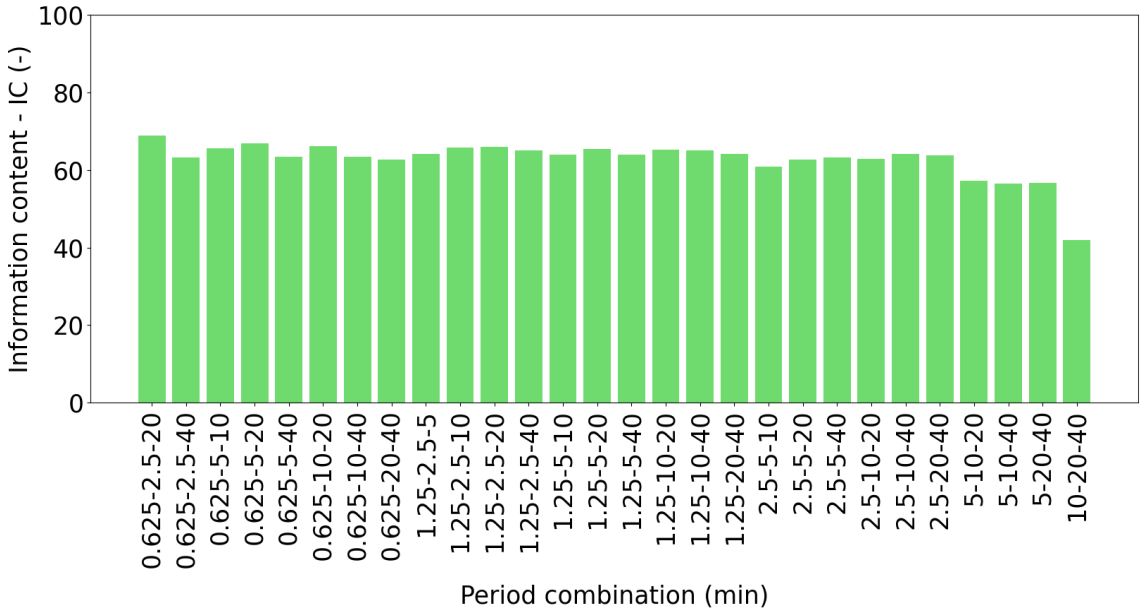

Figure II-17 : Information content (IC) for second part of different triplet combinations of signal periods for periodic tests for the heterogeneous model with rc = 0.0254 m.

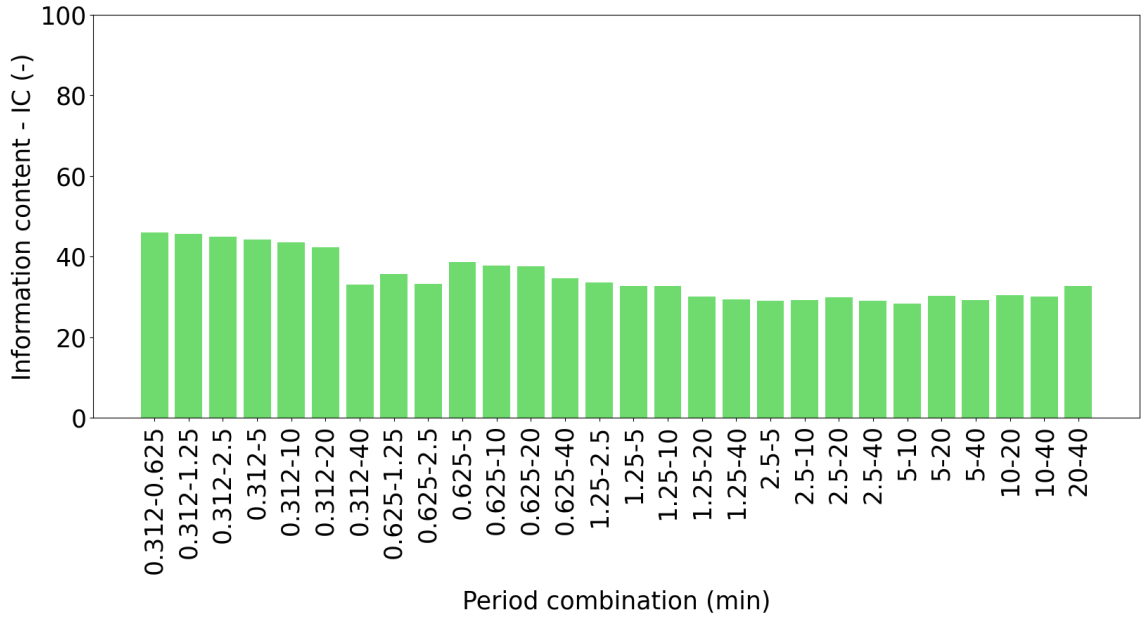

Figure II-18 : Information content (IC) for all different pair combinations of signal periods for periodic tests for the homogeneous model with rc = 0.0077 m.

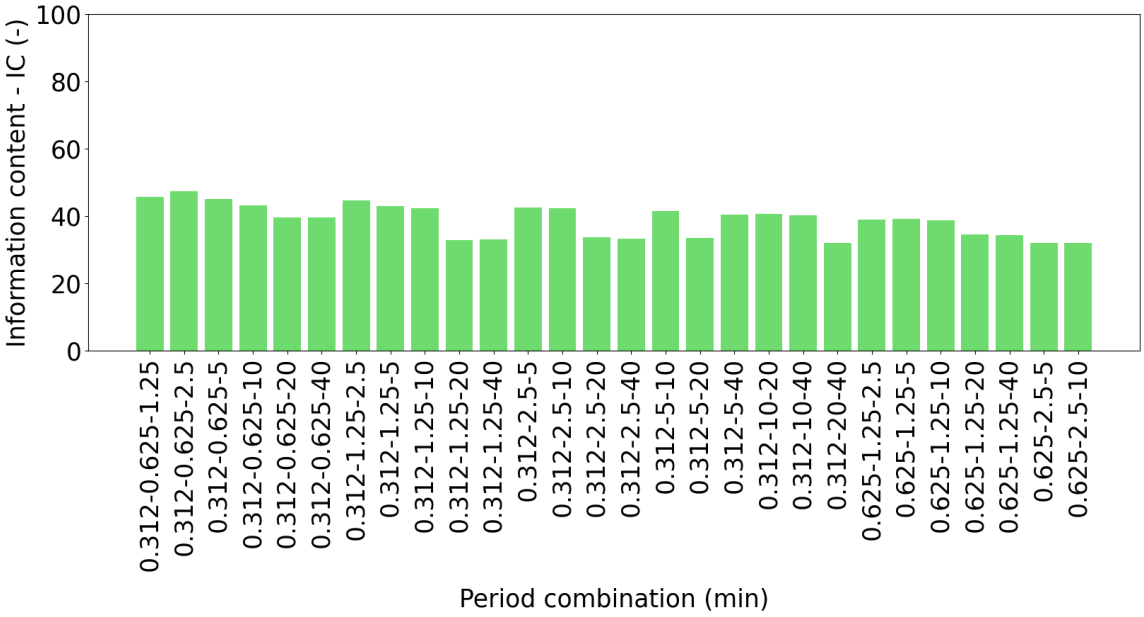

Figure II-19 : Information content (IC) for first part of different triplet combinations of signal periods for periodic tests for the homogeneous model with rc = 0.0077 m.

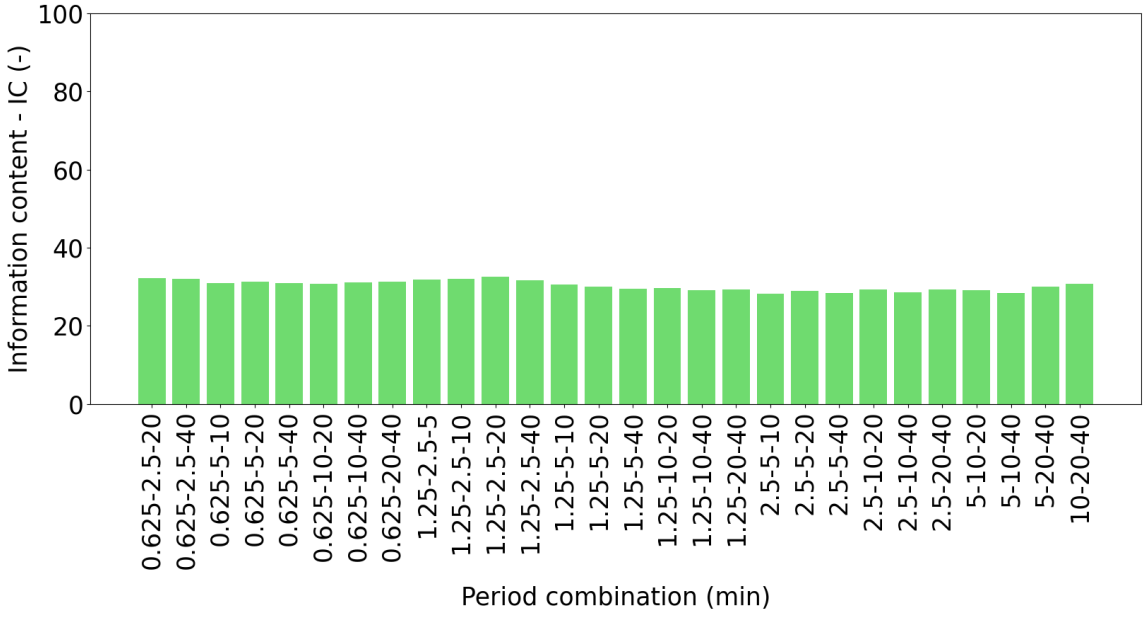

Figure II-20 : Information content (IC) for second part of different triplet combinations of signal periods for periodic tests for the homogeneous model with rc = 0.0077 m.

ANNEXES III : FIGURES SUPPLÉMENTAIRES POUR L'ARTICLE 3

III.1 Inferred hydraulic property values from the numerical inversion with the Ir2dinv model for different combinations of periods

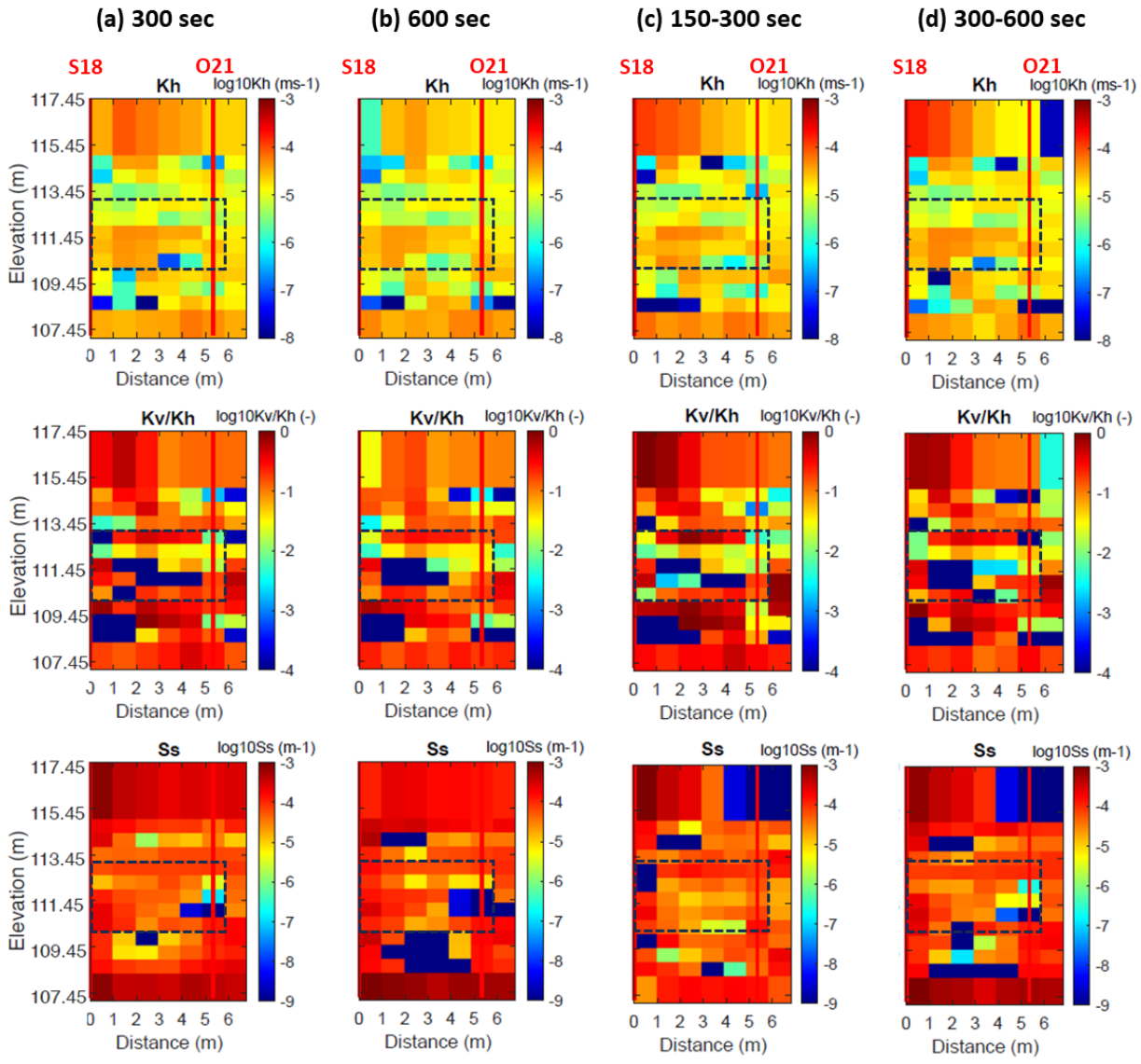

Figure III-1 : Tomograms for Kh, Kv/Kh, and Ss resulting from the inversion of the periodic tests with the (a) 300 sec, (b) 600 sec, (c) 150-300 sec and (d) 300-600 sec. The rectangle outlined by a black dashed line is the focus area for the periodic and slug tests.

III.2 Parameter sensitivities for different single or combined periods

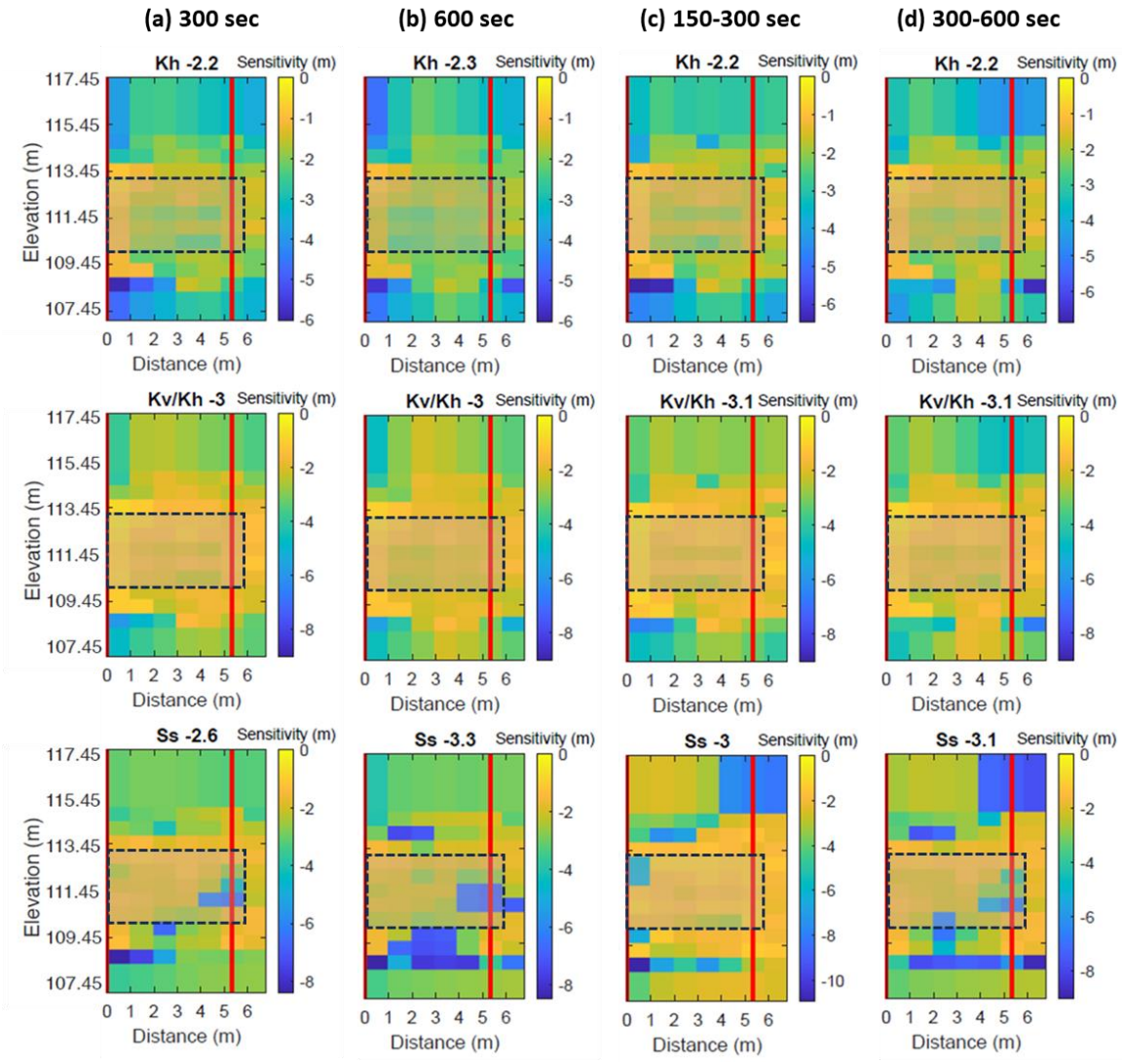

Figure III-2 : Spatial distribution of RMS (root-mean-square) normalized sensitivities for Kh, Kv/Kh and Ss for (a) 300 sec, (b) 600 sec, (c) 150-300 sec, and (d) 300-600 sec. The number next to the name of the hydraulic property is the average RMS sensitivity within the focus area.

III.3 Examples of L-curve used for the resolution analysis for different single or combined periods

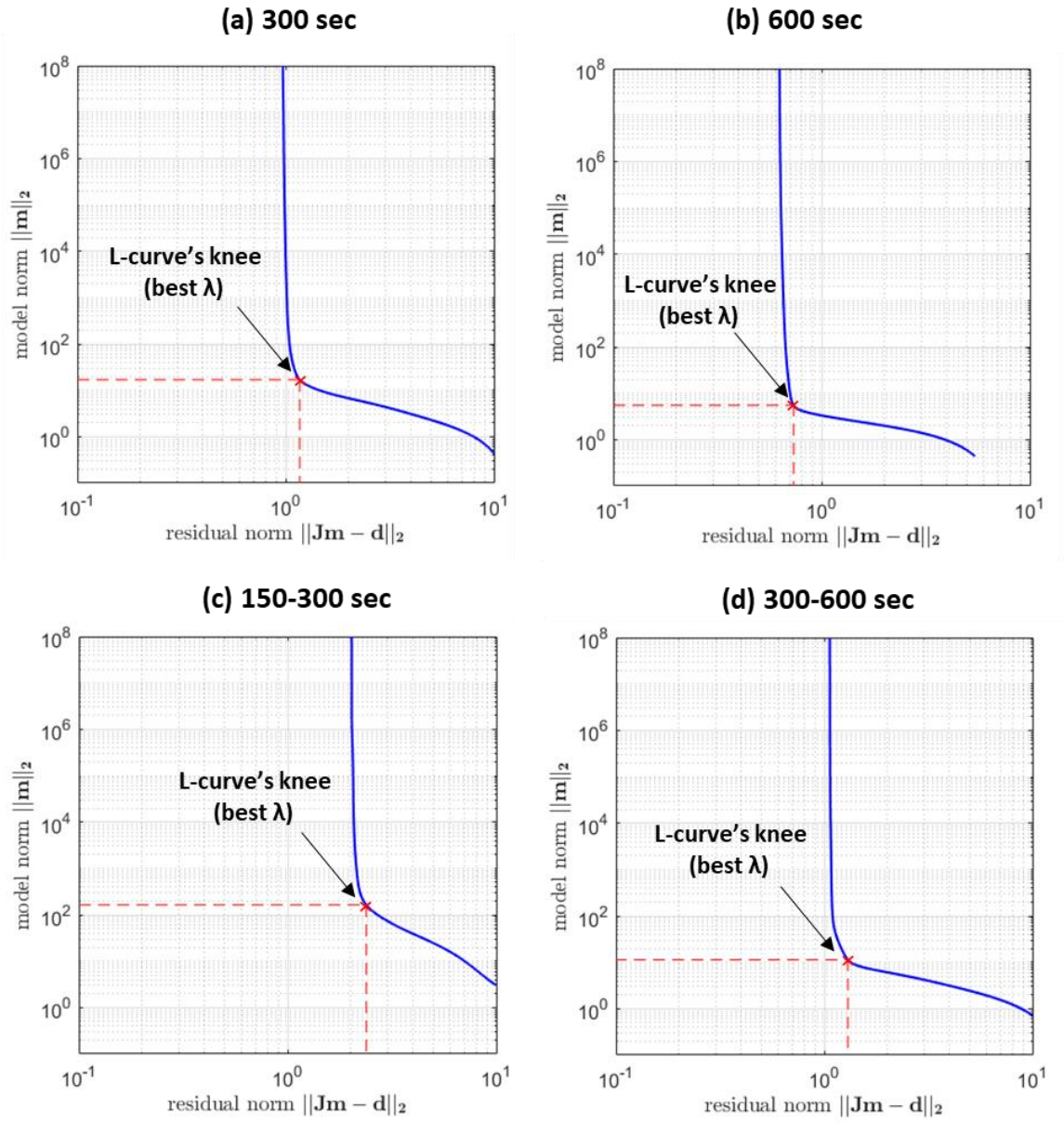

Figure III-3 : Comparison of L-curve plots for simulated tomographic tests: (a) 300 sec, (b) 600 sec, (c) 150-300 sec, and (d) 300-600 sec. The inflexion point of each L-curve is marked by a "x" symbol.

III.4 Parameter resolution associated with the numerical inversion using the lr2dinv model for different single or combined periods

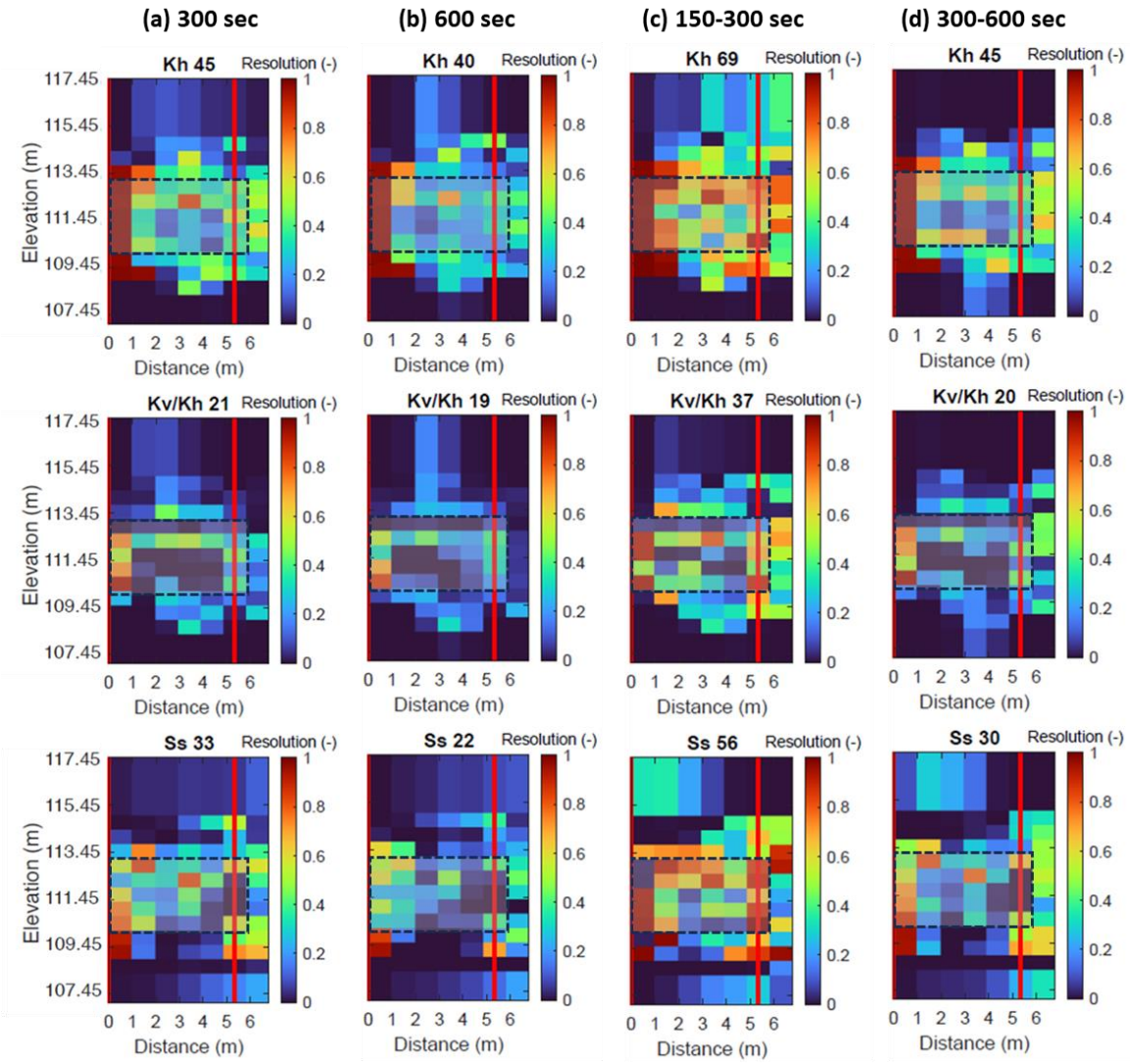

Figure III-4 : Spatial distribution of the resolution for the hydraulic properties Kh, Kv/Kh and Ss for (a) 300 sec, (b) 600 sec, (c) 150-300 sec, and (d) 300-600 sec. The number in the parenthesis next to the name of the hydraulic property is the resolution degree (RD) within the focus area.